



# Effects of corrosion on low-cycle fatigue (seismic) behaviour of high-strength steel reinforcing bars (Rusteel)

**EUROPEAN COMMISSION**

Directorate-General for Research and Innovation  
Directorate D — Key Enabling Technologies  
Unit D.4 — Coal and Steel

E-mail: [rtd-steel-coal@ec.europa.eu](mailto:rtd-steel-coal@ec.europa.eu)  
[RTD-PUBLICATIONS@ec.europa.eu](mailto:RTD-PUBLICATIONS@ec.europa.eu)

Contact: RFCS Publications

European Commission  
B-1049 Brussels

European Commission

# Research Fund for Coal and Steel

## **Effects of corrosion on low-cycle fatigue (seismic) behaviour of high-strength steel reinforcing bars (Rusteel)**

W. Salvatore, S. Caprili

**University of Pisa — Department of Civil and Industrial Engineering**

Largo L. Lazzarino 1, 56126 Pisa PI, ITALY

A. Braconi, M. Finetto

**RIVA Acciaio S.p.A.**

Viale Certosa 249, 20151 Milano MI, ITALY

L. Bianco, C. Ascanio

**Ferriere Nord**

S.S. 463 Zona Industriale, 33010 Osoppo UD, ITALY

J. Moersch

**Institut für Stahlbetonbewehrung e. V.**

Kaiserswether Strasse 137, 40474 Dusseldorf (Germany)

C. Apostolopoulos

**University of Patras**

Rion Patras, 265 04 Patras, GREECE

G. Ferreira Pimenta

**Instituto de Soldadura e Qualidade**

Av. Prof. Dr Cavaco Silva 33, Talaide, 2740-120 Porto Salvo, Oeiras, PORTUGAL

Grant Agreement RFSR-CT-2009-00023

1 July 2009 to 30 June 2012

**Final report**

Directorate-General for Research and Innovation

## **LEGAL NOTICE**

Neither the European Commission nor any person acting on behalf of the Commission is responsible for the use which might be made of the following information.

The views expressed in this publication are the sole responsibility of the authors and do not necessarily reflect the views of the European Commission.

***Europe Direct is a service to help you find answers  
to your questions about the European Union***

**Freephone number (\*):  
00 800 6 7 8 9 10 11**

(\*) Certain mobile telephone operators do not allow access to 00 800 numbers or these calls may be billed.

More information on the European Union is available on the Internet (<http://europa.eu>).

Luxembourg: Publications Office of the European Union, 2014

ISBN 978-92-79-38570-4  
doi:10.2777/7705

© European Union, 2014  
Reproduction is authorised provided the source is acknowledged.

*Printed in Luxembourg*

PRINTED ON WHITE CHLORINE-FREE PAPER

|                          |  |     |
|--------------------------|--|-----|
| <b>Table of Contents</b> |  |     |
| Final Summary            |  | 5   |
| List of Deliverables     |  | 9   |
| <b>1</b>                 | <b>Introduction</b>  | 11  |
| 1.1                      | Mechanical properties of steel reinforcing bars                                | 11  |
| 1.2                      | Durability problems and corrosion phenomena of steel reinforcements            | 14  |
| 1.2.1                    | Concept and definition of durability   | 14  |
| 1.2.2                    | Durability problems of steel reinforcing bars                                  | 15  |
| 1.2.3                    | Durability of concrete structures in the European standards                    | 17  |
| 1.3                      | Actual problems  | 19  |
| 1.4                      | Main objectives of the present work  | 20  |
| 1.5                      | The work - program and the adopted methodology                                 | 21  |
| <b>2</b>                 | <b>Mechanical characterization of steel reinforcing bars</b>                   | 23  |
| 2.1                      | European standards for steel reinforcements: mechanical properties and tests   | 23  |
| 2.2                      | Mechanical characterization of selected reinforcing bars                       | 27  |
| 2.2.1                    | Metallurgical investigation on steel reinforcements                            | 27  |
| 2.2.2                    | Results of experimental tensile tests  | 29  |
| 2.2.2.1                  | Experimental tests executed by UniPi: results                                  | 29  |
| 2.2.2.2                  | Experimental tests executed by ISQ: results                                    | 30  |
| 2.2.2.3                  | Experimental tests executed by UPA: results                                    | 31  |
| 2.2.3                    | Mechanical Characterization of steel reinforcing bars under low-cycle fatigue  | 31  |
| 2.2.3.1                  | Actual literature and standards about LCF tests                                | 31  |
| 2.2.3.2                  | Elaboration of a LCF testing protocol for steel reinforcements                 | 32  |
| 2.2.3.3                  | Experimental LCF tests on steel reinforcements                                 | 35  |
| <b>3</b>                 | <b>Design and modelling of case studies</b>                                    | 39  |
| 3.1                      | Reinforced concrete case study buildings                                       | 39  |
| 3.1.1                    | Structural design of r.c. case studies   | 40  |
| 3.1.2                    | Elaboration of non linear models of r.c. case studies                          | 46  |
| 3.2                      | Steel/concrete composite structures  | 49  |
| 3.2.1                    | Desing of full-scale 3D structure at Ispra laboratory                          | 49  |
| 3.2.2                    | Desing of composite joints   | 51  |
| <b>4</b>                 | <b>Selection of the seismic input for r.c. buildings</b>                       | 53  |
| 4.1                      | Definition of time-histories database and time history processing              | 53  |
| 4.2                      | Application of range counting method to Group 5                                | 54  |
| 4.3                      | Selection of representative time histories for designed structures             | 59  |
| 4.3.1                    | Park and Ang Damage Indicator  | 59  |
| 4.3.2                    | Individuation of the equivalent SDOF model                                     | 60  |
| 4.3.3                    | Selection of representative time histories                                     | 63  |
| <b>5</b>                 | <b>Evaluation of seismic demand on rebars</b>                                  | 67  |
| 5.1                      | Structural assessment of r.c. case studies                                     | 67  |
| 5.2                      | Evaluation of the ductility demand on steel reinforcing bars in r.c. buildings | 76  |
| 5.2.1                    | Calibration of the bar's model   | 76  |
| 5.2.2                    | Axial stress-strain histories on steel reinforcing bars                        | 78  |
| 5.3                      | Evaluation of seismic demand in steel reinforcing bars in composite structures | 90  |
| 5.3.1                    | Calibration of the numerical model of the joint                                | 92  |
| <b>6</b>                 | <b>Durability problems in r.c. structures</b>                                  | 95  |
| 6.1                      | Selection of accelerated corrosion testing procedures                          | 95  |
| 6.2                      | Accelerated corrosion tests in salt spray chamber                              | 99  |
| 6.2.1                    | Elaboration of a protocol for the execution of accelerated corrosion test      | 99  |
| 6.2.2                    | Individuation of a set of representative steel reinforcing bars                | 100 |

|          |  |     |
|----------|--|-----|
| <b>7</b> | <b>Mechanical tests on corroded bars</b>   | 101 |
| 7.1      | Tensile tests on corroded specimens  | 101 |
| 7.1.1    | Results of experimental tensile tests - UniPI  | 101 |
| 7.1.2    | Results of experimental tensile tests – ISQ  | 103 |
| 7.1.3    | Results of experimental tensile tests – UPA  | 106 |
| 7.1.4    | Evaluation of necking of tested steel reinforcing bars   | 107 |
| 7.1.5    | Preliminary observations on experimental tensile tests’ results on corroded bars   | 110 |
| 7.2      | Low-Cycle Fatigue (LCF) tests on corroded specimens  | 117 |
| 7.2.1    | Tests executed by UniPi  | 117 |
| 7.2.2    | Tests executed by UPA  | 120 |
| 7.2.3    | Tests executed by ISQ  | 123 |
| 7.2.4    | Hydrogen concentration measurements of corroded rebars after low-fatigue test  | 124 |
| 7.2.5    | Considerations on the results of LCF tests on corroded bars  | 126 |
| 7.3      | Definition of Corrosion Damage Indicators (CDI) for each type of corrosion induced damage previously classified  | 130 |
| 7.4      | Correlation between corrosion attacks intensity on existing buildings and increasing corrosion damaging levels obtained by accelerated corrosion tests – Corrosion Damage Indicators (CDI) | 132 |
| 7.4.1    | Correlation of mass loss   | 132 |
| 7.4.2    | Correlation of pit depth   | 134 |
| 7.4.3    | Correlation of hydrogen absorption   | 135 |
| 7.4.4    | Example for the correlation of CDI from accelerated corrosion tests to practical corrosion conditions  | 136 |
| 7.5      | Correlation of CDI and Classes of Exposure for buildings with the static and LCF   | 137 |
| 7.5.1    | Performance indicators for static performance - correlation of relevant PI’s to CDI  | 137 |
| 7.5.2    | Performance indicators for LCF- performance - correlation of relevant PI’s to CDI  | 138 |
| 7.5.3    | Correlation of PI’s and CDI’s with practical corrosion conditions  | 140 |
| <b>8</b> | <b>Conclusions</b>   | 141 |
| 8.1      | Exploitation and impact of the research results  | 141 |
| 8.2      | Background document for the execution of LCF tests   | 142 |
| 8.3      | Behaviour of corroded steel reinforcing bars: considerations and practical guidelines  | 145 |
| 8.4      | Dissemination  | 148 |
|          |  |     |
|          | List of figures  | 149 |
|          | List of tables   | 153 |
|          | List of main abbreviations   | 157 |
|          | List of references   | 159 |

## FINAL SUMMARY

---

Modern buildings with r.c. and composite steel/concrete structure are designed according to the capacity design approach, individuating specific structural elements in which plasticizations are expected and oversizing all the other members in order to maintain them in the elastic field. Through an opportune locations of plastic hinges in principal structural members (for example at the ends of beams and columns in r.c. structures), a global ductile collapse mechanism, able to dissipate the energy stored in the building during the earthquake and to avoid at the same time the development of brittle and unexpected failures, can be obtained.

The dissipative capacity of the elements in which plastic hinges are expected strictly depends on their flexural behaviour and on their ability to satisfy the rotational capacity imposed by real seismic event; the structural ductility (i.e. global displacement of the building), the element ductility (i.e. rotational capacity of beams and columns) and the material ductility (i.e. strain in the steel reinforcing bars) are consequently directly connected and a deep knowledge of the effective cyclic/seismic behaviour of steel bars in presence of earthquakes is necessary for the full understanding of the global behaviour of the building, both in the case of r.c. and composite structures.

As a consequence of what already presented, in *Rusteel* research project a detailed investigation of the low-cycle fatigue (LCF)/seismic behaviour of reinforcing steel bars in r.c. and composite steel/concrete structures was executed, aiming to the individuation of the effective mechanical *capacity* of actual European production of reinforcing steels to satisfy the requirements imposed by real earthquake events. The capacity so evaluated was consequently compared to the effective ductility demand imposed on steel reinforcements by real earthquake events, evaluated considering numerical or experimental analyses (respectively in the case of r.c. and composite structures).

Despite a large amount of scientific literature about the modelling and the representation of the cyclic/seismic behaviour of steel reinforcing bars considered as “single elements”, no information are provided about their effective seismic performance inside buildings, their interaction with concrete structure and the ductility requirements imposed by seismic events. The lack of information about the real ductility demand, and the following deficiency of knowledge about the effective seismic performance of steel bars, result in the absence of opportune experimental tests for the production control of the cyclic behaviour of rebars: actual European production standard for reinforcements (EN 10080:2005) does not include LCF tests for the mechanical characterization of the cyclic behaviour of rebars. For sake of clarity, only Spanish and Portuguese standards (UNE 36065 EX:2000, LNEC E-455:2008 and LNEC E-460:2008) prescribe the execution of symmetrical tension/compression cycles for the production control of steel reinforcements. Nevertheless, the testing parameters (imposed deformation, frequency, number of cycles and free length of the specimens) are not based on the results of scientific investigations about the real seismic behaviour of bars in structures and, consequently, more accurate analyses are required.

As a consequence of what already presented, *Rusteel* research project is directly inserted in the widest framework of the revision of European Standards for reinforcements (prEN 10080:2012) and of the indications of Mandate M115, according to which an harmonized low-cycle fatigue test shall be elaborated in order to guarantee the seismic mechanical characterization of steel reinforcements.

Beside what already presented, recent studies in the current literature (Apostolopoulos 2006, Apostolopoulos and Papadakis 2008 and others) evidenced durability problems in concrete structures: in presence of aggressive environmental conditions, both concrete and steel reinforcing bars can be affected by a rapid decrease of their mechanical properties with the following deterioration of the global bearing capacity of the structures in which they are inserted. In particular, problems related to the effects of corrosion phenomena due to carbonation or chloride attack were individuated, causing a decrease of the effective ductility capacity of steel reinforcements, expressed in terms of elongation to maximum load ( $A_{gt}$ ), dissipated energy and number of cycles up to failure (figure I).

Those problems were revealed in particular in the case of TempCore steel reinforcing bars, nowadays mainly used for the realization of modern r.c. and composite steel/concrete structure, underlining the necessity of an accurate study of the ability of actual European production of reinforcing steels to sustain the seismic ductile requirements also in presence of durability problems, corrosion attacks and deterioration phenomena.

It's consequently necessary to understand if reinforcing steel bars, exposed to corrosion attack, are still able to satisfy the ductile requirements due to seismic events.

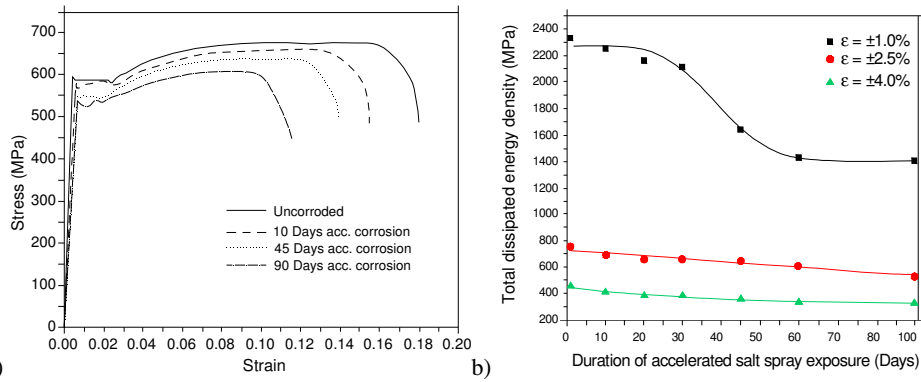


**Figure I:** a) Stress-strain curves for B500St rebars (Apostolopoulos 2006), b) relationship between exposure period and dissipated energy (Apostolopoulos and Michalopoulos 2006).

The objectives of the present work can be so summarized into two different main aspects, that are:

- The evaluation of the effective *ductility demand* imposed by real earthquake events on steel reinforcing bars, expressed in terms of strain level and dissipated energy.
- The evaluation of the mechanical performance (*capacity*) of steel reinforcing bars subjected to low-cycle fatigue (seismic) loading, taking into consideration also the influence of corrosion phenomena on the monotonic and cyclic behaviour of rebars and their ability in sustaining, also after degradation due to corrosion, the effective seismic requirements.

The analysis of the effective cyclic behaviour of reinforcing steels in modern r.c. and composite structures allowed the evaluation of the levels of deformation and energy dissipation effectively required by seismic events, allowing to assess the ability of actual European production to satisfy seismic demand and to individuate a common procedure for the execution of LCF tests able to accurately characterize the seismic behaviour of steel reinforcements, calibrated on the base of scientific investigations. The protocol can be proposed in the framework of the harmonization intent of Mandate M115 for the revision of European standard EN 10080:2005 in order to provide standardized procedures to European steel producers for the factory production control of reinforcing bars. Moreover, the research project aims to provide useful indications for practitioners and designers for what concerns devices to adopt in modern buildings in order to avoid problems related to corrosion attack and degradation, in addition to what already prescribed by Eurocode 2 (EN 1992-1-1:2005).

The simplified scheme of the procedure adopted for the reaching of the objectives above listed is presented in figure II, in which the two main tendencies of capacity and demand are well distinguished.

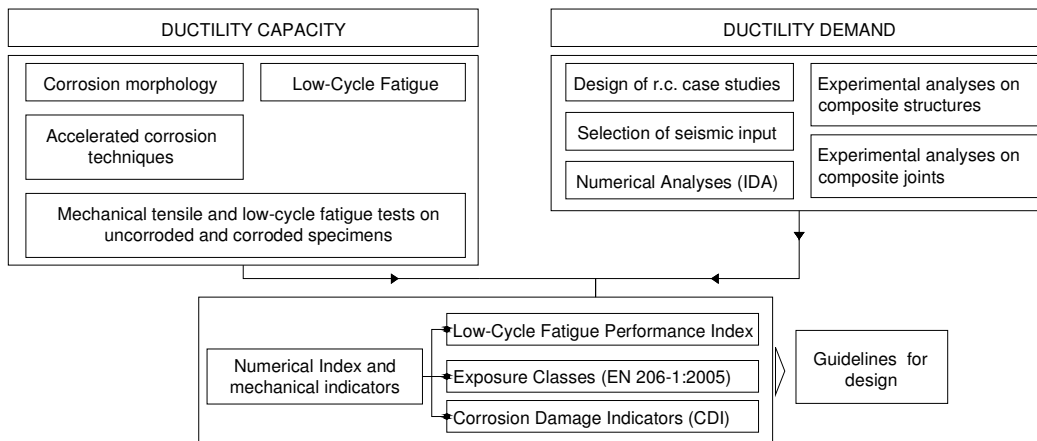


**Figure II:** Simplified scheme of the adopted methodology.

For what concerns the *capacity*, a representative set of steel grades, covering the actual production scenario (strength, ductility classes, diameter and production process), was selected and subjected to tensile and Low-Cycle Fatigue; LCF tests were executed using a preliminary protocol elaborated considering the prescriptions of actual standards and what present in the current literature.

The results of LCF tests, in terms number of cycles and dissipated energy for a specific level of imposed deformation (individuated as *Low-Cycle Fatigue Performance Index – PI*), were compared with the results provided by numerical analyses on r.c. case study buildings and with the data coming

from experimental monotonic and cyclic tests executed on representative steel/concrete composite joints.

The comparison between effective ductility demand and real mechanical cyclic capacity of steel reinforcing bars allowed the definition of a final protocol for the execution of LCF to be adopted as reference testing technique for the production control of the seismic behaviour of steel bars for modern constructions.

Beside what already presented regarding the behaviour of uncorroded (reference) steel reinforcing bars, a detailed investigation of the corrosion process and the analysis of the actual laboratory techniques to artificially reproduce the effects of corrosion phenomena on steel bars were the basis for the elaboration of a specific accelerated corrosion protocol able to artificially reproduce the detrimental effects of environmental conditions on the structural behaviour of steel bars. This task aims to the evaluation of the mechanical behaviour of actual steel reinforcing bars in presence of corrosion exposure, and of their ability to sustain seismic action. Experimental mechanical tests, including again both monotonic and LCF tests (figure III), were executed on a reduced set of corroded steel samples, opportunely individuated for including the most representative European steel grades and diameters.

*Corrosion Damage Indicators (CDI)* were defined considering the severity of corrosion attack in terms of deterioration of the mechanical and mass loss, taking into consideration the influence of several mechanical and production parameters (producer, diameter, process) on the behaviour of corroded specimens. A drastic reduction of ductility in terms of elongation to maximum load ( $A_{gt}$ ) was observed in all the steel reinforcements tested, evidencing the importance and the critical aspects of this situation.

Specific correlation between CDI, Classes of Exposure as defined in Eurocode 2 (EN 1992-1-1:2005) and LCF Performance Index were finally provided analyzing the ability of steel reinforcing bars to maintain an adequate safety level in presence of seismic actions or less.

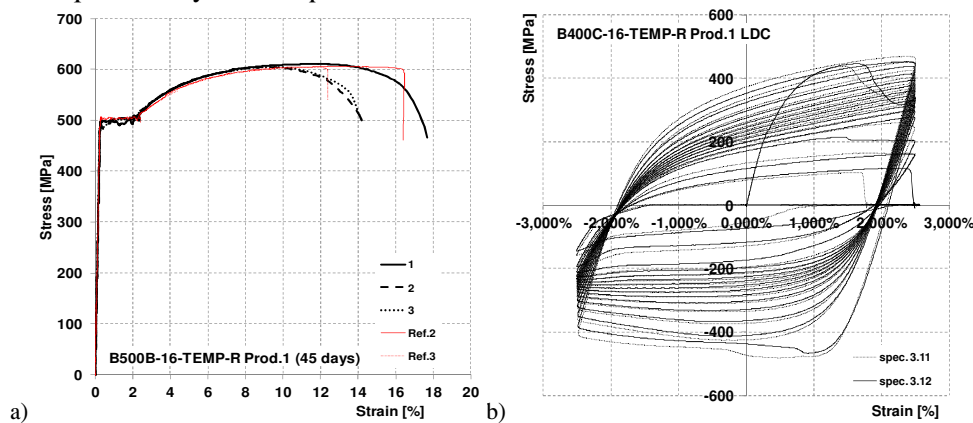


**Figure III:** Execution of experimental tensile (a) and low-cycle fatigue (b) tests on corroded specimens.

For what concerns the individuation of the effective seismic ductility demand on steel reinforcing bars, a different procedure was adopted for r.c. and composite steel/concrete buildings.

MRF r.c. case study buildings designed according to Eurocode 8 were subjected to IDAs using specific accelerograms opportunely selected to maximize the ductility requirements on steel reinforcing bars, individuating the level of maximum deformation and the corresponding dissipated energy. A specific procedure was adopted for the selection of the most requiring seismic inputs, extracted from the European Strong Motion Database (ESMD), and taking into consideration their effects on the designed structures.

All the buildings were designed adopting a design peak ground acceleration (PGA) equal to 0.25g (high seismicity), while both high ductility and low ductility class were considered.

Moreover, for what concerns steel/concrete composite structures the results coming from experimental pseudo-dynamic tests executed on a MRF composite frame tested at ISPRA (Braconi et al. 2008) were compared to the ones directly coming from experimental cyclic tests on interior and exterior beam to column connections tested in the Laboratory of University of Pisa. The good agreement in the results of the cyclic behaviour of joints in PSD and cyclic tests allowed to directly individuate the effective seismic ductility demand on rebars, since specific extensometers were adopted for the monitoring of the stress-strain behaviour of rebars in the joint.

The comparison between the ductility demand obtained from experimental and numerical analyses (IDAs on r.c. structures and cyclic tests on composite structures) and the mechanical capacity of steel reinforcing bars, investigated through the execution of experimental tests, allowed the elaboration of a

common procedure for the control of the production process of steel bars to be used in modern structures.

Looking at the results of mechanical tests on corroded specimens, it was evidenced that the most critical aspect consisted in the high decrease of the elongation to maximum load ( $A_{gt}$ ), while yielding and tensile strengths and dissipative capacity (total energy and number of cycle) less suffered from the effects of corrosion attack, especially in relation to the effective ductile requirements imposed by real seismic events. For example, towards high level of deformation required by seismic action (up to 10% with average values of  $\pm 6.0\%$ ) corrosion degradation led to values of  $A_{gt}$  even lower than 4% (for example in B450C and B500B bars diameter 16 mm, commonly used in constructions) for all types of production processes and ductility class.

The values of ductility showed by corroded steel reinforcing bars were so low and the gap between the mechanical capacity and the ductility demand due to seismic events was so high that any parametric analysis assuming increasing level of seismic intensity (as foreseen in WP6) was considered useless: in any case ductility reduction is not admissible and specific devices and practical operations shall be adopted in the design phase in order to prevent corrosion attack in buildings, especially if located in aggressive environmental conditions.

In present research project it was decided to investigate only the behaviour of buildings designed for high seismicity (with a design PGA equal to 0.25g), paying, on the contrary greater attention to a more accurate identification of cyclic capacity of corroded and uncorroded rebars, increasing the number of experimental tests and elaborations in the WP3, 4 and 5.

Moreover, it's necessary to underline that the recommendations and the guidelines presented in the report as regards the adoption of further protective measurements for rebars in r.c. and composite buildings in aggressive environmental conditions are derived from numerical and experimental simulations executed on buildings and reinforcements without considering the effective development of corrosion attack in structures. The corrosion process should be considered in relation to its effective location in structural elements and, in particular, in the dissipative zones of structural bearing elements in which the ductile requirements due to seismic action are effectively maximized. On the basis of these considerations, a full probabilistic approach, including in the set of basic variables the location and intensity of corrosion attacks, shall be adopted for a complete understanding of the safety level of considered structures.

Looking at the behaviour of composite steel/concrete structures, considering the effective position of steel reinforcing bars in the concrete slab of beam elements, the probability of corrosion attack and of their consequences on steel bars are lower respect to the case of r.c. structures, on which consequently the attention was paid.

## LIST OF DELIVERABLES

| <b>Deliverable</b>   | <b>Due date</b> | <b>Finalization Date</b> | <b>Form</b> | <b>Location</b> |
|--|-----------------|--------------------------|-------------|-----------------|
| <i>D.1.1 Technical report describing the surveyed and recognition of corrosion phenomena on existing structures</i>  | 31/12/2009      | 12/04/2013               | Report      | CIRCA           |
| <i>D.1.2 Descriptive report about past structural failures due to corrosion damaging, considering also the possible presence of seismic actions</i>  | 31/12/2009      | 12/04/2013               | Report      | CIRCA           |
| <i>D.1.3 Technical report containing the description of the structures chosen as case studies</i>  | 31/03/2010      | 12/04/2013               | Report      | CIRCA           |
| <i>D.2.1 Technical report containing the complete description of the designed structural case studies</i>  | 30/06/2010      | 12/04/2013               | Report      | CIRCA           |
| <i>D.2.2 Technical report containing all the main issues related to the definition of seismic demand on steel reinforcing bar: selection of earthquake time-histories, execution of IDA analyses on structural models and definition of the seismic demand for a single reinforcing bar.</i> | 30/09/2010      | 12/04/2013               | Report      | CIRCA           |
| <i>D.2.3 Technical report containing a detailed description of the Low-Cycle-Fatigue test programme, of the obtained test results and of the adopted loading history.</i>  | 31/12/2010      | 12/04/2013               | Report      | CIRCA           |
| <i>D.3.1 Technical report containing the description of available techniques to carry out accelerated corrosion testing programme</i>  | 31/03/2010      | 12/04/2013               | Report      | CIRCA           |
| <i>D.3.2 Technical report describing preliminary corrosion tests performed in order to compare the selected techniques for accelerated corrosion tests and allowing for the choice of the most suitable to be adopted for the research project purposes.</i>                                 | 30/09/2010      | 12/04/2013               | Report      | CIRCA           |
| <i>D.4.1 Technical report containing the description of accelerated corrosion test campaign and an extensive survey of the obtained experimental results</i>   | 30/06/2011      | 12/04/2013               | Report      | CIRCA           |
| <i>D.4.2 Technical report containing the correlation between the Corrosion Damage Index and the Class of Exposure for existing constructions, based on the accelerated corrosion test programme results</i>  | 30/06/2011      | 12/04/2013               | Report      | CIRCA           |
| <i>D.4.3 Technical report about the description of low-cycle fatigue test campaign on corroded bars with the description of the testing set-up and a complete organization of the experimental results</i>   | 30/09/2011      | 12/04/2013               | Report      | CIRCA           |
| <i>D.4.4 Technical report describing the employment of experimental results on Low-Cycle Fatigue tests on corroded bars to correlate the Corrosion Damage Index and the Class of Exposure to the Low-Cycle-Fatigue Performance Index for the single</i>                                      | 30/09/2011      | 12/04/2013               | Report      | CIRCA           |
| <i>D.5.1 Technical report containing numerical results produced using IDA analyses rationally organized to correlate seismic intensity levels, structural ductility levels, Class of Exposure, Corrosion Damage Indicators and LCF Performance Index</i>                                     | 31/12/2011      | 12/04/2013               | Report      | CIRCA           |
| <i>D.5.2 Report containing all the seismic performance assessment executed on exiting constructions employing techniques, instruments and laws developed inside the project</i>  | 31/12/2011      | 12/04/2013               | Report      | CIRCA           |
| <i>D.6.1 Background documents for the assessment of Low-Cycle Fatigue Behaviour of steel reinforcement bars</i>  | 30/03/2012      | 12/04/2013               | Report      | CIRCA           |
| <i>D.6.2 Background documents for Eurocode 8 concerning the definition and evaluation of the LCF Performance Index of the analyzed types of steel reinforcing bars</i>   | 30/03/2012      | 12/04/2013               | Report      | CIRCA           |
| <i>D.6.3 Backgrounds documents for the introduction of Low-Cycle Fatigue performance of steel reinforcing bars in the new harmonized standard EN 10080</i>   | 31/03/2012      | 12/04/2013               | Report      | CIRCA           |
| <i>D.6.4 Backgrounds documents for the assessment of the influence of corrosion phenomena on seismic performance of buildings, to be included in Eurocodes and other international design standards</i>  | 30/06/2012      | 12/04/2013               | Report      | CIRCA           |
| <i>D.6.5 Recommendations for the execution of laboratory accelerated corrosion tests</i>   | 30/06/2012      | 12/04/2013               | Report      | CIRCA           |



## 1. INTRODUCTION

Modern buildings in seismic areas shall be designed according to the philosophy of *capacity design*, nowadays adopted as the reference technique by design codes such as European (EN 1998-1:2005), American (FEMA 356) and New Zealand standards (NZS 1170.5:2004 and NZS 3101:2006). Structures shall be able to satisfy the deformation requirements due to increasing levels of seismic action without the exhibition of significant losses of strength and stiffness, preserving, in such a way, their capacity of dissipating the seismic energy stored during the earthquake. The dissipative capacity of buildings is strictly connected to their structural ductility, defined as the capacity of the structure and of selected structural components to deform beyond their elastic limit without excessive degradation of strength and stiffness and avoiding, consequently, unexpected brittle failures. For the achievement of the global collapse mechanisms, specific elements of the bearing structural system, designed in order to dissipate seismic energy, shall be opportunely detailed in terms of size, number and location of steel reinforcing bars. The regions in which the energy dissipation is expected, and consequently in which plasticization shall be localized, are termed “plastic hinges” and, in moment resisting frames (MRF), generally coincide with the ends of beams. The critical plastic hinge regions are designed and detailed for ductile flexural actions; shear brittle failures can be avoided providing the sections with an adequate overstrength, obtained through a specific disposition of transverse reinforcements satisfying a design shear action evaluated as presented in Eurocode 8 (EN 1998-1:2005). Moreover, all the structural elements in which the dissipation is not foreseen are protected against failure sizing them for actions greater than the ones corresponding to the development of the maximum strength in the potential plastic hinge regions, following the capacity design principle.

The global ability to withstand high displacements is directly influenced by three different “sub-levels” of ductility, that are the element ductility, generally expressed in terms of plastic rotation ( $\mu_\theta = \theta/\theta_y$ ), the section ductility, expressed as a function of curvature ( $\mu_\chi = \chi/\chi_y$ ) and the material ductility, related to the ratio between total strain and strain at yielding ( $\mu_\epsilon = \epsilon/\epsilon_y$ ), figure 1.1 The ductility capacity of steel reinforcing bars (in correspondence of beams and columns - r.c. structures, in the slab of composite structures) is consequently strictly necessary for the global ductile behaviour of r.c. buildings.

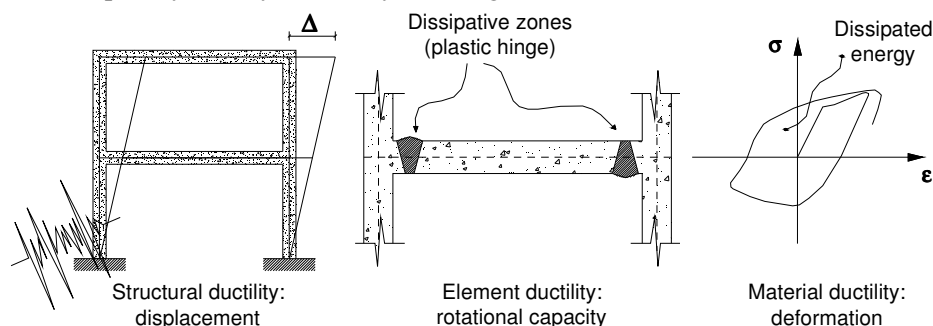


Figure 1. 1: Different ductility levels (structure, element, material).

### 1.1 Mechanical properties of steel reinforcing bars

Actual European and Italian standards prescribe the adoption of steel reinforcing bars (rebars) provided by specific values of the mechanical characteristics, in terms of yielding and tensile strength ( $R_e$  and  $R_m$ ), elongation at ultimate strength ( $A_{gt}$ ) and hardening ratio ( $R_m/R_e$ ). Steel reinforcements shall be characterized by an opportune relationship between ultimate tensile strength and yielding strength, conditioning, in such a way, the hardening behaviour of the material and, moreover, by a moderate variability between the actual and nominal value of the yielding strength, in order to satisfy the principles of capacity design and to avoid unexpected brittle failures due, for example, to the presence of weak columns and strong beams (soft storey) or to development of premature shear mechanisms instead of ductile bending ones.

Annex C of Eurocode 2 (UNI EN 1992-1-1:2005), in relation to the level of elongation at ultimate strength ( $A_{gt}$ ) and to the ratio  $R_m/R_e$ , defines three different ductility classes for steel reinforcing bars, called class “A”, “B” and “C” and respectively characterized by  $A_{gt}$  higher than 2.5%, 5.0% and 7.5% and by hardening ratio higher than 1.05, 1.08 and between 1.15 and 1.35 (Table 1.1). Moreover, Eurocode 8 provides more specifications for the adoption of ductility classes for elements in r.c. structures realized in High Ductility Class (HDC) or Medium/Low Ductility Class (MDC/LDC): for critical regions of HDC buildings, the only use of rebars of class “C” is allowed, while class “B” can be

adopted for critical regions of buildings in LDC. Eurocode 8 forbids the use of class “A” for the seismic desing of buildings, while Italian standards for constructions (D.M. 14/01/2008) allows a lower requirement of ductility for transverse reinforcement only.

**Table 1. 1:** Mechanical properties of rebars according to UNI EN 1992-1-1:2005 prescriptions.

| Ductility Class                        | A                   | B           | C                           |
|--|---------------------|-------------|-----------------------------|
| Characteristic yielding strength (MPa) | Between 400 and 600 |             |                             |
| Hardening ratio ( $R_m/R_e$ )          | $\geq 1.05$         | $\geq 1.08$ | $\geq 1.15$ and $\leq 1.35$ |
| Elongation to max load (%)             | $\geq 2.5$          | $\geq 5.0$  | $\geq 7.5$                  |

For what concerns composite steel/concrete structures, EN 1998-1:2005 provides further prescriptions for the individuation of the ductility class to adopt for the steel reinforcements included in the evaluation of the plastic strength of the dissipative zones: for MDC buildings the adoption of ductility classes B and C (according to what specified in EN 1992-1:2005) is allowed, while in the case of buildings realized in HDC the only employment of ductility class C is imposed.

Nowadays the most diffused typology in Europe of steel reinforcement, able to satisfy the mechanical requirements of strength and ductility presented in table 1.1, is TempCore steel. The TempCore process, characterized by following phases of quenching and tempering, is able to provide optimal mechanical characteristics (figure 1.2), i.e. a high level of yielding strength and ductility and good weldable properties, without any addition of chemical elements and consequently keeping the production costs acceptable. The cross-section of a TempCore rebar is characterized by an external tempered martensite layer and a more soft and ductile central region with a typical ferritic – perlitic microstructure.

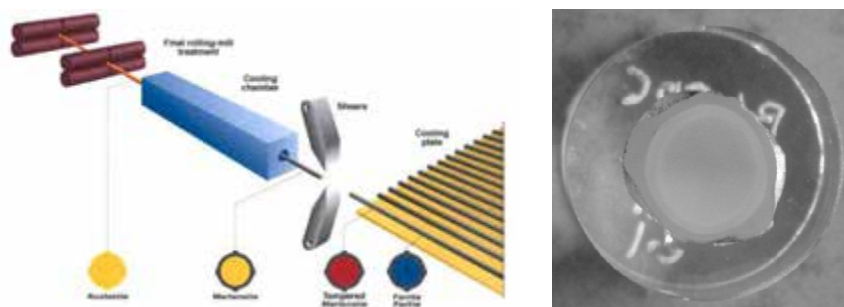


**Figure 1. 2:** TempCore production process and cross-section of TempCore rebar.

Micro-Alloyed (MA) steels, characterized by the addition of small quantities of alloy elements, such as vanadium, titanium, molybdenum and other rare-earth metals, also present excellent qualities of ductility and strength. The yielding strength is, in general, higher than 500 MPa without the necessity of heat treatment; the weldability is good and the threshold of required ductility can be also satisfied. On the other hand, the costs related to the production process for Micro-Alloyed steel is higher than the ones required by TempCore, and consequently their diffusion in the field of r.c. constructions is nowadays quite limited.

The mechanical behaviour of steel reinforcing bars is generally well known under monotonic loading conditions: the limits imposed by Eurocode for  $A_{gt}$  and for  $R_m/R_e$ , as an example, are used for the characterization of the tensile behaviour of reinforcements. On the contrary, no prescriptions are given in order to characterize the real seismic behaviour of reinforcements to be used in new reinforced concrete buildings, aspect that shall be necessarily considered for structures realized in seismic areas, as previously evidenced. An accurate investigation of the actual state of art of standards for the mechanical characterization of steel reinforcements evidenced a large variability in both the mechanical properties and the tests prescribed for the factory production controls. In particular, considering the standards actually used in European Countries with high and moderate seismicity, many differences can be individuated in the required level of minimum yielding and tensile strength  $R_e$  and  $R_m$ , elongation at maximum strength  $A_{gt}$  and ultimate elongation  $A$  and, finally, hardening ratio ( $R_m/R_e$ ). Table 1.2 shows a summary of the most common steel grade actually produced in Europe, while table 1.3 individuates the corresponding prescribed tests.

**Table 1. 2:** Steel grades and mechanical properties of steel reinforcements in European Countries.

| Min. R <sub>e</sub><br>(MPa) | Steel Grade | European<br>country | R <sub>e</sub><br>MPa | R <sub>m</sub><br>MPa | A <sub>gt</sub><br>% | A<br>% | R <sub>m</sub> /R <sub>e</sub><br>- |
|------------------------------|-------------|---------------------|-----------------------|-----------------------|----------------------|--------|-------------------------------------|
| 500                          | A 500 NR SD | Portugal            | 500                   | ≥ 575, ≤ 675          | 8.0                  | -      | ≥ 1.15, <1.35                       |
|                              | B 500 SD    | Spain               | 500                   | 575                   | 9.0                  | ≥ 20   | ≥ 1.15, <1.35                       |
|                              | B 500 A     | Great Britain       | 500                   | 525                   | 2.5                  | -      | 1.05                                |
|                              | B 500 B     |                     | 500                   | 540                   | 5.0                  | -      | 1.08                                |
|                              | B 500 C     |                     | 500                   | ≥ 575, ≤ 675          | 7.5                  | -      | ≥ 1.15, <1.35                       |
|                              | B 500 A     | Germany             | 500                   | 525                   | 2.5                  | -      | 1.05                                |
|                              | B 500 B     |                     | 500                   | 540                   | 5.0                  | -      | ≥ 1.08, <1.35                       |
|                              | B 500 A     | Greece              | ≥ 500                 | ≥ 525                 | ≥ 2.5                | -      | 1.05                                |
|                              | B 500 C     |                     | ≥ 500                 | ≥ 575, ≤ 675          | ≥ 7.5                | -      | ≥ 1.15, <1.35                       |
|                              | B 500 A     | France              | 500                   | ≥ 525                 | 2.5                  | -      | 1.05                                |
|                              | B 500 B     |                     | 500                   | ≥ 540                 | 5.0                  | -      | 1.08                                |
|                              | B 500 A     | Bulgary             | 500                   | 550                   | 2.5                  | -      | 1.05                                |
|                              | B 500 B     |                     | 500                   | 550                   | 5.0                  | -      | 1.08                                |
|                              | B 500 C     |                     | 500                   | 575                   | 7.5                  | -      | ≥ 1.15, <1.35                       |
| 450                          | B 450 B     | France              | 450                   | ≥ 486                 | 5.0                  | -      | 1.08                                |
|                              | B 450 C     |                     | 450                   | ≥ 517.5, ≤ 607.5      | 7.5                  | -      | ≥ 1.15, <1.35                       |
|                              | B 450 A     | Italy               | 450                   | 540                   | ≥ 2.5                | -      | ≥ 1.05                              |
|                              | B 450 C     |                     | 450                   | 540                   | ≥ 7.5                | -      | ≥ 1.15, <1.35                       |
| 400                          | A 400 NR SD | Portugal            | 400                   | ≥ 460, ≤ 540          | 8.0                  | -      | ≥ 1.15, <1.35                       |
|                              | B 400 SD    | Spain               | 400                   | 480                   | 8.0                  | ≥ 16   | ≥ 1.15, <1.35                       |

**Table 1. 3:** Production control tests prescribed by the different standards presented in Table 1.2.

| European country | Tensile tests | Bending test | Bond test | Fatigue tests | Low-cycle fatigue test |
|------------------|---------------|--------------|-----------|---------------|------------------------|
| Portugal         | x             | x            | x         | x             | x                      |
| Spain            | x             | x            | x         | x             | x                      |
| Great Britain    | x             | x            | x         | x *           | -                      |
| Germany          | x             | x            | x         | -             | -                      |
| Greece           | x             | x            | x         | x             | -                      |
| France           | x             | x            | x         | x *           | -                      |
| Bulgary          | x             | x            | x         | x             | -                      |
| Italy            | x             | x            | x         | -             | -                      |
| Algeria          | x             | x            | x         | -             | -                      |
| Serbia           | x             | x            | x         | x             | -                      |
| Romany           | x             | x            | x         | -             | -                      |
| Egypt            | x             | x            | x         | -             | -                      |

As shown in table 1.2, three main classes with yielding strength respectively higher than 400 MPa, 450 MPa and 500 MPa and A<sub>gt</sub> generally corresponding to the three ductility classes defined by Eurocode 2 (EN 1992-1-1:2005) can be individuated. Some exceptions, however, are present: for example, Portugal and Spain require levels of A<sub>gt</sub> higher respect to the ones imposed by Eurocodes, respectively equal to 8.0 and 9.0% for yielding strength higher than 500 MPa and at least 8.0% for R<sub>e</sub> ≥ 400 MPa. Moreover, as shown in the table 1.3, even though the monotonic tensile behaviour of steel reinforcements is well known and qualified by each Country, less information is provided for the characterization of their behaviour under seismic action. The loading condition generated by earthquake, generally known as *Low Cycle Fatigue* (LCF) is characterized by the execution of few cycles with a high level of plastic deformation, more or less equivalent to the stress-strain condition reproduced by a real earthquake; the structural behaviour of steel reinforcements under low-cycle fatigue is actually not accurately investigated. At European level, only two Countries (Spain and Portugal) prescribe the seismic qualification of steel rebars; according to Spanish standard (UNE 36065 EX:2000), three complete symmetric hysteretic cycles for each specimen, with a level of deformation variable between ±1.5 % and ±4.0 % depending on the diameter shall be executed. The frequency to be adopted in the test varies from 1.0 Hz to 3.0 Hz and the length of the specimen shall be equal to 5, 10 or 15 times the nominal diameter, again depending on the diameter of the specimen itself. Portuguese standards (LNEC E-

455:2008 and LNEC E-460:2008, for rebars with nominal yielding strength respectively higher than 400 and 500 MPa) prescribe the execution of 10 complete symmetric cycles tensile/compression with imposed frequency higher than 3.0 Hz, maximum level of deformation equal to  $\pm 2.5\%$  and free length of the specimen equal to 10 times the nominal diameter. The steel reinforcements can be considered in agreement with what required by the standard if able to sustain the 10 cycles with any failure.

The protocols for the execution of LCF tests already presented by both Spanish and Portuguese standards (UNE 36065 and LNEC E-455:2008) are not defined on the base of scientific investigations and the number of cycles to execute, the strain rate of the test, the level of imposed deformation and the free length of the specimens to test are not properly defined in relation to the effective demand imposed by real seismic events. Consequently, despite of the necessity of specific ductile properties of steel reinforcements in critical regions of buildings designed for seismic areas, no prescriptions are given for guaranteeing the satisfaction of those seismic requirements.

Stating the European production scenario already presented in the tables 1.2 and 1.3 for what concerns both the mechanical properties of steel reinforcement and the procedures for the production control of bars, the European Commission evidenced the necessity of a common harmonization of standards inside the revision of European standard EN 10080 (*Steel for the reinforcement of concrete - Weldable reinforcing steel*). In particular, the revision of Mandate M115 tries to solve problems related to the definition of “*the methods (calculation, test methods or others) or a reference to a standard containing the methods for the determination of such characteristics*”, including also the individuation of the cyclic loading performance, actually not completely codified but necessary for earthquake prone areas. The Draft of EN10080 (prEN 10080:2012, rev. 19/01/2012), prescribes the execution of 5 complete hysteretic symmetric cycles using a testing frequency lower than 3.0 Hz, an imposes deformation equal to  $\pm 2.5\%$  and a free length of the specimen, constant for all the considered diameters, equal to 10 times the diameter of the rebar.

## 1.2 Durability problems and corrosion phenomena of steel reinforcements

### 1.2.1 Concept and definition of durability

A definition of “durability” is provided by actual European and Italian standards for constructions.

According to European standard EN 1990:2006 (§ 2.4) “*The structure shall be designed such that deterioration over its design working life does not impair the performance of the structure below that intended, having due regard to its environment and the anticipated level of maintenance*”. The “*design working life*” of the structure is indicatively defined by EN 1990:2006 as presented in table 1.6, and is directly related to the working category.

**Table 1. 4:** Indicative design working life (EN 1990:2006, table 2.1).

| Design working life category | Indicative design working life (years) | Examples  |
|------------------------------|--|---|
| 1                            | 10                                     | Temporary structures <sup>(1)</sup>   |
| 2                            | 10 to 25                               | Replaceable structural parts, e.g. gantry girders bearings                      |
| 3                            | 15 to 30                               | Agricultural and similar structures   |
| 4                            | 50                                     | Building structures and other common structures                                 |
| 5                            | 100                                    | Monumental building structures, bridges, and other civil engineering structures |

<sup>(1)</sup> Structures or parts of structures that can be dismantled with a view to being re-used should not be considered as temporary.

A similar definition is also presented in the actual Italian Standard for Constructions (D.M. 14/01/2008) in which the durability of a structure is defined (§ 2.1) as “*the maintenance of the mechanical and physical characteristics of materials and structure necessary for the preservation of adequate safety levels for the whole building life*”. Similarly to what presented in EN 1990:2006, in D.M. 14/01/2008 the “*building life*” of the structure, generally referred as “nominal life” ( $V_N$ ), is defined as the period in which the structure is able to maintain its efficiency with only the execution of ordinary maintenance (table 1.5). With reference to seismic action, the product between the nominal life ( $V_N$ ) and the “use coefficient” ( $C_U$ ), fixed in relation to the functional destination of the building and to the predicted number of users (table 1.6) provide the “reference life” of the building ( $V_R$ ), to be related to the return period of design seismic action ( $T_R$ ).

**Table 1. 5:** Nominal Life ( $V_N$ ) for different kind of structures (D.M. 14/01/2008, table 2.4.I).

| Construction typology  | $V_N$ [years] |
|--|---------------|
| 1 Provisional structures - Temporary structures - Structure under construction                                       | $\leq 10$     |
| 2 Ordinary structures, bridges, infrastructural structures and dams with moderate dimensions and ordinary importance | $\geq 50$     |
| 3 Large structures, bridges, infrastructural structures and dams with high dimensions and strategic importance       | $\geq 100$    |

**Table 1. 6:** Values for use coefficient  $C_U$  (D.M. 14/01/2008, table 2.4.II).

| Use Class             | I   | II | III | IV |
|-----------------------|-----|----|-----|----|
| Use Coefficient $C_U$ | 0,7 | 1  | 1,5 | 2  |

The durability of the structure is strictly related to the durability of the materials used and to their ability to maintain unchanged the mechanical and physical properties for the entire design working life of the building, in terms of both strength and ductility. The environmental conditions characterizing the site in which the structure is realized shall be identified at the design stage in order to assess their importance in relation to durability and to introduce adequate provisions for the protection of the materials used in the structure. Buildings can be designed everywhere and in every external environmental conditions, if adequate protections for materials and structural elements are provided. As an example, European standard EN 1992-1-1:2005 gives indications for the protection of r.c. buildings and for the reduction of the possible deterioration of structures and materials.

### 1.2.2 Durability problems of steel reinforcing bars

Despite the large use of TempCore steel reinforcing bars in reinforced concrete and composite structures, recent works in the current literature (Apostolopoulos and Papadopoulos 2007, Apostolopoulos and Papadakis 2008, Al Hashemi et al., 2007) evidenced durability problems of TempCore steel bars: the negative effects due to corrosion phenomena on the mechanical properties of rebars, both in terms of strength and ductility, are widely presented and discussed. In ordinary environmental conditions, steel reinforcing bars are generally covered by a thin passive layer able to protect them from corrosion: the passive layer is stable if the pH of the pore solution in which the bar is embedded is higher than 12.8; otherwise, if the passive layer breaks down in relation to particular external conditions, the bar is not yet protected, corrosion can initiate and propagate in the whole reinforcement, leading to potential modifications in the structural behaviour of the bar with consequences, in a long time, on the whole structure.

Corrosion phenomena of steel reinforcements can be classified into two main groups, that are (1) corrosion due to the carbonation of concrete and (2) corrosion due to chlorides' penetration inside the concrete solution. In any case, the propagation of corrosion is due to the cracking of the passive layer originally protecting the bar. The carbonation is the chemical process (both natural or artificial) that, in presence of  $CO_2$ , leads to the generation of carbonates; as an example, in concrete, the calcium hydroxide naturally present in the solution reacts with external  $CO_2$  generating the development of calcium carbonate according to the Eqn. 1.1:



The carbonation of concrete and its relationship with parameters such as water/cement-ratio, binder type and content, crack width, cover depth, water content were widely investigate in the past literature and numerical models to predict the carbonation process in relation to those factors were also provided. The effects of carbonation are not directly related to the mechanical properties of concrete but leads to negative performances of the steel reinforcements embedded; as already said, reinforcing bars behave passively if the pH of the solution is around 13, but if  $CO_2$  begins to spread in the concrete and carbonation starts following Eqn. 1.1, the pH of the pore solution drops below 9, the passive protective film around the rebar cracks, corrosion of steel reinforcements initiates and propagates. In general, carbonation of concrete and following depassivation of the rebar lead to uniform corrosion phenomena on steel rebar; in particular, corrosion due to carbonation begins in localized areas of the surface and then gets more uniform over a part of the surface depending on crack width and deteriorated bond area near the crack (Figure 1.3). The effect of chlorides is the cracking of the passive layer protecting the rebar, with following initiation of localized (pitting) corrosion; at the bottom of the pitting hole, a hydrolysis phenomenon takes place, since the pH drops to values lower than 12.8. In general, chlorides induce localized corrosion phenomena since the portion of the rebar outside the hole remains passive.

Different kinds of pitting corrosion are associated to different concentration of chlorides inside the concrete and the critical chloride content depends on cement type and degree of carbonation.

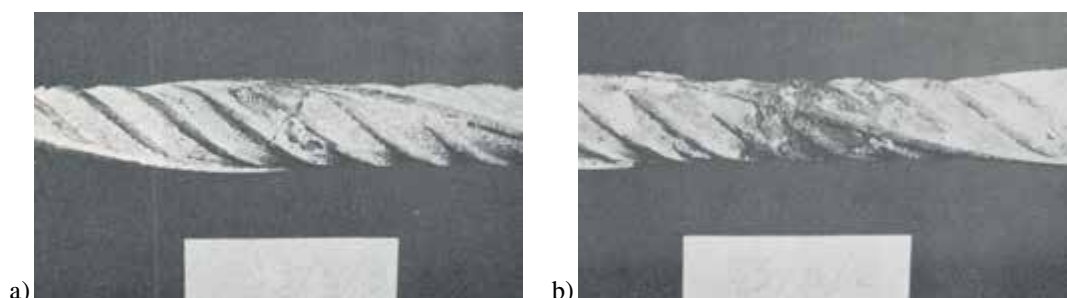


**Figure 1. 3:** a) Starting and b) advanced corrosion in bars due to carbonation of concrete (Schießl P., 1976).

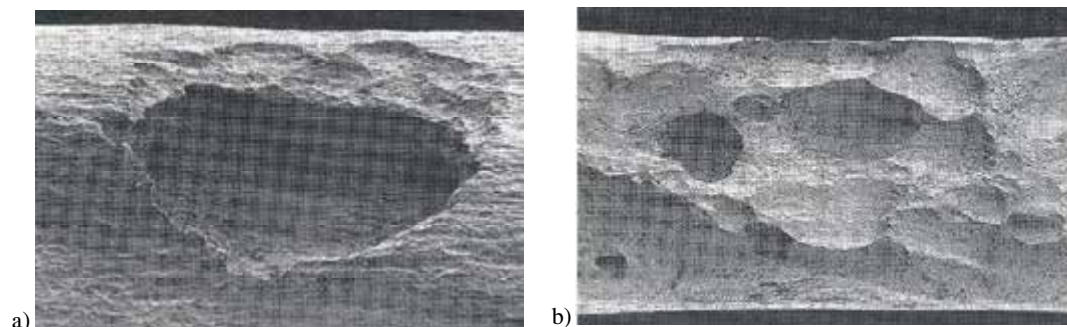


**Figure 1. 4:** Pitting corrosion due to a) low and b) high concentration of chlorides (Nürnberger U., 2005).

As regards the consequences of corrosion phenomena on the mechanical properties of steel rebars, Apostolopoulos and Papadakis (2008) evidenced the detrimental effects of corrosion on steel reinforcements Bst420 ( $\phi 10$  mm), typical steel grade used in Greece during the 1960s, actually no more produced. The corrosion phenomena were artificially reproduced in laboratory using salt spray chamber for several exposure times; the effects of corrosion, in terms of reduction of mechanical properties (yielding and tensile strength and elongation) and cross section reduction, were evaluated in relation to the selected exposure duration by the execution of monotonic tensile tests. Some examples of results are presented in figures 1.5. Similar results were also obtained for reinforcements of 8 mm diameter and with yielding strength of about 500 MPa (Apostolopoulos et al. 2006).

The degradation due to corrosion phenomena was also analyzed considering the cyclic behaviour of steel rebars; low-cycle fatigue tests were executed on small rebars (diameter  $\phi$  equal to 10 mm) after different exposure periods, using a frequency of 0.50 Hz and imposing a level of deformation equal to  $\pm 1.0\%$  on a free length of the specimens equal to 6 times the diameter (Apostolopoulos and Papadopoulos 2008). The results of low-cycle fatigue tests on bars showed a progressive reduction of the energy dissipated (number/shape of the cycles) with the increase of the exposure time (figure 1.6).

Al Hashemi et al. (2007) executed tensile and high cycle fatigue tests on corroded steel reinforcing bars TempCore B450C, diameter 16 mm; corrosion was induced through the application of an anodic current to rebars embedded in chloride contaminated concrete blocks. The results of mechanical tensile tests evidenced a big decrease (about the 60%) of the ductility of the samples, expressed in terms of ultimate elongation, both in the case of uniform and localized corrosion. On the other side, the deterioration due corrosion on the high cycle fatigue behaviour of steel reinforcements was evident in the case of localized (pitting) behaviour but quite negligible in the case of uniform corrosion.

In relation to what already presented, the main consequences of corrosion phenomena on steel reinforcements can be summarized in two different aspects. The first one is the decrease of the bearing capacity of the structure, due to the deterioration of the mechanical characteristics of the reinforcements, under both monotonic and cyclic loading conditions. Apostolopoulos (2007) presents the stress-strain curves obtained from tensile tests on uncorroded specimens B500st (yielding stress equal to 500 MPa) in comparison to the corroded ones after different exposure periods in salt spray chamber (10, 45 and 90 days): the reduction of elongation to failure is evident and drops from the 16.91% to the 11.79% (90 days). The reduction of strength is also visible: after 90 days of exposure yielding stress drops from 575.18 MPa to 524.58 MPa, while tensile stress decreases from 658.52 MPa to 609.23 MPa (Apostolopoulos 2007). Moreover, as regards the cyclic behaviour of steel

reinforcements, with the increase of imposed strain and exposure period, the energy density strongly decreases, evidencing a lower ductile behaviour of the reinforcement.

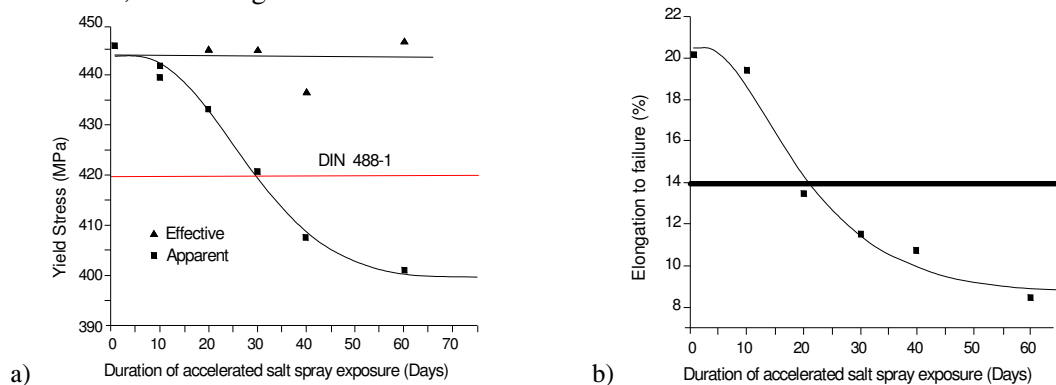


**Figure 1. 5:** Effects of corrosion on bars: a) yielding, b) elongation (Apostolopoulos and Papadakis 2008).

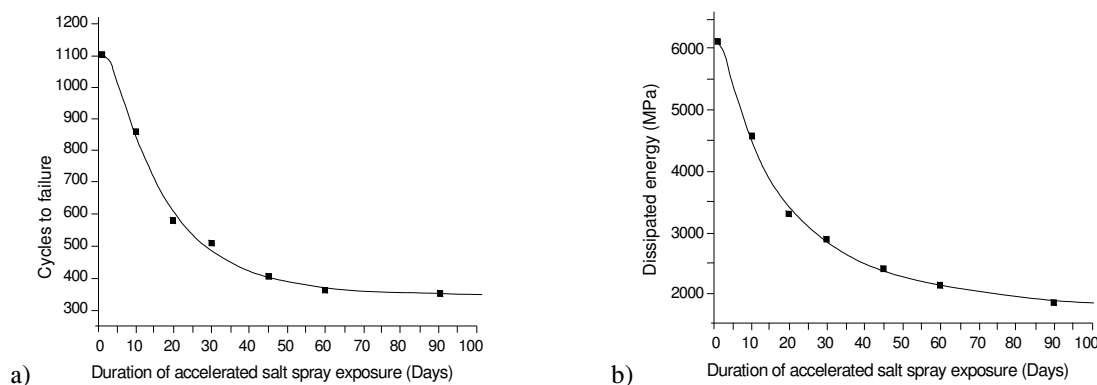


**Figure 1. 6:** Effects of corrosion on the LCF behaviour of bars (Apostolopoulos and Papadopoulos 2007).

The second aspect to be considered is the cracking of the concrete cover: steel corrosion and the associated cracking and spalling of concrete have been identified as the most severe forms of deterioration leading to the progressive damaging of the building before the end of its design working life. The cracking of the concrete cover is also related to the premature buckling of steel reinforcements during a seismic event, since the rebar remains completely exposed to axial compressive stresses and if the spacing of stirrups is not perfectly sized, also in presence of moderated strains, buckling becomes possible.

### 1.2.3 Durability of concrete structures in the European standards

The selection of the most appropriate technique to be used for the preservation of steel reinforcing bars in r.c. and composite structures is related to different aspects, such as the mass volume, the cracking of concrete and, in particular, the quality and thickness of the concrete cover used in the structural elements. The quality of concrete cover can be individuated through two main parameters, i.e. the maximum water/cement ratio and the minimum cement content, as presented in European standard EN 206-1:2006 (*Concrete - Part 1: Specification, performance, production and conformity*); these parameters can be directly associated to a minimum strength class for the concrete that shall be used in relation to the different external environmental conditions. EN 206-1:2006, in fact, individuates different “corrosion classes” in relation to different exposure conditions, as presented in the table 1.7. Class “0” does not present any corrosion risk, class “C” is related to corrosion due to carbonation phenomena, classes “D” and “S” are both related to corrosion due to chlorides, in proximity of the seaside or less. Other classes are also specified for corrosion due to chemical agents or to de-icing cycles. For guaranteeing enough durability to the whole structure and in particular to steel reinforcing bars, Eurocode 2 prescribes the adoption of opportunely sized concrete cover, in relation to the different aggressive environmental conditions and to different structural classes.

**Table 1. 7:** Extracted from table 4.1 of EN 206-1-1:2005 for corrosion classes.

| Class designation                               | Description of the environment                                    | Informative examples where exposure classes may occur   |
|---|---|---|
| 1. No risk of corrosion                         |   |   |
| X0  | For concrete with reinforcement – very dry                        | Concrete inside buildings with very low air humidity  |
| 2. Corrosion induced by carbonation             |   |   |
| XC1   | Dry or permanent dry  | Concrete inside buildings with low air humidity;<br>Concrete permanently submerged in water;            |
| XC2   | Wet, rarely dry   | Concrete surfaces subject to long-term water contact;<br>Many foundations;                              |
| XC3   | Moderate humidity   | Concrete inside buildings with moderate or high air humidity;<br>External concrete sheltered from rain; |
| XC4   | Cyclic wet and dry  | Concrete surfaces subject to water contact, not within exposure class XC2;                              |
| 3. Corrosion induced by chlorides               |   |   |
| XD1   | Moderate humidity   | Concrete surfaces exposed to airborne chlorides   |
| XD2   | Wet, rarely dry   | Swimming pools;<br>Concrete components exposed to industrial waters containing chlorides;               |
| XD3   | Cyclic wet and dry  | Parts of bridges exposed to spray containing chlorides, pavements, car park slabs;                      |
| 4. Corrosion induced by chlorides from seawater |   |   |
| XS1   | Exposed to airborne salt but not in direct contact with sea water | Structures near to or on the coast;   |
| XS2   | Permanently submerged   | Parts of marine structures;   |
| XS3   | Tidal, splash and spray zones                                     | Parts of marine structures;   |

The concrete cover is defined as the distance between the external rebar surface (including stirrups and eventual other reinforcements) and the concrete external surface. The nominal concrete cover can be evaluated as the addition of two different parts, a minimum concrete cover ( $c_{min}$ ) and a further deviation ( $\Delta c_{dev}$ ) that is included in order to avoid unexpected shifts (Eqn. 1.2).

$$c_{nom} = c_{min} + \Delta c_{dev} \quad (1.2)$$

The minimum concrete cover  $c_{min}$  is necessary in order to transmit bond stress, to guarantee enough protection towards corrosion phenomena and an adequate fire resistance.  $C_{min}$  is defined as the maximum value between the following components (Eqn. 1.3):

$$c_{nom} = \max \{ c_{min,b}; c_{min,dur} + \Delta c_{dur,\gamma} - \Delta c_{dur,st} - \Delta c_{dur,add}; 10 \text{ mm} \} \quad (1.3)$$

In Eqn. 1.3  $c_{min,b}$  is minimum concrete cover to satisfy bond requirements,  $c_{min,dur}$  is the minimum concrete cover required for the protection towards environmental conditions,  $\Delta c_{dur,\gamma}$  is the safety range,  $\Delta c_{dur,st}$  is the reduction of minimum concrete cover to apply in presence of stainless steel,  $\Delta c_{dur,add}$  is the reduction of minimum concrete cover to introduce if other additional protections are used. Eurocode 2 (EN 1992-1-1:2005) individuates the minimum values of  $c_{min,b}$ , as presented in table 1.8.

**Table 1. 8:** Minimum concrete cover for bond requirements (EN 1992-1-1:2005, table 4.2).

| Concrete cover for bond requirements |  |
|--------------------------------------|--|
| Disposition of steel reinforcement   | Minimum concrete cover $c_{min,b}$ <sup>*)</sup> |
| Isolated                             | Diameter of steel bar                            |
| Grouped                              | Equivalent diameter                              |

<sup>\*)</sup> If the maximum nominal dimension of the aggregate is higher than 32 mm  $c_{min,b}$  shall be increased of 5 mm

The choice of an adequate durable concrete for the protection of steel bars from corrosion (and for the protection of the concrete itself from environmental attacks) can lead in some cases to the adoption of a higher compressive strength than the one simply required by the structural desing. In the Appendix E of Eurocode 2 (EN 1992-1-1: 2005) the indicative compressive strength classes for concrete to be used in relation to the exposure classes presented in EN 206-1:2006 are presented (table 1.9). The recommended structural class for buildings with a design working life of 50 years is class “S4”.

**Table 1. 9:** Indicative strength classes (Appendix E of EN 1992-1-1:2005, table E 1N).

| Exposition classes according to prospect 4.1 EN 206-1:2006 |         |        |                            |                            |        |        |                          |        |        |        |
|--|---------|--------|----------------------------|----------------------------|--------|--------|--------------------------|--------|--------|--------|
| Corrosion due to carbonation                               |         |        |                            | Corrosion due to chlorides |        |        | Corr. Chlorides -seaside |        |        |        |
|  | XC1     | XC2    | XC3                        | XC4                        | XD1    | XD2    | XD                       | XS1    | XS2    | XS3    |
| Indicative   | C20/25  | C25/30 | C30/37                     |                            | C30/37 | C35/45 |                          | C30/37 | C35/45 |        |
| Damage to concrete   |         |        |                            |                            |        |        |                          |        |        |        |
|  | No risk |        | Ice/de-icing cycles attack |                            |        |        | Chemical attack          |        |        |        |
|  | X0      | XF1    | XF2                        | XF3                        |        |        |                          | XA1    | XA2    | XA3    |
| Indicative   | C12/15  | C30/37 | C25/30                     | C30/37                     |        |        |                          | C30/37 |        | C35/45 |

Further modifications to the indicative strength classes presented in table 1.11 are provided by table 1.10, according to what presented in table 4.3N of Eurocode 2 (EN 1992-1-1:2005). In relation to the structural class, the minimum values of  $c_{min,dur}$  are provided (table 1.11).

**Table 1. 10:** Recommended structural classification (EN 1992-1-1:2005, table 4.3N).

| Structural class   |  |                                     |                                     |                                     |                                     |                                     |                                     |
|--|--|-------------------------------------|-------------------------------------|-------------------------------------|-------------------------------------|-------------------------------------|-------------------------------------|
| Criterion  | Exposition class according to prospect 4.1 EN 206-1:2006 |                                     |                                     |                                     |                                     |                                     |                                     |
|  | X0   | XC1                                 | XC2<br>XC3                          | XC4                                 | XD1                                 | XD2<br>XS1                          | XD3/XS2<br>XS3                      |
| Desing working life equal to 100 years   | Increase 2 classes<br>$\geq C30/37$                      | Increase 2 classes<br>$\geq C30/37$ | Increase 2 classes<br>$\geq C35/45$ | Increase 2 classes<br>$\geq C40/50$ | Increase 2 classes<br>$\geq C40/50$ | Increase 2 classes<br>$\geq C40/50$ | Increase 2 classes<br>$\geq C45/55$ |
| Strength resistance  | decrease 1 class   | decrease 1 class                    | decrease 1 class                    | decrease 1 class                    | decrease 1 class                    | decrease 1 class                    | decrease 1 class                    |
| Element like slabs (position of reinforcements not influenced by the construction process) | decrease 1 class   | decrease 1 class                    | decrease 1 class                    | decrease 1 class                    | decrease 1 class                    | decrease 1 class                    | decrease 1 class                    |
| Specific quality control for concrete production   | decrease 1 class   | decrease 1 class                    | decrease 1 class                    | decrease 1 class                    | decrease 1 class                    | decrease 1 class                    | decrease 1 class                    |

**Table 1. 11:** Minimum values of  $c_{min,dur}$  for different exposure conditions (EN 1992-1-1:2005) for ordinary bars.

| Structural class | Exposure conditions (prospect 4.1 EN 206-1:2006) |     |         |     |         |         |         |
|------------------|--|-----|---------|-----|---------|---------|---------|
|                  | X0   | XC1 | XC2/XC3 | XC4 | XD1/XS1 | XD2/XS2 | XD3/XS3 |
| S1               | 10   | 10  | 10      | 15  | 20      | 25      | 30      |
| S2               | 10   | 10  | 15      | 20  | 25      | 30      | 35      |
| S3               | 10   | 10  | 20      | 25  | 30      | 35      | 40      |
| S4               | 10   | 15  | 25      | 30  | 35      | 40      | 45      |
| S5               | 15   | 20  | 30      | 35  | 40      | 45      | 50      |
| S6               | 20   | 25  | 35      | 40  | 45      | 50      | 55      |

The assumption of an adequate concrete cover in reinforced concrete structures, opportunely sized with reference to tables 1.11, will prevent the exposure of steel reinforcing bars to external environmental conditions and to the degradation processes described in the previous section while the additional values of  $\Delta c_{dev}$  shall avoid eventual shifts due to the execution process; anyway, the effective degradation of steel reinforcements, for what related to both strength and ductility, shall be deeply investigated and studied, in order to evaluated their consequences on the global structural behaviour of the whole building and to prearrange eventual additional protective devices.

### 1.3 Actual problems

The analysis of the effective LCF (seismic) performance of steel reinforcing bars represents, nowadays, a problem of relevant importance in the widest framework of the investigation of the global ductile behaviour of r.c. structures and remains, till now, partially unsolved.

Many works presented in the current literature evidenced the problems related to the numerical modelling of steel reinforcing bars under cyclic actions (Dodd and Restrepo-Posada 1995, Massone and Moroder 2009, Gomes and Appleton 1997, Monti and Nuti 1992, Menegotto and Pinto 1973 and others), providing useful information for the mechanical modeling of steel reinforcements under low-

cycle fatigue seismic action. Despite wide indications on modeling the single rebar element, no information are given for what concerns the effective seismic performance of rebars inside buildings and the ductility requirements imposed by real earthquakes. The lack of information about the real ductility demand on steel reinforcing bars due to seismic event, and the following deficiency of knowledge about the effective seismic performance of steel bars, results in the absence of opportune experimental tests for the production control of the cyclic behaviour of rebars. Actual European production standards for reinforcements (EN 10080:2005) do not include LCF tests for the mechanical characterization of the cyclic behaviour of rebars; only Spanish and Portuguese standards prescribe the execution of symmetrical tension/compression cycles for the production control of steel reinforcements. Nevertheless, the imposed levels of deformation, frequency, number of cycles and free length of the samples are not based on the results of scientific investigations about the real seismic behaviour of bars in structures and consequently, more accurate analyses are required.

The draft of new European standard for reinforcements (prEN 10080:2012) gives some indications for the execution of LCF tests: according to the indications of Mandate M115 inside the revision of EN 10080, in fact, an harmonized low-cycle fatigue test shall be elaborated in order to guarantee the seismic mechanical characterization of steel reinforcements. The standardization of the cyclic testing procedure is necessary since a large variability of parameters used for experimental tests was evidenced both in the current scientific literature (Brown and Kunnath 2004, Mander et al. 1994, Massone and Moroder 2009, Crespi 2002) and in the prescriptions presented by Spanish and Portuguese standards (UNE 36065 EX:2000, LNEC E-455:2008 and LNEC E-460:2008). The testing protocol needs consequently to be defined on the base of accurate analyses about the effective ductility requirements imposed by real earthquake to modern buildings.

In addition, many works in the current literature (Apostolopoulos and Papadakis 2008, Apostolopoulos 2007, Apostolopoulos and Michalopoulos 2006) evidenced durability problems in steel rebars, globally resulting in a rapid decrease of the mechanical properties and of the dissipative capacity of the reinforcements. Once again, no specific information about the effective mechanical performance of reinforcing steel affected by both seismic action and corrosion phenomena are provided in the actual literature and, moreover, no indications for what concerns the influence of corroded steel reinforcement of the global ductile behaviour of the whole building are given.

In order to prevent the above mentioned problems, Eurocode 2 (EN 1992-1-1:2005) introduces specific prescriptions for the sizing of concrete cover, in relation to different external exposition classes (no risk of corrosion, corrosion due to carbonation, presence of chlorides and seaside proximity, chemical attack and ice/de-icing cycles): the adoption of a correctly sized concrete cover shall be able to prevent the cracking and following spalling of the concrete, avoiding the direct exposition of reinforcements to external environmental conditions and the following deterioration of the mechanical behaviour under both monotonic and cyclic actions. Anyway, external events (such as unexpected impacts, particular occasional environmental conditions and others) or even accidental mistakes during the execution and construction phases can lead to the inadequacy or the premature cracking of the concrete cover, with the following possible initiation of corrosion process.

Nevertheless, the studies presented in the current literature generally refer to the mechanical properties of the single corroded steel bar, not including the influence of rebars' deterioration on the global ductile behaviour of the structure. Even if some indications about the reduced mechanical capacity of corroded steel reinforcements are provided, no information related to the effective mechanical demand required to the rebar by seismic events are given, and consequently it's not possible, at this moment, to establish if corroded steel reinforcements are still able to satisfy the ductility (and strength) requirements imposed by earthquakes

#### **1.4 Main objectives of the present work**

The objectives of the present work can be summarized into two different main aspects, respectively related to the evaluation and assessment of the mechanical performance of steel reinforcing bars subjected to low-cycle fatigue (seismic) loading and to the evaluation of the influence of corrosion phenomena on the monotonic and cyclic behaviour of rebars and their consequences on the global ductility of the whole structure, providing suitable indications for the designer in relation to different exposure condition, according to what prescribed by Eurocode 2 (EN 1992-1-1:2005).

A detailed investigation about the effective cyclic performance of steel reinforcing bars in r.c. and composite steel/concrete buildings subjected to seismic events was then executed, aiming at the definition, from one side, of the effective ductility demand due to earthquakes on rebars and, from the

other side, to the evaluation of the real mechanical cyclic capacity of reinforcements, resulting in the assessment of the seismic performance of reinforcing steel bar.

The analysis of the cyclic behaviour of steel bars in r.c. structures, in terms of strength, elongation and dissipated energy, allowed the definition of a procedure for the execution of low-cycle fatigue tests able to accurately characterize the seismic behaviour of steel reinforcements, opportunely calibrated on the base of scientific investigations. The protocol was proposed in the framework of the harmonization intent of Mandate M115 for the revision of European standard EN 10080:2005 in order to provide standardized procedures to European steel producers for the factory production control of reinforcing bars. Moreover, the problems related to the durability of steel reinforcements exposed to corrosion phenomena were deeply considered and investigated in order to individuate the residual mechanical characteristic of corroded steel reinforcing bars (in terms of strength and ductility) and to analyze their ability to withstand the required level of design seismic action. The obtained information provided useful indications for the design of r.c. and composite structures, integrating and completing what presented in Eurocode 2 (EN 1992-1-1:2005) about the protection of steel reinforcements towards corrosion phenomena.

### **1.5 The work - program and the adopted methodology**

The assessment of the cyclic performance of steel rebars required two main following steps, respectively related to the individuation of the effective *ductility demand* imposed to steel reinforcements by seismic action and to the investigation of the real *ductility capacity* of steel reinforcements under low-cycle fatigue seismic action. A simplified scheme of the adopted procedure is presented in figure 1.7. A representative set of steel grades, covering the actual production scenario for what concerns strength, ductility classes, diameters and production processes, was opportunely selected and tested. Experimental tensile and Low-Cycle Fatigue tests were executed on selected rebars; in particular, for monotonic tensile tests European standard EN ISO 15630-1:2010 was followed, while for cyclic tests a specific protocol was opportunely elaborated taking into account the prescriptions imposed by actual standards and by the current literature.

The results of LCF tests, in terms number of cycles and dissipated energy for a specific level of imposed deformation (*Low-Cycle Fatigue Performance Index – PI*), were compared with the results provided by numerical analyses on r.c. case study buildings and with the data coming from experimental monotonic and cyclic tests executed on representative steel/concrete composite joints. The difference in the adopted procedure for r.c. and composite structures (i.e. demand derived numerically for r.c. buildings - obtained from experimental tests for composite structures) can be ascribed to the absence of experimental data related to strain level on reinforcing bars in r.c. structures, needing consequently the execution of IDAs for the individuation of the dissipative behaviour of reinforcements. On the other hand, in the current scientific literature (Braconi et al. 2008, Braconi et al. 2006, Braconi et al. 2010) many results are presented regarding the effective behaviour of reinforcing bars in concrete slab of composite structures, and can be consequently used for the assessment of the effective cyclic behaviour of steel bars.

In particular, for what concerns r.c. buildings, MRF case study buildings designed according to Eurocode 8 were subjected to IDAs using specific accelerograms opportunely selected to maximize the ductility requirements on steel reinforcing bars, individuating the level of maximum deformation and the corresponding dissipated energy.

For what concerns steel/concrete composite structures the results coming from experimental pseudo-dynamic tests executed on a MRF composite frame tested at ISPRA (Braconi et al. 2008) were compared to the ones directly coming from experimental cyclic tests on interior and exterior beam to column connections tested in the Laboratory of University of Pisa. The good agreement in the results of the cyclic behaviour of joints in PSD and cyclic tests allowed to directly individuate the effective seismic ductility demand on rebars, since specific extensometers were adopted for the monitoring of the stress-strain behaviour of rebars in the joint.

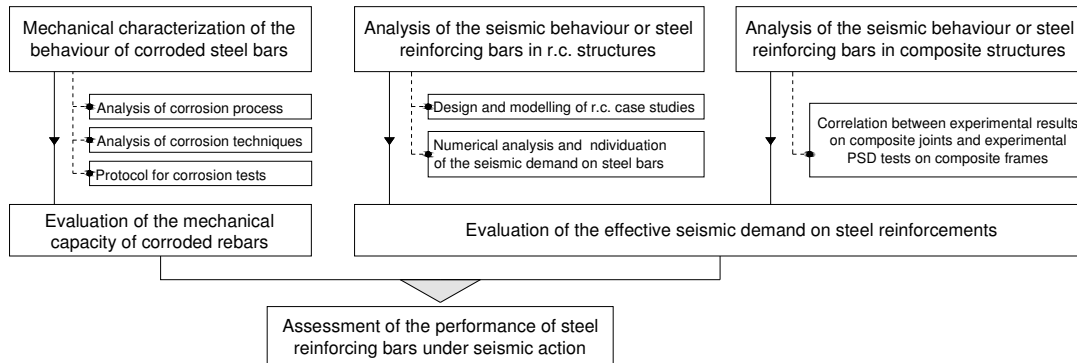


**Figure 1. 7:** Simplified scheme of the methodology adopted for the assessment of the seismic performance of steel bars.

As regards the investigation of the influence of corrosion phenomena on the mechanical performance of reinforcements and of their consequences on the global ductile behaviour of building, two main following steps were followed, respectively related to the analysis of the mechanical monotonic and cyclic capacity of corroded steel reinforcements and to its comparison with the ductility demand individuated as already briefly summarized. A simplified scheme of the main steps for the evaluation of corrosion phenomena on the seismic performance of steel reinforcing bars is presented in figure 1.8.

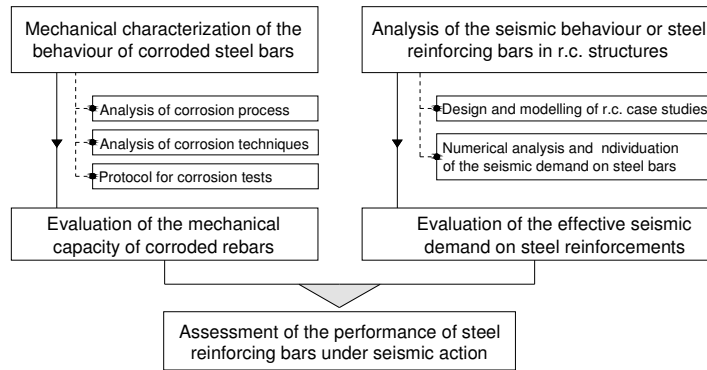


**Figure 1. 8:** Scheme of the methodology adopted for the assessment of the seismic capacity of corroded steel bars.

An opportune investigation of the corrosion morphology process and a detailed analysis of the actual laboratory techniques to artificially reproduce the effects of corrosion phenomena on steel reinforcements were the basis for the elaboration of a specific accelerated corrosion protocol able to artificially reproduce the detrimental effects of environmental conditions on the structural behaviour of steel bars. Experimental mechanical tests, including again both monotonic and low-cycle fatigue tests, were executed on a reduced set of corroded steel samples, opportunely individuated for including the most representative European steel grades and diameters; the experimental test campaign allowed the investigation of the mechanical properties of corroded steel reinforcements and the analysis of the combined effects of corrosion phenomena and seismic action on the structural performance of steel bars. *Corrosion Damage Indicators (CDI)* were opportunely defined considering the severity of corrosion attack in terms of deterioration of the mechanical properties (yielding and tensile strength and elongation to maximum load) and mass loss; specific correlation between CDI, Classes of Exposure as defined in Eurocode 2 (EN 1992-1-1:2005) and LCF Performance Index were finally provided analyzing the ability of steel reinforcing bars to maintain an adequate safety level in presence of seismic actions or less. What herein presented allowed the individuation of additional prescriptions for the protection of steel reinforcing bars from corrosion, respect to the ones already presented in Eurocode 2 (EN 1992-1-1:2005) about the thickness of the concrete cover.

## 2. MECHANICAL CHARACTERIZATION OF STEEL REINFORCING BARS

A set of representative samples, able to reproduce the actual European production scenario, was individuated and tested under monotonic and cyclic loads. Monotonic tensile tests were executed following EN 15630-1:2010, while a specific protocol for Low-Cycle Fatigue tests was elaborated.

### 2.1 European standards for steel reinforcements: mechanical properties and tests

Actual European standards for r.c. constructions (Eurocode 2, EN 1992-1-1:2005) provide the minimum mechanical requirements for reinforcing steels in different delivery conditions (bars, wires, coils and lattice girders), in terms of characteristic yielding strength ( $f_{yk}$  or  $f_{0,2k}$ ), characteristic strain at maximum force ( $\epsilon_{uk}$ ) and hardening ratio ( $f_t/f_{yk}$ ), as presented in table 2.1.

**Table 2. 1:** Mechanical properties of steel reinforcing bars (table C.1 Annex C of EN 1992-1-1:2005).

| Product form   | Bars and de-coiled rods |             |                            | Wire Fabrics                    |             |                            | Quantile value (%) |
|--|-------------------------|-------------|----------------------------|---------------------------------|-------------|----------------------------|--------------------|
| Class  | A                       | B           | C                          | A                               | B           | C                          | -                  |
| Characteristic yield strength $f_{yk}$ or $f_{0,2k}$ (MPa)     | 400 to 600              |             |                            |                                 |             |                            | 5,0                |
| Minimum value of $k = (f_t/f_{yk})_k$                          | $\geq 1,05$             | $\geq 1,08$ | $\frac{\geq 1,15}{< 1,35}$ | $\geq 1,05$                     | $\geq 1,08$ | $\frac{\geq 1,15}{< 1,35}$ | 10,0               |
| Characteristic strain at maximum force, $\epsilon_{uk}$        | $\geq 2,5$              | $\geq 5,0$  | $\geq 7,5$                 | $\geq 2,5$                      | $\geq 5,0$  | $\geq 7,5$                 | 10,0               |
| Bendability  | Bend/Rebend test        |             |                            | -                               |             |                            |                    |
| Shear strength   | -                       |             |                            | 0,3 A $f_{yk}$ (A area of wire) |             |                            | Minimum            |
| Maximum deviation from nominal mass (individual bar or wire %) | Nominal bar size (mm)   |             |                            |                                 |             |                            |                    |
|  | $\leq 8$                | $\pm 6,0$   |                            | 5,0                             |             |                            |                    |
|  | $> 8$                   | $\pm 4,5$   |                            |                                 |             |                            |                    |

Reinforcing steel products are defined mainly in relation to the characteristic yielding strength, varying between 400 and 600 MPa, to the characteristic  $A_{gt}$ , belonging to three different ductility classes (“A”, “B” and “C”) and, finally, to the minimum value of the hardening ratio. Eurocode 2 (EN 1992-1-1:2005) does not differentiate among production processes, diameters of reinforcing steel and metallurgical properties. Nowadays, about 200 different steel grades exist, all over Europe, following the limitations presented in table 2.1; a detailed analysis of the mechanical requirements and of the experimental tests prescribed for the production controls of rebars by European and Mediterranean standards was executed inside the framework of *Rusteel* project and the minimum requirements imposed by each single standard are presented in the tables from 2.2 to 2.13.

**Table 2. 2:** Mechanical properties of steel reinforcements according to Greek standard for reinforcements (ELOT 1421-3:2007), being  $R_e$  the yielding strength,  $R_m$  the tensile strength and  $A_{gt}$  the elongation corresponding to maximum load.

| Steel grade                        | $\phi$<br>[mm] | $R_e$<br>[MPa] | $R_m/R_e$<br>[-]                    | $A_{gt}$<br>[%]                    |
|------------------------------------|----------------|----------------|-------------------------------------|------------------------------------|
| B500 A                             | 5-8            | $\geq 500$     | $\geq 1,05$                         | $\geq 2,5$                         |
|                                    |                |                | $\geq 1,03$ ( $\phi < 6\text{mm}$ ) | $\geq 2,0$ ( $\phi < 6\text{mm}$ ) |
| B500 C<br>Bars, Welded fabric etc. | 6 - 40         | $\geq 500$     | $\frac{\geq 1,15}{\leq 1,35}$       | $\geq 7,5$                         |

**Table 2. 3:** Mechanical properties of steel reinforcements according to Italian standard for constructions (D.M.14/01/2008), in which  $f_{yk}$  and  $f_{tk}$  are the characteristic yield and tensile strength for a 5% fractile.

| Steel grade | $f_{y\text{ nom}}$<br>[MPa] | $f_{t\text{ nom}}$<br>[MPa] | $(f_t/f_y)_k$<br>[-]       | $(f_y/f_{y\text{ nom}})_k$<br>[-] | $(A_{gt})_k$<br>[%] |
|-------------|-----------------------------|-----------------------------|----------------------------|-----------------------------------|---------------------|
| B450 A      | 450                         | 540                         | $\geq 1,05$                | $\leq 1,25$                       | $\geq 2,5$          |
| B450 C      | 450                         | 540                         | $\frac{\geq 1,15}{< 1,35}$ | $\leq 1,25$                       | $\geq 7,5$          |

**Table 2. 4:** Mechanical properties of steel reinforcements according to Spanish standard for steel reinforcements (UNE 36065 EX:2000), being  $R_e$  the yielding strength,  $R_m$  the tensile strength and  $A_{gt}$  the elongation corresponding to maximum load and  $A_5$  the ultimate elongation. In the following table: <sup>(1)</sup> characteristic value, <sup>(2)</sup> means that for the evaluation of stresses it is necessary to use the nominal section of bar, <sup>(3)</sup> real value obtained from tests.

| Steel grade | $R_e$ <sup>(1,2)</sup><br>[MPa] | $R_m$ <sup>(1,2)</sup><br>[MPa] | $R_{e\text{ real}}/R_{e\text{ nominal}}$ <sup>(3)</sup><br>[-] | $A_5$ <sup>(1)</sup><br>[%] | $A_{gt}$ <sup>(1)</sup><br>[%] | $R_m/R_e$ <sup>(1)</sup><br>[-] |
|-------------|---------------------------------|---------------------------------|--|-----------------------------|--------------------------------|---------------------------------|
| B400 SD     | 400                             | 480                             | $\leq 1,20$  | $\geq 20$                   | 9                              | $\frac{\geq 1,20}{\leq 1,35}$   |
| B500 SD     | 500                             | 575                             | $\leq 1,25$  | $\geq 16$                   | 8                              | $\frac{\geq 1,15}{\leq 1,35}$   |

**Table 2. 5:** Mechanical properties of steel reinforcements according to Portuguese standard for steel reinforcements (LNEC E460:2008 and LNEC E455:2008), being  $R_e$  the yielding strength,  $R_m$  the tensile strength and  $A_{gt}$  the elongation corresponding to maximum load. In the following table: <sup>(1)</sup> minimum characteristic value referred to a 5% fractile, <sup>(1)</sup> minimum characteristic value referred to a 10% fractile and <sup>(3)</sup> maximum characteristic value referred to a 90% fractile.

| Steel grade | $R_e$ <sup>(1)</sup><br>[MPa] | $R_m/R_e$ <sup>(2)</sup><br>[-] | $R_m/R_e$ <sup>(3)</sup><br>[-] | $R_e/400$ <sup>(3)</sup><br>[-] | $A_{gt}$ <sup>(2)</sup><br>[%] |
|-------------|-------------------------------|---------------------------------|---------------------------------|---------------------------------|--------------------------------|
| A400 NR SD  | 400                           | 1,15                            | 1,35                            | 1,2                             | 8                              |
| Steel grade | $R_e$ <sup>(1)</sup><br>[MPa] | $R_m/R_e$ <sup>(2)</sup><br>[-] | $R_m/R_e$ <sup>(3)</sup><br>[-] | $R_e/500$ <sup>(3)</sup><br>[-] | $A_{gt}$ <sup>(2)</sup><br>[%] |
| A500 NR SD  | 500                           | 1,15                            | 1,35                            | 1,2                             | 8                              |

**Table 2. 6:** Mechanical properties of steel reinforcements according to British standard for reinforcement of concrete (BS 4449:2005), being  $R_e$  the yielding strength,  $R_m$  the tensile strength and  $A_{gt}$  the elongation corresponding to maximum load. In the following table: <sup>(a)</sup> means that the ratio  $R_m/R_e$  is equal to 1.02 for diameters below 8.0 mm and <sup>(b)</sup> characteristic  $A_{gt}$  is 2.0 for diameters below 8.0 mm.

| Steel grade | $R_e$<br>[MPa] | $R_m/R_e$<br>[-]           | $A_{gt}$<br>[%]    |
|-------------|----------------|----------------------------|--------------------|
| B500A       | 500            | 1,05 <sup>(a)</sup>        | 2,5 <sup>(b)</sup> |
| B500B       | 500            | 1,08                       | 5,0                |
| B500C       | 500            | $\frac{\geq 1,15}{< 1,35}$ | 7,5                |

**Table 2. 7:** Mechanical properties of steel reinforcements according to French standard for steel rebars (NF A35-016-1:2007), being  $R_e$  the yielding strength,  $R_m$  the tensile strength and  $A_{gt}$  the elongation corresponding to maximum load. In the following table: <sup>(a)</sup> means  $R_m/R_e$  equal to 1.03 for diameter 5.0 mm, <sup>(b)</sup> means  $A_{gt}$  equal to 2.0 for diameter 5.0 mm, <sup>(c)</sup> means  $R_m/R_e$  equal to 1.05 for diameter 5.0 mm, <sup>(d)</sup> means  $A_{gt}$  equal to 4.0 for diameter 5.0 mm.

| Steel grade | Re<br>[MPa] | $R_{e\text{ real}}/R_{e\text{ nominal}}$<br>max | $R_m/R_e$<br>min    | $A_{gt}$<br>max | $A_{gt}$<br>[%]    |
|-------------|-------------|---|---------------------|-----------------|--------------------|
| B500A       | 500         | 1,3   | 1,05 <sup>(a)</sup> | -               | 2,5 <sup>(b)</sup> |
| B500B       | 500         | 1,3   | 1,08 <sup>(c)</sup> | -               | 5,0 <sup>(d)</sup> |
| B450B       | 450         | 1,3   | 1,08 <sup>(c)</sup> | -               | 5,0 <sup>(d)</sup> |
| B450C       | 450         | 1,25  | 1,15                | 1,35            | 7,5                |

**Table 2. 8:** Mechanical properties of steel reinforcements according to German standard (DIN 488-1:1984-09), being  $R_e$  the yielding strength,  $R_m$  the tensile strength and  $A_{gt}$  the elongation corresponding to maximum load. In the following table (c) means that  $R_m/R_e$  is equal to 1.03 and minimum  $A_{gt}$  is equal to 2.0 % for diameters between 4.0 and 5.5 mm

| Steel grade | $R_e$<br>[MPa] | $R_m/R_e$<br>[-]    | $R_{e,\text{eff}}/R_{e,\text{nom}}$<br>[-] | $A_{gt}$<br>[%]    |
|-------------|----------------|---------------------|--|--------------------|
| B500A       | 500            | 1,05 <sup>(c)</sup> | -  | 2,5 <sup>(c)</sup> |
| B500B       | 500            | 1,08                | 1,30                                       | 5,0                |

**Table 2. 9:** Mechanical properties of steel reinforcements according to Bulgarian standard for rebars (BG 9252:2007), being  $R_e$  the yielding strength,  $R_m$  the tensile strength and  $A_{gt}$  the elongation corresponding to maximum load.

| Steel grade | $R_e$<br>[MPa] | $R_m$<br>[MPa] | $A_{gt}$<br>[%] | $R_m/R_e$<br>[-]           | $R_{e,\text{act}}/R_{e,\text{nom}}$<br>[-] |
|-------------|----------------|----------------|-----------------|----------------------------|--|
| B500A       | 500            | 550            | 2,5             | 1,05                       | -  |
| B500B       | 500            | 550            | 5               | 1,08                       | $\leq 1,25$                                |
| B500C       | 500            | 575            | 7,5             | $\frac{\geq 1,15}{< 1,35}$ | $\leq 1,25$                                |

**Table 2. 10:** Mechanical properties of steel reinforcements according to Romanian standard (STAS 438/1:1989), in which  $R_e$  is the yielding strength,  $R_m$  is the tensile strength and  $A_{tot}$  is the ultimate total elongation. Steel grade “OB 37” is a kind of carbon steel for round bar, PC 52 and PC 60 are two kinds of low- alloyed steel for deformed bars.

| Steel grade | Diameter<br>[mm] | $R_e$<br>[MPa]                  | $R_m$<br>[MPa] | $A_{tot}$<br>[%] |
|-------------|------------------|---------------------------------|----------------|------------------|
| OB 37       | 6 – 12           | 255                             | 360            | 25               |
|             | 14 – 40          | 235                             |                |                  |
| PC 52       | 6 - 14           | 355                             | 510            | 20               |
|             | 16 – 28          | 345                             |                |                  |
|             | 32 – 40          | 355                             |                |                  |
|             | > 40             | Established conforming contract |                |                  |
| PC 60       | 6 – 12           | 420                             | 590            | 16               |
|             | 14 – 28          | 405                             |                |                  |
|             | 32 – 40          | 395                             |                |                  |

**Table 2. 11:** Mechanical properties of steel reinforcements according to Serbian standard for reinforcing steel (JUS C.K6.020:1987).  $R_{eH}$  is the nominal values for yielding strength.

| Steel grade    | C0002         | C0300         | C0550 |     |     |            | C0551      |
|----------------|---------------|---------------|-------|-----|-----|------------|------------|
|                | GA not ribbed | GA not ribbed | RA1   | RA2 | RA3 | RA4 ribbed | RA2 ribbed |
| $R_{eH}$ (MPa) | 220           | 240           | 400   |     |     |            | 400        |
| $R_m$ (MPa)    | 340           | 360           | 500   |     |     |            | 500        |
| $A_{10}$ (%)   | 18            | 18            | 10    |     |     |            | 10         |

**Table 2. 12:** Mechanical properties of steel reinforcements according to Algerian standard for reinforcing steel (1997), being  $R_{e,min}$  the minimum yielding strength,  $R_{m,min}$  the minimum tensile strength,  $A_{min}$  the elongation to maximum load.

| Steel grade                | $R_{e,min}$ [MPa] | $R_{m,min}$ [MPa] | $A_{min}$ [%] |
|----------------------------|-------------------|-------------------|---------------|
| Not ribbed B22             | 215               | 330               | 22 - 25       |
| Not ribbed B24             | 235               | 430               | 22 - 25       |
| High adherence H.AD/E E400 | 400               | 440               | 12 - 14       |
| High adherence H.AD/E E500 | 500               | 550               | 12 - 14       |

**Table 2. 13:** Mechanical properties of reinforcements according to Egyptian standard for reinforcing steel (262/1988), being  $R_{e,min}$  the minimum yielding strength,  $R_{m,min}$  the minimum tensile strength,  $A_{min}$  the elongation to maximum load.

| Steel grade         | $R_{e,min}$ [MPa] | $R_{m,min}$ [MPa] | $A_{min}$ [%] |
|---------------------|-------------------|-------------------|---------------|
| Plain bars 24/35    | 24                | 35                | 20            |
| Plain bars 28/45    | 28                | 45                | 18            |
| Deformed bars 36/52 | 36                | 52                | 12            |
| Deformed bars 40/60 | 40                | 60                | 10            |

The mechanical properties of steel reinforcements, according to the standards cited above, can be summarized as presented in table 2.14, in which the values of tensile and yielding strength ( $R_m$ ,  $R_e$ ), elongation to maximum load and ultimate elongation ( $A_{gt}$ ,  $A$ ) are provided as well as the hardening ratio ( $R_m/R_e$ ) and the ratio between the real and the nominal yielding strength ( $R_{e,real}/R_{e,nom}$ ). Moreover, an accurate analysis of experimental tests prescribed for the production control of steel reinforcing bars was executed, and the results are briefly summarized in table 2.15.

**Table 2. 14:** Summarizing table for mechanical properties of steel reinforcements in European and other countries.

| European Country | Steel grade | Diameter<br>[mm] | $R_e$<br>[MPa] | $R_m$<br>[MPa] | $R_m/R_e$<br>[-]        | $A_{gt}$<br>[%] | $A$<br>[%] | $R_{e,real}/R_{e,nom}$<br>[-] |
|------------------|-------------|------------------|----------------|----------------|-------------------------|-----------------|------------|-------------------------------|
| Greece           | B500A       | 5-8              | 500            |                | 1,05                    | $\geq 2.0-2.5$  |            |                               |
|                  | B500C       | 6-40             | 500            |                | $\geq 1,15$<br>$< 1,35$ | $\geq 7.5$      |            | $\geq 1.25$                   |
| Italy            | B450A       | 5-12             | 450            |                | $\geq 1,05$             | $\geq 2.5$      |            | $\leq 1.25$                   |
|                  | B450C       | 6-50             | 450            |                | $\geq 1,15$<br>$< 1,35$ | $\geq 7.5$      |            | $\leq 1.25$                   |
| Spain            | B400SD      | 6-40             | 400            |                | $\geq 1,20$<br>$< 1,35$ | 9,0             | $\geq 20$  | $\leq 1.20$                   |
|                  | B500SD      | 6-40             | 500            |                | $\geq 1,15$<br>$< 1,35$ | 8,0             | $\geq 16$  | $\leq 1.25$                   |

|               |                     |       |     |             |             |             |
|---------------|---------------------|-------|-----|-------------|-------------|-------------|
| Portugal      | A400 NR SD          | 6-40  | 400 | $\geq 1,15$ | 8,0         |             |
|               |                     |       |     | $< 1,35$    |             |             |
| Germany       | A500 NR SD          | 6-40  | 500 | $\geq 1,15$ | 8,0         |             |
|               |                     |       |     | $< 1,35$    |             |             |
| Germany       | B500A               | 6-14  | 500 | 1,05        | 2,5         |             |
|               | B500B               | 6-40  | 500 | $\geq 1,08$ | 5,0         | 1,3         |
|               |                     |       |     | $< 1,35$    |             |             |
| Austria       | B420B               | 3-50  | 420 | 1,05 – 1,08 |             | 4-5         |
|               | B500B               | 3-50  | 500 |             |             |             |
|               | B550B               | 3-50  | 550 |             |             |             |
| Great Britain | B500A               |       | 500 | 1,05        | 2,5         |             |
|               | B500B               |       | 500 | 1,08        | 5,0         |             |
|               | B500C               |       | 500 | $\geq 1,15$ | 7,5         |             |
|               |                     |       |     | $< 1,35$    |             |             |
| France        | B500A               |       | 500 | 1,05        | 2,5         | 1,3         |
|               | B500B               |       | 500 | 1,08        | 5,0         | 1,3         |
|               | B450A               |       | 450 | 1,08        | 5,0         | 1,3         |
|               | B450C               |       | 450 | $\geq 1,15$ | 7,5         | 1,3         |
|               |                     |       |     | $< 1,35$    |             |             |
| Romania       | OB 37               | 6-12  | 255 | 360         |             | 25          |
|               |                     | 14-40 | 235 |             |             |             |
|               | PC 52               | 6-14  | 355 | 510         |             | 20          |
|               |                     | 16-28 | 345 |             |             |             |
|               |                     | 32-40 | 355 |             |             |             |
|               | PC 60               | 6-12  | 420 | 590         |             | 16          |
| 14-28         |                     | 405   |     |             |             |             |
| 32-40         |                     | 395   |     |             |             |             |
| Bulgary       | B 500 A             |       | 500 | 550         | 1,05        | 2,5         |
|               | B 500 B             |       | 500 | 550         | 1,08        | 5,0         |
|               | B 500 C             |       | 500 | 575         | $\geq 1,15$ | 7,5         |
|               |                     |       |     |             | $< 1,35$    | $\leq 1,25$ |
| Algeria       | B22 (no ribs)       |       | 215 | 330         |             | 22÷25       |
|               | B24 (no ribs)       |       | 235 | 430         |             | 22÷25       |
|               | H.AD/E E400         |       | 400 | 440         |             | 12÷14       |
|               | H.AD/E E500         |       | 500 | 550         |             | 12÷14       |
| Egypt         | Plain bars 24/35    |       | 240 | 350         |             | 20          |
|               | Plain bars 28/45    |       | 280 | 450         |             | 18          |
|               | Deformed bars 36/52 |       | 360 | 520         |             | 12          |
|               | Deformed bars 40/60 |       | 400 | 600         |             | 10          |

**Table 2. 15:** Experimental tests prescribed by actual standards for steel reinforcements' production control.

| European Country | Tensile tests | Bending test | Bond test | Fatigue tests | LCF test |
|------------------|---------------|--------------|-----------|---------------|----------|
| Portugal         | x             | x            | x         | x             | x        |
| Spain            | x             | x            | x         | x             | x        |
| Great Britain    | x             | x            | x         | x *           |          |
| Germany          | x             | x            | x         |               |          |
| Greece           | x             | x            | x         | x             |          |
| France           | x             | x            | x         | x *           |          |
| Bulgary          | x             | x            | x         | x             |          |
| Italy            | x             | x            | x         |               |          |
| Algeria          | x             | x            | x         |               |          |
| Serbia           | x             | x            | x         | x             |          |
| Romany           | x             | x            | x         |               |          |
| Egypt            | x             | x            | x         |               |          |

What presented in tables 2.14 and 2.15 evidences a large variability of mechanical properties and experimental tests foreseen by actual European standards. As visible from table 2.15, tensile, bending

and bond tests are foreseen by all the countries taken into consideration, 7 Countries prescribe the execution of fatigue tests and only Spain and Portugal introduce a specific protocol for low-cycle fatigue tests on steel reinforcements.

## 2.2 Mechanical characterization of selected reinforcing bars

A significative set of rebars, aiming at the complete representation of the actual European production scenario, was selected for experimental tests. Different steel grades, ductility, diameters and production processes (TempCore - TEMP, Micro-Alloyed MA, Stretched - STR and Cold-Worked - CW) were considered for covering the large variability of rebars used in r.c. structures evidenced in table 2.14. steel reinforcements were taken into account. The variability due to different producers and to different plants was also considered: the samples were provided by two different European producers, in the following presented as “producer 1” and “producer 2”. Table 2.16 presents the complete set of steel reinforcements selected for the execution of mechanical experimental tests.

**Table 2. 16:** Representative set of steel reinforcements selected for mechanical characterization.

| Steel grade | Ductility | Diameter      | Process | Ribs     | Producer                              |
|-------------|-----------|---------------|---------|----------|---------------------------------------|
| B500        | A         | 8             | CW      | Indented | Prod. 1                               |
| B500        | B         | 16            | TEMP    | Ribbed   | Prod. 1 (3 different plants)          |
| B500        | B         | 8             | STR     | Ribbed   | Prod. 1                               |
| B450        | C         | 16            | TEMP    | Ribbed   | Prod. 1 (3 different plants)          |
| B450        | C         | 8             | STR     | Ribbed   | Prod. 1                               |
| B400        | C         | 8, 20, 16     | TEMP    | Ribbed   | Prod. 1                               |
| B500        | A         | 8, 12         | CW      | Ribbed   | Prod. 2                               |
| B500        | B         | 8, 16, 20, 25 | TEMP    | Ribbed   | Prod. 2 (same cast for all diameters) |
| B450        | C         | 16, 20, 25    | TEMP    | Ribbed   | Prod. 2 (same cast for all diameters) |
| B450        | C         | 8, 12         | STR     | Ribbed   | Prod. 2                               |
| B400        | C         | 16, 20, 25    | MA      | Ribbed   | Prod. 2 (same cast for all diameters) |

### 2.2.1 Metallurgical investigation on steel reinforcements

Macrographic and metallographic investigations and hardness tests were executed on 28 specimens belonging to different reinforcing bars classes: TempCore (TEMP), micro alloyed (MA), cold worked (CW), stretched (STR). Specimens taken from bars were prepared for metallographic examination and etched with 3% nital solution, in order to individuate the hardness profile of bars’ cross-sections.

In the figure 2.1, the typical macrostructure of TempCore bars is presented, consisting of three main concentric zones: a skin of tempered martensite on the surface, an intermediate zone with a mixture of bainite and ferrite, and a ferrite–pearlite core. The extension of skin, intermediate zone and core were evaluated by considering the area of the phases on the metallographic samples as evidenced in the figure 2.1. In the table 2.1, the summary of the extension of skin, intermediate zone and core and the hardness of core and skin are reported for all the tested bars.

**Table 2. 17:** Measured bars properties.

| Bar                      | Core Hardness | Skin Hard. | Skin    | Interm. zone | Core diameter |
|--------------------------|---------------|------------|---------|--------------|---------------|
| B400C-8-TEMP-Prod. 1     | 164.5 HV      | 257 HV     | 0.52 mm | 0.28 mm      | 6.79 mm       |
| B400C-16-TEMP- Prod. 1   | 161.0 HV      | 250 HV     | 0.78 mm | 0.54 mm      | 12.47 mm      |
| B400C-20-TEMP- Prod. 1   | 161.5 HV      | 250 HV     | 0.92 mm | 0.67 mm      | 15.34 mm      |
| B450C-16-TEMP- Prod. 1   | 186.0 HV      | 271 HV     | 1.51 mm | 0.93 mm      | 10.11 mm      |
| B450C-16-TEMP- Prod. 1   | 173.5 HV      | 266 HV     | 0.96 mm | 0.83 mm      | 11.52 mm      |
| B450C-16-TEMP- Prod. 1   | 155.0 HV      | 247 HV     | 1.01 mm | 1.57 mm      | 10.75 mm      |
| B450C-16-TEMP- Prod. 2   | 166.5 HV      | 257 HV     | 0.82 mm | 0.78 mm      | 12.20 mm      |
| B450C-20-TEMP- Prod. 2   | 167.0 HV      | 267 HV     | 1.25 mm | 1.69 mm      | 13.50 mm      |
| B450C-25-TEMP- Prod. 2   | 165.0 HV      | 266 HV     | 1.90 mm | 2.10 mm      | 15.65 mm      |
| B500B-16-TEMP- Prod. 1.2 | 177.0 HV      | 271 HV     | 1.16 mm | 0.79 mm      | 11.26 mm      |
| B500B-16-TEMP- Prod. 1.3 | 174.0 HV      | 266 HV     | 1.14 mm | 1.20 mm      | 10.79 mm      |
| B500B-16-TEMP- Prod. 1.1 | 182.0 HV      | 276 HV     | 1.47 mm | 0.69 mm      | 10.60 mm      |
| B500B-16-TEMP- Prod. 2   | 170.0 HV      | 267 HV     | 1.22 mm | 1.30 mm      | 10.49 mm      |
| B500B-20-TEMP- Prod. 2   | 172.5 HV      | 266 HV     | 1.58 mm | 1.47 mm      | 13.12 mm      |
| B500B-25-TEMP- Prod. 2   | 173.0 HV      | 271 HV     | 1.94 mm | 1.87 mm      | 16.30 mm      |

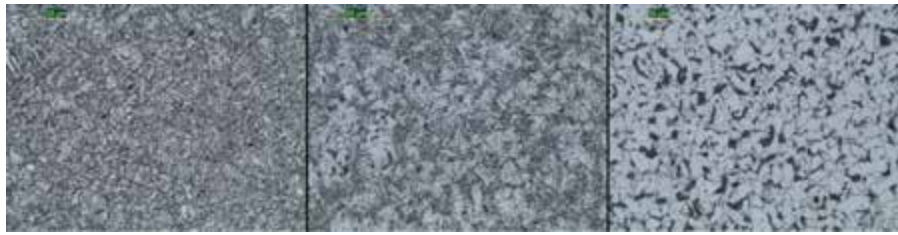


**Figure 2. 1:** Typical microstructures present in a cross-section of B450C-16-TEMP-2.1Tempcore reinforcing bar, (a) skin: tempered martensite, (b) intermediate zone: bainite/ferrite mixture, and (c) core: ferrite–pearlite.

In the figure 2.2a, the typical microstructure of MA steels is presented, consisting of pearlite and ferrite. The ferritic grain size was measured using the intercept method. In the table 2.18, the summary of the microstructural features (ferrite grain size) and the measured hardness are reported for all the tested micro alloyed bars. In the figure 2.2b, the typical microstructure of cold worked steels is shown, consisting of pearlite and ferrite. The ferritic grain size was measured using the intercept method. In the table 2.19, the summary of the micro structural features (ferrite grain size) and the measured hardness are presented for all the tested cold-worked reinforcing bars.

Finally, in the figure 2.3 the typical microstructure of strengthened steels is presented, consisting of pearlite and ferrite. The ferritic grain size was measured using the intercept method. In the table 2.20 the summary of the microstructural features (ferrite grain size) and the measured hardness are reported for all the tested bars.

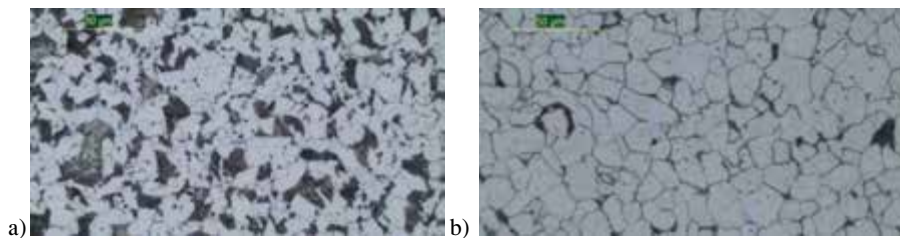


**Figure 2. 2:** a) Typical micro structural in a cross-section of B400C-16 (Prod. 2) Micro alloyed rebar: ferrite–pearlite.

**Table 2. 18:** Measured bars properties (MA specimens), b) Typical micro structural in a cross-section of B500A-8-CW (Producer 2) rebar: ferrite–pearlite.

| Steel grade/diameter/process/producer | Hardness (HV) | FGS ( $\mu\text{m}$ ) |
|---------------------------------------|---------------|-----------------------|
| B400C-16-MA-Prod.2                    | 184           | 9.01                  |
| B400C-20-MA- Prod.2                   | 178           | 8.64                  |
| B400C-25-MA- Prod.2                   | 182           | 12.53                 |

**Table 2. 19:** Measured bars properties (Cold Worked specimens).

| Steel grade/diameter/process/producer | Hardness (HV) | FGS ( $\mu\text{m}$ ) |
|---------------------------------------|---------------|-----------------------|
| B500A-8-CW Prod.2                     | 196           | 12.1                  |
| B500A-8-CW Prod.2                     | 196           | 13.98                 |
| B500A-8-CW Prod.1                     | 201           | 11.08                 |
| B500A-12-CW Prod.2                    | 205           | 14.04                 |
| B500A-12-CW Prod.2                    | 202           | 14.04                 |

**Table 2. 20:** Measured bars properties (Stretched specimens).

| Bar                  | Hardness (HV) | FGS ( $\mu\text{m}$ ) |
|----------------------|---------------|-----------------------|
| B450C-8-STR Prod. 1  | 195           | 5.79                  |
| B500B-8-STR Prod. 1  | 208           | 7.84                  |
| B450C-12-STR Prod. 2 | 186           | 12.09                 |
| B450C-12-STR Prod. 2 | 199           | 8.04                  |



**Figure 2. 3:** Typical micro structural in a cross-section of B500B-8-STR (Producer 1) rebar: ferrite–pearlite.

## 2.2.2 Results of experimental tensile tests

In the following tables the mechanical properties obtained for the different samples are presented. In particular,  $R_m$  is the ultimate tensile stress,  $R_e$  the yielding stress,  $R_m/R_e$  the hardening ratio,  $A_{gt}$  the total elongation corresponding to maximum load and  $A$  the total ultimate elongation.

### 2.2.2.1 Experimental tests executed by UniPi: results

**Table 2. 21:** Mechanical properties of tested rebars.

| Steel grade/diameter/<br>process/rib/producer | Spec.<br>[n°] | d<br>[mm] | A<br>[mm <sup>2</sup> ] | $R_m$<br>[MPa] | $R_e$<br>[MPa] | $R_m/R_e$<br>[-] | A<br>[%] | $A_{gt}$<br>[%] |
|---|---------------|-----------|-------------------------|----------------|----------------|------------------|----------|-----------------|
| B400C-8-TEMP-R Prod. 1                        | 1             | 8,04      | 50,80                   | 567,33         | 442,92         | 1,28             | 33,00    | 15,51           |
|   | 2             | 8,08      | 51,27                   | 567,63         | 452,54         | 1,25             | 31,25    | 17,71           |
|   | 3             | 8,06      | 51,08                   | 574,57         | -              | -                | 35,00    | 16,31           |
| B500A-8-CW-IND Prod. 1                        | 1             | 8,00      | 50,32                   | 581,30         | 582,29         | 1,00             | 17,25    | 3,21            |
|   | 2             | 8,01      | 50,45                   | 592,11         | 564,95         | 1,05             | 22,50    | 4,61            |
|   | 3             | 7,97      | 49,85                   | 591,50         | 581,77         | 1,02             | 17,25    | 4,21            |
| B500B-8-STR-R Prod. 1                         | 1             | 8,12      | 51,80                   | 619,35         | 565,59         | 1,10             | 21,25    | 4,52            |
|   | 2             | 8,11      | 51,63                   | 621,48         | 578,19         | 1,07             | 22,50    | 5,62            |
|   | 3             | 8,06      | 51,08                   | 638,49         | -              | -                | 20,25    | 5,62            |
| B450C-8-STR-R Prod. 1                         | 1             | 8,05      | 50,96                   | 624,76         | -              | -                | 25,00    | 8,62            |
|   | 2             | 8,03      | 50,59                   | 630,86         | -              | -                | 25,00    | 8,92            |
|   | 3             | 8,05      | 50,83                   | 630,99         | -              | -                | 28,00    | 9,62            |
| B500B-8-TEMP-R Prod. 2                        | 1             | 8,14      | 52,01                   | 671,45         | 584,69         | 1,15             | 15,25    | 8,32            |
|   | 2             | 8,13      | 51,89                   | 612,52         | 531,23         | 1,15             | 18,00    | 9,00            |
|   | 3             | 8,13      | 51,85                   | 605,40         | 552,42         | 1,10             | 18,75    | 5,00            |
| B500A-8-CW-R Prod. 2                          | 1             | 7,82      | 48,08                   | 546,83         | 526,42         | 1,04             | 19,50    | 6,00            |
|   | 2             | 7,83      | 48,16                   | 560,20         | 529,65         | 1,06             | 18,00    | 7,10            |
|   | 3             | 7,78      | 47,59                   | 552,43         | 527,69         | 1,05             | 17,50    | 6,20            |
| B500A-12-CW-R Prod. 2                         | 1             | 11,87     | 110,59                  | 588,98         | 567,70         | 1,04             | 20,50    | 7,45            |
|   | 2             | 11,95     | 112,15                  | 589,56         | 570,31         | 1,03             | 19,75    | 6,60            |
|   | 3             | 11,93     | 111,77                  | 581,02         | 552,93         | 1,05             | 16,17    | 6,40            |
| B450C-12-STR-R Prod. 2                        | 1             | 11,81     | 109,60                  | 599,68         | 513,75         | 1,17             | 24,17    | 9,30            |
|   | 2             | 11,80     | 109,31                  | 599,51         | 515,15         | 1,16             | 25,50    | 10,00           |
|   | 3             | 11,82     | 109,72                  | 596,44         | 518,55         | 1,15             | 24,83    | 11,00           |
| B400C-16-TEMP-R Prod. 1                       | 1             | 15,86     | 197,55                  | 547,73         | 446,92         | 1,23             | 24,63    | 16,35           |
|   | 2             | 15,91     | 198,88                  | 544,06         | 428,14         | 1,27             | 29,25    | 15,55           |
|   | 3             | 15,65     | 192,36                  | 560,98         | 442,67         | 1,27             | 29,25    | 15,55           |
| B400C-16-MA-R Prod. 2                         | 1             | 16,17     | 205,48                  | 565,27         | 434,45         | 1,30             | 31,25    | 17,36           |
|   | 2             | 16,22     | 206,66                  | 572,48         | 436,71         | 1,31             | 30,38    | 18,16           |
|   | 3             | 16,17     | 205,39                  | 573,15         | 432,73         | 1,32             | 30,75    | 18,46           |
| B400C-16-TEMP-R Prod. 1                       | 1             | 15,86     | 197,55                  | 547,73         | 446,92         | 1,23             | 24,63    | 16,35           |
|   | 2             | 15,91     | 198,88                  | 544,06         | 428,14         | 1,27             | 29,25    | 15,55           |
|   | 3             | 15,65     | 192,36                  | 560,98         | 442,67         | 1,27             | 29,25    | 15,55           |
| B450C-16-TEMP-R Prod. 1(3)                    | 1             | 16,16     | 205,00                  | 615,41         | 517,78         | 1,19             | 25,38    | 13,76           |
|   | 2             | 16,18     | 205,71                  | 610,42         | 507,42         | 1,20             | 25,13    | 14,96           |
|   | 3             | 16,18     | 205,59                  | 613,65         | 516,30         | 1,19             | -        | 11,96           |
| B450C-16-TEMP-R Prod. 1(2)                    | 1             | 15,97     | 200,29                  | 542,68         | 446,68         | 1,21             | 30,25    | 15,35           |
|   | 2             | 15,91     | 198,91                  | 542,51         | 445,85         | 1,22             | 25,63    | 12,15           |
|   | 3             | 15,96     | 200,13                  | 537,25         | 443,13         | 1,21             | 26,88    | 14,45           |
| B450C-16-TEMP-R Prod. 1(1)                    | 1             | 16,02     | 201,56                  | 640,51         | 537,32         | 1,19             | 23,88    | 8,86            |
|   | 2             | 15,98     | 200,67                  | 703,97         | 586,64         | 1,20             | 21,38    | 10,97           |
|   | 3             | 15,97     | 200,40                  | 681,43         | 581,56         | 1,17             | 22,63    | 9,27            |

|                            |   |       |        |        |        |      |       |       |
|----------------------------|---|-------|--------|--------|--------|------|-------|-------|
| B500B-16-TEMP-R Prod. 1(1) | 1 | 15,93 | 199,30 | 671,40 | 596,58 | 1,13 | 21,88 | 8,07  |
|                            | 2 | 15,89 | 198,26 | 670,97 | 592,79 | 1,13 | 22,50 | 8,07  |
|                            | 3 | 15,74 | 194,63 | 665,33 | 582,67 | 1,14 | 22,38 | 9,26  |
| B500B-16-TEMP-R Prod. 1(2) | 1 | 16,11 | 203,74 | 668,33 | 572,03 | 1,17 | 24,00 | 11,27 |
|                            | 2 | 16,09 | 203,32 | 639,80 | 548,12 | 1,17 | 24,13 | 12,57 |
|                            | 3 | 16,00 | 201,09 | 652,72 | 561,98 | 1,16 | 22,75 | 11,37 |
| B500B-16-TEMP-R Prod. 1(3) | 1 | 16,17 | 205,34 | 616,28 | 513,09 | 1,20 | 25,63 | 11,46 |
|                            | 2 | 16,19 | 205,86 | 614,25 | 513,22 | 1,20 | 24,25 | 13,86 |
|                            | 3 | 16,14 | 204,58 | 611,86 | 514,04 | 1,19 | 23,00 | 11,36 |
| B500B-16-TEMP-R Prod. 2    | 1 | 16,06 | 202,46 | 635,01 |        | -    | 26,38 | 13,80 |
|                            | 2 | 16,07 | 202,70 | 620,93 | 516,88 | 1,20 | 25,50 | 15,50 |
|                            | 3 | 16,08 | 203,06 | 626,55 |        | -    | 22,50 | 13,40 |
| B400C-20-TEMP-R Prod. 1    | 1 | 19,63 | 302,49 | 557,15 | 436,19 | 1,28 | 28,10 | 17,08 |
|                            | 2 | 19,62 | 302,31 | 558,15 | 438,08 | 1,27 | 30,90 | 21,48 |
|                            | 3 | 19,63 | 302,68 | 557,14 | 434,30 | 1,28 | 29,00 | 17,08 |
| B400C-20-MA-R Prod. 2      | 1 | 20,28 | 323,06 | 563,29 | 416,02 | 1,35 | 31,80 | 20,09 |
|                            | 2 | 20,29 | 323,48 | 561,05 | 415,48 | 1,35 | 32,50 | 20,59 |
|                            | 3 | 20,29 | 323,37 | 561,23 | 418,65 | 1,34 | 29,40 | 28,09 |
| B450C-20-TEMP-R Prod. 2    | 1 | 20,14 | 318,47 | 591,43 | 492,85 | 1,20 | 27,30 | 14,10 |
|                            | 2 | 20,12 | 317,96 | 610,89 | 493,65 | 1,24 | 25,10 | 13,80 |
|                            | 3 | 20,13 | 318,37 | 600,86 | 477,61 | 1,26 | 28,00 | 14,20 |
| B500B-20-TEMP-R Prod. 2    | 1 | 20,06 | 316,01 | 621,81 | 515,33 | 1,21 | 24,40 | 11,50 |
|                            | 2 | 20,03 | 315,20 | 628,68 | 519,75 | 1,21 | 26,40 | 12,20 |
|                            | 3 | 20,05 | 315,81 | 643,01 | 528,07 | 1,22 | 24,10 | 15,30 |
| B400C-25-MA-R Prod. 2      | 1 | 25,20 | 498,70 | 577,35 | 432,77 | 1,33 | 29,20 | 20,04 |
|                            | 2 | 25,20 | 498,81 | 576,05 | 434,64 | 1,33 | 32,00 | 18,44 |
|                            | 3 | 25,21 | 499,05 | 574,98 | 433,44 | 1,33 | 30,40 | 16,74 |
| B450C-25-TEMP-R Prod. 2    | 1 | 25,11 | 495,35 | 629,77 | 505,00 | 1,25 | 24,50 | 14,20 |
|                            | 2 | 25,15 | 496,71 | 626,07 | 507,57 | 1,23 | 26,34 | 15,30 |
|                            | 3 | 25,10 | 494,69 | 638,55 | 501,72 | 1,27 | 25,85 | 14,90 |
| B500B-25-TEMP-R Prod. 2    | 1 | 25,16 | 497,19 | 647,18 | 530,76 | 1,22 | 23,92 | 12,70 |
|                            | 2 | 25,14 | 496,49 | 636,23 | 525,58 | 1,21 | 23,29 | 12,90 |
|                            | 3 | 25,18 | 497,99 | 650,07 | 531,88 | 1,22 | 23,58 | 12,50 |

#### 2.2.2.2 *Experimental tests executed by ISO: results*

**Table 2. 22:** Mean values of the mechanical properties of specimens of different diameters.

| Steel grade/diameter/<br>process/rib/producer | D<br>(mm) | R <sub>e</sub><br>MPa | R <sub>m</sub><br>MPa | A <sub>5</sub><br>% | A <sub>gt</sub><br>% |
|---|-----------|-----------------------|-----------------------|---------------------|----------------------|
| B500A-12-CW-I-Prod. 2                         | 12        | 536                   | 574                   | 15,8                | 6,8                  |
| B500B-25-TEMP-R-Prod.2                        | 25        | 547                   | 663                   | 29,1                | 15,1                 |
| B400C-25-TEMP-R-Prod.2                        | 25        | 447                   | 595                   | 23,9                | 14,7                 |
| B450C-25-TEMP-R-Prod.2                        | 25        | 521                   | 634                   | 24,5                | 13,3                 |
| B400C-16-TEMP-R-Prod.2                        | 16        | 464                   | 608                   | ---                 | 21,3                 |
| B450C-16-TEMP-R-Prod.1                        | 16        | 494                   | 616                   | 24,2                | 18,4                 |
| B500B-16-TEMP-R-Prod.1                        | 16        | 544                   | 667                   | 18,5                | 17,1                 |
| B400C-16-TEMP-R-Prod.1                        | 16        | 430                   | 562                   | 23,2                | 20,1                 |
| B450C-16-TEMP-R-Prod.2                        | 12        | 481                   | 641                   | 15,5                | 12,3                 |

### 2.2.2.3 *Experimental tests executed by UPA: results*

**Table 2. 23:** Mechanical properties of specimens of different diameters tested by UPA's laboratory.

| Steel grade/diameter/<br>process/rib/producer | ID             | Diameter<br>(mm) | R <sub>p0,2</sub><br>(MPa) | R <sub>m</sub><br>(MPa) | R <sub>m</sub> /R <sub>p</sub> | A <sub>gt</sub><br>(%) |
|---|----------------|------------------|----------------------------|-------------------------|--------------------------------|------------------------|
| B400C-16-TEMP-R-Prod. 1                       | B400C-1        | 16               | 437                        | 549                     | 1,26                           | 15,6                   |
|   | B400C-2        | 16               | 435                        | 548                     | 1,26                           | 16                     |
|   | B400C-3        | 16               | 433                        | 550                     | 1,27                           | 15,3                   |
|   | <i>Average</i> |                  | <i>435</i>                 | <i>549,2</i>            | <i>1,26</i>                    | <i>15,6</i>            |
| B450C-16-TEMP-R-Prod. 1                       | B450C-1        | 16               | 541                        | 651                     | 1,2                            | 11,3                   |
|   | B450C-2        | 16               | 532                        | 645                     | 1,21                           | 12,3                   |
|   | <i>Average</i> |                  | <i>536,4</i>               | <i>648</i>              | <i>1,21</i>                    | <i>11,8</i>            |
| B500B-16-TEMP-R-Prod. 1                       | B500B-1        | 16               | 522                        | 637,4                   | 1,22                           | 16,1                   |
|   | B500B-2        | 16               | 524                        | 639,3                   | 1,22                           | 12,6                   |
|   | <i>Average</i> |                  | <i>523</i>                 | <i>638,4</i>            | <i>1,22</i>                    | <i>14,4</i>            |
| B500B-16-STR-R-Prod. 1                        | B500B-4        | 16               | 538                        | 605                     | 1,12                           | 7,3                    |
|   | B500B-11       | 16               | 531,8                      | 610                     | 1,15                           | 7,4                    |
|   | B500B-13       | 16               | 518                        | 599                     | 1,16                           | 7,2                    |
|   | <i>Average</i> |                  | <i>529,3</i>               | <i>604,7</i>            | <i>1,14</i>                    | <i>7,3</i>             |
| B450C-16-TEMP-R-Prod. 2                       | B450C-1        | 16               | 473                        | 628                     | 1,33                           | 15                     |
|   | B450C-2        | 16               | 497                        | 622                     | 1,25                           | 13,1                   |
|   | B450C-3        | 16               | 521                        | 630                     | 1,21                           | 12,8                   |
|   | <i>Average</i> |                  | <i>497</i>                 | <i>626,7</i>            | <i>1,26</i>                    | <i>13,6</i>            |

### 2.2.3 *Mechanical Characterization of steel reinforcing bars under low-cycle fatigue*

#### 2.2.3.1 *Actual literature and standards about LCF tests*

The elaboration of a common procedure for the assessing of the LCF behaviour of rebars needs the definition of four main parameters: the level of imposed deformation ( $\epsilon$ ), the frequency used ( $f$ ), the number of cycles to execute ( $N_c$ ) and the free length of the specimen ( $L_0$ ).

The free length of the specimen strongly influences the results of the experimental tests, since buckling phenomena due to compression axial loads can lead to premature unexpected failures of the rebars; in order to avoid this problem, actual standards for r.c. constructions (EN 1998-1:2005, D.M. 14/01/2008) prescribe the adoption of opportune limits for the free length of reinforcements between stirrups, that shall be lower than 6 or 8 times the diameter for buildings respectively designed in high or low ductility class. A detailed investigation of the influence of the free length on the experimental tests' results was provided by Mander et al. (1994); moreover, in Mander's experimental tests, the frequency adopted varied between 0.025 and 0.15 Hz, resulting in an average strain rate of 0.005/s.

Other detailed studies on the cyclic behaviour of steel reinforcements and on the influence of the ratio  $L_0/\phi$  were executed by Cosenza et al. (2008) on smooth bars, used in existing r.c. buildings. Different levels of imposed deformations ( $\pm 1\%$ ,  $\pm 3\%$  and  $\pm 5\%$ ) and different ratios  $L_0/\phi$  (equal to 5, 8, 15 and more) were used, showing a behaviour similar to the one of ribbed bars, except for the critical ratio, equal to 8 instead of 11; the values provided were consequently different from the ones given by Mander et al. (1994). As regards the influence of the strain rate on the results of experimental tests, Crespi (2002) executed preliminary LCF tests on bars diameter 14.0 mm, free length of the specimen equal to  $10\phi$  and using four different loading rates (the time of a complete symmetrical cycle ranges from 600 s to 0.60 s). The results of the tests evidenced that, except for a small shift due to the machine, the cyclic behaviour was nearly independent from the loading rate; moreover, the first quarter of the cyclic tests was very similar to the monotonic behaviour for all the loading rate considered and only the fastest test, with a period of 0.6 s, showed a slight increase of the yield force.

As a consequence of what already presented, Crespi (2002) executed low-cycle fatigue tests on bars of diameter equal to 14 mm and 20 mm using a frequency variable between 1.0 and 3.0 Hz, different levels of imposed deformation, respectively equal to  $\pm 1\%$ ,  $\pm 2.5\%$  and  $\pm 4\%$  and a free length of the specimen of 10 diameters. The tests executed confirmed what presented by Mander et al. (1994): also for larger diameters, ratios  $L_0/\phi$  higher than 6 lead to evident effects of inelastic buckling on the bar with the decrease of compressive strength even below the yielding limit.

Brown and Kunnath (2004) executed low-cycle fatigue tests on steel reinforcements with nominal diameter variable between 20 and 25 mm, imposed deformation equal to  $\pm 1.5\%$ ,  $\pm 1.75\%$ ,  $\pm 2.0\%$ ,  $\pm 2.25\%$ ,  $\pm 2.5\%$ ,  $\pm 2.75\%$  and  $\pm 3.0\%$  and free length of the specimens equal to six times the diameter. The results of experimental tests, analyzed through two cumulative damage parameters, i.e. the total energy to failure and the number of half cycles to failure, evidenced that bars with larger diameters provided a longer fatigue life also for lower strain amplitudes while with the increase of the imposed strain in the plastic range, on the other hand bars with smaller diameter presented a longer fatigue life. Moreover, the tests showed that the deterioration of fatigue life with increasing strain is more severe for larger-diameter bars. As a consequence, in the current literature the largest part of experimental LCF tests were executed using a frequency variable between 0.05 and 2.0 Hz; anyway, for simplifying the procedure and also for specific technical requirements of the testing machines, in some cases the frequency was also lower: Rodriguez et al. (1999) for example, executed low-cycle fatigue tests on steel reinforcing bars using a constant frequency of 0.005 Hz, Hawileh et al. (2010) used a testing frequency of 0.05 Hz. As regards the strain levels, the imposed deformation used generally varied between  $\pm 1.5\%$  and  $\pm 3.0\%$  and, finally, the free length of the specimens was kept near the limit of the critical ratio for inelastic buckling.

For what concerns actual standards on LCF tests, only Spain and Portugal prescribe the execution of low-cycle fatigue tests for steel reinforcing bars; the two protocols, included in UNE 36065 EX:2000 for Spain and in LNEC E 455-2008 for Portugal, show differences from one another and, moreover, differ from the draft of LCF testing protocol included in the revision of European standard EN 10080:2005 (prEN10080:2012). Spanish standard (UNE 36065 EX:2000) prescribes the execution of three complete symmetric hysteresis cycles, using a frequency variable from 1 to 3 Hz and applying at the ends of the sample the levels of deformations (tension and compression) indicated in table 2.28. The deformation imposed is determined in relation to the diameter of the bar, as well as the length of the samples. The test is considered satisfied if the samples are able to sustain the three complete cycles without encountering problems of total or partial failures. Portuguese standard (LNEC E455:2008) prescribes the execution of 10 complete symmetric hysteretic cycles, using a frequency equal to 3.0 Hz and applying at the ends of the sample following deformations of tension and compression. The test can be considered satisfied if the samples arrive to the end of the testing procedure without encountering problems of cracking total or partial failures. The draft of the revision of EN10080:2005 (prEN10080:2012) prescribes the execution of 5 complete hysteretic symmetric tension/compression cycles using a testing frequency lower than 3.0 Hz, an imposed deformation equal to  $\pm 2.5\%$  and a free length of the specimen, constant for all the considered diameters, equal to  $10\phi$ .

**Table 2. 24:** Low-cycle Fatigue testing procedures according to UNE 36065 EX:2000 and LNEC E455:2008.

| UNE 36065 EX:2000.    |             |                 | LNEC E455:2008      |                              |
|-----------------------|-------------|-----------------|---------------------|------------------------------|
| Nominal diameter [mm] | Free length | Deformation [%] | Frequency           | 3 Hz                         |
| $d \leq 16$           | 5 d         | $\pm 4.0$       | Imposed deformation | $\pm 2.5\%$                  |
| $16 < d < 25$         | 10 d        | $\pm 2.5$       | Free length         | 10d                          |
| $25 \leq d$           | 15 d        | $\pm 1.5$       | Temperature         | $10^{\circ} \div 35^{\circ}$ |

### 2.2.3.2 Elaboration of a LCF testing protocol for steel reinforcements

#### Preliminary evaluation of the influence of the strain rate

A preliminary set of experimental low-cycle fatigue tests were executed in order to evaluate the effective influence of the strain rate on test's results, in order to prove what already presented in the current literature (Crespi 2002). Bars of diameter 16 mm, steel grade B450C (yielding strength 450 MPa and ductility class C) were selected; two different strain rates were considered for the tests:

- a first strain rate similar to the one suggested by actual Spanish and Portuguese standards;
- a second strain rate corresponding to the ones used in the current literature (about 0.05 Hz).

Two different levels of imposed deformation, respectively equal to  $\pm 2.5\%$  and  $\pm 4.0\%$  were considered and the number of cycles to execute ( $N_c$ ) was fixed up to 20.

Two different values of the free length  $L_0$  were adopted, respectively equal to 6 and 8 times the diameter of the specimen; the selected values of  $L_0$  correspond to the maximum stirrups' spacing imposed by Eurocode 8 (EN 1998-1:2005) for r.c. structures: in particular  $L_0=6\phi$  is used for steel reinforcing bars in buildings designed in high ductility class and  $L_0=8\phi$  for steel reinforcing bars in buildings designed in low ductility class. The preliminary protocol used for the evaluation of the strain

rate's influence is summarized in the table 2.27. The results of the experimental tests were evaluated in terms of dissipated energy (W) and number of cycles executed ( $N_c$ ).

**Table 2. 25:** Preliminary protocol for the investigation of strain rate influence on low-cycle fatigue behaviour.

|                     |                                    |   |
|---------------------|------------------------------------|---|
| Testing frequency   | 1÷3 Hz (selected 2.0 Hz)           | <i>UNE 36065 ex:2000 / LNEC E455:2008</i> |
|                     | ~ 0.005÷0.15 Hz (selected 0.05 Hz) | <i>current literature</i>                 |
| Imposed deformation | ± 2.5%                             | -   |
|                     | ± 4.0%                             | -   |
| N° of cycles        | Up to failure of at least 20       | -   |
| Bar Diameter $\phi$ | 16 mm                              | -   |
| Free Length         | 6 $\phi$                           | <i>High Ductility Class</i>               |
|                     | 8 $\phi$                           | <i>Low Ductility Class</i>                |

In the figures 2.4 the stress-strain diagrams obtained from LCF tests with imposed deformation equal to  $\pm 2.5\%$  and frequency equal to 0.05 and 2.0 Hz are presented for free length of the specimens respectively equal to 6 and 8 times the diameter; the results in terms of total dissipated energy (and dissipated energy per cycle) are presented in table 2.27.

The dissipated energy density per cycle was evaluated according to the Expression 2.1 (Apostolopoulos et al. 2006), as an approximation from the engineering stress-strain curves.

$$W = \int \sigma d\varepsilon \quad (2.1)$$

As visible from table 2.27, the difference in terms of total dissipated energy (20 cycles or less if premature failure of the rebar occurs) is generally lower than 10%; percentage differences were evaluated only if significative, consequently not considering the last cycles that strongly suffer damaging and deterioration. In general all the specimens are able to sustain at least 15 symmetrical cycles, but a progressive decrease in terms of dissipated energy is evident after the first 5-6 cycles.

**Table 2. 26:** Experimental results of LCF tests for different values of testing frequency.

| L <sub>0</sub> =6 $\phi$<br>Frequency | Energy/cycle  |               | Difference         | L <sub>0</sub> =8 $\phi$<br>2,0 Hz | Energy/cycle  |                    | Difference |
|---------------------------------------|---------------|---------------|--------------------|------------------------------------|---------------|--------------------|------------|
|                                       | 2,0 Hz        | 0,05 Hz       |                    |                                    | 0,05 Hz       | Difference         |            |
| [-]                                   | MPa           | MPa           | [%]                | MPa                                | MPa           | [%]                |            |
| 1                                     | 31,67         | 32,96         | 3,91%              | 31,58                              | 33,74         | 6,39%              |            |
| 2                                     | 31,54         | 33,02         | 4,49%              | 31,67                              | 29,82         | 6,18%              |            |
| 3                                     | 30,90         | 32,43         | 4,71%              | 28,29                              | 27,78         | 1,83%              |            |
| 4                                     | 29,44         | 31,76         | 7,29%              | 25,68                              | 25,21         | 1,86%              |            |
| 5                                     | 29,33         | 31,10         | 5,67%              | 23,68                              | 23,25         | 1,84%              |            |
| 6                                     | 28,35         | 30,51         | 7,07%              | 22,10                              | 21,70         | 1,87%              |            |
| 7                                     | 27,84         | 29,92         | 6,93%              | 20,79                              | 20,38         | 2,01%              |            |
| 8                                     | 27,28         | 29,36         | 7,11%              | 19,63                              | 19,16         | 2,41%              |            |
| 9                                     | 26,22         | 28,81         | 8,99%              | 18,54                              | 17,99         | 3,05%              |            |
| 10                                    | 25,97         | 28,25         | 8,08%              | 17,45                              | 16,92         | 3,15%              |            |
| 11                                    | 25,75         | 27,68         | 6,97%              | 16,30                              | 15,97         | 2,07%              |            |
| 12                                    | 25,21         | 27,06         | 6,84%              | 14,96                              | 15,11         | 0,98%              |            |
| 13                                    | 24,56         | 26,34         | 6,77%              | 13,30                              | 14,27         | 6,75%              |            |
| 14                                    | 23,85         | 25,49         | 6,43%              | 10,47                              | 13,39         | -                  |            |
| 15                                    | 23,23         | 24,24         | 4,18%              | 5,45                               | 12,32         | -                  |            |
| 16                                    | 22,57         | 21,60         | 4,48%              | -                                  | 11,06         | -                  |            |
| 17                                    | 21,83         | 15,11         | -                  | -                                  | 8,59          | -                  |            |
| 18                                    | 20,89         | 2,13          | -                  | -                                  | 3,28          | -                  |            |
| 19                                    | 19,62         | -             | -                  | -                                  | -             | -                  |            |
| 20                                    | 15,20         | -             | -                  | -                                  | -             | -                  |            |
| <i>total</i>                          | <i>511,25</i> | <i>477,76</i> | <i>7,01% (tot)</i> | <i>299,91</i>                      | <i>329,95</i> | <i>9,10% (tot)</i> |            |

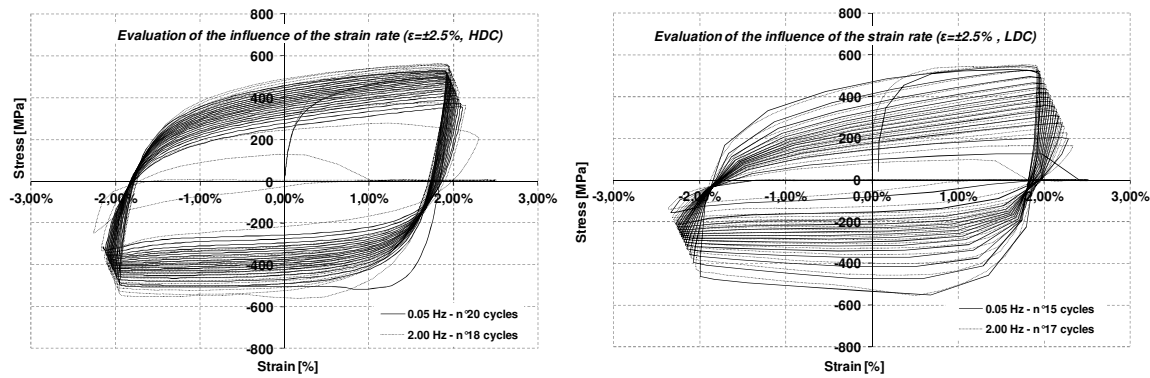


**Figure 2. 4:** a) Stress-strain curve from LCF tests on specimens B450C-Tempcore (producer 2) 16 mm, for imposed deformation equal to  $\pm 2.5\%$ , free length equal to 6 diameters and frequency equal to 0.05 and 2.0 Hz and b) Stress-strain curve from LCF tests on specimens B450C-Tempcore (producer 2) 16 mm, for imposed deformation equal to  $\pm 2.5\%$ , free length equal to 8 diameters and frequency equal to 0.05 and 2.0 Hz.

***Preliminary protocol for the execution of LCF tests on steel reinforcing bars***

A preliminary protocol for the execution of LCF tests on the selected representative steel reinforcements presented in table 2.20 was elaborated. The testing frequency to use in the mechanical tests was generally fixed equal to 2.0 Hz, with possible reduction up to 0.05 Hz in relation to the machine's requirements for large diameter ( $\geq 16.0$  mm). Two levels of imposed deformation, equal to  $\pm 2.5\%$  and  $\pm 4.0\%$  were adopted for the execution of at least 20 symmetrical hysteretic cycles; the free length of the sample was assumed equal to 6 or 8 diameters, in order to perfectly represent the condition of longitudinal rebars in r.c. elements of buildings designed in HDC or LDC according to Eurocode 8 (EN 1998-1:2005). The preliminary protocol can be summarized as follows:

- frequency  $f = 2.0$  Hz (0.05 Hz will be also used for bar of large diameter);
- two levels of imposed deformation:  $\epsilon_1 = \pm 2.5\%$  -  $\epsilon_2 = \pm 4.0\%$ ;
- number of cycles fixed equal to 20 (minimum);
- two different values of the free length:  $L_{0H} = 6\phi$  (HDC) -  $L_{0L} = 8\phi$  (LDC).

The level of elongation imposed to the bar, the free length and the frequency used in the tests of steel reinforcements are summarized in table 2.28.

**Table 2. 27:** Testing procedure for different diameters.

| Diameter [mm] | Frequency [Hz] | Free length $L_0$ | Imposed deformation [%] $\epsilon$ | $\Delta L$ [mm] $\Delta l$ |
|---------------|----------------|-------------------|------------------------------------|----------------------------|
| 20            | 0.05           | $6\phi$           | $\pm 2.5\%$                        | 3                          |
|               |                |                   | $\pm 4.0\%$                        | 4.8                        |
|               |                | $8\phi$           | $\pm 2.5\%$                        | 4                          |
|               |                |                   | $\pm 4.0\%$                        | 6.4                        |
| 16            | 2              | $6\phi$           | $\pm 2.5\%$                        | 2.4                        |
|               |                |                   | $\pm 4.0\%$                        | 3.84                       |
|               |                | $8\phi$           | $\pm 2.5\%$                        | 3.2                        |
|               |                |                   | $\pm 4.0\%$                        | 5.12                       |
| 12            | 2              | $6\phi$           | $\pm 2.5\%$                        | 1.8                        |
|               |                |                   | $\pm 4.0\%$                        | 2.88                       |
| 12            | 2              | $8\phi$           | $\pm 2.5\%$                        | 2.4                        |
|               |                |                   | $\pm 4.0\%$                        | 3.84                       |
| 8             | 2              | $6\phi$           | $\pm 2.5\%$                        | 1.2                        |
|               |                |                   | $\pm 4.0\%$                        | 1.92                       |
|               |                | $8\phi$           | $\pm 2.5\%$                        | 1.6                        |
|               |                |                   | $\pm 4.0\%$                        | 2.56                       |

### 2.2.3.3 *Experimental LCF tests on steel reinforcements*

The results of experimental Low-Cycle Fatigue tests are presented in terms of maximum and minimum strength and deformation and dissipated energy per cycle.

#### *Results obtained from experimental tests executed by UniPI*

**Table 2. 28:** Experimental results of LCF tests on bars.

| Steel grade/diameter/<br>process/rib/producer | ID<br>[-] | L <sub>0</sub><br>[mm] | f<br>[Hz] | Max ε<br>[%] | Min ε<br>[%] | Max σ<br>[MPa] | Min σ<br>[MPa] | Tot. Energy<br>[MPa] | N <sub>cycles</sub><br>[-] |
|---|-----------|------------------------|-----------|--------------|--------------|----------------|----------------|----------------------|----------------------------|
| B500B-8-STR-R-<br>Prod.1                      | 1         | 48                     | 2         | 2,06%        | -2,15%       | 562,76         | -627,82        | 498,29               | 20                         |
|   | 2         | 48                     | 2         | 4,03%        | -3,81%       | 537,31         | -564,44        | 356,76               | 11                         |
|   | 3         | 64                     | 2         | 2,51%        | -2,38%       | 553,42         | -594,18        | 312,7                | 17                         |
|   | 4         | 64                     | 2         | 4,02%        | -3,91%       | 584,82         | -604,68        | 317,77               | 9                          |
| B500A-8-CW-R-<br>Prod.2                       | 1         | 48                     | 2         | 2,13%        | -2,24%       | 495,5          | -627,82        | 498,29               | 20                         |
|   | 2         | 48                     | 2         | 4,03%        | -3,89%       | 499,07         | -434,3         | 322,55               | 14                         |
|   | 3         | 64                     | 2         | 2,51%        | -2,44%       | 512,91         | -431,96        | 246,82               | 19                         |
|   | 4         | 64                     | 2         | 4,02%        | -3,94%       | 514,27         | -395,66        | 226,91               | 12                         |
| B500A-8-CW-I-<br>Prod.1                       | 1         | 72                     | 2         | 2,18%        | -2,26%       | 522,52         | -505,04        | 427,47               | 20                         |
|   | 2         | 72                     | 2         | 4,02%        | -3,90%       | 531,73         | -456,03        | 328                  | 15                         |
|   | 3         | 64                     | 2         | 2,51%        | -2,43%       | 528,64         | -460,01        | 273,8                | 19                         |
|   | 4         | 64                     | 2         | 4,01%        | -3,95%       | 544,77         | -471,05        | 237,47               | 10                         |
| B400C-8-TEMP-R-<br>Prod.1                     | 1         | 48                     | 2         | 2,06%        | -2,16%       | 472,06         | -487,96        | 461,39               | 20                         |
|   | 2         | 48                     | 2         | 4,03%        | -3,82%       | 499,48         | -482,16        | 393,23               | 12                         |
|   | 3         | 64                     | 2         | 2,26%        | -2,35%       | 461,53         | -460,54        | 306,01               | 20                         |
|   | 4         | 64                     | 2         | 4,01%        | -3,92%       | 487,37         | -435,23        | 293,61               | 12                         |
| B500B-8-STR-R-<br>Prod.1                      | 1         | 48                     | 2         | 2,03%        | -2,20%       | 558,36         | -487,57        | 458,7                | 20                         |
|   | 2         | 48                     | 2         | 4,02%        | -3,85%       | 567,67         | -520,4         | 376,91               | 12                         |
|   | 3         | 64                     | 2         | 2,24%        | -2,35%       | 571,29         | -454,28        | 334,18               | 20                         |
|   | 4         | 64                     | 2         | 4,01%        | -3,91%       | 582,29         | -458,67        | 277,38               | 10                         |
| B450C-8-STR-R-<br>Prod.1                      | 1         | 48                     | 2         | 2,00%        | -2,17%       | 511,35         | -490,59        | 456,06               | 20                         |
|   | 2         | 48                     | 2         | 4,03%        | -3,78%       | 516,25         | -456,14        | 428,7                | 11                         |
|   | 3         | 64                     | 2         | 2,14%        | -2,29%       | 504,78         | -415,38        | 339,41               | 20                         |
|   | 4         | 64                     | 2         | 4,01%        | -3,89%       | 525,32         | -410,67        | 332,04               | 16                         |
| B500A-12-CW-R-<br>Prod.2                      | 1         | 72                     | 2         | 2,51%        | -2,29%       | 464,8          | -459,84        | 355,63               | 20                         |
|   | 2         | 72                     | 2         | 4,02%        | -3,86%       | 502,81         | -459,82        | 255,6                | 8                          |
|   | 3         | 96                     | 2         | 2,51%        | -2,41%       | 513,38         | -441,74        | 250,42               | 17                         |
|   | 4         | 96                     | 2         | 4,01%        | -3,92%       | 509,23         | -439,82        | 187,19               | 8                          |
| B450C-12-STR-R-<br>Prod.2                     | 1         | 72                     | 2         | 2,09%        | -2,23%       | 492,45         | -452,12        | 446,23               | 20                         |
|   | 2         | 72                     | 2         | 4,01%        | -3,80%       | 544,57         | -388,47        | 341,63               | 14                         |
|   | 3         | 96                     | 2         | 2,26%        | -2,36%       | 495,29         | -426,99        | 351,04               | 20                         |
|   | 4         | 96                     | 2         | 4,01%        | -3,93%       | 506,25         | -361,73        | 270,3                | 12                         |
| B500B-16-TEMP-R<br>Prod. 2                    | 1         | 96                     | 2         | 2,09%        | -2,18%       | 529,38         | -532,07        | 488,4                | 20                         |
|   | 2         | 96                     | 2         | 4,00%        | -3,88%       | 580,27         | -478,11        | 355,53               | 11                         |
|   | 3         | 128                    | 2         | 2,51%        | -2,38%       | 524,06         | -540,25        | 285,09               | 14                         |
|   | 4         | 128                    | 2         | 4,02%        | -3,92%       | 506,88         | -537,26        | 213,15               | 7                          |
| B400C-16-TEMP-R<br>Prod. 1                    | 1         | 96                     | 2         | 2,50%        | -2,29%       | 467,88         | -452,24        | 385,78               | 18                         |
|   | 2         | 96                     | 2         | 4,01%        | -3,84%       | 488,34         | -437,37        | 276,43               | 8                          |
|   | 3         | 128                    | 2         | 2,50%        | -2,41%       | 461,31         | -442,7         | 258,2                | 15                         |
|   | 4         | 128                    | 2         | 4,00%        | -3,93%       | 462,93         | -403,85        | 245,36               | 10                         |
| B450C-16-TEMP-R<br>Prod.1.1                   | 1         | 96                     | 2         | 2,07%        | -2,10%       | 616,66         | -575,38        | 558,67               | 19                         |
|   | 2         | 96                     | 2         | 4,01%        | -3,77%       | 631,22         | -591,83        | 378,13               | 9                          |
|   | 3         | 128                    | 2         | 2,58%        | -2,39%       | 572,16         | -607,34        | 261,5                | 13                         |
|   | 4         | 128                    | 2         | 4,02%        | -3,91%       | 613,85         | -540,82        | 471,51               | 11                         |
| B450C-16-TEMP-R<br>Prod.1.3                   | 1         | 96                     | 2         | 2,19%        | -2,10%       | 537,65         | -557,82        | 532,15               | 19                         |
|   | 2         | 96                     | 2         | 4,03%        | -3,76%       | 465,48         | -515,36        | 550,99               | 14                         |
|   | 3         | 128                    | 2         | 2,51%        | -2,37%       | 501,91         | -550,97        | 291,96               | 15                         |
|   | 4         | 128                    | 2         | 4,50%        | -3,92%       | 598,09         | -491,88        | 380,03               | 9                          |

|                              |   |     |      |       |        |        |         |        |    |
|------------------------------|---|-----|------|-------|--------|--------|---------|--------|----|
| B450C-16-TEMP-R<br>Prod.1.2  | 1 | 96  | 2    | 2,23% | -2,18% | 483,44 | -508,73 | 516,86 | 18 |
|                              | 2 | 96  | 2    | 4,01% | -3,80% | 550,74 | -483,86 | 726,01 | 18 |
|                              | 3 | 128 | 2    | 2,51% | -2,43% | 482,54 | -508,39 | 353,75 | 18 |
|                              | 4 | 128 | 2    | 4,01% | -3,93% | 494,73 | -477,06 | 230,29 | 9  |
| B400C-16-MA-R<br>Prod. 2     | 1 | 96  | 2    | 2,12% | -2,18% | 466,28 | -465,93 | 429,61 | 20 |
|                              | 2 | 96  | 2    | 4,03% | -3,81% | 450,84 | -465,99 | 418,72 | 12 |
|                              | 3 | 128 | 2    | 2,51% | -2,34% | 535,65 | -418,31 | 377,57 | 17 |
|                              | 4 | 128 | 2    | 4,05% | -3,93% | 475,19 | -445,46 | 211,11 | 8  |
| B450C-16-TEMP-R<br>Prod. 2   | 1 | 96  | 2    | 2,51% | -2,26% | 562,5  | -560,12 | 477,75 | 18 |
|                              | 2 | 96  | 2    | 2,51% | -2,41% | 552,44 | -555,05 | 329,95 | 8  |
|                              | 3 | 128 | 2    | 4,10% | -3,81% | 531,52 | -502,24 | 316,67 | 18 |
|                              | 4 | 128 | 2    | 4,11% | -3,92% | 510,48 | -471,7  | 224,46 | 7  |
| B500B-16-TEMP-R<br>Prod. 1.1 | 1 | 96  | 2    | 2,50% | -2,21% | 565,59 | -571,8  | 488,44 | 19 |
|                              | 2 | 96  | 2    | 4,02% | -3,78% | 583,6  | -586,71 | 328,93 | 8  |
|                              | 3 | 128 | 2    | 2,51% | -2,39% | 560,39 | -566,43 | 293,63 | 15 |
|                              | 4 | 128 | 2    | 4,02% | -3,90% | 625,72 | -510,02 | 360,65 | 10 |
| B500B-16-TEMP-R<br>Prod. 1.2 | 1 | 96  | 2    | 2,10% | -2,00% | 577,66 | -605,08 | 570,67 | 19 |
|                              | 2 | 96  | 2    | 4,01% | -3,74% | 583,01 | -601,27 | 338,79 | 8  |
|                              | 3 | 128 | 2    | 2,51% | -2,36% | 564,78 | -585,17 | 325,64 | 15 |
|                              | 4 | 128 | 2    | 4,02% | -3,90% | 587,68 | -541,79 | 212,8  | 6  |
| B500B-16-TEMP-R<br>Prod. 1.3 | 1 | 96  | 2    | 2,08% | -2,05% | 530,34 | -534,52 | 529,94 | 19 |
|                              | 2 | 96  | 2    | 4,14% | -3,79% | 572,58 | -543,1  | 407,67 | 9  |
|                              | 3 | 128 | 2    | 2,61% | -2,39% | 513,79 | -502,47 | 268,29 | 13 |
|                              | 4 | 128 | 2    | 4,01% | -3,93% | 550,21 | -524,26 | 246,62 | 8  |
| B400C-20-TEMP-R-<br>Prod. 1  | 1 | 120 | 0,5  | 2,12% | -2,10% | 411,26 | -416,88 | 407,64 | 20 |
|                              | 2 | 120 | 0,5  | 3,67% | -3,60% | 458,1  | -436,31 | 230,29 | 7  |
|                              | 3 | 160 | 0,5  | 3,87% | -3,85% | 368    | -430,79 | 182,53 | 7  |
| B400C-20-MA-R-<br>Prod. 2    | 1 | 120 | 0,5  | 2,51% | -2,02% | 430,39 | -448,98 | 431,26 | 20 |
|                              | 2 | 120 | 0,5  | 4,01% | -3,57% | 495,13 | -501,11 | 351,34 | 9  |
|                              | 3 | 160 | 0,5  | 2,38% | -2,32% | 466,15 | -450,66 | 320,86 | 18 |
|                              | 4 | 160 | 0,5  | 3,83% | -3,84% | 446,75 | -438,95 | 231,42 | 9  |
| B450C-20-TEMP-R-<br>Prod. 2  | 1 | 120 | 0,5  | 1,86% | -1,89% | 497,74 | -521,42 | 493,38 | 19 |
|                              | 2 | 120 | 0,5  | 4,01% | -3,52% | 521,47 | -535,9  | 283,77 | 7  |
|                              | 3 | 160 | 0,5  | 2,42% | -2,31% | 509,34 | -532,42 | 411,05 | 19 |
|                              | 4 | 160 | 0,5  | 3,92% | -3,81% | 493,8  | -531,24 | 212,19 | 7  |
| B500B-20-TEMP-R-<br>Prod. 2  | 1 | 120 | 2    | 2,00% | -2,03% | 570,51 | -511,41 | 540,62 | 20 |
|                              | 2 | 120 | 0,05 | 3,66% | -3,62% | 597,48 | -504,72 | 363,85 | 9  |
|                              | 3 | 160 | 0,5  | 2,56% | -2,24% | 545,51 | -518,43 | 362,08 | 16 |
|                              | 4 | 160 | 0,05 | 3,96% | -3,84% | 509,5  | -503,19 | 222,77 | 7  |

*Results obtained from experimental tests executed by ISQ*

**Table 2. 29:** Experimental results of LCF on specimens tested by ISQ.

| Steel grade/diameter/<br>process/rib/ producer | ID        | f    | L <sub>0</sub> | Δε   | N <sub>cycles</sub> / break | Tot. Energy |        |
|--|-----------|------|----------------|------|-----------------------------|-------------|--------|
|  |           | [Hz] | [mm]           | [%]  | [-]                         | [MPa]       | [MPa]  |
| B500A-12-CW-R-Prod.2                           | D9/D10    | 2    | 72             | ±2.5 | 20/20 No Break              | 382,97      | 335,53 |
|  | D12/D14   |      |                | ±4.0 | 16/15 Break                 | 343,47      | 323,22 |
|  | D3/D4     |      | 96             | ±2.5 | 14/11 Break                 | 268,06      | 214,28 |
|  | D5/D6     |      |                | ±4.0 | 20/12 Break                 | 227,30      | 212,51 |
| B450C-12-STR-R-Prod.1                          | I19/I21   | 2    | 72             | ±2.5 | 20/20 No Break              | 481,58      | 466,50 |
|  | I22/I23   |      |                | ±4.0 | 10/9 Break                  | 347,21      | 310,08 |
|  | I26/I28   |      | 96             | ±2.5 | 16/13 Break                 | 359,51      | 291,89 |
|  | I29/I30   |      |                | ±4.0 | 7/5 Break                   | 256,41      | 193,14 |
| B400C-16-TEMP-R-Prod.1                         | SE9/S10   | 2    | 96             | ±2.5 | 18/18 Break                 | 440,90      | 425,95 |
|  | SE12/SE13 |      |                | ±4.0 | 6/5 Break                   | 250,32      | 202,74 |
|  | S1/S14    |      | 128            | ±2.5 | 13/11 Break                 | 239,33      | 208,15 |
|  | S21/S23   |      |                | ±4.0 | 5/4 Break                   | 151,34      | 117,98 |

|                        |           |     |           |                       |        |        |
|------------------------|-----------|-----|-----------|-----------------------|--------|--------|
| B400C-16-MA-R-Prod.2   | C1/C2     | 96  | $\pm 2.5$ | 20 break /20 no break | 478,50 | 509,62 |
|                        | C3/C4     |     | $\pm 4.0$ | 12/13 Break           | 357,22 | 334,36 |
|                        | C9/C10    | 128 | $\pm 2.5$ | 15/16 Break           | 271,25 | 290,11 |
|                        | C11/C12   |     | $\pm 4.0$ | 16/8 Break            | 244,10 | 205,10 |
| B450C-16-TEMP-R-Prod.1 | R1/R7     | 96  | $\pm 2.5$ | 20 Break/20 No Break  | 474,17 | 520,01 |
|                        | R14/R17   |     | $\pm 4.0$ | 13/13 Break           | 389,69 | 399,05 |
|                        | R4/R26    | 128 | $\pm 2.5$ | 19/18 Break           | 335,28 | 306,17 |
|                        | R27/R28   |     | $\pm 4.0$ | 12/12 Break           | 249,01 | 246,87 |
| B500B-16-TEMP-R-Prod.1 | P10B      | 96  | $\pm 2.5$ | 20 No Break           | 532,75 |        |
|                        | P17B      |     | $\pm 4.0$ | 14 Break              | 373,70 |        |
|                        | P5B       | 128 | $\pm 2.5$ | 17 Break              | 323,22 |        |
|                        | P12B      |     | $\pm 4.0$ | 11 Break              | 228,71 |        |
| B400C-25-MA-R-Prod.2   | 1LCF/2LCF | 150 | $\pm 2.5$ | -                     | -      |        |
|                        | -         |     | $\pm 4.0$ | -                     | -      |        |
|                        | B73/B74   | 200 | $\pm 2.5$ | 17/13 Break           | 390,06 | 271,35 |
| B79/B80                | $\pm 4.0$ |     | 6/5 Break | 218,17                | 185,89 |        |
| B450C-25-TEMP-R-Prod.2 | B81/B82   | 150 | $\pm 2.5$ | 19/19 No Break        | 571,52 | 525,92 |
|                        | B83/B84   |     | $\pm 4.0$ | B83- 9 Break          | -      | -      |
|                        | B89/B90   | 200 | $\pm 2.5$ | 14/17 Break           | 313,29 | 349,48 |
|                        | B91/B95   |     | $\pm 4.0$ | 6/7 Break             | 223,62 | 256,33 |
| B500B-25-TEMP-R-Prod.2 | B97/B98   | 150 | $\pm 2.5$ | 22/20 No Break        | 611,84 | 538,76 |
|                        | B101/B103 |     | $\pm 4.0$ | 19/9 Break            | 472,43 | 417,33 |
|                        | B109/B110 | 200 | $\pm 2.5$ | 14/19 Break           | 298,69 | 374,90 |
|                        | B111/B112 |     | $\pm 4.0$ | 9/8 Break             | 258,03 | 233,46 |

*Results obtained from experimental tests executed by UPA*

**Table 2. 30:** Experimental results of LCF on specimens tested by UPA.

| B450C-12- STR Prod. 1 |          |                  |                      |                       |                      |              |             |
|-----------------------|----------|------------------|----------------------|-----------------------|----------------------|--------------|-------------|
| ID                    | $L_0$    | $\Delta\epsilon$ | $\sigma_{max}$ [MPa] | $\sigma_{MINe}$ [MPa] | $\sigma_{min}$ [MPa] | $N_{cycles}$ | Energy[MPa] |
| B450C-41              |          |                  | 542                  | -537,7                | -544,4               | 38           | 893         |
| B450C-42              |          |                  | 534,5                | -533,5                | -539                 | 32           | 741         |
| B450C-43              | 6 $\Phi$ |                  | 543,7                | -554,5                | -558,2               | 36           | 838         |
| B450C-44              |          |                  | 540,6                | -539                  | -544,5               | 37           | 834,5       |
| B450C-45              |          |                  | 542,4                | -544,8                | -554                 | 35           | 803         |
| B450C-46              |          | $\pm 2,5\%$      | 581,8                | -462,9                | -510,4               | 24           | 462,5       |
| B450C-47              |          |                  | 584,6                | -488                  | -532,7               | 22           | 452         |
| B450C-48              | 8 $\Phi$ |                  | 585,3                | -465,3                | -515,6               | 23           | 442,5       |
| B450C-49              |          |                  | 587                  | -495                  | -532,4               | 20           | 407         |
| B450C-50              |          |                  | 582,7                | -475,5                | -523,7               | 21           | 431,2       |
| B450C-51              |          |                  | 580                  | -409,8                | -514,3               | 8            | 268         |
| B450C-52              |          |                  | 580,7                | -401,4                | -511,8               | 9            | 289         |
| B450C-53              | 8 $\Phi$ |                  | 571,6                | -405,3                | -506,8               | 8            | 276,5       |
| B450C-54              |          |                  | 578,6                | -414,6                | -504,4               | 9            | 302,7       |
| B450C-55              |          |                  | 581                  | -399                  | -500,8               | 7            | 238         |
| B450C-56              |          | $\pm 4\%$        | 579                  | -561,2                | -574                 | 12           | 489,8       |
| B450C-57              |          |                  | 588,6                | -577                  | -592,6               | 12           | 498,7       |
| B450C-58              | 6 $\Phi$ |                  | 586                  | -574                  | -584,5               | 11           | 495         |
| B450C-59              |          |                  | 583,2                | -560                  | -576,3               | 13           | 527         |
| B450C-60              |          |                  | 591                  | -582                  | -594,4               | 11           | 485         |

| B500B-12- STR - Prod. 1 |       |        |         |         |    |        |
|-------------------------|-------|--------|---------|---------|----|--------|
| B500B -41               |       | 566,38 | -546,2  | -553,6  | 48 | 1152,8 |
| B500B- 42               |       | 580,72 | -554    | -563,1  | 49 | 1141,7 |
| B500B -43               | 6Φ    | 568,8  | -530,5  | -542    | 37 | 878,4  |
| B500B -44               |       | 568,7  | -539,5  | -546,6  | 48 | 1144,7 |
| B500B -45               |       | 565,3  | -531,2  | -530,3  | 42 | 976,5  |
| B500B-46                | ±2,5% | 545,2  | -482,4  | -510,5  | 20 | 388    |
| B500B-47                |       | 545,1  | -480,8  | -508,4  | 20 | 391    |
| B500B-48                | 8Φ    | 549,4  | -473,8  | -511,7  | 19 | 381    |
| B500B-49                |       | 549,7  | -462,7  | -507,6  | 23 | 423    |
| B500B-50                |       | 549,5  | -475,5  | -507,5  | 19 | 375    |
| B500B-51                |       | 607,5  | -404,7  | -503,1  | 11 | 348    |
| B500B-52                |       | 606,5  | -386,5  | -498    | 9  | 276    |
| B500B-53                | 8Φ    | 598,5  | -395,7  | -502,6  | 10 | 309    |
| B500B-54                |       | 614,4  | -417,5  | -522,6  | 9  | 311,6  |
| B500B-55                | ±4%   | 607,4  | -404,2  | -502,3  | 9  | 290    |
| B500B-56                |       | 610    | -546,3  | -565,4  | 13 | 574    |
| B500B-57                |       | 613,8  | -570,7  | -582,4  | 13 | 554,6  |
| B500B-58                | 6Φ    | 613,2  | -583,3  | -590,6  | 13 | 544,5  |
| B500B-59                |       | 608,5  | -551,2  | -573,8  | 13 | 528,5  |
| B500B-60                |       | 609,5  | -545    | -564,9  | 13 | 533    |
| B500A-12-CW (Prod. 2)   |       |        |         |         |    |        |
| B500A-41                |       | 552    | -510,6  | -532    | 33 | 711,4  |
| B500A-42                |       | 546    | -498,6  | -529,4  | 23 | 497,6  |
| B500A-43                | 6Φ    | 550    | -516    | -532    | 31 | 683,8  |
| B500A-44                |       | 553    | -511,8  | -538,3  | 39 | 814,8  |
| B500A-45                |       | 557,4  | -529,2  | -538,3  | 32 | 707    |
| B500A-46                | ±2,5% | 549    | -439,5  | -514,7  | 15 | 274    |
| B500A-47                |       | 554,2  | -429    | -515    | 16 | 289    |
| B500A-48                | 8Φ    | 553,37 | -438,14 | -511,3  | 17 | 308    |
| B500A-49                |       | 553,2  | -427,3  | -516,4  | 21 | 354    |
| B500A-50                |       | 549,2  | -423,4  | -509    | 16 | 284    |
| B500A-51                |       | 559,5  | -347,7  | -498    | 8  | 232    |
| B500A-52                |       | 552,5  | -332,5  | -488    | 8  | 221,5  |
| B500A-53                | 8Φ    | 555,7  | -337,4  | -488,4  | 8  | 247    |
| B500A-54                |       | 556,1  | -337,2  | -495,5  | 7  | 226,5  |
| B500A-55                | ±4%   | 560,34 | -344    | -496,8  | 7  | 231    |
| B500A-56                |       | 565,2  | -505,2  | -541,5  | 10 | 379    |
| B500A-57                |       | 566,17 | -494    | -542,6  | 11 | 401,3  |
| B500A-58                | 6Φ    | 564,5  | -500    | -536,9  | 11 | 413    |
| B500A-59                |       | 569    | -500    | -542,35 | 11 | 402,65 |
| B500A-60                |       | 568,9  | -495    | -537    | 10 | 372    |

### 3. DESIGN AND MODELLING OF CASE STUDIES

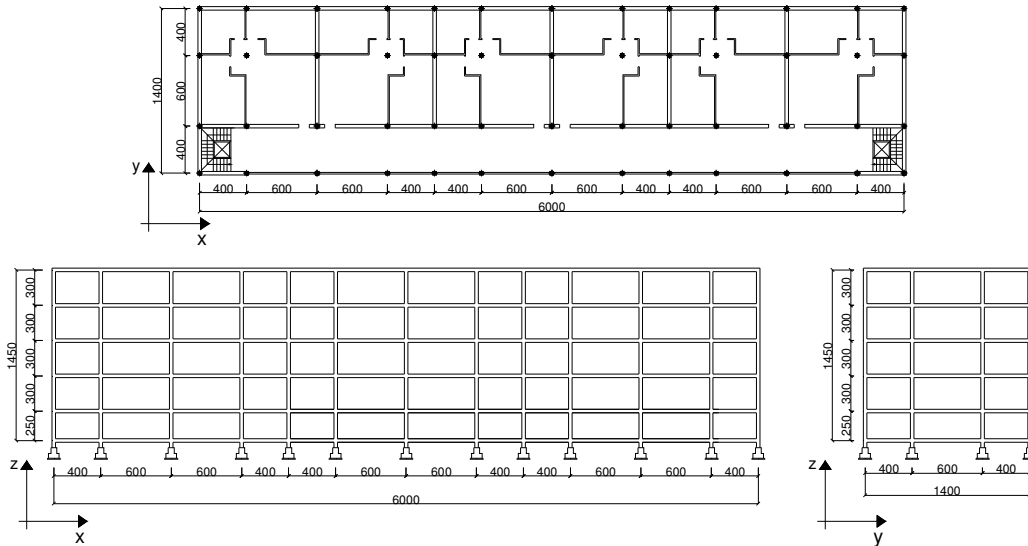
#### 3.1 Reinforced concrete case study buildings

Different reinforced concrete case studies were designed following the prescriptions imposed by actual European and Italian standards for constructions (EN 1992-1-1:2005, EN 1998-1:2005, D.M. 14/01/2008). Different distributions of structural elements in both plan and elevation, different functional destinations (commercial, residential and office buildings), different seismicity areas (high seismicity with a design PGA equal to 0.25 g and medium seismicity with a design PGA of 0.15 g) and different ductility classes (high ductility class – HDC and medium ductility class – MDC) were considered; steel grade B450C was used for the design. Table 3.1 summarizes the r.c. buildings designed as case studies.

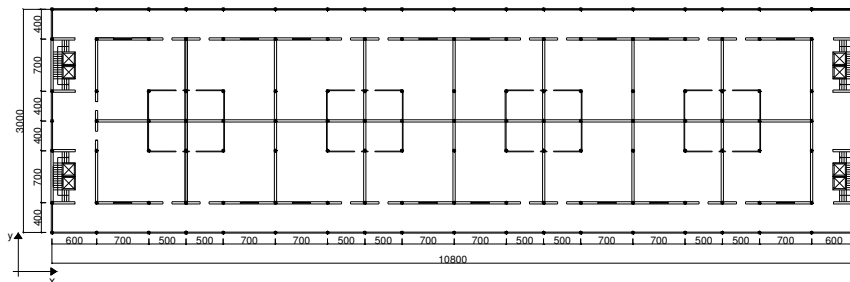
**Table 3. 1:** Designed reinforced concrete case studies.

| Functional destination | PGA [g] | Ductility class | Steel grade |
|------------------------|---------|-----------------|-------------|
| Residential building   | 0,25    | HDC             | B450C       |
| Residential building   | 0,25    | MDC             | B450C       |
| Commercial building    | 0,25    | HDC             | B450C       |
| Office building        | 0,25    | HDC             | B450C       |

Moment resisting frames (MRF) with span length of beams variable between 4.0 m and 7.0 m and storey height between 2.5 m and 5.0 m were adopted for the design of the selected buildings in relation to the functional destination foreseen. The stiffening contribution of stairs and lift's rooms was directly taken into account through the introduction of opportune elements in the numerical models. Residential buildings in both HDC and MDC present the same geometrical disposition of structural elements, resulting in an area of 60,0x14,0 m<sup>2</sup> and a total height of 14,0 m; commercial building in HDC is characterized by an area of 36,0x34,0 m<sup>2</sup> and a total height of 19,0 m and, finally, office building in HDC presents an area of 108,0x30,0 m<sup>2</sup> and a global height of 19,0 m. Figures from 3.1 to 3.3 present the geometrical schemes, in plan and elevation, of the case studies.



**Figure 3. 1:** Geometrical schemes adopted for residential buildings.



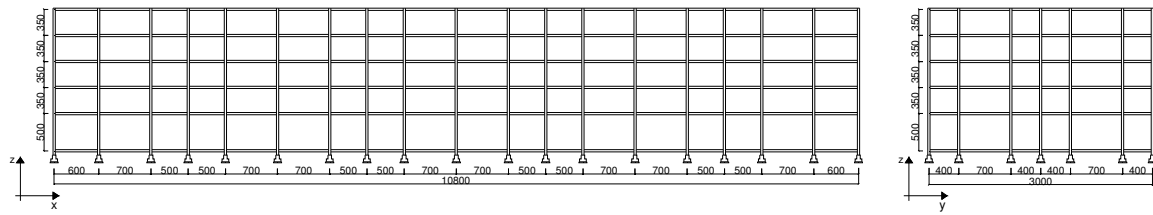


Figure 3. 2: Geometrical schemes adopted for office building.

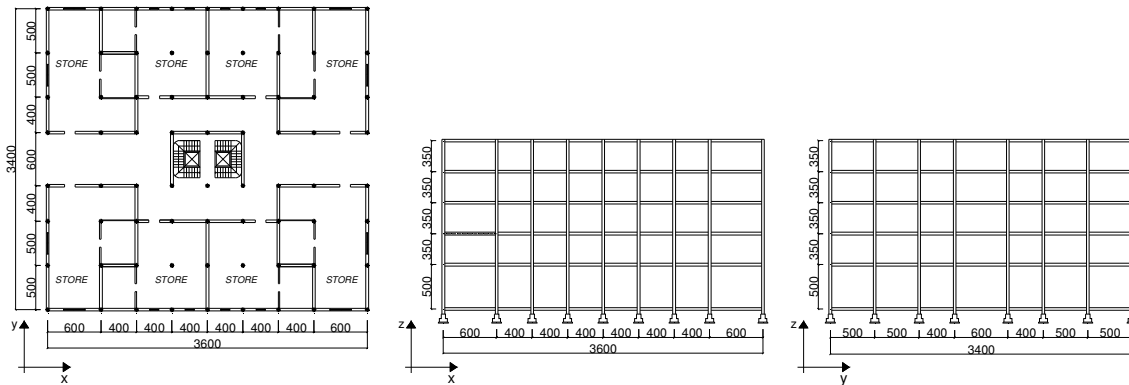


Figure 3. 3: Geometrical schemes adopted for commercial building.

### 3.1.1 Structural design of r.c. case studies

A preliminary pre-sizing of structural elements was executed considering only vertical loads, including both gravitational and live loads with reference to the selected case study; the formula provided by Eurocode (EN 1990:2006) for the fundamental combination of loads, with opportune values of partial coefficients, was used.

Simplified expressions were adopted for the definition of the bending action on beams and for the individuation of the height of the section, as well as for the evaluation of column's section.

Vertical loads acting on selected case studies were defined in relation to the typology of structural and not structural elements used (for storey slab, roof, internal and external infills, equipments, etc...) and in relation to the functional destination of the buildings (for live loads). For residential buildings in both high and low ductility class, storey slabs "Predalle H24-i50", characterized by a total height of 24 cm and spacing between longitudinal joists equal to 50 cm were used, resulting in a vertical load ( $G_k$ ) equal to 3.35 kN/m<sup>2</sup>.

For commercial building storey slab "Predalle H24-i40", characterized by a total height of 24 cm and spacing between longitudinal joists equal to 40 cm were used, resulting in a vertical load ( $G_k$ ) equal to 4.00 kN/m<sup>2</sup>. For office building storey slab "Predalle H28-i50", characterized by a total height of 28 cm and spacing between longitudinal joists equal to 50 cm were used, resulting in a vertical load ( $G_k$ ) equal to 3.70 kN/m<sup>2</sup>. Additional vertical loads due to concrete slabs, floor and internal infills (considered uniformly distributed on the storey slab) were considered, resulting in values of actions respectively equal to 2.80 kN/m<sup>2</sup>, 2.35 kN/m<sup>2</sup> and 2.50 kN/m<sup>2</sup> for residential (both HDC and MDC), commercial and office buildings. The values of accidental loads (Q) were derived from both EN 1991-1-1:2004 with reference also to D.M. 14/01/2008, in relation to the functional destination chosen for each building; live loads are summarized in table 3.2. The accidental live loads acting on roof slab was generally considered equal to 0.50 kN/m<sup>2</sup> (used for not practicable roofs). Wind and snow actions were also evaluated and included in the design according to the fundamental gravitational combination proposed by actual standards.

Table 3. 2: Loads acting on r.c. case studies.

| Functional Destination | Ductility Class | Structural loads (kN/m <sup>2</sup> ) | Not structural loads (kN/m <sup>2</sup> ) | Q (kN/m <sup>2</sup> ) |
|------------------------|-----------------|---------------------------------------|---|------------------------|
| Residential building   | HDC             | 3,35                                  | 2,80                                      | 2,00                   |
| Residential building   | MDC             | 3,35                                  | 2,80                                      | 2,00                   |
| Office Building        | HDC             | 3,70                                  | 2,50                                      | 3,00                   |
| Commercial Building    | HDC             | 4,00                                  | 2,35                                      | 5,00                   |

Seismic action was opportunely evaluated using the design response spectra defined in Eurocode 8 (EN 1998-1:2005) and taking into account also the prescriptions of actual Italian Standards for Constructions (D.M. 14/01/2008), in order to achieve the required level of design seismic action, expressed in terms of peak ground acceleration (PGA). Buildings were designed considering soil category “B”, characterized by a speed of propagation of shear waves in the first 30 m of depth between 360 and 800 m/s. According to EN 1998-1:2005 response spectrum of Type 1 can be adopted, in the assumption that earthquakes with magnitude higher than 5.5 can take place.

Considering also the prescriptions imposed by D.M. 14/01/2008, an opportune response spectrum was individuated for each building in relation to the effective reference life ( $V_R$ ) of the structure, defined as function of the nominal life ( $V_N$ ) and of the use coefficient ( $C_U$ ), whose values are given by the Italian standard. As an example, for ordinary constructions,  $C_U$  is assumed equal to 1.0, while for strategic buildings (i.e. hospitals and others) and for schools is respectively equal to 2.0 and 1.5. The nominal life  $V_N$  is equal to 50 years for ordinary constructions, 100 years for strategic buildings and 10 years for temporary constructions. The design PGA ( $a_g$ ) and other two significative parameters ( $F_0$ , related to the amplification of spectral acceleration and  $T_C^*$ , period corresponding to the beginning of the constant velocity branch of the spectrum) are opportunely defined in relation to the site in which the building is designed, considering the rigid reference soil.

For the designed case studies, the reference life  $V_R$  was assumed equal to 50 years, the coefficient  $C_U$  is unitary and the nominal life  $V_N$  is consequently equal to 50 years; buildings were designed with reference to two different limit state, i.e. Life Safety limit state (LS), as regards strength, and Damage Limitation limit state (DL), as regards stiffness and displacements. For the selected buildings, the return periods are respectively equal to 475 and 75 years for LS and DL.

The behaviour factors for case-study buildings were evaluated considering the prescriptions imposed by both actual European and Italian standards for constructions (EN 1998-1:2005, D.M. 14/01/2008). For the selected case studies, the values of the behaviour factors are summarized in the table 3.3, while figure 3.4 shows the horizontal response spectra used for design of buildings according to what prescribed by D.M. 14/01/2008.

**Table 3. 3:** Values of the q factors adopted for designed buildings.

| Functional destination | PGA [g] | Ductility class | q factor |
|------------------------|---------|-----------------|----------|
| Residential building   | 0,25    | HDC             | 5,85     |
| Residential building   | 0,25    | MDC             | 3,90     |
| Commercial building    | 0,25    | HDC             | 5,85     |
| Office building        | 0,25    | HDC             | 5,85     |

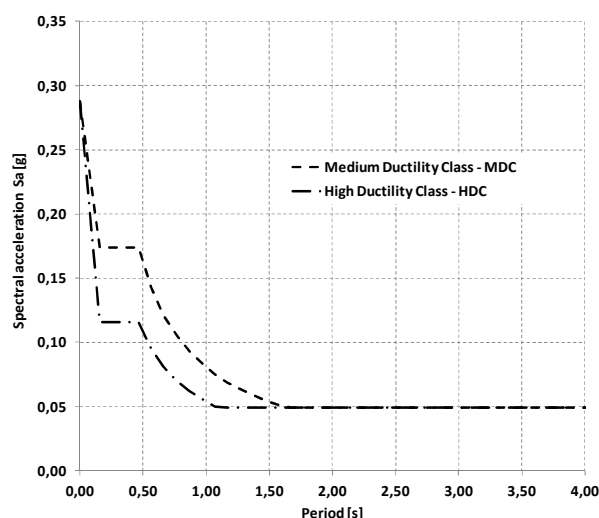


**Figure 3. 4:** Response spectra used for the design of case studies in HDC and MDC to 0.25g (D.M.14/01/2008).

The fundamental combination for gravitational loads is expressed through Eqn. 6.10 from § 6.4.3.2 of EN 1990:2006, while for the seismic combination, the expression 6.12.a from § 6.4.3.2 of EN 1990:2006) was adopted, in which  $G_{k,j}$  are the gravitational loads due to structural and not structural elements,  $P$  is the pre-compression load,  $Q_{k,j}$  are the live loads and  $A_{Ed}$  refers to seismic event.

Seismic masses to be considered in the desing are defined according to equation 3.17 of EN 1998-1:2005, in which  $\psi_{E,i}$  is a coefficient used for taking into account the possibility that accidental loads are not always totally present during a seismic event.

$$\sum G_{k,j} + \sum \psi_{E,i} \cdot Q_{k,i} \quad (3.1)$$

The values of  $\psi_{E,i}$ , according to what presented in EN 1998-1:2005, are equal to  $\psi_{E,i} = \varphi \cdot \psi_{2,i}$ , where  $\psi_{2,i}$  are defined in Table A.1.1 of Annex A1 of EN 1990:2006 and  $\varphi$  is defined in Table 4.2 of EN 1998-1:2005. Tridimensional linear models were elaborated for each case study using SAP 2000 (v.14.1) software, according to what imposed by actual standards for seismic constructions. Mono-dimensional “frame” elements were used for both beams and columns, while for the slabs of the stairs, two-dimensional plane “shell” elements with opportune thickness were adopted. Columns were fixed at the base and opportune diaphragms were applied in correspondence of each floor in order to represent the rigid contribution of the storey slab, previously defined and characterized by a concrete slab with reinforcement grid of 40 mm of thickness. Figures 3.5 present the simple schemes of the linear models, including, as already mentioned, the stiffening contribution of stairs and lift’s rooms.

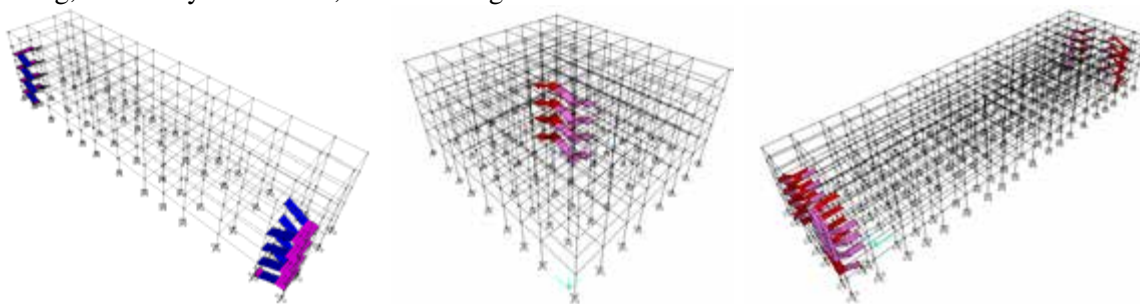


**Figure 3. 5:** Tridimensional linear model for residential, commercial and office buildings case studies.

As regards the choice of materials, concrete class C25/30 was adopted for concrete elements, while steel grade B450C was used for steel reinforcements. The mechanical characteristics of materials, in terms of compressive strength for concrete and yielding and tensile strength for steel.

Vertical loads were directly applied to bearing structural elements as linear distributed loads and opportune torsional moments were introduced for taking into account the effects of the centroid eccentricity, accepted to be equal to the 5% of the maximum dimension of the building in the perpendicular direction respect to the seismic action according to what prescribed by EN 1998-1:2005 and D.M.14/01/2008. For taking into account the cracking phenomena of concrete at life safety limit state (LS), a reduction of stiffness of primary structural elements (beams and columns) was adopted. In general, a reduction of stiffness equal to 50% was adopted for beam elements and a reduction of stiffness equal to 30% was adopted for column elements, characterized by a significative axial load, for all the designed case study buildings.

Reinforced concrete buildings were designed following the criteria and the indications presented in Eurocode 8 and Italian standards for constructions (EN 1998-1:2005, D.M. 14/01/2008) for both structures in high and low ductility classes, considering the results of linear modal analysis above presented, the loads and behaviour factors already described.

The capacity design approach was adopted, localizing plastic hinges in correspondence of the ends of the elements (both beams and columns), in order to achieve the development of ductile global collapse mechanisms instead of local brittle ones. The shear design forces were defined considering the localization of flexural plastic hinges at the ends of the elements, according to EN 1998-1:2005.

The expressions used for the determination of the shear strength, on the other hand, are the same generally used for buildings not in seismic areas (Eqn. 3.2), as presented in EN 1992-1-1:2005, in which  $V_{Rd}$  is the design shear resistance for the selected element,  $V_{Rd,S}$  the shear resistance due to steel stirrups,  $V_{Rd,C}$  the shear resistance due to compression strut,  $\alpha$  the angle between shear reinforcement and the beam axis perpendicular to the shear force,  $\theta$  the angle between the concrete compression strut and the beam axis perpendicular to the shear force,  $b_w$  the minimum width between tension and compression chords,  $z$  the inner lever arm,  $A_{sw}$  the cross-sectional area of the shear reinforcement,  $s$  the spacing of the stirrups,  $f_{ywd}$  the design yield strength of the shear reinforcement,  $v_1$  a strength reduction factor for concrete cracked in shear and  $\alpha_{cw}$  a coefficient taking account the stress condition in the compression chord.

$$V_{Rd} = \min[V_{Rd,s}; V_{Rd,max}]$$

$$V_{Rd,s} = \frac{A_{sw}}{s} z f_{ywd} (\cot \theta + \cot \alpha) \sin \alpha \quad (3.2)$$

$$V_{Rd,max} = \alpha_{cw} b_w z v_1 f_{cd} (\cot \theta + \cot \alpha) / (1 + \cot^2 \theta)$$

The design of beams and columns was optimized in order to achieve sections with the minimum requirement of reinforcements: one of the main aims of the design is, in fact, the maximization of the ductility requirements imposed by seismic action to the rebar. As a consequence, steel bars of different diameters were used for longitudinal reinforcements, varying from 14 to 18 mm in both beams and columns.

As regards transversal reinforcements, stirrups of diameter 8.0 mm and 10 mm were generally used, respectively in beams and columns; in particular, rectangular double stirrups with four branches were often used in columns of the first and of the second floor, while simple rectangular stirrups were always used in beams. The spacing of stirrups generally varies from 50 mm to 100 mm in correspondence of the critical zones of beams and columns. The length of the critical zones of elements is defined according to what presented in EN 1998-1:2005.

Tables from 3.4 to 3.7 summarize the geometrical characteristics of structural elements of the different buildings selected as case studies, while figures from 3.6 to 3.16 present the some structural details of reinforcements in beams' and columns' sections. The whole structural desing of buildings is better detailed in the corresponding deliverable (D.2.1).

### Residential building in HDC

**Table 3. 4:** Dimensions and height of structural elements for residential building in HDC.

| Floor | Columns [cm x cm] | Beams [cm x cm] | Concrete Class | Storey height [m] |
|-------|-------------------|-----------------|----------------|-------------------|
| 1     | 40x70             | 40x50           | C25/30         | 2,50              |
| 2     | 40x60             | 40x50           | C25/30         | 3,00              |
| 3     | 40x50             | 40x50           | C25/30         | 3,00              |
| 4     | 40x50             | 40x50           | C25/30         | 3,00              |
| 5     | 40x50             | 40x50           | C25/30         | 3,00              |

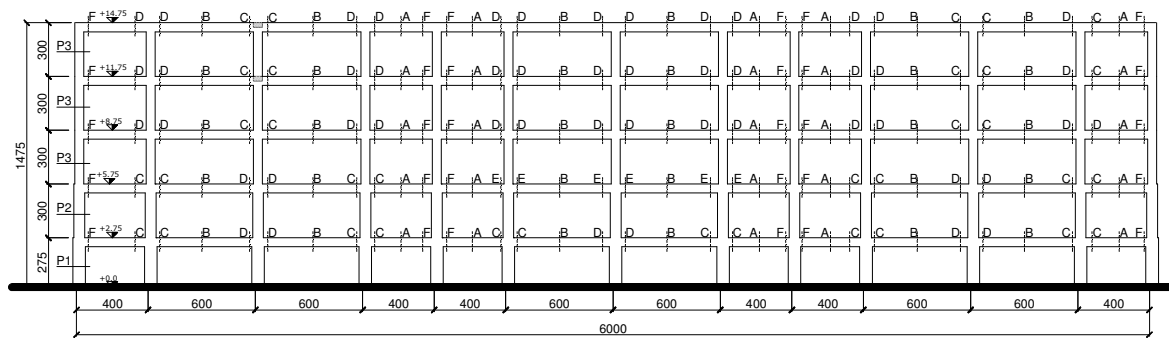


**Figure 3. 6:** Scheme of elements' sections disposition for residential building in HCD (main frame).

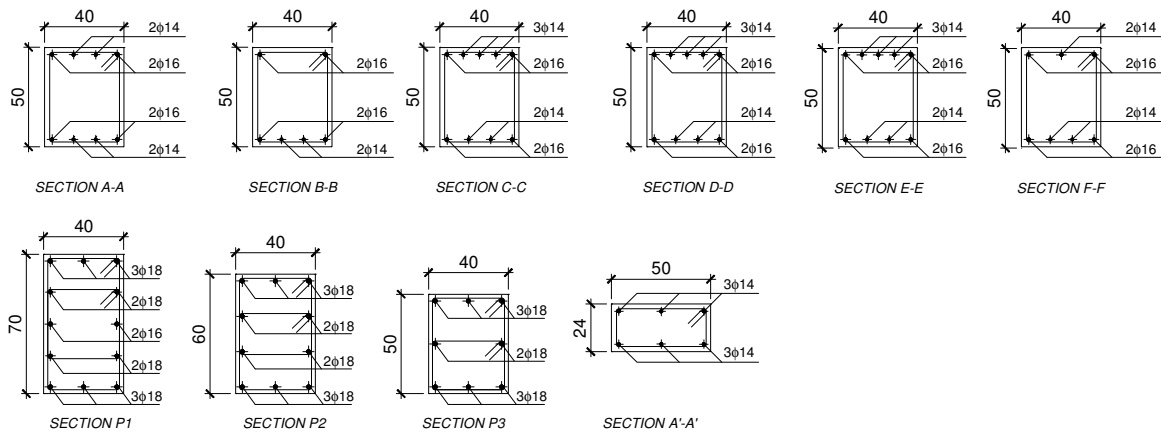


**Figure 3. 7:** Typical sections of beam and column elements in residential building in HDC.

*Residential building in MDC*

**Table 3. 5:** Dimensions and height of structural elements for residential building in MDC.

| Floor | Columns [cm x cm] | Beams [cm x cm] | Concrete Class | Storey height [m] |
|-------|-------------------|-----------------|----------------|-------------------|
| 1     | 40x50             | 40x50           | C25/30         | 2,50              |
| 2     | 40x50             | 40x50           | C25/30         | 3,00              |
| 3     | 40x50             | 40x50           | C25/30         | 3,00              |
| 4     | 40x50             | 40x50           | C25/30         | 3,00              |
| 5     | 40x50             | 40x50           | C25/30         | 3,00              |

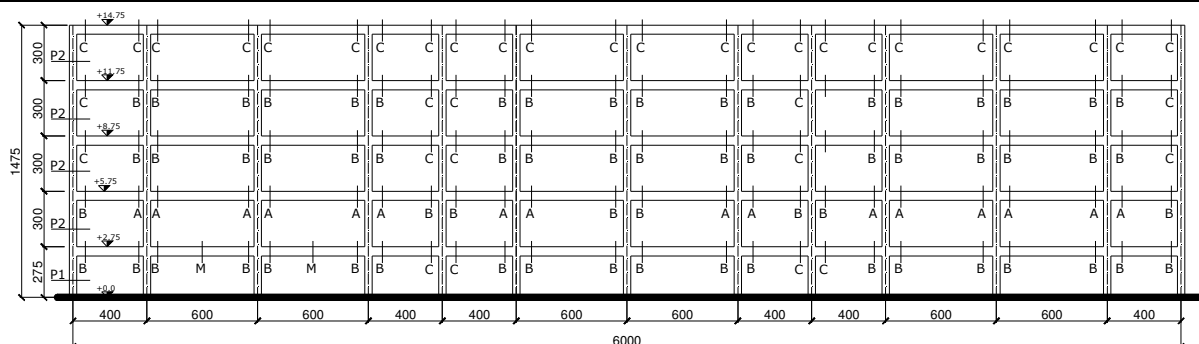


**Figure 3. 8:** Scheme of elements' sections disposition for residential building in MCD (main frame).

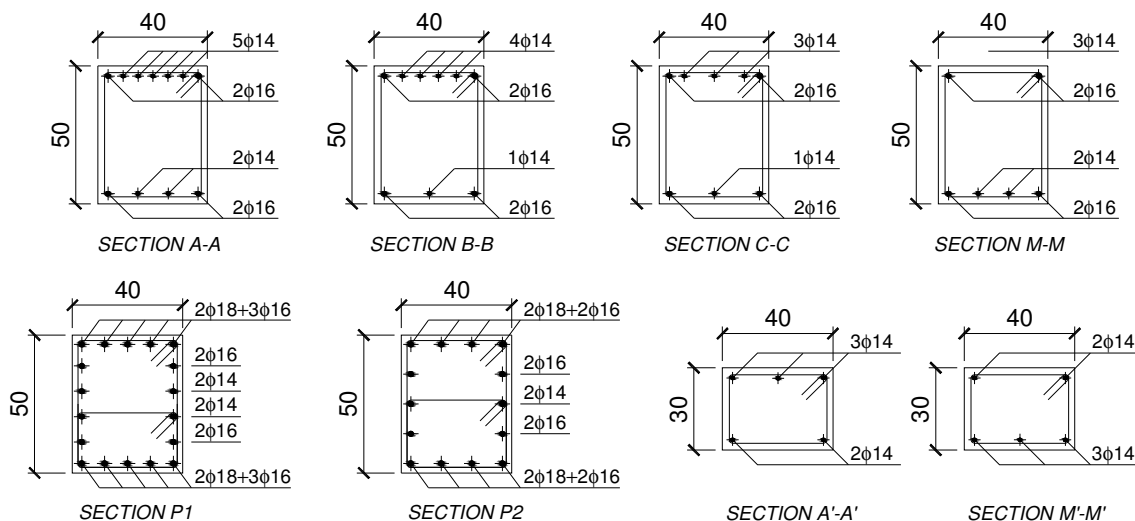


**Figure 3. 9:** Typical sections of beam and column elements in residential building in MDC.

*Commercial building in HDC*

**Table 3. 6:** Dimensions and height of structural elements for commercial building in HDC.

| Floor | Columns [cm x cm] | Beams [cm x cm] | Concrete Class | Storey height [m] |
|-------|-------------------|-----------------|----------------|-------------------|
| 1     | 40x80             | 40x60           | C25/30         | 5,00              |
| 2     | 40x70             | 40x60           | C25/30         | 3,50              |
| 3     | 40x60             | 40x60           | C25/30         | 3,50              |
| 4     | 40x60             | 40x60           | C25/30         | 3,50              |
| 5     | 40x60             | 40x60           | C25/30         | 3,50              |

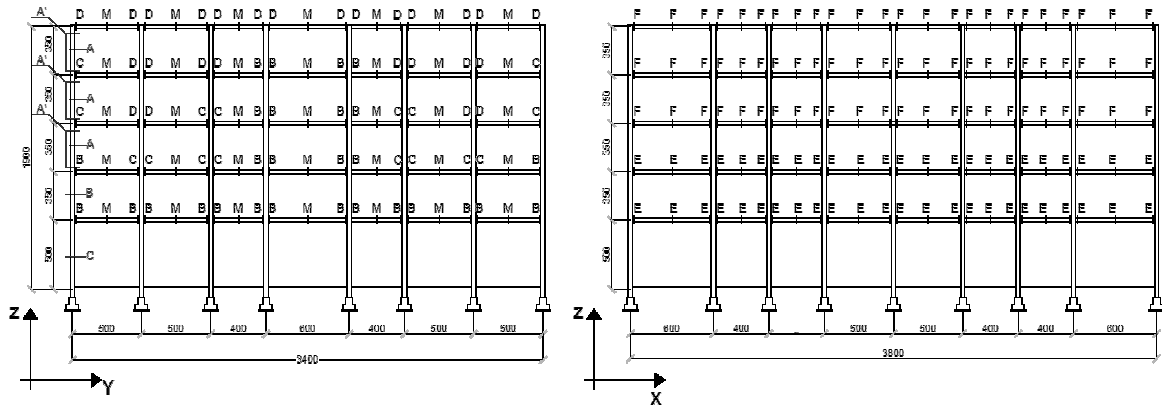


Figure 3. 10: Schemes of elements' sections for commercial building (main frame yz, secondary frame xz).

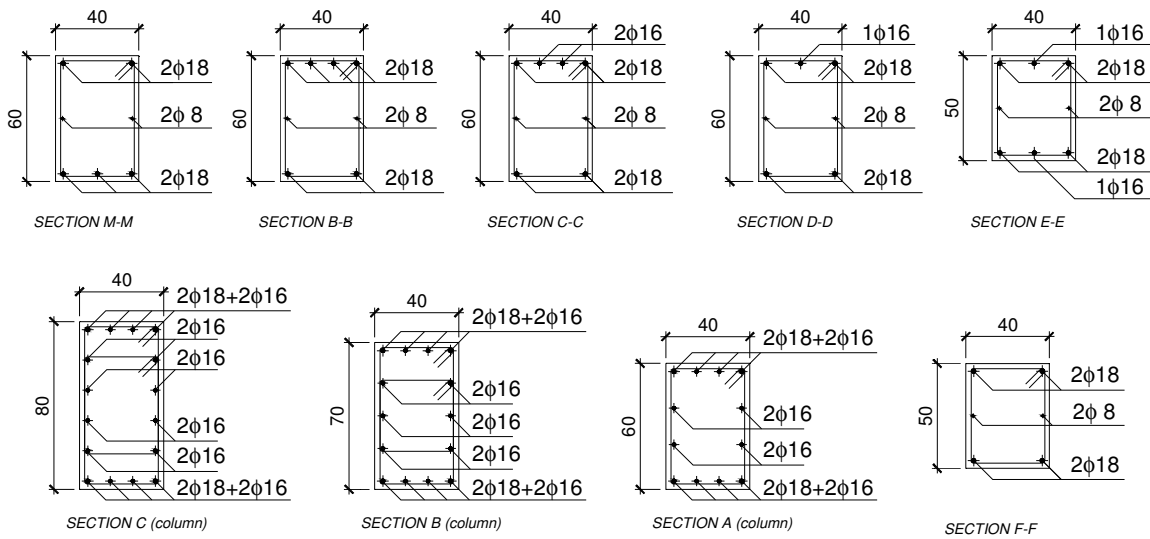


Figure 3. 11: Typical sections of beam and column elements in commercial building in HDC.

### Office building in HDC

Table 3. 7: Dimensions and height of structural elements for office building in HDC.

| Floor | Columns [cm x cm] | Beams [cm x cm] | Concrete Class | Storey height [m] |
|-------|-------------------|-----------------|----------------|-------------------|
| 1     | 40x80             | 40x60           | C25/30         | 5,00              |
| 2     | 40x70             | 40x60           | C25/30         | 3,50              |
| 3     | 40x60             | 40x60           | C25/30         | 3,50              |
| 4     | 40x60             | 40x60           | C25/30         | 3,50              |
| 5     | 40x60             | 40x60           | C25/30         | 3,50              |

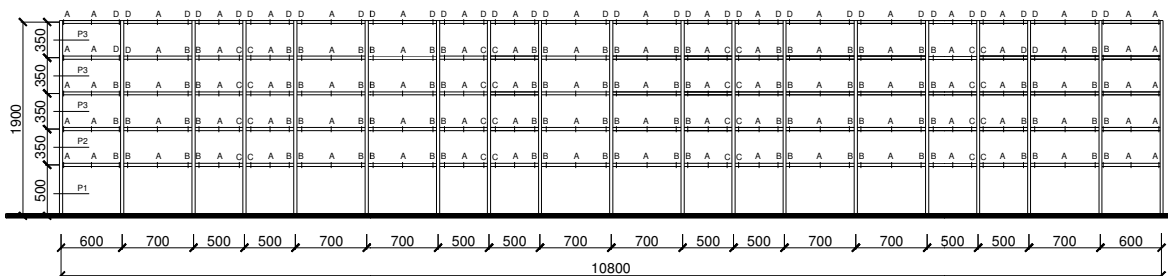


Figure 3. 12: Scheme of elements' sections disposition for office building in HCD (main frame).

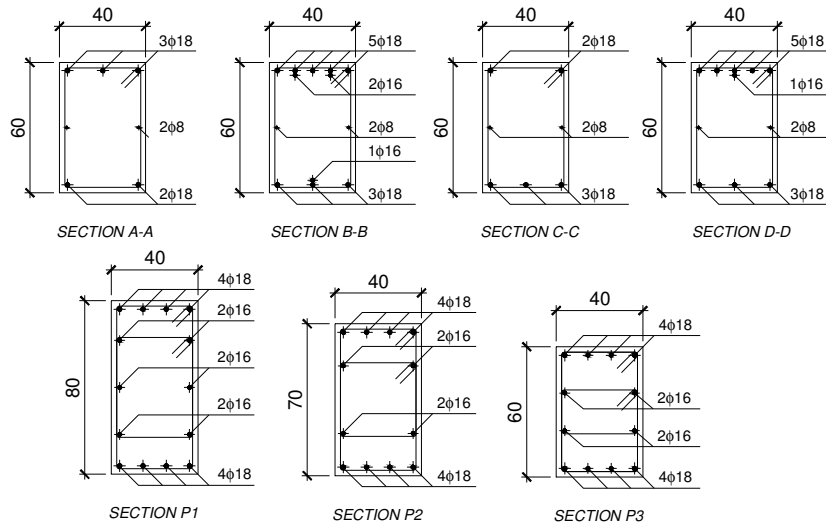


Figure 3.13: Typical sections of beam and column elements in office building in HDC.

### 3.1.2 Elaboration of non linear models of r.c. case studies

Non linear two-dimensional models were elaborated for each of the two main directions of designed case studies using OpenSees software (Mazzoni et al. 2007).

Beams and columns were modelled as *beam with hinge* (BWH) elements: each single element was divided into three different portions, two plastic hinges in correspondence of the two ends and an elastic central part (figure 3.14). The definition of the section in correspondence of the central part of the element required only the individuation of the transversal area ( $A$ ) and of the elastic modulus of material ( $E_m$ ); on the other hand, the sections in correspondence of the two ends of beams and columns were modeled as “fiber sections” and an opportune length ( $L_p$ ) for plastic hinges was defined, based on the definition proposed by Fardis (2001) for cyclic loading condition (eqn. 3.3).

Columns were considered fixed in correspondence of the base and seismic masses were concentrated in correspondence of the top of the columns, as well as vertical loads. In order to reproduce the stiffening contribution of storey slab, additional truss elements, opportunely sized, were introduced in the model between column elements (figure 3.14a).

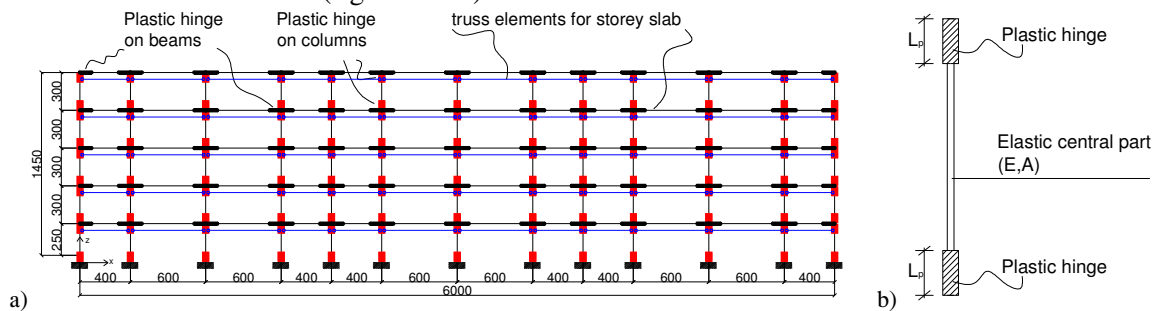
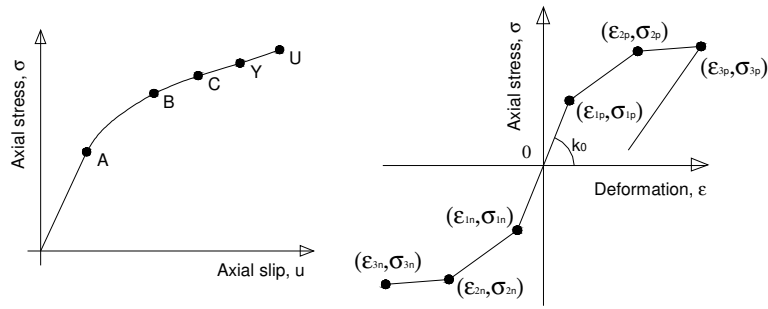


Figure 3.14: a) Simplified scheme of non linear model with beam with hinges elements, b) BWH element.

The selection of opportune constitutive laws for both concrete and steel materials was necessary in order to provide significative and reliable results for the deformation levels obtained in reinforcements. For concrete material, the constitutive law proposed by Braga, Gigliotti and Laterza (2006) was used, in order to directly represent the confinement contributions due to both longitudinal and transversal reinforcements; the BGL model was recently implemented in OpenSees (D’Amato 2008) considering different possible layouts of transversal stirrups. For steel reinforcing bars, the “modified slip model” presented by Braga et al. (2013) was adopted, allowing to consider the relative slip phenomena between steel reinforcements and concrete. Different coordinates, in terms of axial stress-slip and axial stress-fictitious strain, were derived in relation to the different bar diameters used in the design for beams and columns; the modified slip model was implemented in OpenSees using the trilinear hysteretic material, with the three characteristic points of the loading envelopes opportunely determined in relation to the energy equivalence principle (figure 3.15).



**Figure 3.15:** Shift from axial stress-slip model to axial stress-fictitious strain model for steel reinforcements.

For the modified slip model, the following hypothesis were adopted:

- The constitutive *stress-strain* relationship of steel was assumed elastic-plastic with hardening (figure 3.16); the values adopted for yielding and tensile strength and for the elongation to maximum load were calibrated in relation to the mean values of the experimental tests' results presented in Chapter 2 for the corresponding steel grade used in the design (B450C).

**Table 3.8:** Mean values of experimental test on B450C-TempCore rebars and assumed values for simplified model.

| B450C – TempCore steel   | $f_u$ [MPa] | $f_y$ [MPa] | $f_u/f_y$ [-] | A [%] | $A_{gt}$ [%] |
|--------------------------|-------------|-------------|---------------|-------|--------------|
| Mean (Experimental test) | 596.60      | 488.00      | 1.22          | 26.40 | 14.10        |
| Assumed for model        | 600.00      | 490.00      | 1.22          | 26.40 | 14.00        |

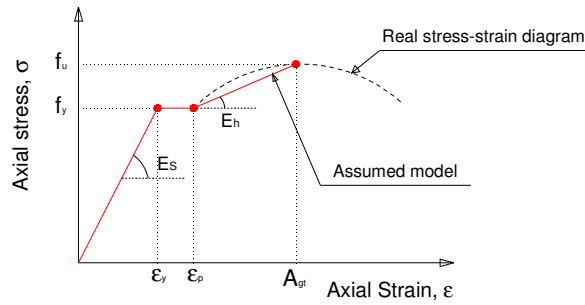


**Figure 3.16:** Simplified stress-strain relationship assumed for steel constitutive law.

- The *bond stress-slip* relationship was assumed elasto-plastic (figure 3.17), in agreement with what already presented by Braga et al. (2004). In particular, the simplification adopted in the slip model was extended to the case of ribbed bars and the values provided by Model Code 90 were assumed; in order to consider the progressive deterioration and damaging of bond between steel and concrete due to cycling actions, the residual bond stress to use in the model ( $\tau_d$ ) was taken equal to the one prescribed for poor bond conditions in confined concrete. For  $u_l$  the value obtained from the intersection between the residual bond stress and the linear approximation of the first branch of the Model Code relationship was assumed.

**Table 3.9:** Assumed values for the bond stress-slip relationship in modified slip model.

| Confined concrete - All other bond condition |                     |  |      |
|--|---------------------|--|------|
| Model Code 90                                |                     | Assumed values for modified slip model |      |
| $s_1$ [mm]                                   | 1.0                 | $s_b$ [mm]                             | 0.4  |
| $s_2$ [mm]                                   | 3.0                 | $s_2$ [mm]                             | -    |
| $s_3$ [mm]                                   | Clear rib spacing   | $s_3$ [mm]                             | -    |
| $\alpha$                                     | 0.4                 | $f_{ck}$ [MPa]                         | 33   |
| $\tau_{max}$ [MPa]                           | $1.25\sqrt{f_{ck}}$ | $\tau_{max}$ [MPa]                     | 7.18 |
| $\tau_f$ [MPa]                               | $0.40\tau_{max}$    | $\tau_f$ [MPa]                         | 2.87 |

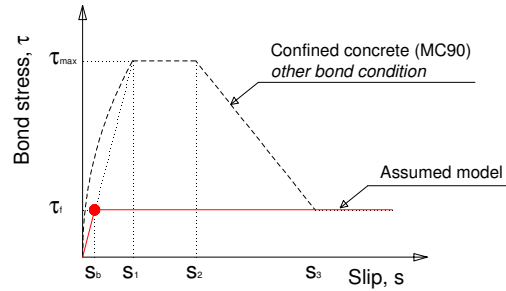


**Figure 3.17:** Bond stress-slip relationship assumed for the modified slip model.

- The axial stress-strain to be used in the numerical models was obtained, according to what provided by D'Amato (2008); a fictitious strain  $\varepsilon^*$  was individuated through equation presented below, in which the plastic hinge length  $L_p$  was defined according to Panagiotakos and Fardis (2001), as presented by equation 3.4:

$$\varepsilon^* = \frac{u_{L,tot}}{L_p}, \quad L_{pl,cy} = 0.12 \cdot L_v + 0.014 a_{sl} d_b f_y \quad (3.4)$$

Being  $L_v$  the shear span length,  $a_{sl}$  a coefficient for slip equal to 1 if there is slippage of the longitudinal bars from their anchorage beyond the section of maximum moment, or to 0 if there is not slip,  $d_b$  is the bar diameter and  $f_y$  the yielding strength. In the present work, the value of  $a_{sl}$  was assumed equal to zero, since the relative slip phenomena between bars and the surrounding concrete was directly taken into consideration in the modified slip model.

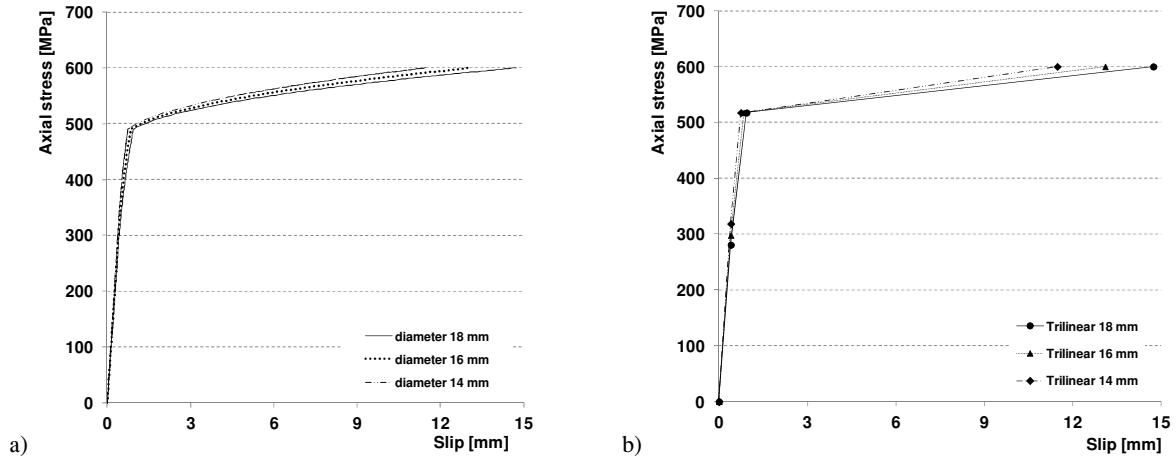


**Figure 3.18:** Bond stress-slip relationship and trilinear equivalent model.

**Table 3.10:** Assumed values for the axial stress-slip model.

| Mechanical properties of material |         |     | Axial stress-slip relationships: coordinates of significative points |        |     |               |        |     |               |        |     |
|-----------------------------------|---------|-----|--|--------|-----|---------------|--------|-----|---------------|--------|-----|
| $f_y$                             | 490     | MPa | d  | 14     | mm  | d             | 16     | mm  | d             | 18     | mm  |
| $f_u$                             | 600     | MPa | $u_{p1}$   | 0.400  | mm  | $u_{p1}$      | 0.400  | mm  | $u_{p1}$      | 0.400  | mm  |
| $\varepsilon_y$                   | 0.24    | %   | $\sigma_{p1}$  | 318.56 | MPa | $\sigma_{p1}$ | 297.80 | MPa | $\sigma_{p1}$ | 280.77 | MPa |
| $A_{gt}$                          | 12.50   | %   | $u_{p2}$   | 0.743  | mm  | $u_{p2}$      | 0.839  | mm  | $u_{p2}$      | 0.936  | mm  |
| $E_s$                             | 206000  | MPa | $\sigma_{p2}$  | 517.30 | MPa | $\sigma_{p2}$ | 517.44 | MPa | $\sigma_{p2}$ | 517.59 | MPa |
| $E_h$                             | 1047.00 | MPa | $u_{p3}$   | 11.475 | mm  | $u_{p3}$      | 13.104 | mm  | $u_{p3}$      | 14.734 | mm  |
| $\tau_d$                          | 2.87    | MPa | $\sigma_{p3}$  | 600.00 | MPa | $\sigma_{p3}$ | 600.00 | MPa | $\sigma_{p3}$ | 600.00 | MPa |
| $u_1$                             | 0.4     | Mm  |  |        |     |               |        |     |               |        |     |

## 3.2 Steel/concrete composite structures

For what concerns steel/concrete composite case study structures, differently from what already presented for r.c. structures that were opportunely designed and modeled for the execution of numerical analyses, a real existing 3D full-scale composite building was used for the individuation of the ductility demand on steel bars. This choice was due to the presence in the current scientific literature of a large amount of experimental tests on the whole structure and on beam/column sub-assemblages with the recording of the effective strain histories on steel reinforcements, to be used and analyzed for the aims of the research project. Stating these considerations, in the present work the results obtained from an experimental tests' campaign executed on the two-storey full-scale 3D prototype structure at the European Laboratory for Structural Assessment (ELSA) of the Joint Research Centre at Ispra (Italy) were used for the individuation of the effective ductility demand on steel reinforcements present in the concrete slab.

As already presented in the current literature in fact (Braconi et al. 2008 and 2007), the dynamic behaviour of joints, obtained through the execution of pseudo-dynamic (PSD) tests at ELSA, was comparable to the one obtained through cyclic tests executed on sub-assemblages at University of Pisa, in which moreover a specific instrumentation was adopted for the individuation of the effective level of strain on reinforcing bars. The experimental tests presented in the following paragraphs and used for Rusteel elaborations were executed inside the frameworks of two European research project ("*3-D full-scale seismic testing of a steel– concrete composite building at ELSA*", Contract No. HPR-CT-1999-000594 and "*Applicability of composite structures to sway frames*", ECSC Contract No. 7210-PR-250, 2002).

### 3.2.1 *Desing of full-scale 3D structure at Ispra laboratory*

Steel-concrete composite MRF structures are characterized by a high lateral stiffness if compared with steel MRF constructions; beam-to-column joints can be realized at a lower cost taking advantage of the concrete slab to develop the required flexural stiffness and strength under gravity and lateral loads. Considering the seismic design, beam and column sizes are controlled by lateral drift limits, so that an interesting design option is represented by partial-strength (PS) beam-to-column joints, detailed to accommodate relevant inelastic rotations through ductile inelastic connection components' response.

Eurocode 8 (EN 1998-1:2005) allows the design realization of composite frames according to different design concepts, in relation to the expected yielding in structural elements (low dissipation - DCL; medium dissipation – DCM and high dissipation - DCH). The dissipation induced by plastic deformations can be located, for DCM and DCH structures, in composite or bare steel parts as beam ends, PR/PS beam-to-column joint or bracing systems, leading to different dissipative structural types.

As well as for r.c. buildings, Eurocode 8 provisions adopt the *capacity design* approach for the final design of structural elements in dissipative seismic-resistant systems, with specific elements in which plasticization is expected and other structural components designed to remain in the elastic field.

For the design of the 3D full-scale structure and to develop a global hinging composite frame mechanism, a strong column-weak beam or partial strength (PS) connection strategy was adopted; the PS connections were designed to exhibit a ductile failure mode for energy dissipation accommodating a rotation capacity consistent with the global deformations expected from the frame, localizing the plastic phenomena mainly in ductile components of PS/PR composite joints.

The designed structure includes five identical two-bay MRFs with different spans (5+7m) and spaced 3m apart. The frames are built with composite beams connected to partially encased composite columns with PS end-plate joints (figure 3.19). Traditional end-plated connections were adopted at the base of the columns to establish an effective restraint at the structure/foundation interface. In the direction normal to the MRFs, lateral resistance is provided by two concentrically braced steel frames located along the exterior walls (figure 3.19a). The building erected at the ELSA included the three interior MRFs along with secondary beams and transverse cross bracings in order to optimize the experimental effort.

The prototype structure was designed according to Eurocode provisions for all static load combinations involving gravity, wind, snow and live loads, and seismic combinations; the frame was assumed to be constructed on rock in an active seismic region with a design ground acceleration equal to 0.4g.

A capacity design approach was followed for the sizing of the structure. A beam end-plate design was selected for the PS joints; beam end-plates and web column zones were designed to resist the actions obtained from the elastic analysis: their strength was kept close so that yielding will develop

simultaneously in both components. In order to ensure an effective hierarchy of yielding under strong ground motion shaking, beams, columns, and components were checked against design forces compared with those that lead to yield dissipative mechanisms in the end-plates and column web panels. For end-plate bolts, premature failure of the bolts prior to flexural yielding of the end-plates was prevented, satisfying the following conditions. Figure 3.19 and table 3.11 briefly summarize the main characteristics of the realized structure and of material properties, while more details can be found in Braconi et al. (2008). On the 3D full-scale structure PSD tests were executed considering generated time-history (PGA 0.46g) able to maximize the damage in in beam-to-column joints and to limit the damage in the columns.

Prior to performing the PSD test programme, full-scale sub-assembly monotonic and quasi-static cyclic tests were performed at the University of Pisa on interior and exterior beam-to-column joint specimens to validate design assumptions and to obtain data required to develop a numerical model capable of predicting the behaviour of the test structure.

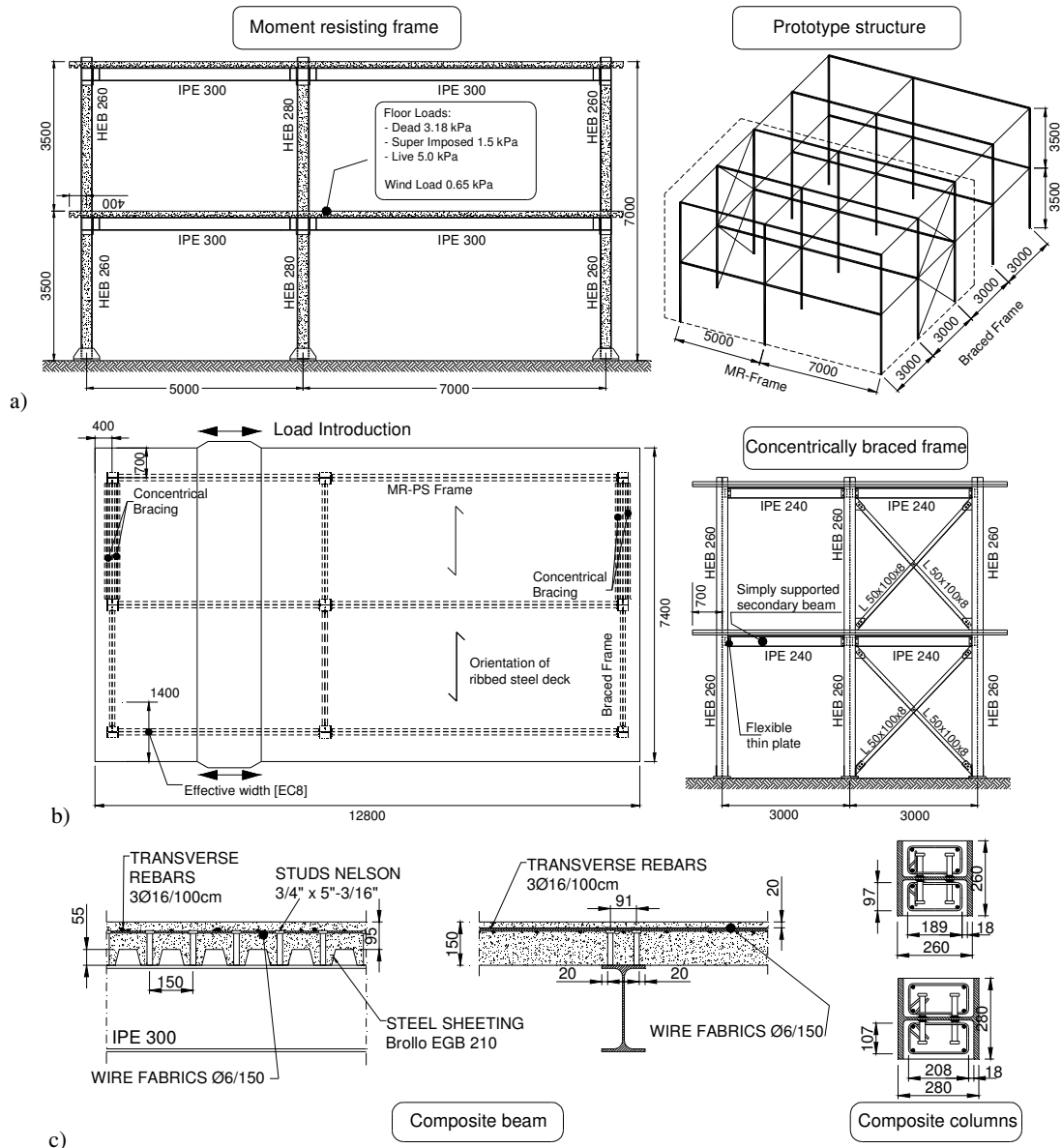


**Figure 3.19:** Designed prototype structure: a) moment-resisting frame and designed structure; b) concrete slab plan view of the realized prototype at JRC and concentrically braced frame, c) main geometrical features of composite beams and columns.

**Table 3.11:** Nominal and actual steel and concrete material properties.

| Component                       |        | $f_{y,nom}$<br>(MPa) | $f_{u,nom}$<br>(MPa) | $f_{u,nom}/f_{y,nom}$ | $\epsilon_{u,nom}$<br>(%) | $f_y$<br>(MPa) | $f_u$<br>(MPa) | $f_u/f_y$ | $\epsilon_u$<br>(%) | $f_y/f_{y,nom}$ | $f_u/f_{u,nom}$ | $f_{cm}$<br>(MPa) |
|---------------------------------|--------|----------------------|----------------------|-----------------------|---------------------------|----------------|----------------|-----------|---------------------|-----------------|-----------------|-------------------|
| <i>Structural steel S235 J0</i> |        |                      |                      |                       |                           |                |                |           |                     |                 |                 |                   |
| IPE 300                         | Flange | 235                  | 360                  | 1,53                  | 28                        | 313            | 480            | 1,53      | 30,7                | 1,33            | 1,33            |                   |
|                                 | Web    | 235                  | 360                  | 1,53                  | 28                        | 370            | 489            | 1,32      | 35,6                | 1,57            | 1,36            |                   |
| IPE 240                         | Flange | 235                  | 360                  | 1,53                  | 28                        | 315            | 448            | 1,42      | 31                  | 1,34            | 1,24            |                   |



these connections. Precast partially encased composite columns made with steel profiles were used for the exterior and interior joints, respectively. Eurocode 8 capacity design provisions were followed such that energy dissipation is shared between beam end plate flexural yielding and shear yielding of the column web panel zone. Expected material overstrength was taken into account in the process to ensure that the intended yielding mechanisms would develop. The nominal material properties of the materials Class S235 structural steel, Class C25/30 concrete and Class B450-C reinforcing steel. In the tests, a displacement controlled actuator was used to impose a pre-determined storey drift to the specimens (figure 3.20). More details related to the characteristics of the sub-assemblages are presented in Braconi et al. 2007. A simplified scheme of the considered interior joint tested in Pisa is presented in figure 3.23.

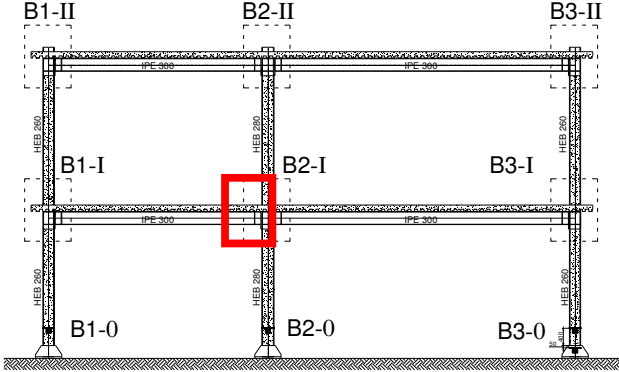


Figure 3.21: Instrumented frame of the full-scale structure at Ispra (considered interior joint B2-I of the internal frame).

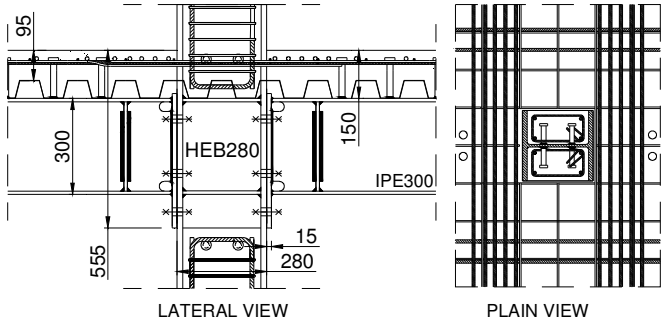


Figure 3.22: Detail of tested internal joint of full scale structure at Ispra laboratory (B2-I).

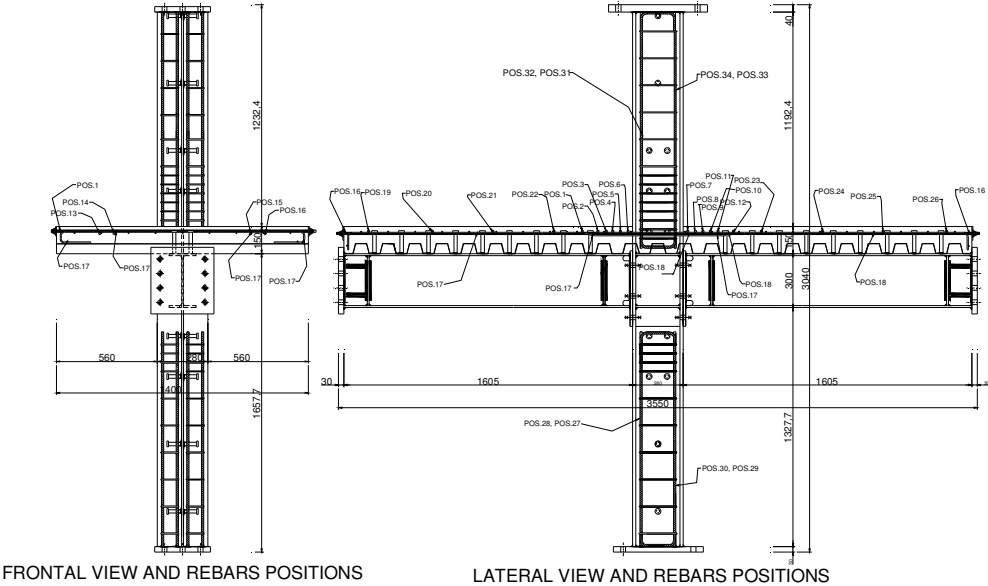


Figure 3.23: Substructure of an interior joint (CJ1) tested at the University of Pisa.

#### 4. SELECTION OF THE SEISMIC INPUT FOR R.C. CASE STUDY BUILDINGS

The earthquake time-histories to be used in the numerical simulations were opportunely selected from a reduced database including natural accelerograms taken from European Strong Motion Database (ESMD) and other significative recent recorded seismic events.

According to actual standards for constructions (Eurocode 8 EN 1998-1:2005, Italian Standard D.M.14/01/2008), at least seven artificial accelerograms shall be used for the execution of non linear dynamic analyses, considering as results the mean values of the outputs obtained from each time history. In the present work, a specific investigation of most significative natural ground motions for each of the designed r.c. structures, to be adopted for numerical simulations (IDA), was executed.

##### 4.1 Definition of time-histories database and time history processing

A first group of earthquake time-histories was selected among the ones used in the definition of European hazard and of most recent attenuation models. Time-histories from 1976 to 2000 from EMSD were considered: 157 accelerograms were taken into account with their three different components (N-S, E-W, Up-Down). The preliminary selection of seismic events was executed on the base of the following parameters:

- All the European regions in the Mediterranean areas and Turkey were considered.
- The maximum focal depth was fixed up to 30 km.
- The surface magnitude ( $M_S$ ) was fixed higher than 4.0.
- Different site conditions – rock (A), stiff soil (B), soft soil (C) were considered.
- Tri-axial records (three wave's components).

Earthquake time histories with frequencies lower than 0.25 Hz and higher than 25 Hz were neglected; the selected accelerograms were grouped according to the classes presented in the figure 4.1 and each group was processed separately, providing consequently homogeneous geological site conditions and magnitude variation ranges. After the individuation of groups (figure 4.1), time histories were analyzed in order to determine their demand in terms of number of cycles ( $N_{Cycles}$ ) and excursion of ground acceleration during the cycles ( $\Delta_{g.a.}$ ). Appropriate counting techniques were employed to define  $N_{Cycles}$  and  $\Delta_{g.a.}$ ; in particular, peak counting method, level crossing counting method, range counting method and indirect estimation were considered. Peak counting technique considered only the maximum points of an earthquake, neglecting the intermediate cycles and the local unloading phenomena usually present during a ground motion (figure 4.2a). Level crossing counting technique prescribed the measure of threshold over-passing (figure 4.2b): this technique appeared quite artificial and, also in this case, the complete physical meaning of the phenomena was not fully identified.

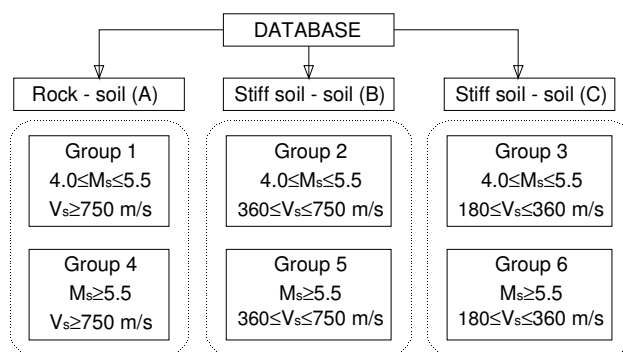


**Figure 4. 1:** Subdivision of time-histories in homogeneous classes: same magnitude range and geological local conditions.

Range counting technique, on the contrary, was able to represent the cyclic behaviour of the ground shaking and the amplitude of cycles, including the ones that did not pass through the zero and that consequently did not reverse the sign of peak ground acceleration (figure 4.3). Different methodologies were presented in the current literature for the execution of the range counting; in the present work, the *rain flow counting method* was used for the processing of time histories.

In particular, the application of the rain flow method to time histories belonging to group 5 is presented, since all the presented case studied were designed considering soil type “B” and high seismicity area (magnitude higher than 5.5).

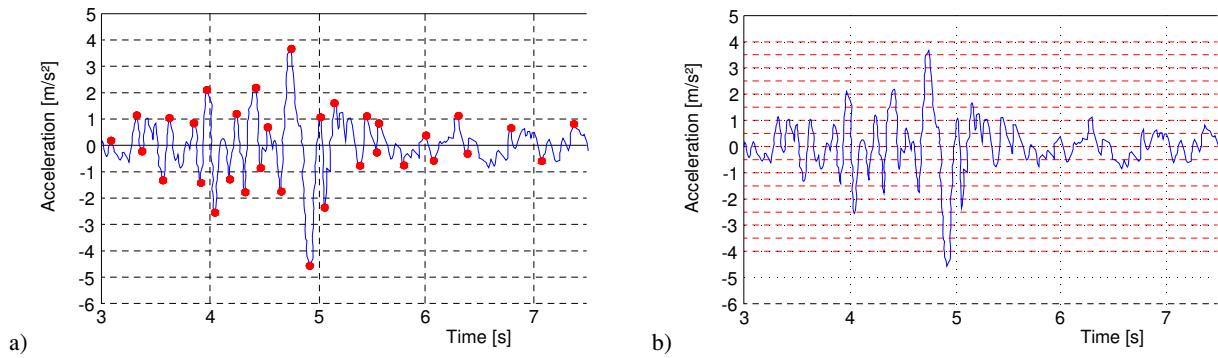


Figure 4. 2: a) Peak counting technique, b) Level crossing counting technique.

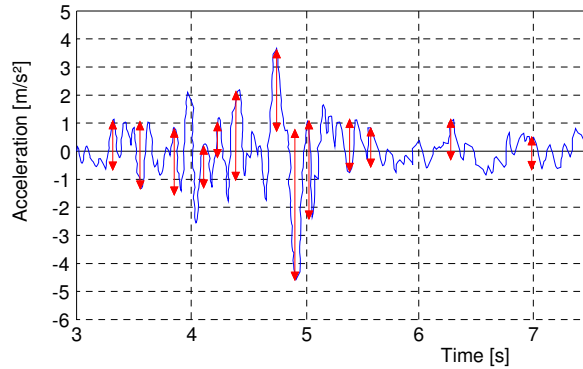


Figure 4. 3: Range counting technique using rain-flow method.

## 4.2 Application of range counting method to Group 5

Each time history belonging to group 5 (table 4.1) was analyzed with the rain-flow method; the individuated cycles were classified into three different amplitude intervals related to the maximum value recognized during the processing: 25%÷50% of maximum amplitude, 50%÷75% of maximum amplitude and higher than 75% of maximum amplitude.

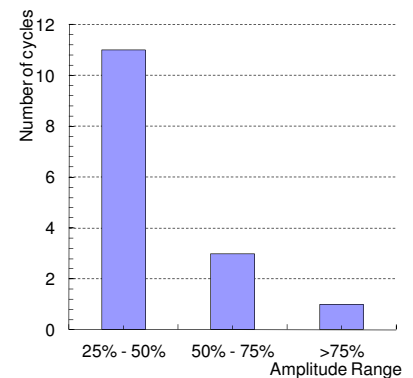
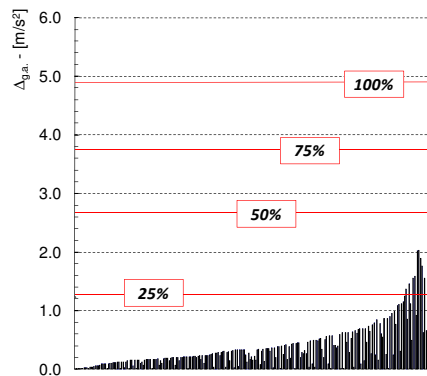
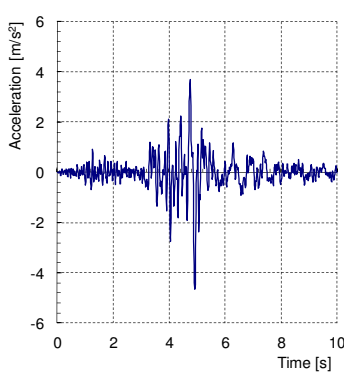
Figure 4.4 presents an example of the application of the rain-flow method to the three components (x, y and z) of a generic accelerogram.

The preliminary results obtained from the application of rain-flow method to all the time histories presented in table 4.1 were used for a more accurate characterization of accelerograms, in terms of number of cycles ( $N_{cycles}$ ), amplitude ( $\Delta_{g.a.}$ ), correlation with epicentre distance and strong motion duration. As visible from figure 4.4, the number of cycles characterized by high amplitude was very low compared to the ones respectively associated to medium and low amplitude, considering for “low amplitude” the range 25%-50% of the maximum amplitude, for “medium amplitude” the 50%-75% of the maximum amplitude and for “high amplitude” values higher than 75% of the maximum amplitude. Figure 4.5.b confirmed what already presented: blue rhomboidal points referred to high amplitude, red squares to medium amplitude and orange triangle to low amplitude.

As visible from figure 4.5, the number of cycles increased with the epicentre distance and decreased with the increasing of peak ground acceleration (PGA). These phenomena were related to the distribution of the energy associated to the earthquake: the epicentre distance increased with the energy distributed among frequencies, reducing the amplitude of cycles and increasing, on the other hand, their total number. The number of cycles, obviously, increased also with the increase of strong motion duration (figure 4.5d). Figures 4.5 and 4.6, provide general descriptive parameters of the analyzed earthquake time histories; PGA and maximum amplitude of cycles were perfectly correlated quantities, while magnitude of earthquake and maximum amplitude of cycles were not completely associated. According to these preliminary observations, the maximum amplitude of cycles was assumed as intensity measure of seismic input and hazard parameter related to low-cycles fatigue demand.

**Table 4. 1:** Earthquakes belonging to group 5 and analyzed with rain flow technique.

| ID  | Name                  | Distance<br>[km] | Depth<br>[km] | $M_s$ | ID   | Name              | Distance<br>[km] | Depth<br>[km] | $M_s$ |
|-----|-----------------------|------------------|---------------|-------|------|-------------------|------------------|---------------|-------|
| 48  | Friuli                | 132              | 6             | 6.5   | 366  | Lazio Abruzzo     | 33               | 8             | 5.9   |
| 49  | Friuli                | 48               | 6             | 6.5   | 367  | Lazio Abruzzo     | 67               | 8             | 5.9   |
| 50  | Friuli                | 93               | 6             | 6.5   | 370  | Lazio Abruzzo     | 72               | 8             | 5.9   |
| 119 | aftershock Friuli     | 83               | 16            | 5.7   | 376  | Lazio Abruzzo     | 64               | 8             | 5.9   |
| 120 | aftershock Friuli     | 16               | 16            | 5.7   | 436  | Killini           | 19               | 12            | 5.65  |
| 123 | aftershock Friuli     | 16               | 16            | 5.7   | 535  | Erzincan          | 13               | 10            | 6.75  |
| 126 | aftershock Friuli     | 18               | 15            | 6.2   | 536  | Erzincan          | 65               | 10            | 6.75  |
| 129 | aftershock Friuli     | 40               | 15            | 6.2   | 537  | Erzincan          | 76               | 10            | 6.75  |
| 130 | aftershock Friuli     | 84               | 15            | 6.2   | 538  | Pulumur           | 45               | 10            | 5.8   |
| 131 | aftershock Friuli     | 17               | 15            | 6.2   | 547  | Izmir             | 63               | 17            | 6     |
| 134 | aftershock Friuli     | 17               | 15            | 6.2   | 548  | Izmir             | 30               | 17            | 6     |
| 139 | aftershock Friuli     | 22               | 12            | 6.1   | 549  | Izmir             | 41               | 17            | 6     |
| 142 | aftershock Friuli     | 42               | 12            | 6.1   | 550  | Gulf of Corinth   | 25               | 15            | 5.9   |
| 143 | aftershock Friuli     | 83               | 12            | 6.1   | 569  | Patras            | 29               | 15            | 5.6   |
| 146 | aftershock Friuli     | 17               | 12            | 6.1   | 572  | Patras            | 25               | 15            | 5.6   |
| 147 | aftershock Friuli     | 17               | 12            | 6.1   | 591  | Umbro-Marchigiano | 3                | 7             | 5.7   |
| 153 | Caldiran              | 52               | 10            | 7.34  | 592  | Umbro-Marchigiano | 5                | 6             | 6     |
| 171 | Basso Tirreno         | 18               | 15            | 5.83  | 595  | Umbro-Marchigiano | 25               | 7             | 5.7   |
| 196 | Montenegro            | 25               | 12            | 7.04  | 596  | Umbro-Marchigiano | 23               | 6             | 6     |
| 197 | Montenegro            | 24               | 12            | 7.04  | 601  | Umbro-Marchigiano | 27               | 7             | 5.7   |
| 209 | aftershock Montenegro | 24               | 7             | 5.8   | 602  | Umbro-Marchigiano | 27               | 6             | 6     |
| 210 | aftershock Montenegro | 63               | 7             | 5.8   | 619  | Umbro-Marchigiano | 78               | 6             | 6     |
| 227 | aftershock Montenegro | 54               | 5             | 6.34  | 640  | aftershock Umbro  | 20               | 7             | 5.6   |
| 244 | Valnerina             | 39               | 4             | 5.84  | 643  | aftershock Umbro  | 37               | 7             | 5.6   |
| 247 | Valnerina             | 23               | 4             | 5.84  | 645  | aftershock Umbro  | 26               | 7             | 5.6   |
| 248 | Valnerina             | 37               | 4             | 5.84  | 648  | aftershock Umbro  | 13               | 7             | 5.6   |
| 288 | Campano Lucano        | 43               | 16            | 6.87  | 906  | Norcia            | 18               | 6             | 5.9   |
| 291 | Campano Lucano        | 16               | 16            | 6.87  | 947  | Potenza           | 31               | 12            | 5.6   |
| 294 | Campano Lucano        | 26               | 16            | 6.87  | 1214 | Kocaeli           | 214              | 17            | 7.8   |
| 295 | Campano Lucano        | 58               | 16            | 6.87  | 1225 | Kocaeli           | 330              | 17            | 7.8   |
| 299 | Campano Lucano        | 52               | 16            | 6.87  | 1233 | Kocaeli           | 34               | 17            | 7.8   |
| 300 | Campano Lucano        | 100              | 16            | 6.87  | 1312 | Athens            | 25               | 9             | 5.9   |
| 351 | Biga                  | 84               | 7             | 6.02  | 1559 | Duzce             | 304              | 14            | 7.3   |
| 352 | Biga                  | 45               | 7             | 6.02  | 1566 | Duzce             | 65               | 14            | 7.3   |
| 353 | Biga                  | 95               | 7             | 6.02  | 1702 | Duzce             | 372              | 14            | 7.3   |
| 354 | Kars                  | 33               | 14            | 6.74  | 2015 | Ionian            | 18               | 3             | 6.16  |



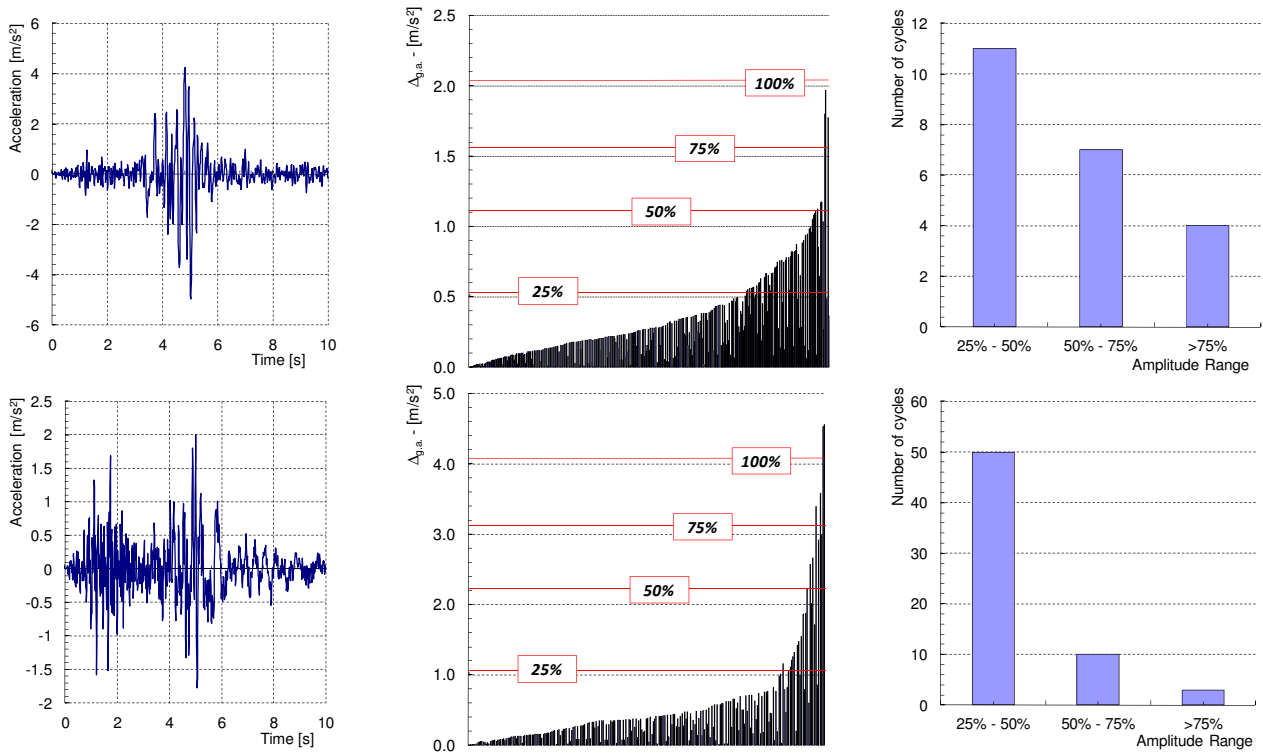


Figure 4. 4: Example of application of the rain flow counting technique.

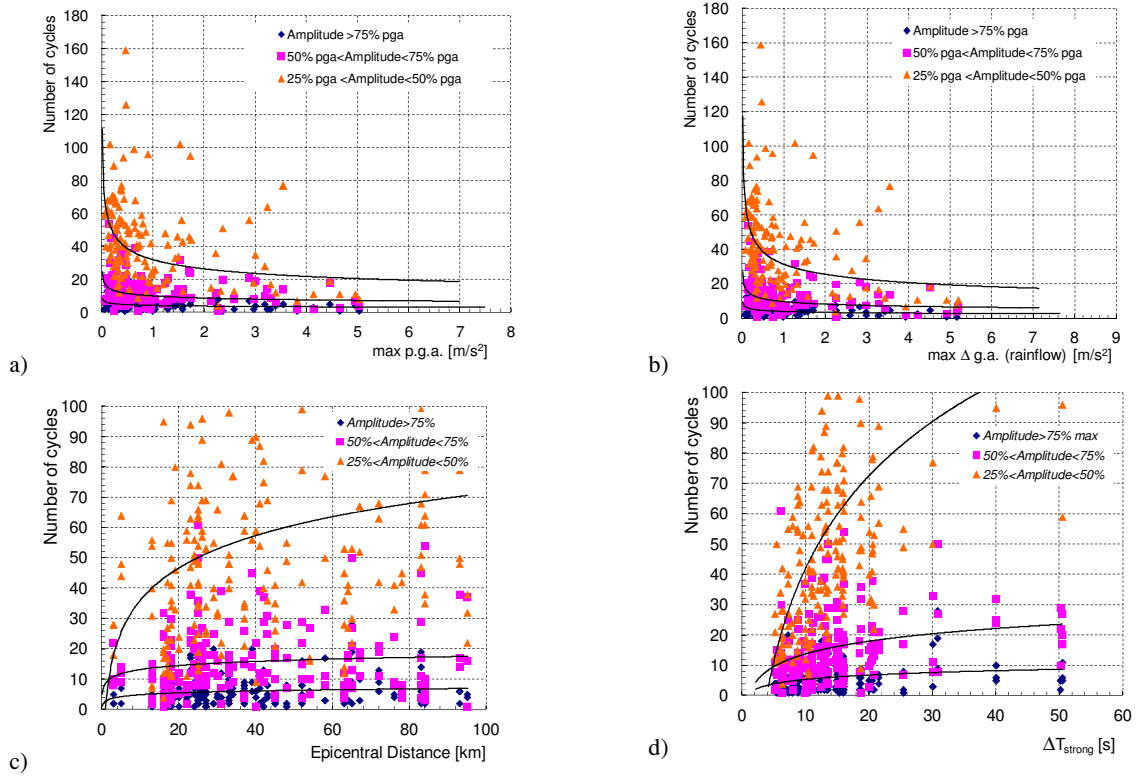
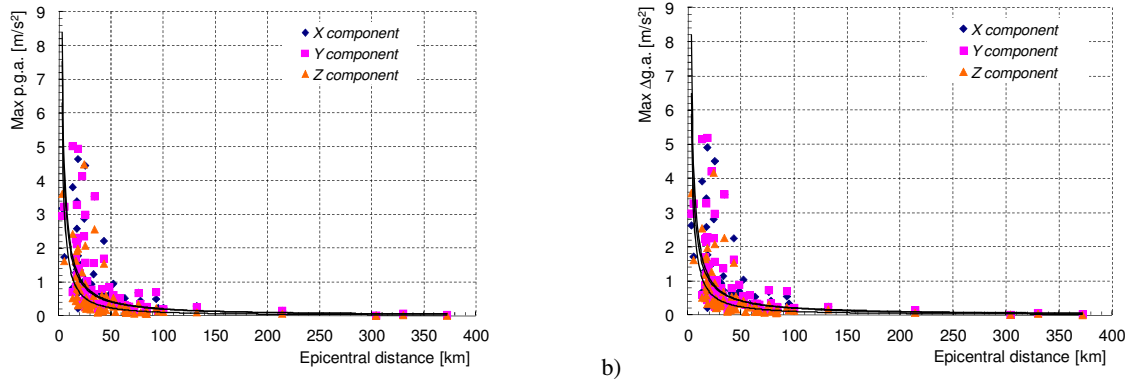
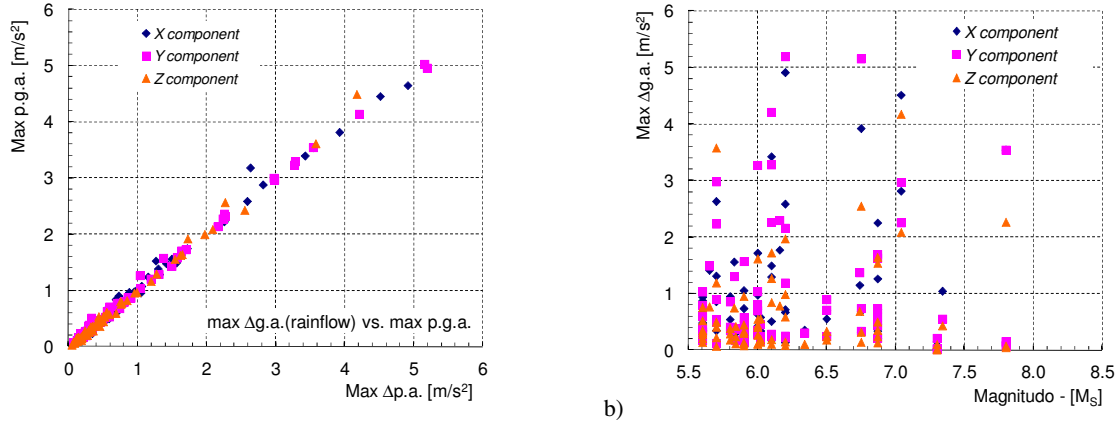


Figure 4. 5: a)  $N_{cycles}$  – PGA of input, b)  $N_{cycles}$  – max amplitude of acceleration cycles, c)  $N_{cycles}$  – epicentre distance, d)  $N_{cycles}$  – strong motion duration.



**Figure 4. 6:** a) PGA – epicentre distance, b) Max amplitude of cycles – epicentre distance.



**Figure 4. 7:** a) Correlation between PGA and maximum cycles amplitude, b) Correlation between maximum amplitude cycles and earthquake magnitude

A first selection of the time histories presented in table 4.1 was directly made neglecting the earthquakes characterized by very low peak ground acceleration values, with too high number of cycles (usually associated to very low levels of acceleration) and the ones characterized by a low number of cycles with low peak ground acceleration. In the tables 4.2 and 4.3 the first organization of database Group 5 according to the previous considerations is presented.

The earthquakes presented in tables 4.2 and 4.3 were then ordered in relation to the increasing epicentre distance and to the increasing values of amplitude of maximum cycles, considering the three components of the seismic event; moreover, earthquakes characterized by PGA lower than 0.05g were not considered. All the other natural time histories were processed again for individuating those ones able to maximize the demand on structural designed case studies. The procedure adopted is presented in the following paragraphs.

**Table 4. 2:** First set of analyzed time-histories.

| ID  | Name                  | Distance [km] | $\Delta_{g.a.x}$ m/s <sup>2</sup> | $\Delta_{g.a.y}$ m/s <sup>2</sup> | $\Delta_{g.a.z}$ m/s <sup>2</sup> | 75% $\Delta_{g.a.x}$ N <sub>Cycles</sub> | 75% $\Delta_{g.a.y}$ N <sub>Cycles</sub> | 75% $\Delta_{g.a.z}$ N <sub>Cycles</sub> |
|-----|-----------------------|---------------|-----------------------------------|-----------------------------------|-----------------------------------|--|--|--|
| 126 | aftershock Friuli     | 18            | 4.913                             | 5.192                             | 1.971                             | 1  | 4  | 10                                       |
| 196 | Montenegro            | 25            | 4.514                             | 2.972                             | 2.085                             | 5  | 4  | 17                                       |
| 146 | aftershock Friuli     | 17            | 3.425                             | 3.280                             | 1.725                             | 4  | 2  | 8  |
| 197 | Montenegro            | 24            | 2.816                             | 2.255                             | 4.174                             | 7  | 1  | 50                                       |
| 134 | aftershock Friuli     | 17            | 2.588                             | 2.161                             | 0.990                             | 2  | 7  | 18                                       |
| 288 | Campano Lucano        | 43            | 2.253                             | 1.634                             | 1.540                             | 5  | 8  | 15                                       |
| 171 | Basso Tirreno         | 18            | 1.562                             | 1.307                             | 0.752                             | 5  | 2  | 15                                       |
| 139 | aftershock Friuli     | 22            | 1.495                             | 4.209                             | 1.272                             | 4  | 3  | 7  |
| 123 | aftershock Friuli     | 16            | 1.313                             | 2.236                             | 1.194                             | 3  | 8  | 5  |
| 147 | aftershock Friuli     | 17            | 1.297                             | 2.264                             | 0.844                             | 4  | 3  | 8  |
| 291 | Campano Lucano        | 16            | 1.264                             | 1.698                             | 1.645                             | 10                                       | 5  | 31                                       |
| 354 | Kars                  | 33            | 1.151                             | 1.375                             | 0.685                             | 4  | 2  | 37                                       |
| 153 | Caldiran              | 52            | 1.046                             | 0.555                             | 0.435                             | 3  | 16                                       | 11                                       |
| 209 | Aftershock Montenegro | 24            | 0.949                             | 0.859                             | 0.386                             | 5  | 7  | 13                                       |
| 120 | aftershock Friuli     | 16            | 0.862                             | 0.900                             | 0.501                             | 5  | 6  | 4  |

|     |                       |     |       |       |       |    |    |    |
|-----|-----------------------|-----|-------|-------|-------|----|----|----|
| 294 | Campano Lucano        | 26  | 0.726 | 0.735 | 0.503 | 6  | 5  | 25 |
| 129 | aftershock Friuli     | 40  | 0.719 | 0.252 | 0.151 | 1  | 4  | 15 |
| 49  | Friuli                | 48  | 0.710 | 0.895 | 0.337 | 8  | 2  | 23 |
| 131 | aftershock Friuli     | 17  | 0.672 | 1.191 | 0.590 | 10 | 6  | 6  |
| 352 | Biga                  | 45  | 0.584 | 0.457 | 0.558 | 3  | 3  | 3  |
| 50  | Friuli                | 93  | 0.555 | 0.712 | 0.240 | 2  | 6  | 28 |
| 210 | aftershock Montenegro | 63  | 0.544 | 0.345 | 0.289 | 3  | 5  | 15 |
| 142 | aftershock Friuli     | 42  | 0.511 | 0.287 | 0.190 | 1  | 13 | 6  |
| 299 | Campano Lucano        | 52  | 0.464 | 0.438 | 0.356 | 2  | 10 | 11 |
| 227 | Aftershock Montenegro | 54  | 0.358 | 0.307 | 0.107 | 6  | 5  | 6  |
| 247 | Valnerina             | 23  | 0.348 | 0.371 | 0.421 | 18 | 17 | 14 |
| 353 | Biga                  | 95  | 0.342 | 0.174 | 0.147 | 1  | 5  | 10 |
| 295 | Campano Lucano        | 58  | 0.340 | 0.589 | 0.238 | 17 | 3  | 27 |
| 244 | Valnerina             | 39  | 0.328 | 0.174 | 0.239 | 6  | 20 | 27 |
| 248 | Valnerina             | 37  | 0.303 | 0.380 | 0.114 | 9  | 3  | 26 |
| 48  | Friuli                | 132 | 0.256 | 0.249 | 0.182 | 8  | 5  | 4  |
| 351 | Biga                  | 84  | 0.221 | 0.238 | 0.194 | 3  | 5  | 10 |
| 300 | Campano Lucano        | 100 | 0.215 | 0.219 | 0.133 | 7  | 9  | 22 |
| 143 | aftershock Friuli     | 83  | 0.175 | 0.249 | 0.109 | 14 | 11 | 29 |
| 130 | aftershock Friuli     | 84  | 0.140 | 0.224 | 0.086 | 8  | 4  | 22 |
| 119 | aftershock Friuli     | 83  | 0.138 | 0.118 | 0.068 | 2  | 6  | 38 |

**Table 4. 3:** Second set of analyzed time-histories.

| ID   | Name              | Distance<br>[km] | $\Delta_{g.a.x}$<br>m/s <sup>2</sup> | $\Delta_{g.a.y}$<br>m/s <sup>2</sup> | $\Delta_{g.a.z}$<br>m/s <sup>2</sup> | 75% $\Delta_{g.a.x}$<br>N <sub>Cycles</sub> | 75% $\Delta_{g.a.y}$<br>N <sub>Cycles</sub> | 75% $\Delta_{g.a.z}$<br>N <sub>Cycles</sub> |
|------|-------------------|------------------|--------------------------------------|--------------------------------------|--------------------------------------|---|---|---|
| 535  | Erzincan          | 13               | 3.924                                | 5.156                                | 2.550                                | 1   | 1   | 4   |
| 1233 | Kocaeli           | 34               | 3.543                                | 3.543                                | 2.266                                | 5   | 5   | 7   |
| 591  | Umbro-Marchigiano | 3                | 2.633                                | 2.981                                | 3.580                                | 5   | 2   | 2   |
| 2015 | Ionian            | 18               | 1.772                                | 2.295                                | 0.786                                | 8   | 6   | 6   |
| 592  | Umbro-Marchigiano | 5                | 1.718                                | 3.271                                | 1.618                                | 7   | 2   | 9   |
| 436  | Killini           | 19               | 1.415                                | 1.494                                | 0.769                                | 5   | 4   | 9   |
| 1312 | Athens            | 25               | 1.057                                | 1.569                                | 0.953                                | 5   | 4   | 2   |
| 602  | Umbro-Marchigiano | 27               | 0.975                                | 1.038                                | 0.444                                | 1   | 2   | 3   |
| 947  | Potenza           | 31               | 0.942                                | 0.797                                | 0.318                                | 4   | 4   | 12  |
| 640  | aftershock Umbro  | 20               | 0.877                                | 1.035                                | 0.758                                | 4   | 7   | 1   |
| 366  | Lazio Abruzzo     | 33               | 0.739                                | 0.582                                | 0.451                                | 2   | 10  | 3   |
| 596  | Umbro-Marchigiano | 23               | 0.725                                | 0.699                                | 0.407                                | 5   | 13  | 17  |
| 537  | Erzincan          | 76               | 0.690                                | 0.740                                | 0.320                                | 4   | 5   | 8   |
| 648  | aftershock Umbro  | 13               | 0.686                                | 0.594                                | 0.523                                | 5   | 5   | 2   |
| 549  | Izmir             | 41               | 0.637                                | 0.803                                | 0.549                                | 7   | 2   | 2   |
| 572  | Patras            | 25               | 0.484                                | 0.391                                | 0.350                                | 2   | 7   | 17  |
| 601  | Umbro-Marchigiano | 27               | 0.459                                | 0.495                                | 0.224                                | 5   | 6   | 1   |
| 619  | Umbro-Marchigiano | 78               | 0.430                                | 0.357                                | 0.114                                | 4   | 8   | 6   |
| 550  | Gulf of Corinth   | 25               | 0.390                                | 0.263                                | 0.296                                | 3   | 10  | 2   |
| 569  | Patras            | 29               | 0.348                                | 0.331                                | 0.283                                | 2   | 20  | 2   |
| 595  | Umbro-Marchigiano | 25               | 0.347                                | 0.539                                | 0.411                                | 9   | 8   | 2   |
| 645  | aftershock Umbro  | 26               | 0.343                                | 0.325                                | 0.211                                | 6   | 4   | 7   |
| 536  | Erzincan          | 65               | 0.323                                | 0.340                                | 0.143                                | 2   | 7   | 13  |
| 538  | Pulumur           | 45               | 0.308                                | 0.410                                | 0.181                                | 2   | 3   | 19  |
| 548  | Izmir             | 30               | 0.307                                | 0.297                                | 0.270                                | 4   | 5   | 4   |
| 547  | Izmir             | 63               | 0.301                                | 0.276                                | 0.110                                | 4   | 2   | 7   |
| 643  | aftershock Umbro  | 37               | 0.291                                | 0.170                                | 0.139                                | 2   | 7   | 2   |
| 367  | Lazio Abruzzo     | 67               | 0.264                                | 0.312                                | 0.137                                | 11  | 3   | 10  |
| 906  | Norcia            | 18               | 0.225                                | 0.450                                | 0.332                                | 5   | 4   | 4   |
| 376  | Lazio Abruzzo     | 64               | 0.195                                | 0.211                                | 0.122                                | 3   | 3   | 3   |
| 1566 | Duzce             | 65               | 0.151                                | 0.213                                | 0.102                                | 9   | 28  | 19  |
| 1214 | Kocaeli           | 214              | 0.150                                | 0.156                                | 0.076                                | 10  | 7   | 4   |

|      |               |     |       |       |       |    |    |     |
|------|---------------|-----|-------|-------|-------|----|----|-----|
| 370  | Lazio Abruzzo | 72  | 0.104 | 0.140 | 0.083 | 13 | 6  | 9   |
| 1225 | Kocaeli       | 330 | 0.076 | 0.075 | 0.047 | 2  | 3  | 2   |
| 1702 | Duzce         | 372 | 0.027 | 0.032 | 0.010 | 28 | 4  | 300 |
| 1559 | Duzce         | 304 | 0.020 | 0.015 | 0.014 | 43 | 22 | 9   |

### 4.3 Selection of representative time histories for designed structures

#### 4.3.1 Park and Ang Damage Indicator

Among the pre-selected natural time histories presented in the tables 4.2 and 4.3, a further choice needed to be executed in order to individuate about 3 or 4 accelerograms to be used for the non linear analyses on designed r.c. buildings. The evaluation of the most representative strong motions was executed taking into account their effects on the structural behaviour of buildings (for example in terms of dissipated energy or displacement). Opportune analyses were executed for the evaluation of specific damage parameters able to provide significative information about the seismic performance of each considered case study.

Nowadays, the most used damage indicator is the Park and Ang index ( $DI_{PA}$ ), generally defined as the combination of dissipated energy and plastic deformation, simply expressed in terms of displacement. The original formulation of the damage indicator (Wen, Park and Ang 1989) was provided by equation 4.1, in which  $\delta_m$  was the maximum response deformation,  $\delta_u$  the ultimate deformation under monotonic loads,  $Q_y$  the yielding strength,  $dE$  the dissipated energy and  $\beta$  a parameter.

$$DI_{PA} = \frac{\delta_m}{\delta_u} + \frac{\beta}{Q_y \delta_u} \int dE \quad (4.1)$$

Park and Ang damage index generally assumed values lower than 0.2 if no damage was evidenced, values between 0.2 and 0.5 in the case of structural but reparable damages, values between 0.5 and 1.0 for structural not reparable damages and, finally, values higher than 1.0 in case of structural collapse. Table 5.4 summarizes the meaning of the different values assumed by  $DI_{PA}$ .

The main problem of the application of Park and Ang index was the definition of the parameter  $\beta$ ; according to the original formulation, equation 4.2 should be followed, in which  $\rho_w$  was the confinement ration,  $l/d$  the shear span ratio,  $\rho_l$  the longitudinal reinforcement ratio and  $n_0$  the normalized axial force.

$$\beta = 0.7^{\rho_w} \left( -0.447 + 0.073 \cdot \frac{l}{d} + 0.24n_0 + 0.314\rho_l \right) \quad (4.2)$$

**Table 4. 4:** Park and Ang Damage Index Performance (Oyarzo Vera 2006).

| $DI_{P\&A}$   | Level damage    |   |
|---------------|-----------------|---|
| 0.00 - 0.10   | No damage       | Localized minor cracking at worst                     |
| 0.10 - 0.25   | Light damage    | Minor cracking throughout                             |
| 0.25 - 0.40   | Moderate damage | Severe cracking and localized spalling                |
| 0.40 - 1.00   | Severe damage   | Crushing of concrete and exposure of reinforcing bars |
| 1.00 and more | Collapse        | Total failure of the structure                        |

The experimental determination of the parameter  $\beta$  was quite complex; the relationship between  $\beta$  and the dissipated energy was evidenced by Cosenza and Manfredi (2000) for the case of an elasto-perfectly plastic (EPP) reference systems with no degradation. In particular, the cited work evidenced that  $DI_{PA}$  evaluated for  $\beta$  values between 0.6 and 0.8 generally provided similar results respect to the ones simply obtained from energy based methodologies, while energy dissipation did not affect the results for very low values of  $\beta$  parameters.

Moreover, several experimental tests were executed in order to evaluate the level of damaging of structural elements and its correlation to Park and Ang index; as an example Fardis (1995) used the results of experimental tests for the evaluation of the efficiency of damage index, suggesting also some modifications to the original formulation of  $DI_{PA}$ , substituting the maximum rotation with the peak value of the member deformation energy.

For  $\beta$  value equal to 0.15 the results obtained from Park and Ang index and from low-cycle fatigue damage parameters mainly coincided; as a consequence, in general for r.c. structure the assumption  $\beta=0.15$  was generally adopted (Cosenza and Manfredi 2000). Despite the introduction of other

modified and refined structural damage indicators (Bozorgnia and Bertero 2001), the Park and Ang damage indicator still remain the most common used for the evaluation of the global behaviour of structures under seismic events.

In the present work, the assessment of the damaging and deterioration of structures was executed following a macroscopic approach: equivalent SDOF models were opportunely individuated for each of the designed r.c. structures and the execution of non linear monotonic and cyclic analyses allowed the evaluation of the Park and Ang damage indicators corresponding to different seismic events, finally individuating the most requiring natural time histories.

#### 4.3.2 Individuation of the equivalent SDOF model

In order to individuate the most requiring natural time histories for each designed r.c. building, simplified models representative of the monotonic and cyclic behaviour of the structures were subjected to non linear dynamic analyses using the pre-selected accelerograms evidenced in the tables 4.2 and 4.3, and opportune damage index parameters were evaluated.

Different techniques were presented in the current literature for the individuation of Single Degree Of Freedom (SDOF) models able to correctly represent the behaviour of complex structures in which the first mode of vibration prevailed over the others. Specific indications were provided by Eurocode 8 (EN 1998-1:2005), American Standard for r.c. buildings (FEMA 356) and Italian standards for constructions (D.M. 14/01/2008); all the above cited methodologies were elaborated on the base of the N2 method proposed by Fajfar and Fischinger (1988).

The N2 method, firstly proposed at the end of the 1980s and further detailed to be applied to different structural typologies, allowed the individuation of an equivalent SDOF model starting from the original MDOF model representative of the global structure.

An opportune distribution of lateral increasing forces was selected and applied to the considered structure; starting from the consideration that a unique solution for the choice of load pattern did not exist, Fajfar (2000) proposed the adoption of a load vector defined according to equation 6, in which  $p$  was the parameter controlling the magnitude of lateral loads,  $M$  was the mass matrix and  $\Phi$  the displacement shape. As visible from equation 4.3, the displacement shape and the lateral loads adopted were not mutually independent as in the majority of pushover analyses.

$$P = p \cdot \Psi = p \cdot M \cdot \Phi \quad (4.3)$$

The lateral force corresponding to the  $i$ -th level of the building was proportional to the single component  $\Phi_i$  of the displacement shape  $\Phi$ , weighted through the use of the mass  $m_i$ :

$$P_i = p \cdot m_i \cdot \Phi_i \quad (4.4)$$

The approach presented by Fajfar (2000) for the individuation of the lateral forces distribution allowed the rapid transformation of the original MDOF system into an equivalent SDOF one using simple mathematical expressions and without the necessity of additional approximations.

The capacity curve of the SDOF system was derived from the one corresponding to the MDOF system reducing the values of force and displacement by the modal participation factor  $\Gamma$ , defined by equation 4.5:

$$\Gamma = \frac{\Phi^T M 1}{\Phi^T M \Phi} = \frac{\sum m_i \Phi_i}{\sum m_i \Phi_i^2} = \frac{m^*}{\sum m_i \Phi_i^2} \quad (4.5)$$

The mass characterizing the bilinear equivalent SDOF model proposed by Fajfar (2000) was defined by equation 4.6, while the displacements  $D^*$  and forces  $F^*$  were described by equations 4.7 and 4.8, being  $V$  the shear base of the MDOF model. In the presented expressions, the values of modal displacements  $\Phi_i$  were normalized respect to the top, assumed unitary.

$$m^* = \Phi^T M 1 = \sum m_i \Phi_i \quad (4.6)$$

$$D^* = \frac{D}{\Gamma} \quad (4.7)$$

$$F^* = \frac{V}{\Gamma} = \frac{\sum P_i}{\Gamma} = \frac{\Phi^T M 1 \cdot p_i}{\Gamma} = \frac{p \sum m_i \Phi_i}{\Gamma} \quad (4.8)$$

The slope of elastic branch of the bilinear law allowed the evaluation of the first period of the idealized structure, defined by equation 4.9, being  $F_y^*$  and  $D_y^*$  the force and the displacement corresponding to yielding.

Fajfar (2000) provided some indications for the determination of an equivalent bilinear elasto-plastic SDOF system, underlining, anyway, the possibility of using different methodologies.

Eurocode 8 (EN 1998-1:2005) suggested to define the initial stiffness of the idealized system on the base of energy equivalence considerations, while Italian Standard for constructions (D.M. 14/01/2008) defined the linear branch of the bilinear system imposing the passage for the capacity curve point corresponding to the 60% of the maximum load. Moreover, American Standard FEMA 356 individuated a bilinear equivalent SDOF system characterized by an initial stiffness  $K_e$ , defined as the secant stiffness calculated at a base shear force equal to 60% of the effective yielding strength of the structure, and a post-yield slope  $\alpha$  determined by a line segment passing through the evaluated target displacement.

$$T^* = 2\pi \sqrt{\frac{m^* D^*}{F_y^*}} \quad (4.9)$$

In the present work, the necessity to individuate an equivalent SDOF able to reproduce both the monotonic and the cyclic behaviour of the real structure led to the definition of an equivalent trilinear system, opportunely calibrated taking into account the effects of degradation and deterioration due to the cyclic loading condition on r.c. structures. In the following, the expression “SDOF model” refers to the reduced system obtained from MDOF structure using modal participation factor  $\Gamma$ , while “equivalent SDOF system”

Monotonic pushover analyses were executed on plane MDOF models of the designed r.c. structures, using the distribution load pattern presented by equation 7 and the displacement shapes obtained from the results of linear modal analyses. According to the procedure proposed by Fajfar (2000), a preliminary bilinear elasto-plastic SDOF model was elaborated (figure 4.9): the equivalent mass of the structure was defined by equation 4.6, the indications provided by Italian D.M.14/01/2008 and FEMA 356 allowed the individuation of the initial stiffness and, finally, the principle of energy equivalence led to the evaluation of the equivalent yielding displacement (figure 4.9).

A preliminary structural assessment of the analyzed building, following the indications provided by Eurocode 8 (EN 1998-1:2005) for both ductile and brittle elements and local and global collapse mechanisms, was executed, allowing the individuation of the effective structural behaviour of the building and the individuation of the corresponding ultimate condition (ultimate rotation of beams and columns, shear brittle mechanisms in beams and columns, overcoming of the admissible interstorey drift, according to European and American standards EN 1998-1:2005, FEMA 356).

An idealized *trilinear equivalent SDOF system* was then individuated (figure 4.8), on the base the following considerations:

- The ultimate point of the trilinear law was defined in relation to the global assessment of the structure, considering all the significative collapse criteria for a r.c. building. The point characterized by ultimate strength  $F_u^*$  and ultimate displacement  $d_u^*$  was individuated.
- The first point of the trilinear law was defined imposing the passage of the initial secant stiffness from the point corresponding to the 30% of the ultimate strength ( $F_u^*$ ); this assumption was executed in relation to the effective behaviour of the structure, whose linear field was generally limited up to a force equal to the 30%-35% of the ultimate load.
- The intermediate point was defined considering the energy equivalence between the trilinear model and the original SDOF system; the displacement of the second characteristic point of the idealized system was fixed equal to the yielding one, opportunely defined according to the indications provided by FEMA 356 and D.M.14/01/2008.

In the figure 4.8 the idealized trilinear system is presented, as well as the bilinear elasto-plastic SDOF model obtained from the application of the traditional N2 method. As an example, table 4.5 presents the values characterizing the trilinear equivalent system of residential building in HDC.

In this case, the ultimate condition coincided with the over passing of the interstorey drift limit (4%), leading to the individuation of the final point of the curve ( $d_u^*$ ,  $F_u^*$ ) and of the initial one ( $0.30d_u^*$ ,  $0.30F_u^*$ ). The yielding displacement ( $d_y^*$ ) was evaluated according to the energy equivalence between the SDOF model and the bilinear elasto-plastic one; moreover, energy equivalence was used for the determination of the force corresponding to the second point of the idealized trilinear law.

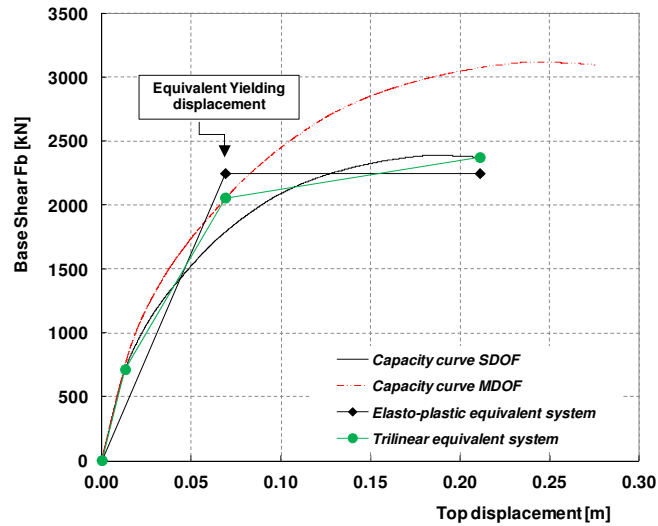


Figure 4. 8: Pushover analysis on residential building in HDC and trilinear equivalent SDOF system.

Table 4. 5: Trilinear equivalent system for residential building in HDC: values of forces and displacements.

| Residential building HDC                               |        |      |  |                |                              |
|--|--------|------|--|----------------|------------------------------|
| Ultimate collapse criteria: interstorey drift limit 4% |        |      | Determination of the equivalent trilinear system |                |                              |
| $d_u^*$  | 0.2098 | m    | ultimate displacement                            |                |                              |
| $F_u^*$  | 2369   | kN   | ultimate force                                   | First point    | $d_1^* = 0.30d_u^*$ 0.0130 m |
| $0.60 d_u^*$   | 0.0440 | m    | initial secant stiffness: 60% of ultimate load   | Second point   | $F_1^* = 0.30F_u^*$ 711 kN   |
| $0.60 F_u^*$   | 1457   | kN   |  |                | $d_2^* = d_y^*$ 0.069 m      |
| $K^*$  | 33080  | kN/m |  |                | $F_2^*$ 2210 kN              |
| $d_y^*$  | 0.0689 | m    | yielding displacement                            | Ultimate point | $d_3^* = d_u^*$ 0.2098 m     |
| $F_y^*$  | 2278.6 | kN   | yielding force                                   |                | $F_3^* = F_u^*$ 2369 kN      |

A *zero-length element* model was then elaborated in OpenSees (Mazzoni et al., 2007) in order to represent the effective monotonic and cyclic behaviour of the designed structures; the assumed mass of the system was defined according to equation 4.6 and the trilinear force-displacement law already defined was opportunely calibrated in order to include deterioration due to cycling action.

“*Pinching4*” material, already implemented in OpenSees, was used allowing the direct representation of the two symmetrical envelopes in tension and compression and the introduction of specific parameters for taking into account the damaging due to unloading and reloading stiffness, strength degradation and dissipation of adsorbed energy.

In order to calibrate the cyclic behaviour of the numerical models, cyclic static analyses were executed on bi-dimensional frames of the designed r.c. buildings; the displacement histories used were defined in relation to the equivalent yielding displacement previously defined for each structure. In particular, different cycles with imposed displacement equal to  $\pm d_y, \pm 2d_y, \pm 3d_y, \dots$  were executed on the SDOF systems (figure 4.9), using the same lateral load distribution adopted for monotonic pushover.

As an example, figure 4.9a presents the base shear – lateral top displacement behaviour of the SDOF model for residential building in HDC, while in the figure 4.9b, the comparison between the SDOF model and the trilinear equivalent system is showed. The parameters characterizing the *pinching 4* material consequently describing the cyclic behaviour of the simplified model were opportunely calibrated on the base of the energy equivalence principle. The procedure presented for residential building in HDC was extended to all the designed r.c. case studies.

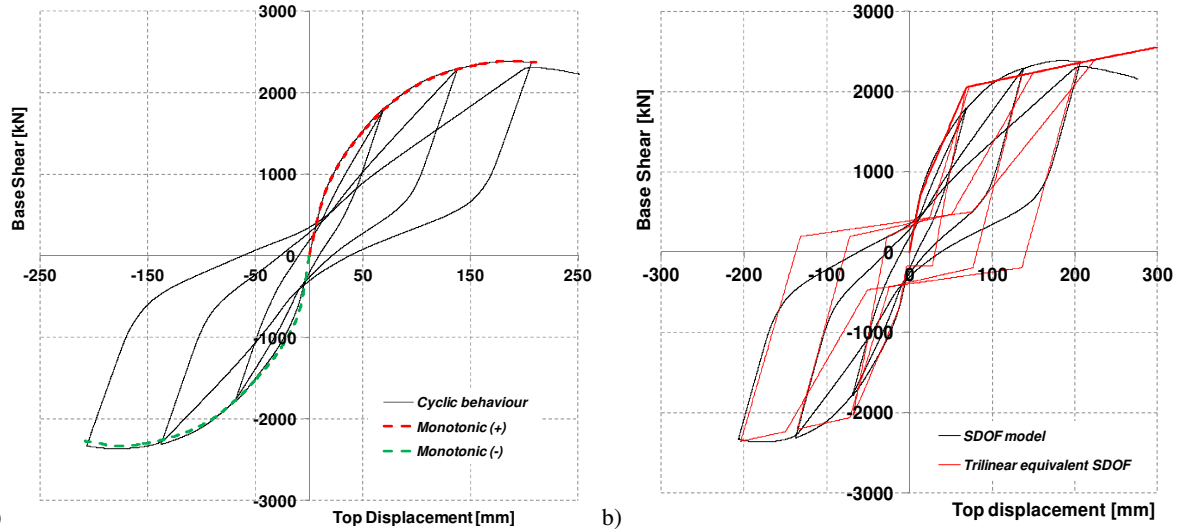


**Figure 4. 9:** a) Base shear vs lateral top displacement under cyclic and monotonic pushover analyses; b) Comparison between the cyclic response of the SDOF model and the trilinear equivalent hysteretic model.

### 4.3.3 Selection of representative time histories

On the individuated zero-length element models with pinching material, Incremental Dynamic Analyses (IDA) were executed, using the pre-selected natural accelerograms characterized by a PGA equal or higher than 0.15 g (evidenced in yellow and orange): this choice was related to the seismic action used for the design of presented r.c. case studies. Both the two horizontal components of the natural time histories, provided by ESMD, were considered, associating a progressive number, as presented in table 4.6. A PGA increment equal to 0.05 g was assumed and IDAs were executed between 0.05 and 1.0 g.

**Table 4. 6:** ID number assigned to the considered accelerograms (PGA  $\geq 0.15$  g, soil type B and magnitude  $\geq 5.5$ ).

| Group 5 (M>5.5, soil B, PGA $\geq 0.15$ g) |                                 |         |       |         |       |
|--|---------------------------------|---------|-------|---------|-------|
| ID   | Name                            | Comp. X | ID n° | Comp. Y | ID n° |
| 1233                                       | Kocaeli                         | x       | 0     | y       | 0     |
| 123  | aftershock of Friuli earthquake | x       | 1     | y       | 2     |
| 126  | aftershock of Friuli earthquake | x       | 3     | y       | 4     |
| 134  | aftershock of Friuli earthquake | x       | 5     | y       | 6     |
| 139  | aftershock of Friuli earthquake | x       | 7     | y       | 8     |
| 146  | aftershock of Friuli earthquake | x       | 9     | y       | 10    |
| 147  | aftershock of Friuli earthquake | x       | 11    | y       | 12    |
| 171  | Basso Tirreno                   | x       | 13    | y       | 14    |
| 196  | Montenegro                      | x       | 15    | y       | 16    |
| 197  | Montenegro                      | x       | 17    | y       | 18    |
| 288  | Campano Lucano                  | x       | 19    | y       | 20    |
| 291  | Campano Lucano                  | x       | 21    | y       | 22    |
| 535  | Erzincan                        | x       | 23    | y       | 24    |
| 591  | Umbro-Marchigiano               | x       | 25    | y       | 26    |
| 592  | Umbro-Marchigiano               | x       | 27    | y       | 28    |
| 2015                                       | Ionian                          | x       | 29    | y       | 30    |
| 436  | Killini                         | x       | 31    | y       | 32    |
| 1312                                       | Athens                          | x       | 33    | y       | 34    |

The expression used for the evaluation of the Park & Ang damage index is presented by equation 4.10, in which  $u_{max}$  is the maximum displacement associated to the selected time history for a certain level of PGA,  $u_{mon}$  is the maximum lateral displacement obtained from a monotonic pushover analysis,  $E_H$  represents the dissipated energy,  $F_y$  is the yielding force and, finally,  $\beta$  is a parameter whose value is equal to 0.15 (Cosenza and Manfredi 2000).

$$DI_{PA} = \frac{u_{max}}{u_{mon}} + \beta \frac{E_H}{F_y u_{mon}} \quad (4.10)$$

The values used for  $u_{mon}$  and  $F_y$  were derived from the procedure adopted for the individuation of the equivalent trilinear SDOF system presented in the previous paragraph.

Figure 4.10 presents the values obtained for the Park & Ang damage index for the considered accelerograms and for different levels of PGA in the case of residential building in HDC; obviously, the damage index rapidly increased with the increase of seismic input, related to both dissipated energy and top displacement. The red dashed line indicated the unitary value of Park & Ang index and, consequently, the sudden collapse of the structural equivalent system.

Natural time histories to be used in the numerical simulations of r.c. designed buildings were chosen in relation to the Park & Ang indexes overpassing the unitary value (i.e. the structural collapse) for the lower level of the seismic input. Tables from 4.7 to 4.11 provide the values of damage indicators for selected accelerograms in relation to the increase of PGA.

In general the most requiring seismic events for all the designed r.c. buildings were:

- Erzincan earthquake (x component), characterized by a PGA equal to 0.389 g and a duration of about 21 s;
- Montenegro earthquake, characterized by PGA values respectively equal to 0.294 g and 0.241 g for x and y components and a duration of about 48 s;
- Campano Lucano earthquake, by PGA values respectively equal to 0.156 g and 0.176 g for x and y components and a duration of about 86 s;
- Kocaeli earthquake (y component), characterized by a PGA equal to 0.361 g and a duration of about 388 s.

Moreover, in order to evaluate the differences in the obtained results, also Umbro-Marchigiano time histories were considered, even if the values generally obtained for the Park & Ang damage indicators were lower. In figure 4.11a the horizontal components of the selected time histories are presented, while figure 4.11b presents the corresponding response spectra (taken from the European Strong Motion Database).

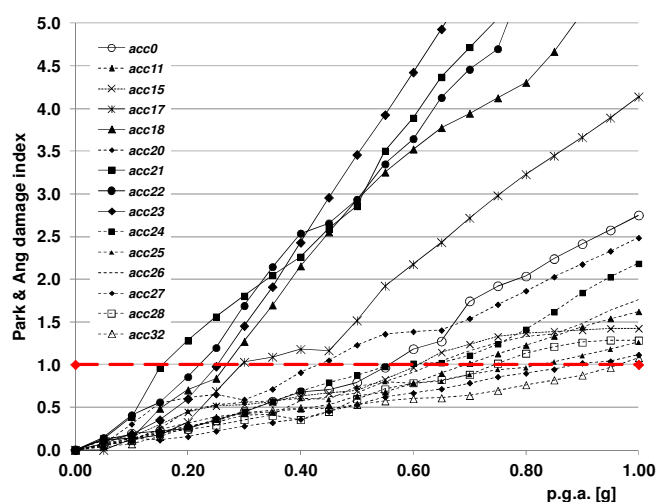


**Figure 4.10:** Park & Ang damage index vs PGA for significative accelerograms for residential building in HDC.

**Table 4.7:** Park & Ang damage index vs PGA for selected time histories (residential building in HDC).

| Accelerogram | Kocaeli | Montenegro | Campano Lucano | Erzincan | Umbro Marchigiano |
|--------------|---------|------------|----------------|----------|-------------------|
| ID n°        | acc0    | acc17      | acc21          | acc23    | acc27             |
| max PGA [g]  | 0.361   | 0.294      | 0.156          | 0.389    | 0.178             |
| Duration [s] | 388.85  | 48.21      | 86.05          | 21.27    | 48.32             |
| 0.00         | 0,00    | 0,000      | 0,000          | 0,000    | 0,000             |
| 0.05         | 0,05    | 0,070      | 0,134          | 0,116    | 0,110             |
| 0.10         | 0,10    | 0,195      | 0,164          | 0,467    | 0,182             |
| 0.15         | 0,15    | 0,247      | 0,283          | 0,970    | 0,336             |
| 0.20         | 0,20    | 0,238      | 0,662          | 1,298    | 0,549             |
| 0.25         | 0,25    | 0,336      | 1,016          | 1,582    | 0,906             |
| 0.30         | 0,30    | 0,423      | 1,184          | 1,797    | 1,368             |
| 0.35         | 0,35    | 0,502      | 1,220          | 2,010    | 1,858             |
| 0.40         | 0,40    | 0,669      | 1,173          | 2,262    | 2,379             |
| 0.45         | 0,45    | 0,838      | 1,349          | 2,727    | 2,914             |

**Table 4. 8:** Park & Ang damage index vs PGA for selected time histories (residential building in LDC).

| Accelerogram | Kocaeli | Montenegro | Campano Lucano | Erzincan | Umbro Marchigiano |
|--------------|---------|------------|----------------|----------|-------------------|
| ID n°        | acc0    | acc17      | acc21          | acc23    | acc27             |
| max PGA [g]  | 0.361   | 0.294      | 0.156          | 0.389    | 0.178             |
| Duration [s] | 388.85  | 48.21      | 86.05          | 21.27    | 48.32             |
| 0,00         | 0,000   | 0,000      | 0,000          | 0,000    | 0,000             |
| 0,05         | 0,091   | 0,142      | 0,259          | 0,135    | 0,148             |
| 0,10         | 0,219   | 0,267      | 0,797          | 0,297    | 0,527             |
| 0,15         | 0,229   | 0,701      | 1,128          | 0,521    | 0,652             |
| 0,20         | 0,338   | 1,024      | 1,531          | 0,890    | 0,653             |
| 0,25         | 0,518   | 1,132      | 1,823          | 1,384    | 0,589             |
| 0,30         | 0,628   | 1,235      | 2,093          | 1,913    | 0,773             |
| 0,35         | 0,702   | 1,244      | 2,322          | 2,476    | 0,981             |
| 0,40         | 0,800   | 1,637      | 2,497          | 3,085    | 1,143             |
| 0,45         | 0,879   | 2,073      | 3,146          | 3,674    | 1,327             |
| 0,50         | 0,998   | 2,326      | 3,774          | 4,230    | 1,436             |
| 0,55         | 1,162   | 2,630      | 4,175          | 4,801    | 1,474             |

**Table 4. 9:** Park & Ang damage index vs PGA for selected time histories (commercial building in HDC).

| Accelerogram | Kocaeli | Montenegro | Campano Lucano | Erzincan | Umbro Marchigiano |
|--------------|---------|------------|----------------|----------|-------------------|
| ID n°        | acc0    | acc18      | acc22          | acc23    | acc27             |
| max PGA [g]  | 0.361   | 0.241      | 0.176          | 0.389    | 0.178             |
| Duration [s] | 388.85  | 48.16      | 86.03          | 21.27    | 48.32             |
| 0,00         | 0,000   | 0,000      | 0,000          | 0,000    | 0,000             |
| 0,05         | 0,104   | 0,153      | 0,112          | 0,114    | 0,110             |
| 0,10         | 0,117   | 0,275      | 0,258          | 0,258    | 0,153             |
| 0,15         | 0,169   | 0,496      | 0,512          | 0,445    | 0,234             |
| 0,20         | 0,183   | 0,736      | 0,824          | 0,719    | 0,330             |
| 0,25         | 0,285   | 0,979      | 1,020          | 1,056    | 0,411             |
| 0,30         | 0,406   | 1,202      | 1,080          | 1,350    | 0,517             |
| 0,35         | 0,534   | 1,356      | 1,260          | 1,658    | 0,548             |
| 0,40         | 0,798   | 1,445      | 1,567          | 2,021    | 0,560             |
| 0,45         | 0,836   | 1,479      | 1,713          | 2,371    | 0,631             |
| 0,50         | 0,873   | 1,737      | 1,856          | 2,736    | 0,730             |
| 0,55         | 1,002   | 2,024      | 1,863          | 3,072    | 0,840             |
| 0,60         | 1,123   | 2,320      | 2,162          | 3,346    | 0,960             |
| 0,65         | 1,246   | 2,610      | 2,225          | 3,647    | 1,084             |

**Table 4. 10:** Park & Ang damage index vs PGA for selected time histories (office building in HDC).

| Accelerogram | Kocaeli | Montenegro | Campano Lucano | Erzincan | Umbro Marchigiano |
|--------------|---------|------------|----------------|----------|-------------------|
| ID n°        | acc0    | acc18      | acc22          | acc23    | acc27             |
| max PGA [g]  | 0.361   | 0.241      | 0.176          | 0.389    | 0.178             |
| Duration [s] | 388.85  | 48.16      | 86.03          | 21.27    | 48.32             |
| 0,00         | 0,000   | 0,000      | 0,000          | 0,000    | 0,000             |
| 0,05         | 0,087   | 0,124      | 0,161          | 0,111    | 0,095             |
| 0,10         | 0,143   | 0,300      | 0,291          | 0,245    | 0,155             |
| 0,15         | 0,154   | 0,505      | 0,543          | 0,404    | 0,229             |
| 0,20         | 0,232   | 0,726      | 0,812          | 0,660    | 0,325             |
| 0,25         | 0,317   | 0,945      | 0,804          | 1,002    | 0,418             |
| 0,30         | 0,455   | 1,151      | 1,020          | 1,313    | 0,512             |
| 0,35         | 0,643   | 1,282      | 1,307          | 1,621    | 0,543             |
| 0,40         | 0,803   | 1,329      | 1,425          | 1,950    | 0,548             |
| 0,45         | 0,781   | 1,361      | 1,555          | 2,274    | 0,595             |
| 0,50         | 0,910   | 1,630      | 1,614          | 2,607    | 0,689             |
| 0,55         | 1,016   | 1,894      | 1,778          | 2,898    | 0,796             |
| 0,60         | 1,126   | 2,172      | 1,944          | 3,175    | 0,912             |
| 0,65         | 1,237   | 2,457      | 2,136          | 3,437    | 1,046             |

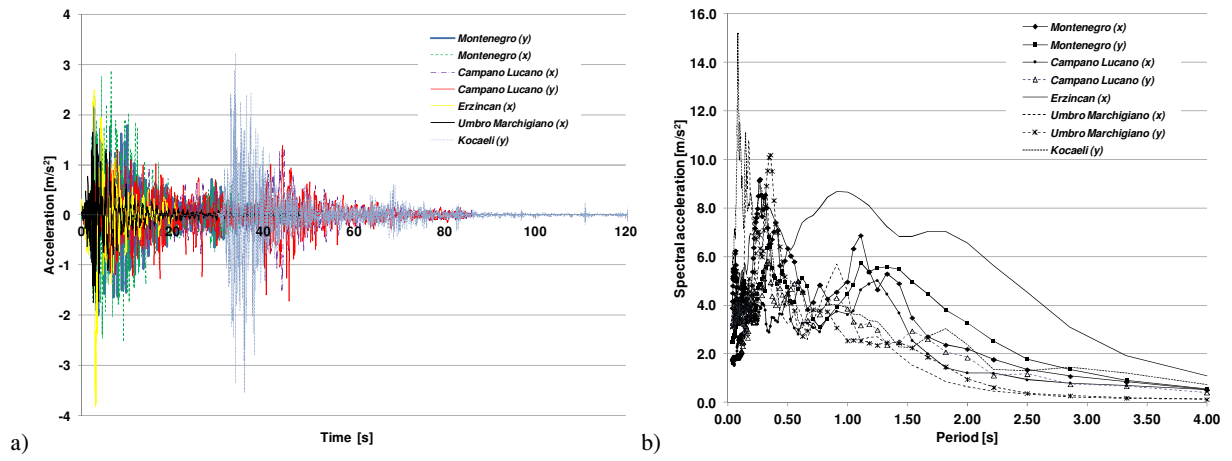


**Figure 4. 11:** a) Horizontal components of the selected time histories (ESMD); b) Response spectra for the selected time histories (ESMD).

## 5. EVALUATION OF SEISMIC DEMAND ON REBARS

### 5.1 Structural assessment of r.c. case studies

The r.c. case studies designed as already presented in Chapter 2 were consequently subjected to IDAs using 3 different natural accelerograms opportunely selected for maximizing the seismic demand in terms of both displacement and energy dissipation, following the procedure presented in Chapter 4; an additional accelerogram with lower value of the Park & Ang damage index was also considered in order to provide a comparison with the other cases. Both the horizontal and the vertical components of accelerograms were considered. All the time histories were scaled to obtain a common maximum acceleration equal to 1.0g and IDAs were executed for increasing level of PGA until the reaching of the structural collapse, with PGA increment equal to 0.05g.

In the case of non linear analyses, both static and dynamic, the structural safety of the building was checked comparing the capacity of the structure, evaluated in terms of strength or deformation respectively for brittle and ductile elements (or mechanisms), with the corresponding demand due to seismic events, opportunely derived from the analyses.

The ductile mechanisms were assessed at the member level, evaluating the chord rotation demand and the corresponding capacity at the ends of each structural element (both beams and columns); according to Mpampatsikos et al. (2008), the chord rotation was defined as the angle between the chord connecting the considered end section of the member to the one in which the bending moment was equal to zero, and the tangent to the member axis at the end section. The brittle elements/mechanisms were assessed evaluating their strength capacity, to be compared to the strength demand due to seismic loading action.

According to actual standards for constructions (Eurocode 8, D.M. 14/01/2008), the capacity of reinforced concrete elements towards seismic action was evaluated through the definition of chord rotation (at yielding and ultimate conditions) and shear strength, respectively for ductile (beams and column in flexure, with or without axial force) and brittle elements (shear in beams and columns).

In particular, the capacity of r.c. structural members at Damage Limitation limit state (DL), expressed in terms of chord rotation at yielding  $\theta_y$ , was evaluated using the expression A.10b presented in the Annex A of Eurocode 8 (EN 1998-3:2005), as reported in equation 5.1:

$$\theta_y = \varphi_y \frac{L_v + a_v z}{3} + 0.0013 \left( 1 + 1.5 \frac{h}{L_v} \right) + 0.13 \varphi_y \frac{d_{bL} f_y}{\sqrt{f_c}} \quad (5.1)$$

Being:  $\varphi_y$  the yielding curvature of the element's section,  $a_v z$  is the tension shift of the bending moment diagram, with  $z$  defined as the length of the internal level arm and  $a_v$  equal to zero if no shear cracking was expected before flexural yielding,  $h$  the height of the section,  $L_v$  the shear length,  $f_y$  and  $f_c$  respectively the strength of steel reinforcement and concrete and  $d_{bL}$  the mean diameter of longitudinal rebars.

The value of total chord rotation capacity (considering both the elastic and the inelastic part) at ultimate (Near Collapse, NC) limit state was evaluated with the expression 5.2 (EN 1998-3:2005):

$$\theta_{um} = \frac{1}{\gamma_{el}} 0.016 \cdot (0.3^\nu) \left[ \frac{\max(0.01; \omega')}{\max(0.01; \omega)} f_c \right]^{0.225} \left( \min \left( 9; \frac{L_v}{h} \right) \right)^{0.35} \cdot 25 \left( \alpha \rho_{sx} \frac{f_{yw}}{f_c} \right) \cdot (1.25^{100 \rho_d}) \quad (5.2)$$

In which  $\gamma_{el}$  was equal to 1.5 or 1.0 respectively for primary and secondary elements,  $\nu$  the compression stress normalized to  $f_c$ ,  $\omega$  and  $\omega'$  the mechanical reinforcement ratios of the tension and compression longitudinal reinforcement,  $\alpha$  the confinement effectiveness factor,  $\rho_{sx}$  the ratio of transverse steel parallel to the direction of loading,  $\rho_d$  the steel ratio of diagonal reinforcement (if present),  $f_{yw}$  and  $f_c$  the strength of stirrup and concrete respectively.

Expressions 5.1 and 5.2 evidenced the relationship between the deformation capacity of ductile mechanisms and the geometrical and mechanical properties of the elements themselves; in particular, the dependence of chord rotation from the shear span length ( $L_v$ ) underlined the strong influence of the seismic input:  $L_v$  was defined as the ratio between bending moment demand and shear demand and, moreover, the curvature  $\varphi_y$  was related to the amount of axial load. Mpampatsikos et al. (2008) in particular, evidenced that the adoption of a simplified expression for the evaluation of the shear span length (assumed to be equal to half the member span length) generally provided good results in the prediction of the effective capacity of ductile r.c. elements, consequently reducing the computational effort and simplifying the safety assessment of the whole building.

For what concerns brittle elements/mechanisms, they were assessed at the section level, through the evaluation of the effective shear demand and of the corresponding capacity at the two ends of each structural member. According to Eurocode 8 (EN 1998-1:2005) both the “static” and the “cyclic” shear capacity of elements was taken into account, since the effects of the inelastic response in the assessment of the shear capacity was necessarily taken into account decreasing the shear strength with the progressive increase of the cyclic inelastic deformations.

The “static” shear static strength was evaluated according to Eurocode 2 (EN 1992-1-1:2005). The cyclic shear resistance  $V_{R,cyclic}$  was also evaluated at ultimate limit state (NC), according to the formula presented in the Annex A of Eurocode 8 (expression A.12 of EN 1998-3:2005):

$$V_{R,cyclic} = \frac{1}{\gamma_{el}} \cdot \left[ \frac{h-x}{L_v} \min(N; 0.55 A_c f_c) + (1 - 0.05 \min(5; \mu_{\Delta}^{pl})) \cdot \left[ 0.16 \max(0.5; 100 \rho_{tot}) \left( 1 - 0.16 \min\left(5; \frac{L_v}{h}\right) \right) \sqrt{f_c} A_c + V_w \right] \right] \quad (5.3)$$

In which:  $V_w = \rho_w b_w z f_{yw}$  was the contribution of transverse reinforcement to shear resistance for cross sections with rectangular web,  $b_w$  the width of the web,  $\rho_{tot}$  the total longitudinal reinforcement ratio,  $x$  the compressive zone depth and  $\gamma_{el}$  a coefficient equal to 1.15 or 1.0 respectively for primary and secondary elements.

Each of the designed reinforced concrete buildings was deeply analyzed in order to understand its behaviour under increasing levels of seismic action; IDAs were executed considering the combined horizontal and vertical components of time histories (table 5.1). Moreover, the overcoming of the interstorey drift limit for Collapse Prevention (CP) limit was considered; the limit was fixed according to the indications provided by American Standard (FEMA 356) up to 4.0% (case of reinforced concrete frames).

**Table 5. 1:** Selected time histories for non linear dynamic analyses.

| Building        | Time histories |              |                    |                       |
|-----------------|----------------|--------------|--------------------|-----------------------|
| Residential HDC | Montenegro x+z | Erzincan x+z | Campano Lucano x+z | Umbro Marchigiano x+z |
| Residential LDC | Montenegro x+z | Erzincan x+z | Campano Lucano x+z | Umbro Marchigiano x+z |
| Commercial      | Montenegro y+z | Erzincan x+z | Campano Lucano y+z | Umbro Marchigiano x+z |
| Office          | Montenegro y+z | Erzincan x+z | Campano Lucano y+z | Umbro Marchigiano x+z |

### **Residential building in High Ductility Class**

The global structural behaviour of the residential building in HDC for increasing levels of seismic action is summarized in the figure 5.1a. IDAs using Campano Lucano and Umbro Marchigiano natural time histories were executed until a maximum level of PGA equal to 0.60 g, corresponding to a maximum top displacement respectively equal to 477 and 290 mm; in the case of Erzincan accelerogram, the analysis reached a maximum PGA of 0.45 g, corresponding to a top displacement of about 870 mm and, finally, considering Montenegro time history, a maximum displacement equal to 559 mm was obtained for a PGA equal to 0.45g. The limit of the maximum interstorey drift (4.0%, according to FEMA 356) was reached in correspondence of the 3<sup>rd</sup> floor, for a PGA equal to 0.30g for Erzincan and Campano Lucano time histories, and for PGA equal to 0.35g for Montenegro accelerogram (even if at 0.35g the interstorey drift was already equal to 3.59%, figure 5.1b).

**Table 5. 2:** Values of the interstorey drift for PGA equal to 0.30g.

| Height [m]                     | Erzincan | Campano Lucano | Montenegro | Umbro Marchigiano |
|--------------------------------|----------|----------------|------------|-------------------|
|                                | 0,30g    | 0,30g          | 0,30g      | 0,60g             |
| 1 <sup>st</sup> floor – 2.5 m  | 1,47%    | 1,55%          | 1,12%      | 1,90%             |
| 2 <sup>nd</sup> floor – 5.5 m  | 2,05%    | 2,36%          | 1,85%      | 2,50%             |
| 3 <sup>rd</sup> floor – 8.5 m  | 4,12%    | 4,63%          | 3,59%      | 3,77%             |
| 4 <sup>th</sup> floor – 11.5 m | 2,88%    | 2,78%          | 2,29%      | 1,80%             |
| 5 <sup>th</sup> floor – 14.5m  | 0,80%    | 1,04%          | 0,82%      | 0,91%             |

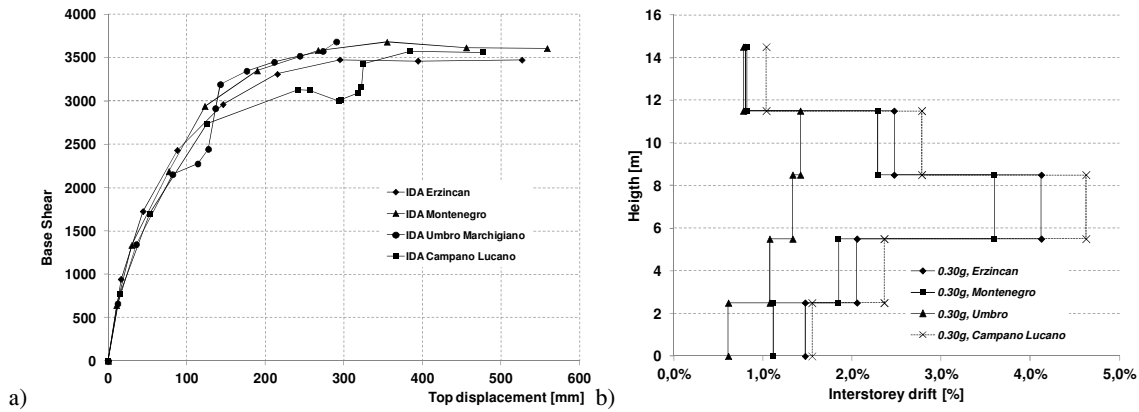


**Figure 5. 1:** a) Capacity curves obtained for the different time histories (kN-mm), b) Interstorey drift profiles for the different time histories and for PGA equal to 0.30g.

No shear mechanisms (i.e. overcoming of the maximum shear strength in beams and columns) were individuated; on the other hand, ductile mechanisms were revealed in both beams and columns.

First yielding in the columns of the first floor generally activated for PGA equal to 0.20 g or 0.25g (Campano Lucano, Erzincan and Montenegro time histories). For PGA equal to 0.30g, in general, the majority of beams' end sections in correspondence of the 1<sup>st</sup> and of the 2<sup>nd</sup> floor reached the yielding limit of the chord rotation for all the three accelerograms considered.

In the case of Campano Lucano earthquake, for PGA equal to 0.20g all the columns of the 1<sup>st</sup> floor and several beams section of the 1<sup>st</sup>, 2<sup>nd</sup> and 3<sup>rd</sup> floor got the yielding point, as visible from figure 6.5, in which the filled red circles and the filled blue squares indicated the overcoming of the yielding chord rotation capacity respectively for PGA equal to 0.20 and 0.25g. For PGA equal to 0.45g the ultimate rotation limit was reached by several columns of the 3<sup>rd</sup> floor.

A situation similar to the one already presented was individuated also in the cases of Montenegro and Erzincan time histories. For Montenegro accelerogram (figure 5.2) first plastic hinges in correspondence of the base of the columns of the first floor and of the end sections of beams of the 2<sup>nd</sup> and 3<sup>rd</sup> levels developed for PGA equal to 0.20g (filled red circles), while for PGA of 0.25g (blue filled squares) all the critical sections of beams of the 2<sup>nd</sup> and 3<sup>rd</sup> floors got the yielding chord rotation. For PGA of 0.40g some base sections of the 1<sup>st</sup> and 3<sup>rd</sup> floor columns over passed the ultimate chord rotation (red line), while for 0.45g also in the ends of some beams elements of the third floor the ultimate ductile limit for rotation was reached (red cross).

The progressive evolution of the structural behaviour of the building under Erzincan natural accelerogram is presented in the figure 5.2; the situation was similar to the one obtained from Montenegro and Campano Lucano time histories, with the full plasticization of beams' end sections of the first, second and third floor for PGA between 0.20g and 0.30g. Also in this case, for PGA equal to 0.35-0.40g all the end sections of the columns of the 3<sup>rd</sup> floor reached the ultimate rotation.

Figures from 5.3 to 5.4 evidenced a relatively uniform distribution of the development of plastic hinges, generally involving beams of the first three levels and columns of the first and third floor. In particular the overcoming of the interstorey drift limit (usually for PGA of about 0.30-0.35g) was strictly connected to the reaching of the ultimate rotation of columns of the 3<sup>rd</sup> floor. Probably the fact that the maximum interstorey drift was reached in correspondence of the 3<sup>rd</sup> floor was the consequence of reduced section of columns' elements (equal to 50x50 cm<sup>2</sup> respect to the 70x50 cm<sup>2</sup> of the first floor and to the 60x50 cm<sup>2</sup> of the second one). Finally, no (or few) plastic hinges developed in correspondence of beams and columns of the 4<sup>th</sup> and 5<sup>th</sup> floors, underlining that the collapse mechanisms generally did not involve the higher levels of the building.

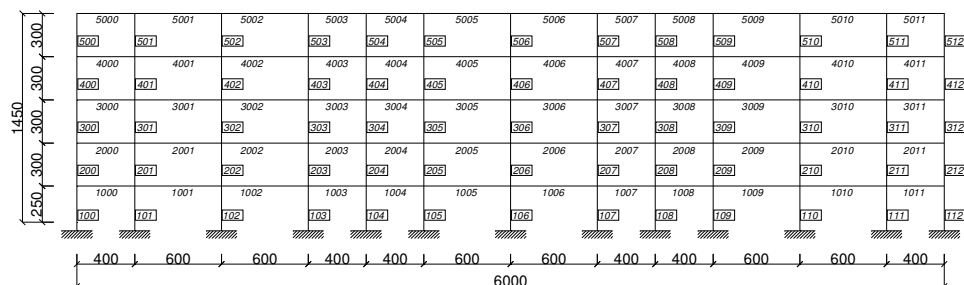


**Figure 5. 2:** Numbering of beam and column elements for residential building in HDC.

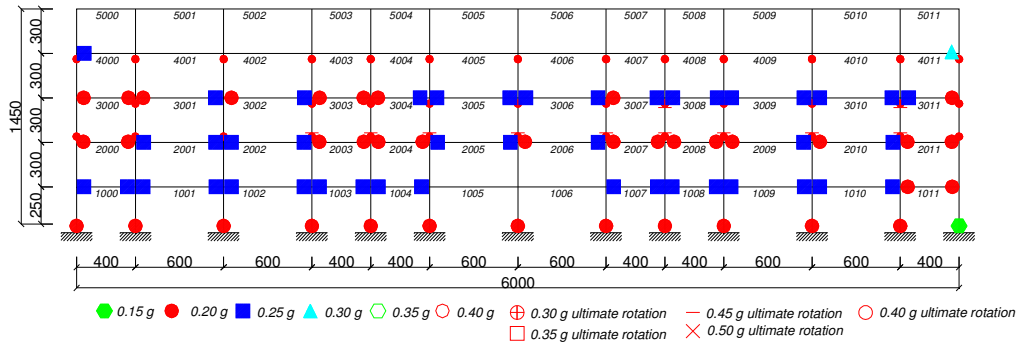


Figure 5. 3: Progressive evolution of the structural behaviour of residential building in HDC for Campano earthquake.

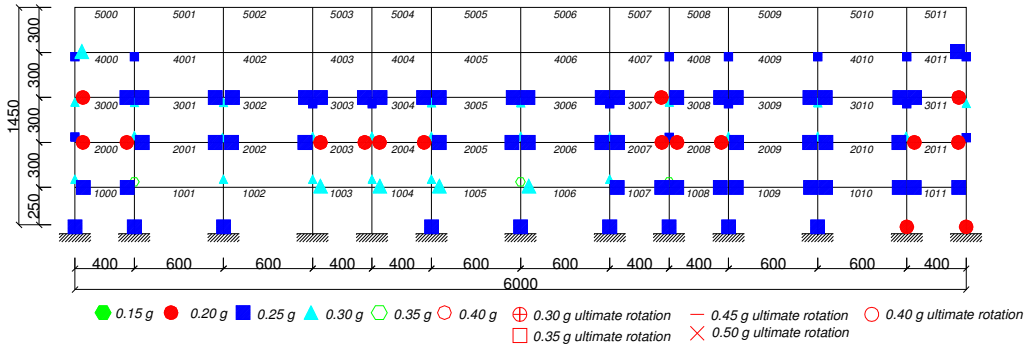


Figure 5. 4: Progressive evolution of the structural behaviour of residential building in HDC for Montenegro earthquake.

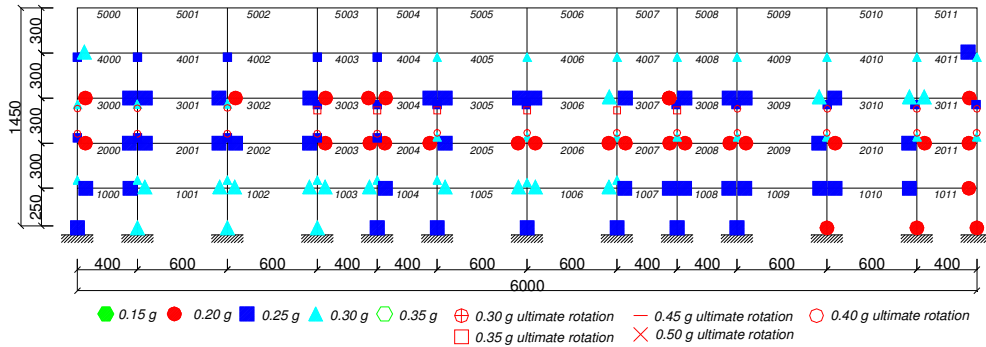


Figure 5. 5: Progressive evolution of the structural behaviour of residential building in HDC for Erzincan earthquake.

### Commercial building in High Ductility Class

The global structural behaviour of commercial building in HDC, in terms of capacity curves (top displacement – base shear) for the different natural time histories considered is summarized in the figure 5.6a.

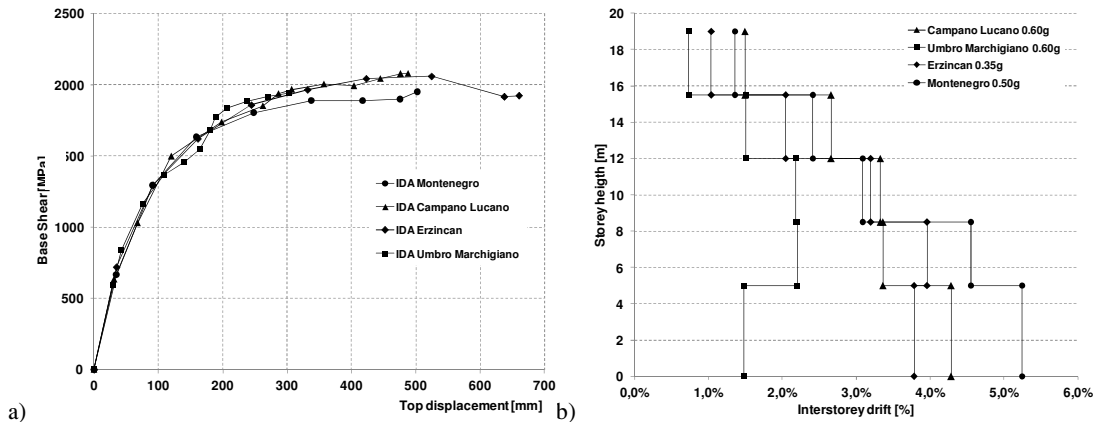


Figure 5. 6: a) Capacity curves for the different time histories (kN-mm), b) Interstorey drift profiles for different levels of PGA.

IDAs were executed until a PGA equal to 0.60g in the cases of Campano Lucano and Umbro Marchigiano earthquakes, while using Erzincan and Montenegro time histories non linear analyses were

limited to 0.50 and 0.40g, since higher displacements were obtained for lower levels of seismic action. The interstorey drift profiles obtained from analyses are presented in the figure 5.6b and in table 5.3: as visible, the limit of 4.0% (FEMA 356) was reached for different levels of PGA, respectively equal to 0.35g for Erzincan time history (2<sup>nd</sup> floor), 0.50g for Montenegro time history (1<sup>st</sup> floor) and 0.60g for Campano Lucano accelerogram (1<sup>st</sup> floor); once again, the displacements obtained from Umbro Marchigiano for the same levels of PGA were lower than the other ones.

**Table 5. 3:** Values of the interstorey drift for the considered time histories and different PGA levels.

| Storey height [m]              | Campano [0.60g] | Montenegro [0.50g] | Erzincan [0.35g] | Umbro [0.60g] |
|--------------------------------|-----------------|--------------------|------------------|---------------|
| 1 <sup>st</sup> floor – 5.0 m  | 4,28%           | 5,24%              | 3,78%            | 1,48%         |
| 2 <sup>nd</sup> floor – 8.5 m  | 3,36%           | 4,55%              | 3,96%            | 2,21%         |
| 3 <sup>rd</sup> floor – 12.0 m | 3,33%           | 3,09%              | 3,19%            | 2,18%         |
| 4 <sup>th</sup> floor – 15.5 m | 2,66%           | 2,42%              | 2,05%            | 1,51%         |
| 5 <sup>th</sup> floor – 19.0m  | 1,50%           | 1,36%              | 1,04%            | 0,73%         |

As well as in the case of residential building in HDC, no shear mechanisms were individuated, according to the capacity design methodology adopted; on the other hand, ductile mechanisms were revealed in both beams and columns, and several elements reached not only the yielding but also the ultimate chord rotation. First yielding in the columns of the first floor generally activated for PGA equal to 0.15 g (Erzincan and Montenegro time histories) or 0.20g (Campano Lucano earthquake); for PGA equal to 0.20g or 0.25g all the base sections of the 1<sup>st</sup> floor columns were already yielded (respectively in the case of Erzincan and Montenegro or Campano Lucano earthquakes). The yielding chord rotation  $\theta_y$  was reached by the end sections of beams of the 1<sup>st</sup> or 2<sup>nd</sup> floors for very low values of PGA, respectively equal to 0.15g for Erzincan and Montenegro time histories and 0.20g for Campano Lucano. In the case of Campano Lucano earthquake (fig. 5.8) plastic hinges were already developed in all the critical sections of the 1<sup>st</sup> and 2<sup>nd</sup> floor for PGA equal to 0.20g, while at 0.25g all the beams of the 3<sup>rd</sup> floor reached their yielding point as well as columns' base sections. In four columns of the first floor the ultimate chord rotation was over passed for a PGA level equal to 0.50g.

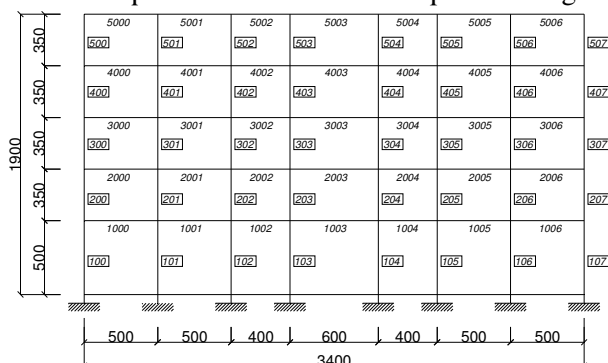


**Figure 5. 7:** Numbering of beam and column elements for commercial building in HDC.

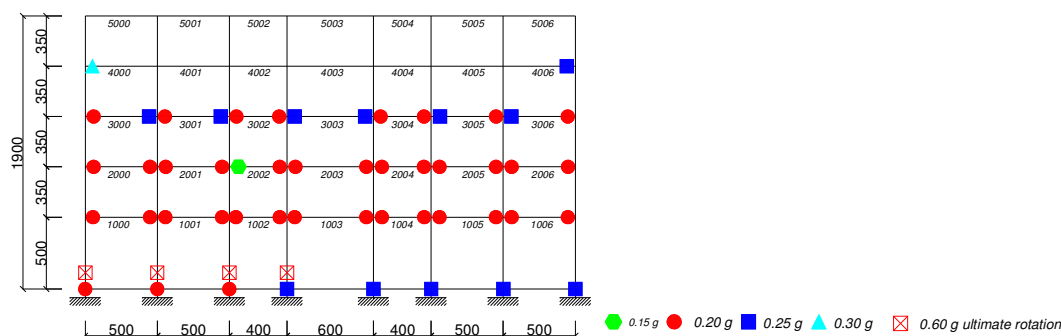


**Figure 5. 8:** Progressive evolution of the structural behaviour of commercial building in HDC for Campano earthquake.

The situation coming from analyses with Montenegro time history was a little more complicated (figure 5.9): all the beams of the first, second and third floors already reached their critical yielding point for PGA equal to 0.25g, and in particular, for 0.15 - 0.20g all the beams of the first two floors overpassed their corresponding yielding chord rotation. Moreover, at 0.20g also all the columns' base sections were completely yielded. As regards the reaching of the ultimate chord rotation, two columns' base sections

reached their collapse limit for 0.40g and about all the other ones overcame  $\theta_u$  for a PGA equal to 0.50g, in agreement to what evidenced by the interstorey drift profiles. A similar situation was obtained also from IDA executed considering Erzincan time history (figure 5.10), even if in this case several columns' base sections reached the ultimate limit for chord rotation for lower values of PGA (equal to 0.30g) and also in beam elements of the 2<sup>nd</sup> and 3<sup>rd</sup> floors, for PGA equal to 0.35g, the ultimate rotation was reached. Considerations similar to the ones argued for residential building in HDC were made. For each one of the three considered natural time histories, a global uniform distribution of plastic hinges in the beams of the first three floors, for increasing levels of PGA, was found; moreover, in general, yielding rotations developed in beams for lower values of the PGA causing the yielding of columns' end sections, according to the capacity design approach. No (or, at the worst, few) plastic hinges developed in correspondence of beams and columns of the 4<sup>th</sup> and 5<sup>th</sup> floors, underlining that the collapse mechanisms generally did not involve the higher levels of the building, as already found for the other considered r.c. case study.

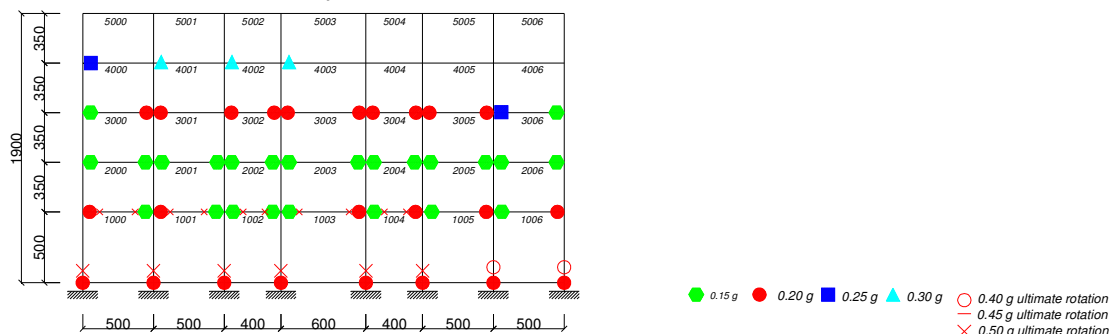


Figure 5. 9: Progressive evolution of the structural behaviour of commercial building in HDC for Montenegro earthquake.

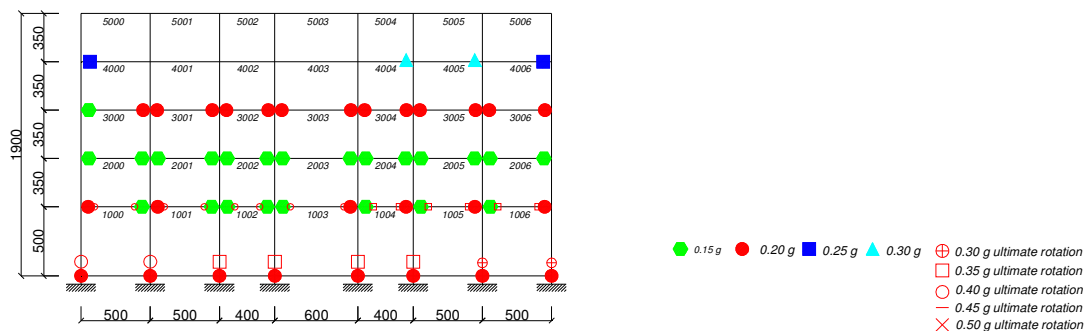


Figure 5. 10: Progressive evolution of the structural behaviour of commercial building in HDC for Erzincan earthquake.

### Office building in High Ductility Class

The global structural behaviour of office building in HDC, in terms of capacity curves for the different natural time histories considered is summarized in the figure 5.11a. IDAs were limited to a PGA respectively equal to 0.55g and 0.60g for Campano Lucano and Umbro Marchigiano time histories, while in the case of Erzincan and Montenegro earthquakes maximum levels of PGA up to 0.35g and 0.50g were reached. Figure 5.11b presents the interstorey drift profiles obtained from the different natural time histories adopted in the analyses, while table 5.4 directly presents the values obtained from IDAs. As visible, the interstorey drift limit (4.0% according to FEMA 356) was reached for PGA respectively equal to 0.55g, 0.40g and 0.40g in the case of Campano Lucano, Montenegro and Erzincan earthquakes, generally in correspondence of the 1<sup>st</sup> floor.

Table 5. 4: Values of the interstorey drift for the considered time histories and different PGA levels.

| Storey height [m]              | Campano [0.55g] | Montenegro [0.40g] | Erzincan [0.40g] | Umbro [0.60g] |
|--------------------------------|-----------------|--------------------|------------------|---------------|
| 1 <sup>st</sup> floor – 5.0 m  | 4,44%           | 4,15%              | 4,16%            | 1,21%         |
| 2 <sup>nd</sup> floor – 8.5 m  | 2,80%           | 2,85%              | 3,49%            | 1,87%         |
| 3 <sup>rd</sup> floor – 12.0 m | 3,79%           | 3,84%              | 3,89%            | 2,34%         |
| 4 <sup>th</sup> floor – 15.5 m | 2,71%           | 3,23%              | 2,63%            | 1,74%         |
| 5 <sup>th</sup> floor – 19.0m  | 1,17%           | 1,36%              | 1,19%            | 0,84%         |

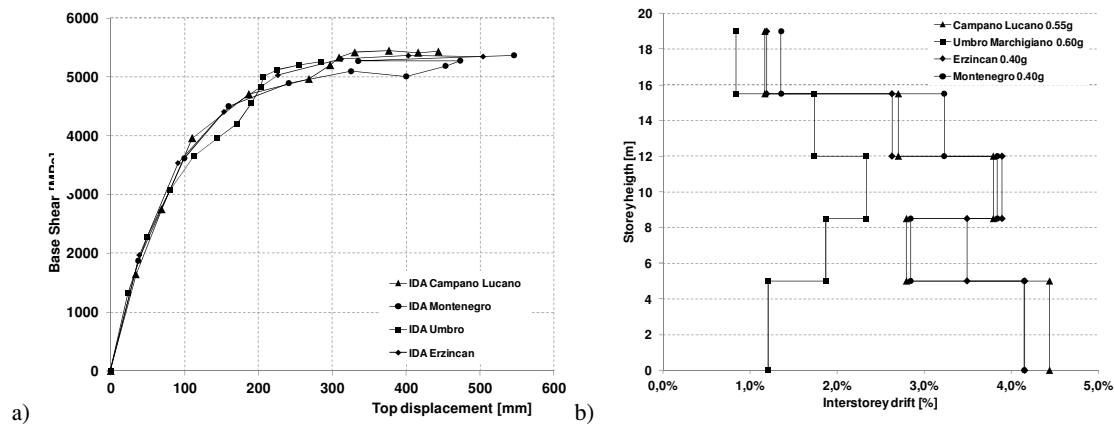


Figure 5. 11: a) Capacity curves obtained for the different time histories and from pushover (kN-mm), b) drift profiles.

No shear mechanisms were individuated, according to the capacity design methodology adopted; on the other hand, ductile mechanisms were revealed in both beams and columns, and several elements reached not only the yielding but also the ultimate chord rotation.

Considering the behaviour of the office building under Campano Lucano time history (figure 5.12), for a PGA equal to 0.20g first yielding rotations in columns of the first floor and in beams of the first and second floors developed; the whole plasticization of end sections was generally reached for PGA of 0.25g (1<sup>st</sup> and 2<sup>nd</sup> floor), while in correspondence of the 3<sup>rd</sup> floor, several sections overpassed the yielding chord rotation limit for PGA equal to 0.30g. As regards the reaching of the ultimate chord rotation, several base sections of the 1<sup>st</sup> floor columns collapsed for PGA between 0.40g and 0.50g. At PGA equal to 0.55g, the majority of columns of the first floor (except columns from n°106 to 111) reached the limit rotation  $\theta_u$ . Considering the results provided by IDA executed with Erzincan natural accelerogram, in several beams' end sections of the 1<sup>st</sup>, 2<sup>nd</sup> and 3<sup>rd</sup> floor plastic hinges developed for a PGA level equal to 0.15g and in general, for PGA equal to 0.25g all the sections were completely yielded (1<sup>st</sup>, 2<sup>nd</sup> and 3<sup>rd</sup> floor). As regards columns, several of the base sections of the 1<sup>st</sup> floor developed plastic hinges for PGA equal to 0.15g, and all of them were yielded at 0.20g; moreover, for PGA equal to 0.30-0.35g many columns reached their ultimate chord rotation limit.

A very similar situation was also evidenced by the results coming from IDA with Montenegro natural time history (figure 5.14), in which the majority of beams' and columns' end sections were completely yielded for a PGA level equal to 0.25g, with first yielding in correspondence of 0.15g. Also in this case, for PGA equal to 0.30-0.35g several columns of the first floor developed ultimate chord rotation.

A uniform distribution of plastic hinges developed for PGA levels in the range 0.20-0.30g, involving only the first three floors and non including the higher storeys of the buildings.

Moreover, even if no shear brittle mechanisms were evidenced, in some cases (Erzincan and Montenegro time histories) ultimate chord rotations developed before in the columns' sections than in beams' ones, not in agreement with what imposed according to the capacity design approach.

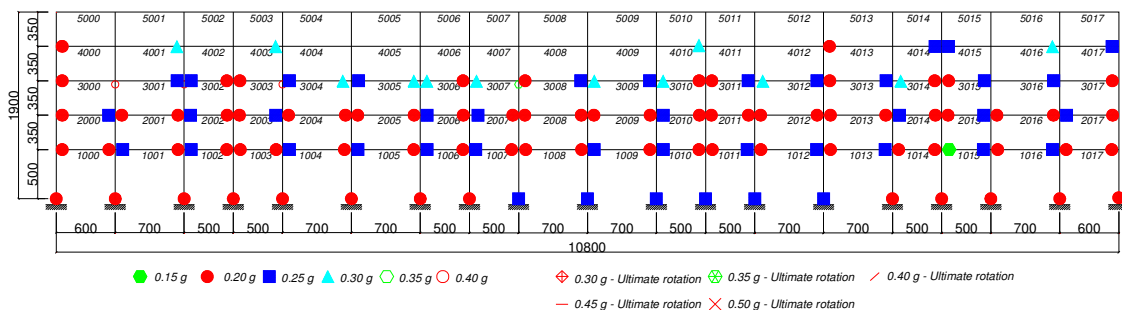


Figure 5. 12: Progressive evolution of the structural behaviour of office building in HDC for Campano earthquake.

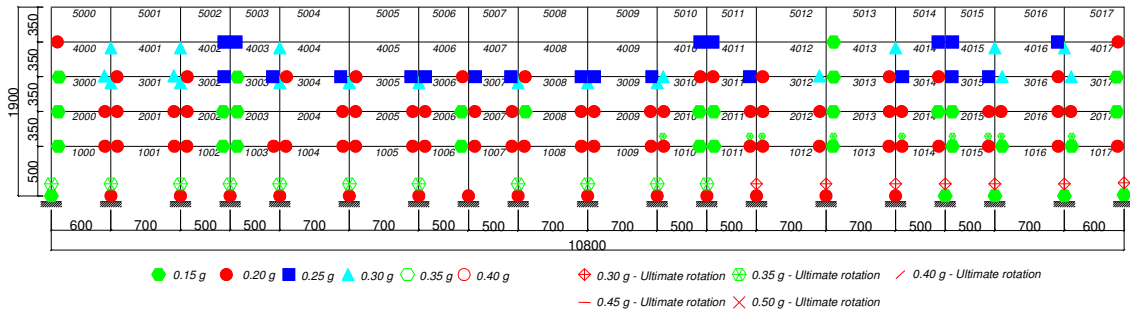


Figure 5. 13: Progressive evolution of the structural behaviour of office building in HDC for Erzincan earthquake.

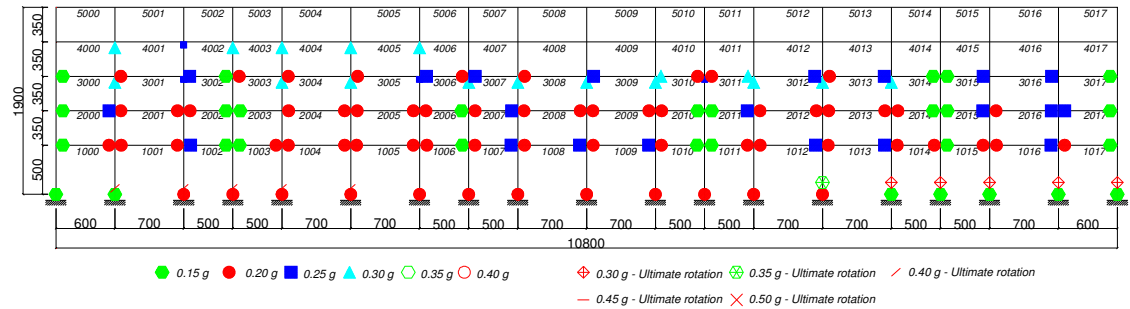


Figure 5. 14: Progressive evolution of the structural behaviour of office building in HDC for Montenegro earthquake.

### Residential building in Low Ductility Class

The results of Incremental Dynamic Analyses on residential building in Low Ductility Class (LDC) evidenced a different behaviour respect to what already presented for the other case studies. Figure 5.15a shows the top displacement-base shear curves obtained from the four natural time histories selected. IDAs were executed until a maximum PGA equal to 0.40g for Erzincan and Montenegro time histories, while Campano Lucano and Umbro Marchigiano earthquakes were analyzed respectively until a PGA equal to 0.60g and 0.55 was reached; the results evidenced, once again, the lower displacements induced by Umbro Marchigiano earthquakes and a comparable behaviour in the cases of the other seismic inputs, whose analysis was stopped in correspondence of a top displacement varying between 500 and 570 mm. As regards the evaluation of the interstorey drift profiles (figure 5.15b, table 5.5), the maximum interstorey drift (4.0%, according to FEMA 356) was generally reached in correspondence of the 2<sup>nd</sup> floor for a PGA equal to 0.35g (Montenegro and Erzincan earthquakes) or 0.55g (Campano Lucano time history). In the case of Umbro Marchigiano accelerogram, at 0.60g the interstorey drift limit was not yet overpassed.

Differently from what evidenced by the non linear analysis of building in HDC, in this case some brittle shear mechanisms were individuated in both beams and columns, as presented in the figures 5.16-5.18, respectively for Campano Lucano, Montenegro and Erzincan time histories.

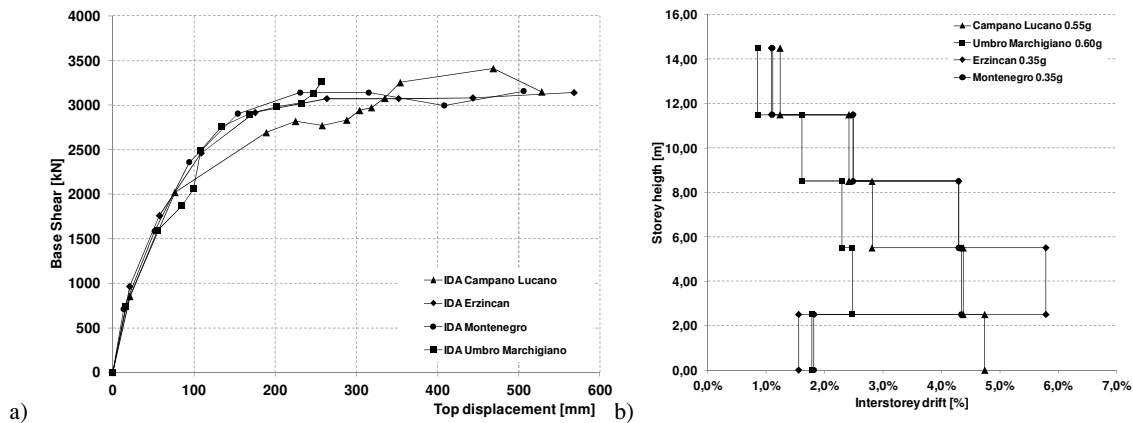
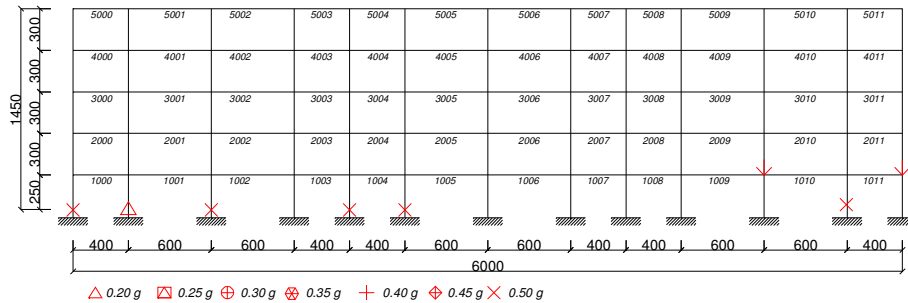


Figure 5. 15: a) Capacity curves for the different time histories and from pushover analysis, b) Interstorey drift profiles.

**Table 5. 5:** Values of the interstorey drift for the considered time histories and different PGA levels.

| Storey height [m]              | Campano [0.55g] | Montenegro [0.35g] | Erzincan [0.35g] | Umbro [0.60g] |
|--------------------------------|-----------------|--------------------|------------------|---------------|
| 1 <sup>st</sup> floor – 2.5 m  | 4,74%           | 1,82%              | 1,55%            | 1,78          |
| 2 <sup>nd</sup> floor – 5.5 m  | 4,37%           | 4,34%              | 5,79%            | 2,48%         |
| 3 <sup>rd</sup> floor – 8.5 m  | 2,81%           | 4,29%              | 4,30%            | 2,30%         |
| 4 <sup>th</sup> floor – 11.5 m | 2,42%           | 2,49%              | 2,48%            | 1,61%         |
| 5 <sup>th</sup> floor – 14.5m  | 1,24%           | 1,11%              | 1,09%            | 0,85%         |



**Figure 5. 16:** Development of shear mechanisms in beams and columns for increasing levels of PGA (Campano Lucano).

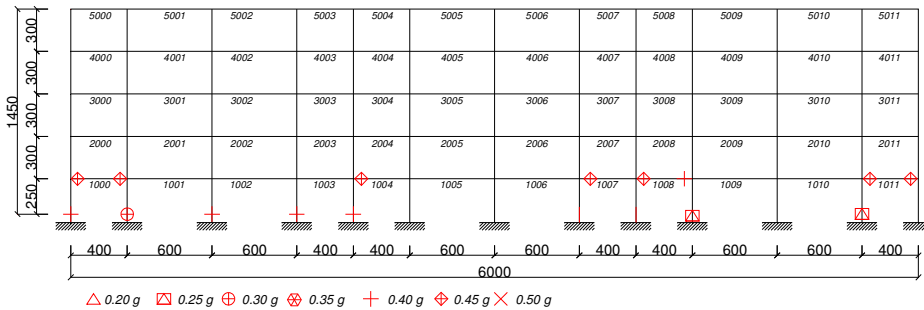


**Figure 5. 17:** Development of brittle shear mechanisms in beams and columns for increasing levels of PGA (Montenegro).

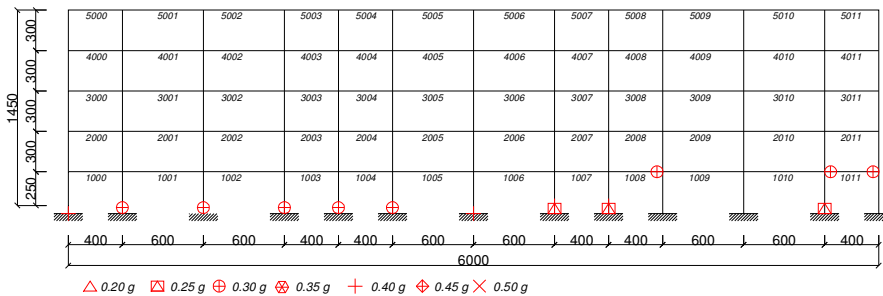


**Figure 5. 18:** Development of brittle shear mechanisms in beams and columns for increasing levels of PGA (Erzincan).

In the case of Campano Lucano time history, the first shear failures in the columns of the 1<sup>st</sup> floor happened for PGA equal to 0.20g; for higher levels of PGA (about 0.50g) also several other columns of the 1<sup>st</sup> floor were involved in brittle shear mechanisms. Only in two sections of the 1<sup>st</sup> level, beams overpassed their shear strength (both static and cyclic). On the other hand, the results of analyses with Erzincan and Montenegro time histories evidenced shear mechanisms in both beams and columns of the 1<sup>st</sup> floor, for PGA levels generally varying between 0.25g and 0.40g (columns) and between 0.35g and 0.45g (beams). Considering, on the other hand, the development of ductile mechanisms in beams and columns, the first yielding rotations developed in beams and columns of the 1<sup>st</sup> floor for PGA equal to 0.15g; moreover, for PGA equal to 0.20g all the beams' end sections (1<sup>st</sup>, 2<sup>nd</sup> and 3<sup>rd</sup> floor) and all the columns' base sections (1<sup>st</sup> floor) already developed plastic hinges. The ultimate chord rotation was reached in correspondence of the base section of columns of the first level (n°100 and 101) for PGA equal to 0.30 (figure 5.18). Figures 5.20 and 5.21 show the behaviour of ductile elements for increasing levels of PGA for Montenegro and Erzincan time histories, respectively. As visible, once again, beams' end sections and columns' base sections generally developed rotations higher than the yielding chord rotation for PGA levels between 0.20g and 0.35g, while ultimate chord rotations usually took place for PGA higher than 0.30g, in correspondence of the base of the columns of the 1<sup>st</sup> floor. The results already presented evidenced a different behaviour between residential building in HDC and LDC; in particular, in the case of low ductility class structures, brittle shear mechanisms developed in both

beams and columns for moderate values of the PGA, differently from what foreseen during the design phase according to the capacity design approach. Moreover, as well as in the case of HDC, despite a uniform distribution of plastic hinges among the elements of the first three levels (both beams and columns), the higher floors were not directly involved in the structural collapse mechanisms.

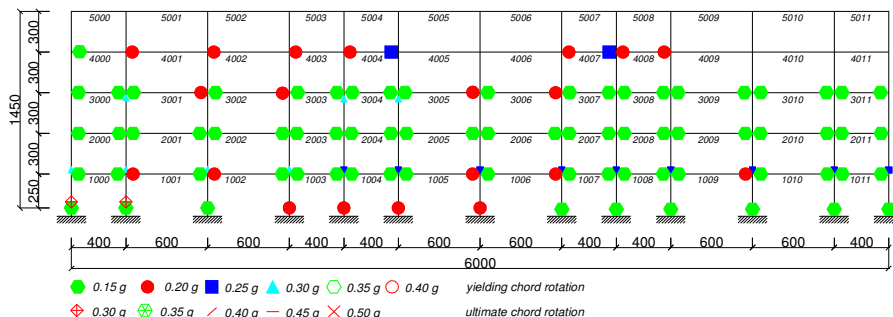


Figure 5. 19: Progressive evolution of the structural behaviour of residential building in LDC for Campano earthquake.

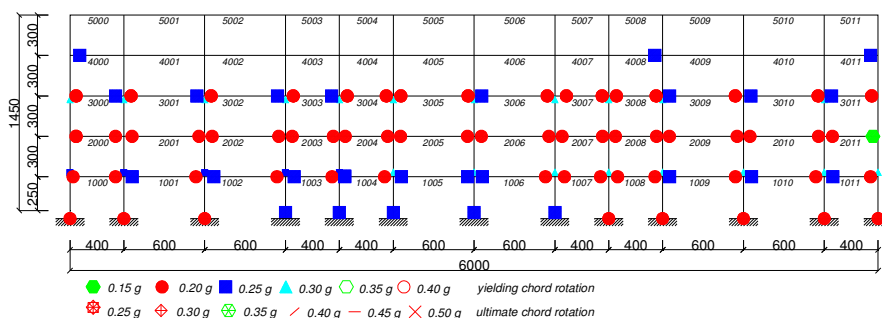


Figure 5. 20: Progressive evolution of the structural behaviour of residential building in LDC for Montenegro earthquake.

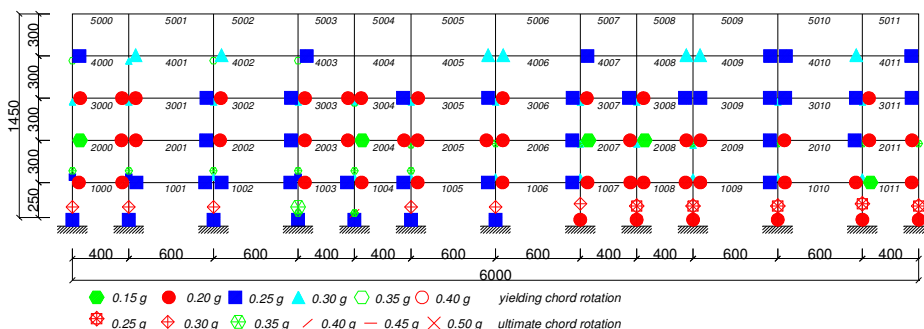
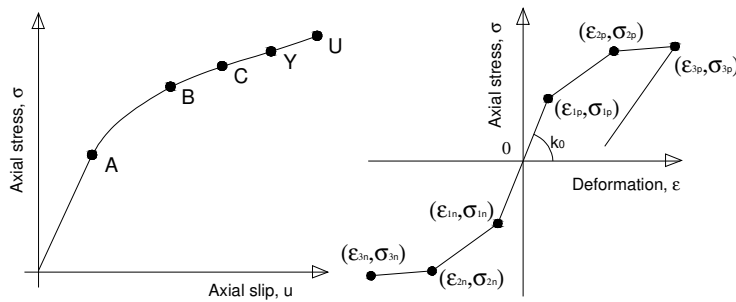


Figure 5. 21: Progressive evolution of the structural behaviour of residential building in LDC for Erzincan earthquake.

## 5.2 Evaluation of the ductility demand on steel reinforcing bars in r.c. buildings

### 5.2.1 Calibration of the bar's model

The *modified hardening slip model* was used as constitutive law for rebars in the models of r.c. case studies. In particular, an axial stress-slip ( $\sigma-u$ ) law was preliminarily derived; then, the shift to an axial stress-strain relationship ( $\sigma-\epsilon$ ) was executed through the use of simple practical considerations and adopting the plastic hinge formulation proposed by Panagiotakos and Fardis (2001), as briefly summarized in the figure 5.22. The results coming from the IDAs with the natural accelerograms opportunely selected to maximize the seismic response of each structure, provided, at steel fiber level, a *stress - fictitious strain* ( $\sigma-\epsilon^*$ ) history; according to the *modified hardening slip model* in fact, the stresses coming from the analyses coincided with the effective strength on bars due to earthquakes, while the strains were affected by the plastic hinge length, defined, as already presented, according to the formulation provided by Panagiotakos and Fardis (2001).



**Figure 5. 22:** Modified slip model: shift from axial stress-slip law to trilinear hysteretic stress-fictitious strain relationship.

In order to individuate and evaluate the effective seismic ductility demand on steel reinforcements, in terms of both deformation and energy dissipation, an opportune simplified model for the steel bar was elaborated, once again using OpenSees software; the real strains were individuated subjecting the reinforcements to the effective stress history directly derived from the execution of Incremental Dynamic Analyses on plane frame models.

The Menegotto-Pinto model (1973) was used for the representation of the effective deformations induced by seismic events, since able to reproduce the cyclic behaviour of reinforcements including Baushinger effect and hardening phenomena. The Menegotto-Pinto constitutive law was already implemented in OpenSees (*Steel02 material*); several parameters were introduced in order to control the transition from the elastic to the hardening branch ( $R0$ ,  $cR1$ ,  $cR2$ ), to include hardening phenomena ( $a1$ ,  $a2$ ,  $a3$ ,  $a4$ ) and strain hardening ratio ( $b$ ). The calibration of the above mentioned parameter was executed on the base of the results coming from experimental Low-Cycle Fatigue (LCF) tests presented in Chapter 2; a short description of the results of the calibration process is presented in the following paragraph.

A simple model was elaborated using OpenSees software for representing the effective cyclic behaviour of steel reinforcements under reversal tension-compression cycles. A *zero-length element* model (Mazzoni et al. 2007) was used; the mechanical properties selected for the material constitutive law were defined according to the mean values obtained from the experimental tests executed on the corresponding steel reinforcements. *Steel02 material* model (following the Giuffrè-Menegotto-Pinto law) was opportunely calibrated, providing the most correct values of the already listed parameters.

The simplified model of the steel reinforcing bar was subjected to tension-compression cycles with the same level of imposed strain, in agreement to the mechanical LCF tests executed on the specimens, as presented in Chapter 2. The experimental LCF tests generally showed buckling of reinforcements after the first one/two cycles in compression and, moreover, the progressive deterioration of the rebar led to the decrease of strength, until failure occurred. Obviously, the calibration of the simplified zero-length element model was executed considering only the first cycle and the degradation phenomena were not directly taken into account. In the figure 5.27 the comparison between the results provided by the numerical model and the experimental LCF tests is presented, considering an imposed deformation varying between 1.85% and 1.93%. For the *Steel02 material* model, the values adopted for  $R0$ ,  $cR1$  and  $cR2$  were respectively equal to 20, 0.925 and 0.15 (suggested values, according to Mazzoni et al. 2007). The percentage errors between numerical and experimental results in terms energy dissipation were lower than 5%.

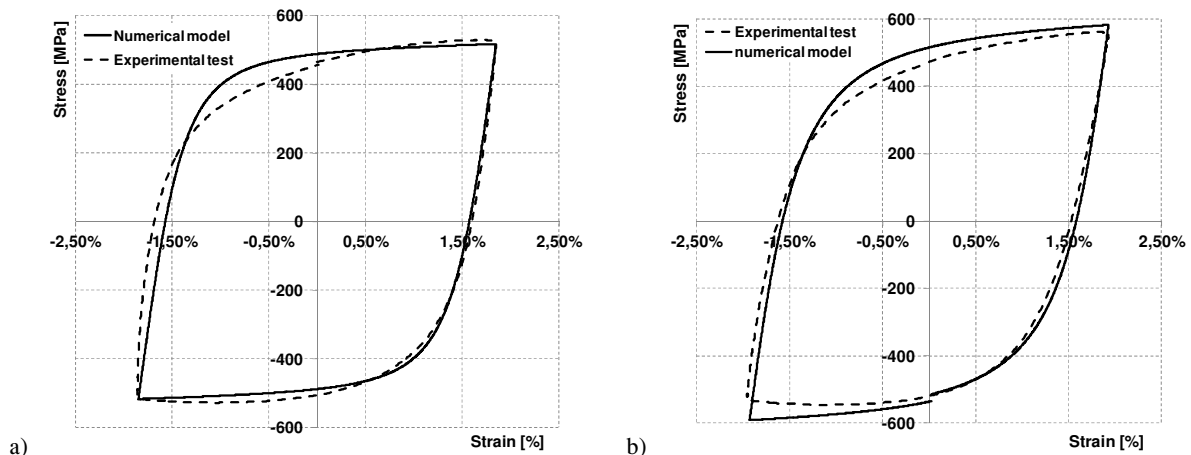


**Figure 5. 23:** Formulation of the Steel02 material in OpenSees (Mazzoni et al. 2007) for deformations around 2.2%.

As a consequence of what already presented, the parameters adopted in the *Steel02* model were:

- Mean values of the mechanical properties (yielding strength  $R_e$ , tensile strength  $R_m$ , elongation to maximum load  $A_{gt}$ ) of the corresponding steel grades, coming from the experimental mechanical tensile tests presented in the Chapter 2;
- The hardening branch slope was defined according to equation, in which  $\varepsilon_p$  represents the strain corresponding to the end of the yielding plateau ( $\cong 2.0\%$ );

$$E_h = \frac{R_m - R_e}{A_{gt} - \varepsilon_p}$$

- The parameters assumed for the Menegotto-Pinto law were:  $R0 = 0.20$ ,  $cR1 = 0.925$ ,  $cR2 = 0.15$ , coinciding with the usually suggested values for the Steel02 material model (Mazzoni et al., 2007).

### 5.2.2 Axial stress-strain histories on steel reinforcing bars

For the individuation of the effective level of deformation reached by the steel reinforcing bars during the seismic event, PGA equal to 0.25g, i.e. the design PGA for LS, according to the design codes used in the design (Eurocode 8 EN 1998-1:2005, D.M. 14/01/2008), was considered. In agreement to what already presented in the previous paragraphs about the global structural behaviour of the building and of beams and columns, steel fibres of 1<sup>st</sup> floor columns' base section and of 1<sup>st</sup> and 2<sup>nd</sup> floors beams were mainly taken into account, evaluating their axial stress-strain relationships. In the present work, only some of the results obtained are reported, in order not to weigh down in an excessive way the presentation of data obtained. In the following pages, the tables and the figures of the results obtained from the execution of IDAs on designed case studies are presented; steel reinforcements are individuated with the number of the correspondent element (i.e. column 100 – 1<sup>st</sup> column element of the 1<sup>st</sup> level), the section (i.e. s1 is the starting section and s6 the end section, figure 5.24) and the corresponding fiber (J or K, respectively on the top or on the bottom of the transversal plane section). In the following paragraphs, the most significant stress-strain histories obtained from steel reinforcing bars of different case studies (and considering different natural accelerograms) are presented.

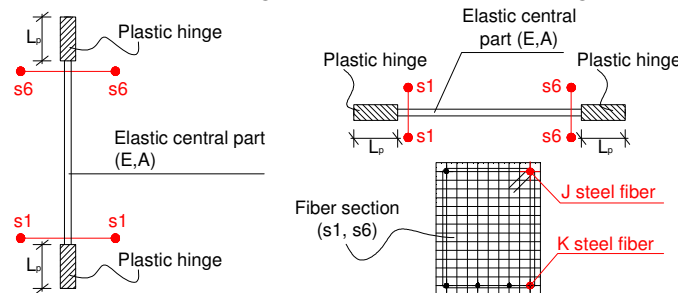
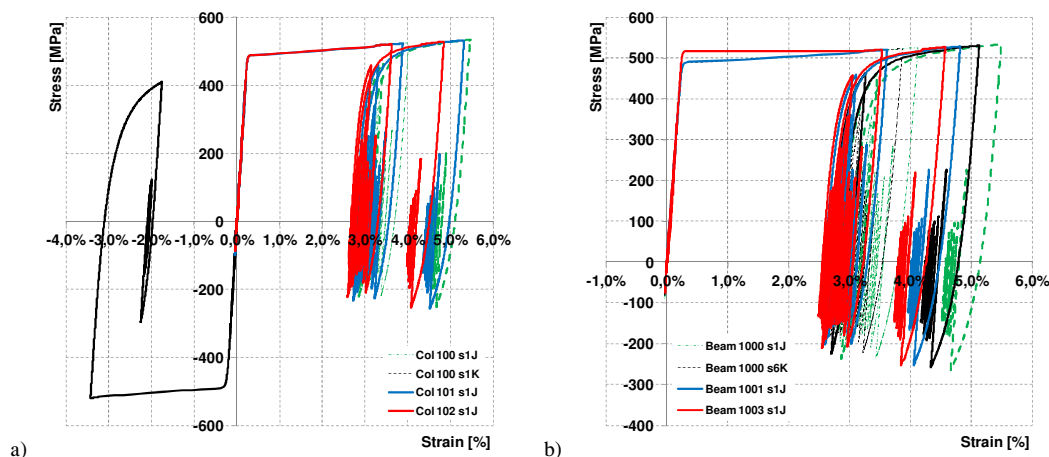


Figure 5. 24: Schematization of output section and steel fiber.

Residential building in HDC: PGA equal to 0.25g

In the tables from 5.6 to 5.29 the maximum levels of deformation and strength and the total density of dissipated energy obtained in rebars of some significative structural elements are presented for all the natural accelerograms considered; moreover, figures from 5.25 to 5.36 present representative stress-strain diagrams of beams' and columns' reinforcements.

Campano Lucano accelerogram



**Figure 5. 25:** Stress-strain histories on bars for Campano earthquake: a) columns 1<sup>st</sup> floor, b) beam 1<sup>st</sup> level.

**Table 5. 6:** Maximum and minimum strength and deformation and density of dissipated energy for steel bars of representative columns of residential building in HDC for Campano Lucano earthquake.

| Residential building in HDC – Campano Lucano time history - COLUMNS |       |             |             |                |                |              |
|---|-------|-------------|-------------|----------------|----------------|--------------|
| PGA   | 0,25g | max def [%] | min def [%] | max Tens [MPa] | min Tens [MPa] | Energy [MPa] |
| 100   | s1 J  | 5,45%       | -0,04%      | 534,45         | -249,83        | 33,49        |
|   | s1 K  | 0,22%       | -3,43%      | 437,42         | -519,24        | 19,70        |
| 101   | s1 J  | 5,31%       | -0,05%      | 533,00         | -257,01        | 32,27        |
|   | s1 K  | 0,17%       | -1,08%      | 355,82         | -497,69        | 4,49         |
| 102   | s1 J  | 4,84%       | -0,04%      | 528,78         | -252,43        | 28,42        |
|   | s1 K  | 0,19%       | -3,27%      | 396,82         | -517,81        | 16,68        |

**Table 5. 7:** Maximum and minimum strength and strain and density of dissipated energy for steel bars of significative beams of residential building in HDC (Campano Lucano).

| Residential building in HDC – Campano Lucano time history - BEAMS |       |             |             |                |                |              |
|---|-------|-------------|-------------|----------------|----------------|--------------|
| PGA   | 0,25g | max def [%] | min def [%] | max Tens [MPa] | min Tens [MPa] | Energy [MPa] |
| 1000  | s1 J  | 5,49%       | -0,04%      | 533,86         | -262,66        | 34,81        |
|   | s1 K  | 0,24%       | -0,12%      | 470,14         | -267,18        | 0,00         |
|   | s6 J  | 0,21%       | -0,11%      | 424,59         | -222,33        | 0,00         |
|   | s6 K  | 5,13%       | -0,04%      | 530,77         | -257,27        | 32,00        |
| 1003  | s1 J  | 4,57%       | -0,03%      | 526,24         | -243,55        | 26,97        |
|   | s1 K  | 3,27%       | -0,06%      | 517,82         | -213,20        | 16,11        |
|   | s6 J  | 3,36%       | -0,05%      | 518,62         | -204,52        | 16,47        |
|   | s6 K  | 4,58%       | -0,04%      | 525,92         | -243,67        | 27,32        |

Montenegro accelerogram

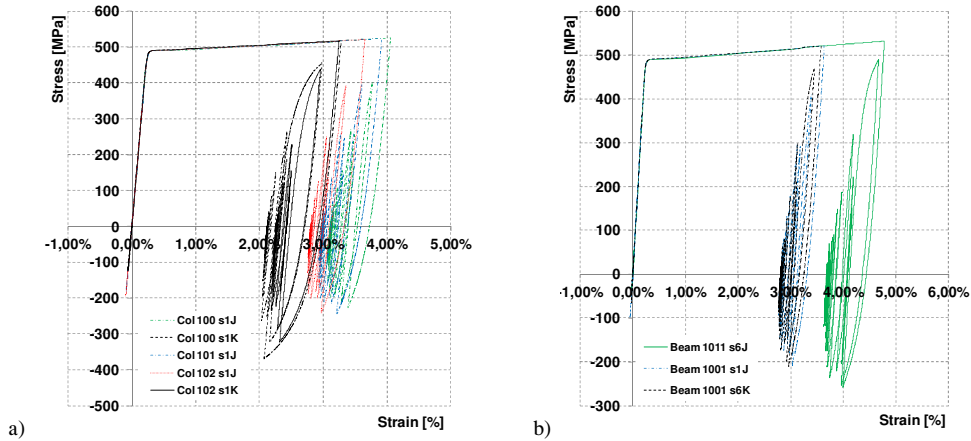


**Figure 5. 26:** Stress-strain histories on bars for Montenegro time history: a) columns 1<sup>st</sup> floor, b) beams 1<sup>st</sup> level.

**Table 5. 8:** Maximum and minimum strength and deformation and density of dissipated energy for steel bars (Montenegro).

| Residential building in HDC – Montenegro time history - COLUMNS |       |             |             |                |                |              |
|---|-------|-------------|-------------|----------------|----------------|--------------|
| PGA   | 0,25g | max def [%] | min def [%] | max Tens [MPa] | min Tens [MPa] | Energy [MPa] |
| 100   | s1 J  | 4,06%       | -0,05%      | 525,03         | -227,37        | 20,21        |
|   | s1 K  | 3,28%       | -0,06%      | 517,92         | -369,44        | 20,15        |
| 101   | s1 J  | 3,92%       | -0,09%      | 523,76         | -246,08        | 19,59        |
|   | s1 K  | 0,24%       | -0,14%      | 466,76         | -311,94        | 0,00         |
| 102   | s1 J  | 3,66%       | -0,09%      | 521,33         | -242,11        | 18,01        |
|   | s1 K  | 3,25%       | -0,06%      | 517,61         | -322,90        | 17,66        |
| 112   | s1 J  | 0,16%       | -0,25%      | 358,33         | -476,43        | 0,00         |
|   | s1 K  | 5,14%       | -0,02%      | 534,95         | -250,85        | 27,33        |

**Table 5. 9:** Maximum and minimum strength and deformation and density of dissipated energy for steel bars of beams of residential building in HDC for Montenegro earthquake.

| Residential building in HDC – Montenegro time history - BEAMS |       |             |             |                |                |              |
|---|-------|-------------|-------------|----------------|----------------|--------------|
| PGA   | 0,25g | max def [%] | min def [%] | max Tens [MPa] | min Tens [MPa] | Energy [MPa] |
| 1001  | s1 J  | 3,64%       | -0,05%      | 521,18         | -210,63        | 17,78        |
|   | s1 K  | 3,30%       | -0,04%      | 518,02         | -186,35        | 15,97        |
|   | s6 J  | 0,25%       | -0,05%      | 482,70         | -148,77        | 0,00         |
|   | s6 K  | 3,79%       | -0,06%      | 522,60         | -228,54        | 18,88        |
| 1011  | s1 J  | 0,18%       | -0,09%      | 375,42         | -194,41        | 0,00         |
|   | s1 K  | 4,47%       | -0,02%      | 528,81         | -251,48        | 23,88        |
|   | s6 J  | 4,78%       | -0,02%      | 531,64         | -257,89        | 25,78        |
|   | s6 K  | 0,20%       | -0,11%      | 412,48         | -231,27        | 0,00         |

Erzincan accelerogram

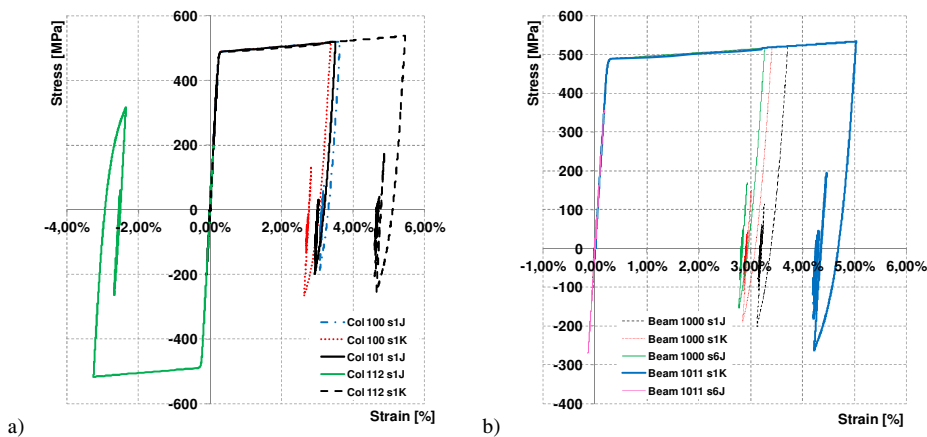


**Figure 5. 27:** Stress-strain histories on steel bars for Erzincan time history: a) columns 1<sup>st</sup> floor, b) beams 1<sup>st</sup> level.

**Table 5. 10:** Maximum and minimum strength and deformation and dissipated energy for steel bars for Erzincan earthquake.

| Residential building in HDC – Erzincan time history - COLUMNS |       |             |             |                |                |              |
|---|-------|-------------|-------------|----------------|----------------|--------------|
| PGA   | 0,25g | max def [%] | min def [%] | max Tens [MPa] | min Tens [MPa] | Energy [MPa] |
| 100   | s1 J  | 3,63%       | -0,05%      | 521,13         | -193,24        | 17,11        |
|   | s1 K  | 3,37%       | -0,06%      | 518,74         | -266,61        | 16,11        |
| 101   | s1 J  | 3,51%       | -0,10%      | 520,02         | -200,33        | 16,49        |
|   | s1 K  | 2,76%       | -0,05%      | 513,08         | -242,09        | 12,79        |
| 112   | s1 J  | 0,10%       | -3,26%      | 316,36         | -517,67        | 16,00        |
|   | s1 K  | 5,45%       | -0,02%      | 537,79         | -254,33        | 27,08        |

**Table 5. 11:** Maximum and minimum strength and deformation and dissipated energy for steel bars of beams (Erzincan).

| Residential building in HDC – Erzincan time history - BEAMS |       |             |             |                |                |              |
|---|-------|-------------|-------------|----------------|----------------|--------------|
| PGA   | 0,25g | max def [%] | min def [%] | max Tens [MPa] | min Tens [MPa] | Energy [MPa] |
| 1000  | s1 J  | 3,72%       | -0,05%      | 521,88         | -201,11        | 17,55        |
|   | s1 K  | 3,41%       | -0,03%      | 519,09         | -189,63        | 15,98        |
|   | s6 J  | 3,27%       | -0,03%      | 517,81         | -153,94        | 15,19        |
|   | s6 K  | 3,52%       | -0,06%      | 520,09         | -179,71        | 16,50        |
| 1011  | s1 J  | 0,16%       | -0,11%      | 334,62         | -227,15        | 0,00         |
|   | s1 K  | 4,69%       | -0,02%      | 530,84         | -255,81        | 23,02        |
|   | s6 J  | 5,03%       | -0,02%      | 533,96         | -261,45        | 24,87        |
|   | s6 K  | 0,17%       | -0,13%      | 357,39         | -271,17        | 0,00         |

All the bottom and the top steel reinforcements of 1<sup>st</sup> floor columns reached the yielding strength in tension; on the other hand, only in some cases the same stress level was obtained for the compression condition: as an example, in the case of Erzincan time history, steel bars at the base of column n°112 reached respectively a strain level equal to 5.45% (in tension) and -3.26% (in compression), with a corresponding dissipated energy density respectively equal to 27.5 MPa and 16 MPa. Considering, on the other hand, the behaviour of steel reinforcing bars in beam elements, only tensile deformations were revealed, with a maximum value equal to 5.49% for Campano Lucano earthquake.

For rebars characterized by yielding strength reached in tension or in compression, the corresponding dissipated energy density mainly varied between 34.8 MPa (Campano Lucano time history, beam n°1000) and 4.5 MPa (Campano Lucano time history, column n°101). The values of maximum deformation in tension and minimum deformation in compression reached were respectively equal to 5.49 % (steel bar in beam n°1000, section s1, Erzincan time history) and -3.43% (steel bar at the base of column n°100, Erzincan accelerogram). All the time histories evidenced that in general, even if yielding was reached, the complete reversal of the stress did not take place, and consequently the total density of dissipated energy was relatively low and, at the most, equal to 30-37 MPa.

Commercial building in HDC: PGA equal to 0.25g

Campano Lucano accelerogram

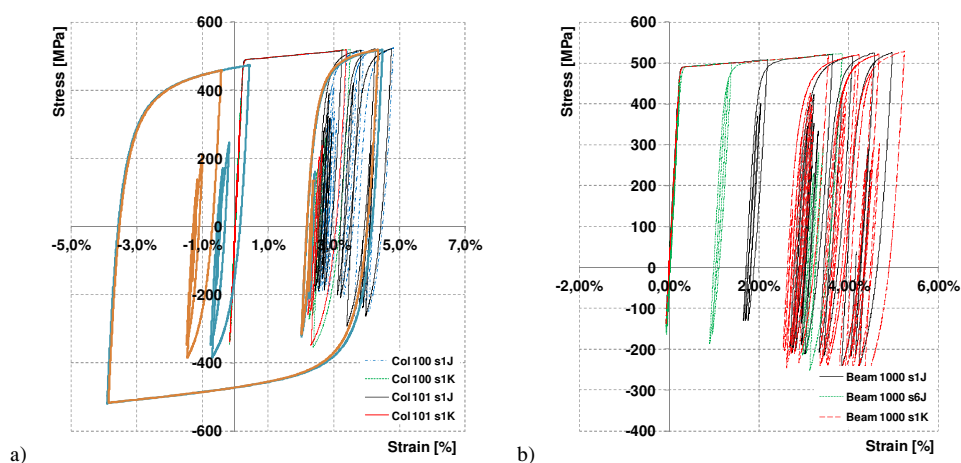


**Figure 5. 28:** Stress-strain histories on bars for Campano Lucano: a) column 1<sup>st</sup> floor, b) beams 1<sup>st</sup> level.

**Table 5. 12:** Max and min strength and deformation and dissipated energy for steel bars of beams (Campano Lucano).

| Residential building in HDC – Campano Lucano time history - BEAMS |       |             |             |                |                |              |
|---|-------|-------------|-------------|----------------|----------------|--------------|
| PGA   | 0,25g | max def [%] | min def [%] | max Tens [MPa] | min Tens [MPa] | Energy [MPa] |
| 1000  | s1 J  | 5,85%       | -0,056%     | 534,58         | -269,94        | 44,71        |
|   | s1 K  | 5,44%       | -0,068%     | 528,05         | -360,97        | 55,37        |
|   | s6 J  | 4,02%       | -0,072%     | 523,18         | -275,65        | 25,99        |
|   | s6 K  | 6,56%       | -0,039%     | 538,23         | -283,45        | 59,83        |
| 1002  | s1 J  | 5,58%       | -0,059%     | 531,61         | -271,62        | 42,04        |
|   | s1 K  | 5,32%       | -0,066%     | 528,82         | -360,10        | 53,73        |
|   | s6 J  | 4,65%       | -0,043%     | 526,01         | -280,04        | 37,43        |
|   | s6 K  | 6,26%       | -0,038%     | 535,07         | -286,76        | 56,79        |

**Table 5. 13:** Max and min strength and deformation and dissipated energy for steel bars of columns (Campano Lucano).

| Commercial building in HDC – Campano Lucano time history - COLUMNS |       |             |             |                |                |              |
|--|-------|-------------|-------------|----------------|----------------|--------------|
| PGA  | 0,25g | max def [%] | min def [%] | max Tens [MPa] | min Tens [MPa] | Energy [MPa] |
| 100  | s1 J  | 5,99%       | -0,05%      | 537,35         | -281,72        | 43,73        |
|  | s1 K  | 4,49%       | -3,90%      | 520,08         | -518,65        | 80,90        |
| 101  | s1 J  | 5,88%       | -0,07%      | 534,96         | -296,61        | 43,82        |
|  | s1 K  | 4,36%       | -3,86%      | 519,43         | -518,18        | 73,83        |

Montenegro Accelerogram

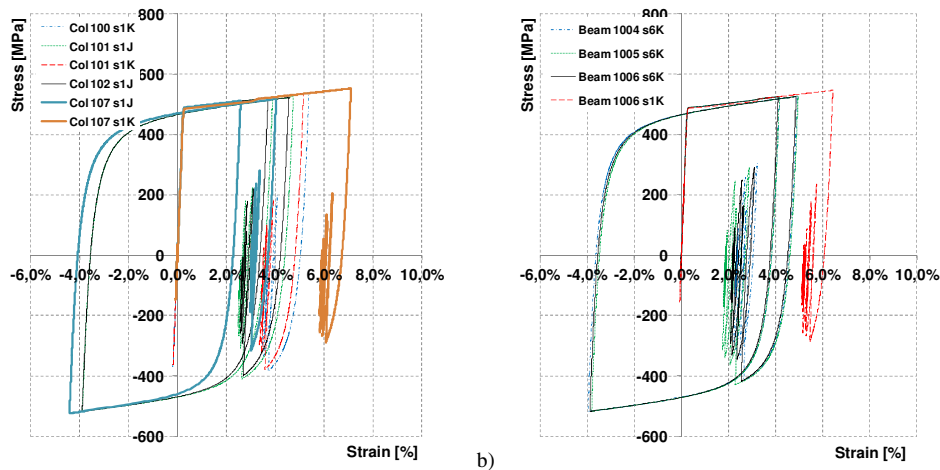


**Figure 5. 29:** Stress-strain histories on steel bars for Montenegro time history: a) columns 1<sup>st</sup> floor , b) beams 1<sup>st</sup> level.

**Table 5. 14:** Max and min strength and deformation and dissipated energy for steel bars of columns (Montenegro).

| Commercial building in HDC – Montenegro time history - COLUMNS |       |             |             |                |                |              |
|--|-------|-------------|-------------|----------------|----------------|--------------|
| PGA  | 0,25g | max def [%] | min def [%] | max Tens [MPa] | min Tens [MPa] | Energy [MPa] |
| 100  | s1 J  | 4,94%       | -0,01%      | 527,29         | -304,74        | 27,65        |
|  | s1 K  | 5,38%       | -0,18%      | 537,15         | -383,32        | 30,26        |
| 101  | s1 J  | 4,74%       | -3,89%      | 525,29         | -518,20        | 92,59        |
|  | s1 K  | 5,16%       | -0,18%      | 535,10         | -379,84        | 28,61        |
| 107  | s1 J  | 4,04%       | -4,41%      | 518,86         | -523,70        | 77,35        |
|  | s1 K  | 7,10%       | -0,07%      | 552,87         | -287,01        | 36,86        |

**Table 5. 15:** Max and min strength and deformation and dissipated energy for steel bars of (Montenegro).

| Commercial building in HDC – Montenegro time history - BEAMS |       |             |             |                |                |              |
|--|-------|-------------|-------------|----------------|----------------|--------------|
| PGA  | 0,25g | max def [%] | min def [%] | max Tens [MPa] | min Tens [MPa] | Energy [MPa] |
| 1004   | s1 J  | 4,90%       | -0,018%     | 524,27         | -370,48        | 30,14        |
|  | s1 K  | 5,99%       | -0,093%     | 542,75         | -289,40        | 30,98        |
|  | s6 J  | 5,51%       | -0,062%     | 538,31         | -278,93        | 27,94        |
|  | s6 K  | 4,92%       | -3,971%     | 527,12         | -519,10        | 98,80        |
| 1005   | s1 J  | 4,53%       | -0,020%     | 522,18         | -337,98        | 26,29        |
|  | s1 K  | 6,31%       | -0,084%     | 545,64         | -288,24        | 32,68        |
|  | s6 J  | 5,69%       | -0,057%     | 539,94         | -277,76        | 28,89        |

|      |      |       |         |        |         |       |
|------|------|-------|---------|--------|---------|-------|
|      | s6 K | 4,95% | -3,819% | 527,34 | -517,54 | 99,83 |
|      | s1 J | 4,47% | -0,021% | 521,52 | -338,50 | 25,85 |
| 1006 | s1 K | 6,43% | -0,076% | 546,73 | -287,39 | 33,34 |
|      | s6 J | 5,90% | -0,050% | 541,91 | -277,75 | 30,06 |
|      | s6 K | 4,86% | -3,890% | 526,48 | -518,25 | 97,58 |

### Erzincan accelerogram

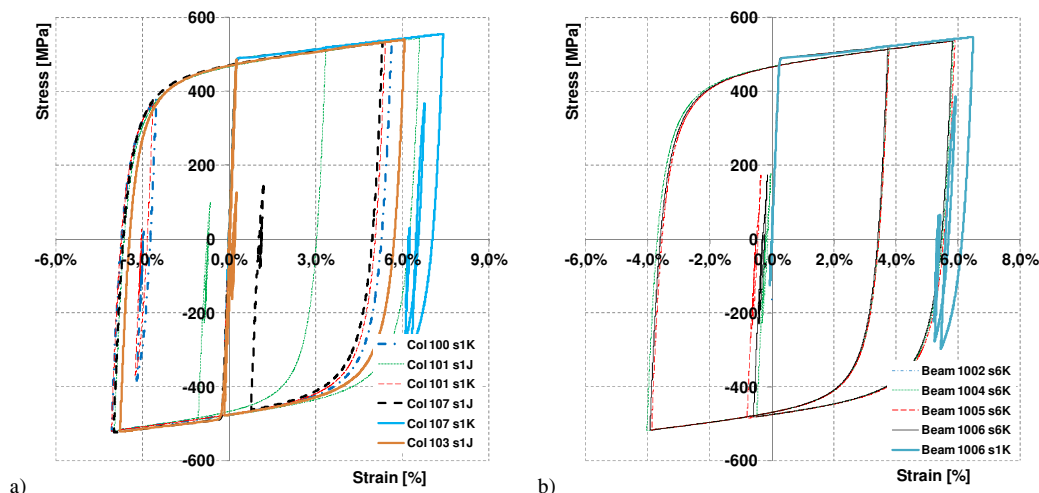


**Figure 5. 30:** Stress-strain histories on bars for Erzincan: a) columns 1<sup>st</sup> floor , b) beams 1<sup>st</sup> level.

**Table 5. 16:** Max and min strength and deformation and dissipated energy for steel bars of columns (Erzincan).

| Commercial building in HDC – Erzincan time history - COLUMNS |       |             |             |                |                |              |
|--|-------|-------------|-------------|----------------|----------------|--------------|
| PGA  | 0,25g | max def [%] | min def [%] | max Tens [MPa] | min Tens [MPa] | Energy [MPa] |
| 101  | s1 J  | 6,60%       | -3,97%      | 544,05         | -518,95        | 121,83       |
|  | s1 K  | 5,41%       | -4,08%      | 537,39         | -520,64        | 68,98        |
| 103  | s1 J  | 6,08%       | -3,78%      | 540,04         | -522,47        | 84,11        |
|  | s1 K  | 5,81%       | -3,81%      | 541,04         | -518,07        | 71,37        |
| 107  | s1 J  | 5,31%       | -4,00%      | 532,49         | -524,49        | 74,37        |
|  | s1 K  | 7,42%       | -0,05%      | 555,80         | -294,51        | 39,17        |

**Table 5. 17:** Max and min strength and deformation and dissipated energy for steel bars of beams (Erzincan).

| Commercial building in HDC – Erzincan time history - BEAMS |       |             |             |                |                |              |
|--|-------|-------------|-------------|----------------|----------------|--------------|
| PGA  | 0,25g | max def [%] | min def [%] | max Tens [MPa] | min Tens [MPa] | Energy [MPa] |
| 1002   | s1 J  | 5,46%       | -0,011%     | 534,89         | -351,68        | 32,14        |
|  | s1 K  | 5,83%       | -0,081%     | 541,30         | -470,25        | 50,49        |
|  | s6 J  | 5,46%       | -0,057%     | 537,91         | -312,72        | 28,60        |
| 1004   | s6 K  | 6,08%       | -3,852%     | 538,78         | -517,80        | 120,85       |
|  | s1 J  | 5,40%       | -0,012%     | 533,46         | -387,31        | 33,09        |
|  | s1 K  | 6,09%       | -0,072%     | 543,68         | -399,72        | 37,16        |
| 1006   | s6 J  | 5,58%       | -0,050%     | 539,00         | -292,56        | 28,83        |
|  | s6 K  | 5,85%       | -4,030%     | 536,59         | -519,60        | 116,42       |
|  | s1 J  | 4,88%       | -0,013%     | 530,86         | -352,06        | 28,16        |
| 1006   | s1 K  | 6,49%       | -0,060%     | 547,34         | -297,64        | 34,16        |
|  | s6 J  | 5,95%       | -0,041%     | 542,38         | -283,86        | 30,63        |
|  | s6 K  | 5,82%       | -3,930%     | 536,23         | -518,56        | 115,44       |

Considering the level of strain and the dissipated energy of steel reinforcements under different natural time histories, the most critic conditions (in terms of dissipated energy and deformation level) were individuated under Montenegro and Erzincan accelerograms.

In the first case, several steel rebars of 1<sup>st</sup> floor's columns were subjected to complete reversed tension/compression cycles, resulting in high values of the total dissipated energy respect to other conditions in which rebars were not able to completely invert the sign of the deformation. As an example, considering all the rebars involved in complete reversed cycles (1<sup>st</sup> floor columns), the average values of maximum deformation in tension and minimum deformation in compression were

respectively around 4.3% and -4.1% (with absolute maximum and minimum strains equal to 4.74% and -4.41%); the maximum dissipated energy was equal to 92.6 MPa, with an average value generally around 80 MPa. On the other hand, for steel reinforcements mainly subjected to only tension (with no strength sign reversal), the maximum strain in tension was equal to 7.10%, with a corresponding dissipated energy density equal to 36.9 MPa. In the case of beam n°1005, the maximum density of dissipated energy was equal to 99.83 MPa and the corresponding strains in tension and compression respectively equal to 4.95% and -3.82%. In the case of Erzincan time history, considering all the rebars involved in complete reversed cycles (both beams and columns), the average values of the maximum and minimum strains in tension and compression were respectively equal to 5.85% and -3.91% (table 6.29); the dissipated energy was generally higher than the one obtained from Montenegro earthquake, with a maximum value equal to 121 MPa. Moreover, for steel reinforcements that were not able to completely reverse the sign of deformation (i.e. yielding in tension but not in compression), the maximum strain in tension was equal to 7.42% (column n°107). As regards Campano Lucano time history, the values obtained for deformations in rebars subjected to complete tension/compression cycles were lower than the ones coming from Montenegro accelerogram, while the level of total density of dissipated energy was, in general, lower, with an average value equal to 50.6 MPa and a maximum one up to 80.9 MPa. The results coming from Umbro-Marchigiano time history were lower than the other ones, both for what concerns deformation and dissipated energy. Considering all the steel reinforcements analyzed, the maximum strain level reached in tension was equal to 7.42% (Erzincan time history), while the minimum one in compression was equal to -4.41% (Montenegro). The results of IDAs on steel reinforcing bars of the 1<sup>st</sup> floor evidenced only in few cases the complete reversal of the cycle tension/compression and, moreover, complete cycles usually took place in correspondence of columns' bars: in general, the deformations of steel rebars in beams reached the higher values in tension. As an example, for Erzincan time history, fibre K of beam element n°1002 (section s6) evidenced a maximum strain in tension equal to 6.10% and a minimum strain in compression equal to -3.85%, resulting in a total density of dissipated energy equal to 120.85 MPa; moreover, the maximum strain in tension in beams' bars was equal to 6.50%. As a consequence of what already presented, the deformation levels reached in beams were, in general, higher than the one obtained in columns; on the other hand, the dissipation of seismic energy was higher in column elements, since steel reinforcements were, usually, subjected to complete reversed tension/compression cycles.

Office building in HDC: PGA equal to 0.25g

Campano Lucano accelerogram

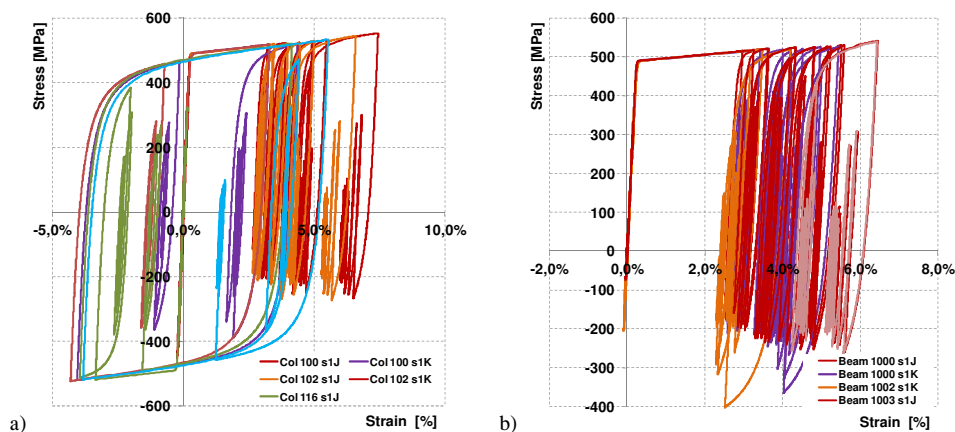


**Figure 5. 31:** Stress-strain histories on bars for Campano Lucano time history: a) columns 1<sup>st</sup> floor , b) beams 1<sup>st</sup> level.

**Table 5. 18:** Max and min strength and deformation and dissipated energy for steel bars of columns (Campano Lucano).

| Office building in HDC – Campano Lucano time history - COLUMNS |       |             |             |                |                |              |
|--|-------|-------------|-------------|----------------|----------------|--------------|
| PGA  | 0,25g | max def [%] | min def [%] | max Tens [MPa] | min Tens [MPa] | Energy [MPa] |
| 100  | s1 J  | 7,44%       | -0,05%      | 552,92         | -267,69        | 56,36        |
|  | s1 K  | 4,36%       | -4,05%      | 518,69         | -520,10        | 79,65        |
| 102  | s1 J  | 6,59%       | -0,06%      | 544,19         | -273,75        | 48,19        |
|  | s1 K  | 3,29%       | -4,30%      | 517,97         | -522,38        | 60,80        |
| 116  | s1 J  | 4,15%       | -3,95%      | 521,07         | -518,54        | 83,60        |
|  | s1 K  | 5,57%       | -0,04%      | 533,99         | -286,52        | 44,95        |

**Table 5. 19:** Max and min strength and deformation and dissipated energy for steel bars of beams (Campano Lucano).

| Office building in HDC – Campano Lucano time history - BEAMS |       |             |             |                |                |              |
|--|-------|-------------|-------------|----------------|----------------|--------------|
| PGA  | 0,25g | max def [%] | min def [%] | max Tens [MPa] | min Tens [MPa] | Energy [MPa] |
| 1000   | s1 J  | 6,45%       | -0,03%      | 540,41         | -258,23        | 52,03        |
|  | s1 K  | 5,45%       | -0,06%      | 526,22         | -363,71        | 50,47        |
|  | s6 J  | 0,20%       | -0,13%      | 415,98         | -268,87        | 0,00         |
|  | s6 K  | 5,89%       | -0,06%      | 535,77         | -259,55        | 45,48        |
| 1002   | s1 J  | 6,44%       | -0,04%      | 538,68         | -264,82        | 55,12        |
|  | s1 K  | 4,87%       | -0,05%      | 526,12         | -340,84        | 43,21        |
|  | s6 J  | 3,36%       | -0,08%      | 517,72         | -289,71        | 19,90        |
|  | s6 K  | 5,47%       | -0,06%      | 532,19         | -261,02        | 39,89        |

Montenegro accelerogram

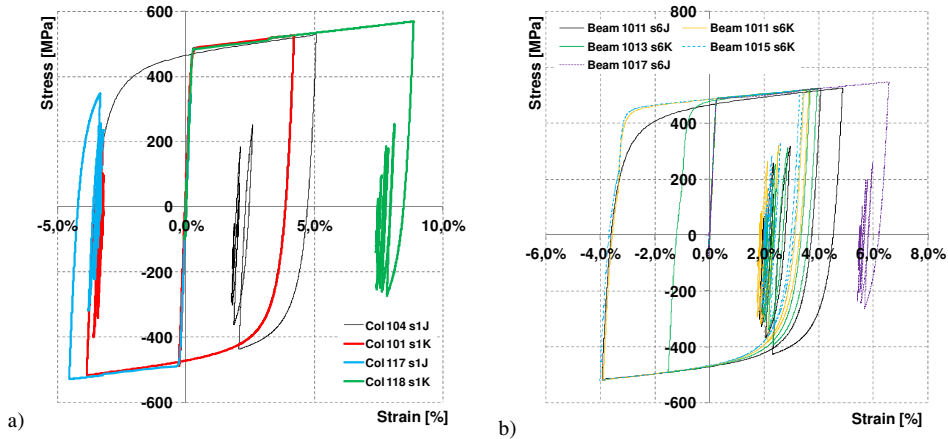


**Figure 5. 32:** Stress-strain histories on bars for Montenegro time history: a) columns 1<sup>st</sup> floor , b) beams 1<sup>st</sup> level.

**Table 5. 20:** Max and min strength and deformation and dissipated energy for steel bars of columns (Montenegro).

| Office building in HDC – Montenegro time history - COLUMNS |       |             |             |                |                |              |
|--|-------|-------------|-------------|----------------|----------------|--------------|
| PGA  | 0,25g | max def [%] | min def [%] | max Tens [MPa] | min Tens [MPa] | Energy [MPa] |
| 104  | s1 J  | 5,08%       | -3,86%      | 528,63         | -517,93        | 101,18       |
|  | s1 K  | 4,90%       | -0,19%      | 532,70         | -416,94        | 29,97        |
| 117  | s1 J  | 0,17%       | -4,54%      | 349,51         | -529,48        | 24,14        |
|  | s1 K  | 7,92%       | -0,09%      | 560,38         | -274,88        | 41,38        |
| 118  | s1 J  | 2,41%       | -4,03%      | 502,49         | -524,79        | 45,70        |
|  | s1 K  | 8,86%       | -0,05%      | 569,05         | -271,37        | 46,90        |

**Table 5. 21:** Max and min strength and deformation and dissipated energy for steel bars of beams (Montenegro).

| Office building in HDC – Montenegro time history - BEAMS |       |             |             |                |                |              |
|--|-------|-------------|-------------|----------------|----------------|--------------|
| PGA  | 0,25g | max def [%] | min def [%] | max Tens [MPa] | min Tens [MPa] | Energy [MPa] |
| 1011   | s1 J  | 4,87%       | -3,94%      | 526,63         | -518,75        | 99,31        |
|  | s1 K  | 5,79%       | -0,07%      | 540,86         | -266,63        | 29,45        |
|  | s6 J  | 4,93%       | -0,07%      | 532,98         | -259,83        | 24,60        |
|  | s6 K  | 3,64%       | -3,89%      | 520,78         | -518,12        | 83,49        |
| 1015   | s1 J  | 4,68%       | -4,02%      | 524,76         | -519,50        | 95,24        |
|  | s1 K  | 6,15%       | -0,05%      | 544,21         | -264,80        | 31,40        |
|  | s6 J  | 5,24%       | -0,05%      | 535,82         | -258,50        | 26,25        |
| 1017   | s6 K  | 3,42%       | -4,02%      | 518,95         | -519,41        | 80,48        |
|  | s1 J  | 0,19%       | -0,17%      | 388,01         | -352,46        | 0,00         |
|  | s1 K  | 6,02%       | -0,05%      | 543,02         | -265,13        | 30,83        |
|  | s6 J  | 6,57%       | -0,04%      | 548,02         | -263,71        | 33,62        |
|  | s6 K  | 4,74%       | -3,89%      | 525,28         | -518,18        | 95,73        |

### Erzincan accelerogram

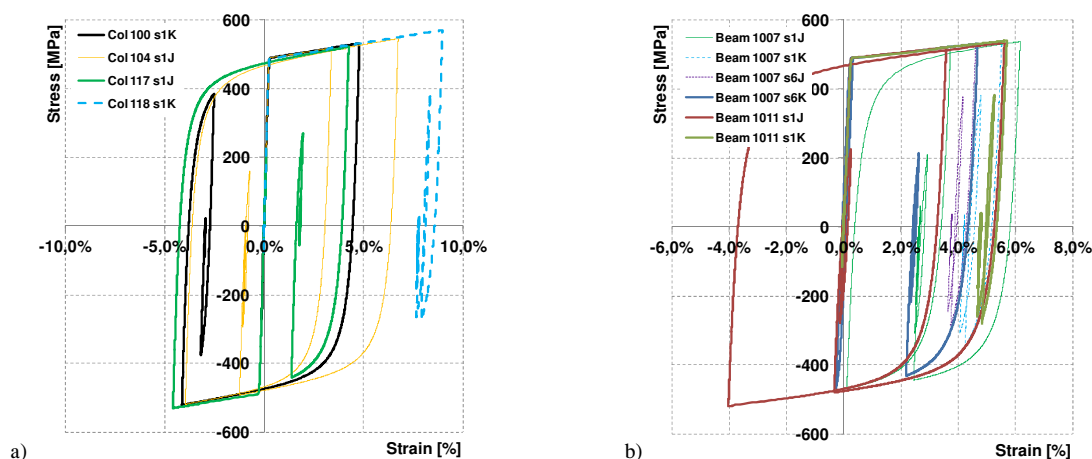


Figure 5. 33: Stress-strain histories on bars for Erzincan: a) columns 1<sup>st</sup> floor , b) beams 1<sup>st</sup> level.

Table 5. 22: Max and min strength and deformation and dissipated energy for steel bars of columns (Erzincan).

| Office building in HDC – Erzincan time history – COLUMNS |       |             |             |                |                |              |
|--|-------|-------------|-------------|----------------|----------------|--------------|
| PGA  | 0,25g | max def [%] | min def [%] | max Tens [MPa] | min Tens [MPa] | Energy [MPa] |
| 104  | s1 J  | 6,74%       | -3,95%      | 545,43         | -518,76        | 124,32       |
|  | s1 K  | 5,08%       | -4,14%      | 534,43         | -521,11        | 66,39        |
| 117  | s1 J  | 4,25%       | -4,58%      | 522,09         | -529,80        | 67,48        |
|  | s1 K  | 8,01%       | -0,06%      | 561,24         | -327,83        | 43,65        |
| 118  | s1 J  | 4,62%       | -4,05%      | 525,68         | -524,97        | 65,04        |
|  | s1 K  | 8,96%       | -0,04%      | 569,94         | -272,91        | 47,61        |

Table 5. 23: Max and min strength and deformation and dissipated energy for steel bars of beams (Erzincan).

| Office building in HDC – Erzincan time history - BEAMS |       |             |             |                |                |              |
|--|-------|-------------|-------------|----------------|----------------|--------------|
| PGA  | 0,25g | max def [%] | min def [%] | max Tens [MPa] | min Tens [MPa] | Energy [MPa] |
| 1011   | s1 J  | 5,61%       | -4,03%      | 534,30         | -519,53        | 111,99       |
|  | s1 K  | 5,70%       | -0,06%      | 540,04         | -279,17        | 29,12        |
|  | s6 J  | 4,87%       | -0,05%      | 532,48         | -270,88        | 24,57        |
| 1007   | s6 K  | 4,37%       | -3,32%      | 527,77         | -518,23        | 64,34        |
|  | s1 J  | 6,16%       | -0,01%      | 537,34         | -468,45        | 67,26        |
|  | s1 K  | 5,52%       | -0,06%      | 538,40         | -346,00        | 30,05        |
| 1017   | s6 J  | 4,61%       | -0,06%      | 530,10         | -285,36        | 23,38        |
|  | s6 K  | 4,68%       | -0,27%      | 530,75         | -464,13        | 30,43        |
|  | s1 J  | 3,37%       | -0,16%      | 518,73         | -337,42        | 16,21        |
| 1017   | s1 K  | 5,82%       | -0,04%      | 541,19         | -270,15        | 29,83        |
|  | s6 J  | 6,40%       | -0,03%      | 546,49         | -264,70        | 32,84        |
|  | s6 K  | 5,56%       | -3,85%      | 533,64         | -517,65        | 110,31       |

The maximum density of dissipated energy was individuated for steel reinforcements of 1<sup>st</sup> floor columns in the case of Erzincan earthquake, and was equal to 124.32 MPa (column n°104), in correspondence of complete reversed tension/compression cycles with maximum deformation in tension equal to 6.74% and minimum deformation in compression equal to -3.95%. A similar situation was evidenced also in the case of beam n°1011, with a total dissipated energy density up to 112 MPa, a maximum deformation in tension equal to 5.61% and a minimum in compression equal to -4.03%. The absolute maximum level of strain obtained was equal to 8.96% (steel bar in column n°118), while the minimum one in compression was equal to -4.58% (steel bar in column n°117).

Considering Montenegro and Campano Lucano time histories, lower values of the dissipated energy density were revealed, respectively equal to 100 MPa (Montenegro, maximum value in beams and columns' steel reinforcements) and 83 MPa or 55 MPa (Campano Lucano, maximum value respectively in columns' and beams' steel bars). Also in the case of Montenegro earthquake, a deformation equal to 8.86% was obtained for steel bar in column n°118, while in beams the maximum deformation level was up to 6.57%. Once again, the results of numerical analyses showed a different behaviour of steel reinforcing bars in beam elements: in general, only few steel bars were able to complete full

tension/compression cycles (with yielding stresses reached both in tension and in compression), in the case of Montenegro and Erzincan natural time histories, with maximum density of dissipated energy about equal to 112 MPa; on the other hand, in the case of Campano Lucano accelerogram, the values of dissipated energy obtained were lower (maximum 55 MPa), due to the fact that in general, rebars were not able to fully recover the reached strains in tension.

*Residential building in MDC: PGA equal to 0.25g*

*Campano Lucano accelerogram*

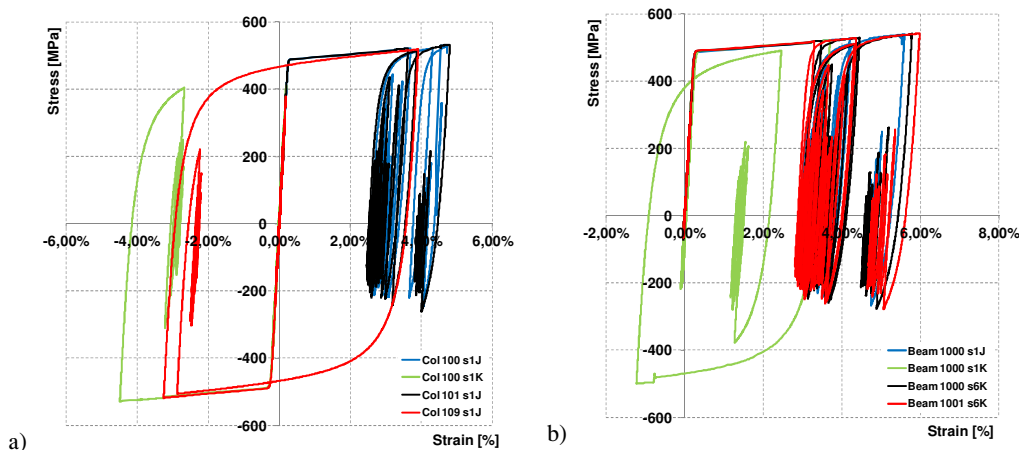


**Figure 5. 34:** Stress-strain histories on bars for Campano Lucano time history: a) columns 1<sup>st</sup> floor , b) beams 1<sup>st</sup> level.

**Table 5. 24:** Max and min strength and deformation and dissipated energy for steel bars of columns (Campano Lucano).

| Residential building in MDC – Campano Lucano time history - COLUMNS |       |             |             |                |                |              |
|---|-------|-------------|-------------|----------------|----------------|--------------|
| PGA   | 0,25g | max def [%] | min def [%] | max Tens [MPa] | min Tens [MPa] | Energy [MPa] |
| 100   | s1 J  | 4,72%       | -0,07%      | 530,05         | -245,96        | 30,27        |
|   | s1 K  | 0,20%       | -4,49%      | 411,84         | -528,98        | 26,20        |
| 101   | s1 J  | 4,80%       | -0,07%      | 531,81         | -261,85        | 31,63        |
|   | s1 K  | 0,17%       | -3,68%      | 360,17         | -521,53        | 19,16        |
| 109   | s1 J  | 3,91%       | -3,25%      | 518,28         | -517,66        | 71,96        |
|   | s1 K  | 3,67%       | -0,09%      | 521,46         | -275,51        | 19,27        |

**Table 5. 25:** Max and min strength and deformation and dissipated energy for steel bars of beams (Campano Lucano).

| Residential building in MDC – Campano Lucano time history - BEAMS |       |             |             |                |                |              |
|---|-------|-------------|-------------|----------------|----------------|--------------|
| PGA   | 0,25g | max def [%] | min def [%] | max Tens [MPa] | min Tens [MPa] | Energy [MPa] |
| 1000  | s1 J  | 5,60%       | -0,04%      | 539,13         | -267,90        | 37,96        |
|   | s1 K  | 3,70%       | -1,23%      | 521,73         | -499,09        | 51,03        |
|   | s6 J  | 0,27%       | -0,10%      | 486,35         | -270,40        | 0,00         |
|   | s6 K  | 5,79%       | -0,03%      | 540,78         | -275,71        | 43,25        |
| 1001  | s1 J  | 5,15%       | -0,04%      | 534,59         | -263,51        | 32,73        |
|   | s1 K  | 3,70%       | -0,09%      | 521,64         | -313,01        | 20,72        |
|   | s6 J  | 0,23%       | -0,09%      | 456,42         | -201,28        | 0,00         |
|   | s6 K  | 5,98%       | -0,03%      | 541,57         | -277,89        | 44,00        |

Montenegro accelerogram

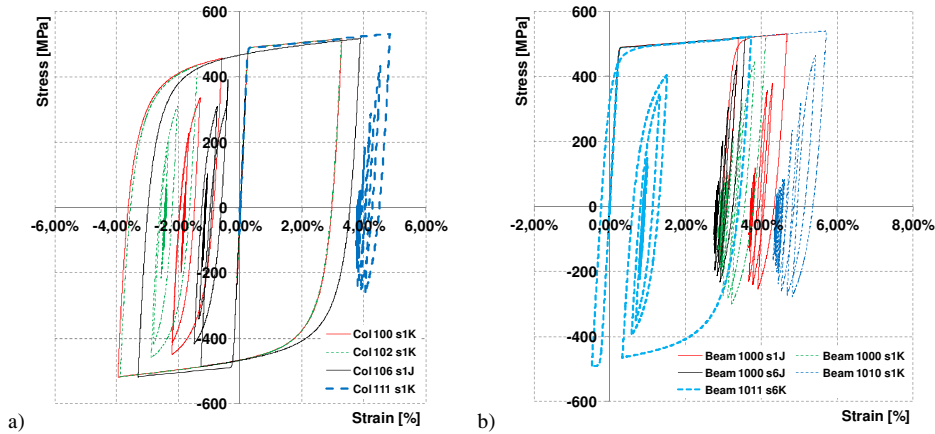


**Figure 5. 35:** Stress-strain histories on bars for Montenegro time history: a) columns 1<sup>st</sup> floor , b) beams 1<sup>st</sup> level.

**Table 5. 26:** Max and min strength and deformation and dissipated energy for steel bars of columns (Montenegro).

| Residential building in MDC – Montenegro time history - COLUMNS |       |             |             |                |                |              |
|---|-------|-------------|-------------|----------------|----------------|--------------|
| PGA   | 0,25g | max def [%] | min def [%] | max Tens [MPa] | min Tens [MPa] | Energy [MPa] |
| 100   | s1 J  | 3,88%       | -3,31%      | 518,00         | -518,12        | 67,93        |
|   | s1 K  | 3,78%       | -0,07%      | 522,43         | -334,41        | 21,08        |
| 111   | s1 J  | 0,13%       | -3,86%      | 367,47         | -523,17        | 24,08        |
|   | s1 K  | 4,84%       | -0,04%      | 532,18         | -262,71        | 25,07        |
| 112   | s1 J  | 0,15%       | -4,31%      | 413,92         | -527,35        | 32,28        |
|   | s1 K  | 4,75%       | -0,02%      | 531,29         | -249,47        | 24,31        |

**Table 5. 27:** Max and min strength and deformation and dissipated energy for steel bars of beams (Montenegro).

| Residential building in MDC – Montenegro time history - BEAMS |       |             |             |                |                |              |
|---|-------|-------------|-------------|----------------|----------------|--------------|
| PGA   | 0,25g | max def [%] | min def [%] | max Tens [MPa] | min Tens [MPa] | Energy [MPa] |
| 1010  | s1 J  | 0,22%       | -0,11%      | 448,00         | -221,07        | 0,00         |
|   | s1 K  | 5,71%       | -0,04%      | 540,18         | -277,63        | 31,01        |
|   | s6 J  | 4,89%       | -0,03%      | 532,63         | -261,71        | 25,54        |
|   | s6 K  | 3,66%       | -0,16%      | 521,40         | -329,09        | 19,69        |
| 1011  | s1 J  | 0,26%       | -0,15%      | 479,53         | -308,93        | 0,00         |
|   | s1 K  | 5,58%       | -0,03%      | 538,93         | -274,78        | 30,14        |
|   | s6 J  | 5,42%       | -0,02%      | 537,49         | -266,72        | 28,59        |
|   | s6 K  | 3,73%       | -0,47%      | 522,00         | -492,14        | 35,39        |

Erzincan accelerogram

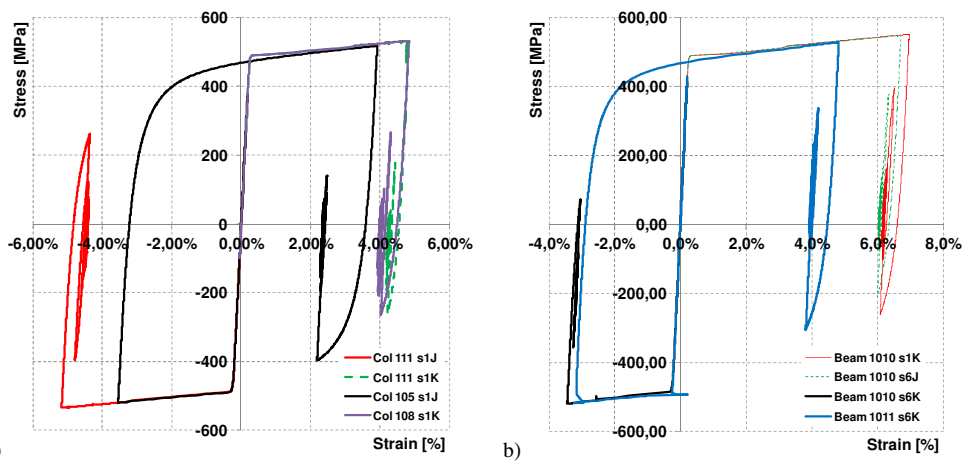


**Figure 5. 36:** Stress-strain histories on bars for Erzincan time history: a) columns 1<sup>st</sup> floor , b) beams 1<sup>st</sup> level.

**Table 5. 28:** Max and min strength and deformation and dissipated energy for steel bars of columns (Erzincan).

| Residential building in MDC – Erzincan time history - COLUMNS |       |             |             |                |                |              |
|---|-------|-------------|-------------|----------------|----------------|--------------|
| PGA   | 0,25g | max def [%] | min def [%] | max Tens [MPa] | min Tens [MPa] | Energy [MPa] |
| 109   | s1 J  | 0,15%       | -5,06%      | 413,78         | -534,25        | 30,66        |
|   | s1 K  | 4,08%       | -0,04%      | 525,24         | -263,35        | 19,65        |
| 105   | s1 J  | 3,92%       | -3,54%      | 518,41         | -520,31        | 51,06        |
|   | s1 K  | 3,92%       | -0,06%      | 523,80         | -279,76        | 19,26        |
| 111   | s1 J  | 0,13%       | -5,18%      | 261,19         | -535,26        | 25,88        |
|   | s1 K  | 4,84%       | -0,04%      | 532,24         | -262,58        | 23,65        |

**Table 5. 29:** Max and min strength and deformation and dissipated energy for steel bars of beams (Erzincan).

| Residential building in MDC – Erzincan time history - BEAMS |       |             |             |                |                |              |
|---|-------|-------------|-------------|----------------|----------------|--------------|
| PGA   | 0,25g | max def [%] | min def [%] | max Tens [MPa] | min Tens [MPa] | Energy [MPa] |
| 1010  | s1 J  | 0,14%       | -0,15%      | 283,58         | -312,18        | 0,00         |
|   | s1 K  | 6,96%       | -0,04%      | 551,64         | -260,57        | 35,53        |
|   | s6 J  | 6,71%       | -0,03%      | 549,36         | -210,40        | 33,68        |
|   | s6 K  | 0,20%       | -3,44%      | 414,56         | -519,36        | 15,71        |
| 1011  | s1 J  | 3,63%       | -0,16%      | 521,09         | -321,58        | 16,95        |
|   | s1 K  | 5,63%       | -0,03%      | 539,39         | -280,50        | 27,91        |
|   | s6 J  | 5,44%       | -0,02%      | 537,73         | -271,56        | 26,20        |
|   | s6 K  | 4,82%       | -3,24%      | 528,38         | -517,50        | 50,31        |

The absolute higher level of deformation was reached in correspondence of steel reinforcements of 1<sup>st</sup> floor's beams under Erzincan earthquake, and was equal to 6.96% (in tension).

Several steel rebars of 1<sup>st</sup> floor columns were subjected to reversal tension/compression cycles, resulting in average values of strains in tension and compression respectively equal to 3.90% and -3.72%, with a correspondent total medium dissipated energy equal to 62 MPa, with a maximum value up to 68 MPa (Montenegro time history). On the other hand, rebars whose behaviour was characterized essentially by deformations in tension or in compression (i.e. for which the yielding strength was reached only in tension or in compression), the maximum strain was equal to 6.96% and the minimum one to -5.18% (Erzincan accelerogram). For what concerns the dissipated energy density, in the case of Campano Lucano and Erzincan earthquakes the maximum levels of energy were respectively equal to 51 MPa and 71.96 MPa.

Moreover, as regards the behaviour of beams' steel reinforcements, only few elements rebars were subjected to complete reversal of strain, since it was not possible to completely recover the initial deformation reached (in tension or in compression, in relation to the considered element).

In the case of Campano Lucano time history, steel bar of beam n°1000 executed complete cycles, resulting in a total dissipated energy equal to 51 MPa and tension and compression strains up to 3.70% and -1.23% (maximum absolute values); moreover, the highest level of deformation was equal to 5.98% (in tension). As already observed, in general steel reinforcements were not subjected to the complete reversal of the strain sign, resulting in higher strain levels (up to 7.0% - Erzincan) but lower values of the total dissipated energy.

### **Conclusive remarks of IDAs on r.c. buildings**

Numerical analyses were executed on designed r.c. case studies and the global structural assessment was executed following the prescriptions imposed by actual standards for constructions, individuating the collapse modalities and the levels of seismic action leading to the development of ductile and brittle elements. In the case of buildings designed in high ductility class (HDC), according to what established during the design process, no shear mechanisms in beams and columns were activated, while chord rotation at yielding ( $\theta_y$ ) was overpassed by several elements, for increasing levels of seismic action. Moreover, in general, structural elements of the 4<sup>th</sup> and 5<sup>th</sup> floors (beams and columns) were not involved in the development of ductile mechanisms for moderate levels of seismic action, and only for values of the PGA higher than 0.40-0.50g some plastic hinges were activated.

A different behaviour was evidenced, on the other hand, in the case of residential building in low ductility class (MDC), in which several elements (usually beams and columns of the first levels) reached the maximum shear strength for levels of PGA equal (or at least a little big higher) than the one adopted in the design.

As regards the stress-strain behaviour of steel reinforcing bars, the results presented in the previous paragraphs evidenced the higher levels of deformations in correspondence of the elements of the first floor, both beams and columns. In general, the complete reversal of the tension/compression cycle was obtained in the reinforcements of base columns' sections, resulting in higher values of the total dissipated energy density; on the other hand, in the case of beams, the behaviour of steel reinforcements was essentially characterized by simple tension or compression condition, resulting in lower values of the dissipated energy and higher levels of absolute deformation.

On the base of those observation and comparing the ductility capacity obtained from experimental tests with the ductility demand coming from non linear analyses, a protocol for the execution of Low-Cycle Fatigue (LCF) tests on reinforcements, aiming to the assessing of the effective ductility capacity of steel rebars under seismic action and to the control of the production process, was elaborated.

### 5.3 Evaluation of seismic demand in steel reinforcing bars in composite structures

According to what already presented in the previous paragraphs, in the present work the results directly coming from the experimental tests on joints sub-assemblages (CJ1 type) executed at University of Pisa were adopted for the determination of the effective seismic demand on steel reinforcing bars in steel-concrete composite structures. To do this, a direct comparison between the data coming from PSD tests executed at Ispra laboratory on a full scale composite structure and the results of cyclic tests on internal joints executed at University of Pisa was carried out and is herein briefly summarized.

The good agreement between the two different experimental tests allowed the calibration of a numerical model of the PS interior joint of steel-concrete composite structures, used for the individuation of the cyclic demand on the steel reinforcing bars present in correspondence of the concrete slab.

For what concerns PSD tests executed on the full-scale structure at Ispra laboratory, in order to evaluate the response of the structure under code compatible seismic demand at all natural frequencies, a suite of artificial accelerograms were generated to match the EC8 Type 1 elastic response spectrum.

The accelerogram selected for the PSD tests was the one able to cause the highest level of damage in beam-to-column joints and limited damage induced in columns. The ground motion time history was characterized by a peak ground acceleration equal to 0.46g, a 10 s strong motion duration with rise and decay periods of 2.5 and 5.0 s, respectively. More details and information can be found in Braconi et al. (2007), in which the test setup was widely described.

In particular, for the aims of the present research project, PSD tests executed considering the accelerogram scaled up to a PGA equal to 1.40g were adopted. This amplification was necessary, taking into account overstrength phenomena, to maximize the seismic response of PS joints, obtaining joint plastic rotations near the limit of 35 mrad with less than 20% of strength degradation (Braconi et al. 2007). Figure 5.37a presents the accelerogram used for considered PSD tests.

Moreover, cyclic tests following the displacement history represented in the figure 5.37b were executed on joint CJ1 at Pisa laboratory; the selected joint strictly reproduced the one present in the full scale structure tests at Ispra, as already presented in Chapter 3.

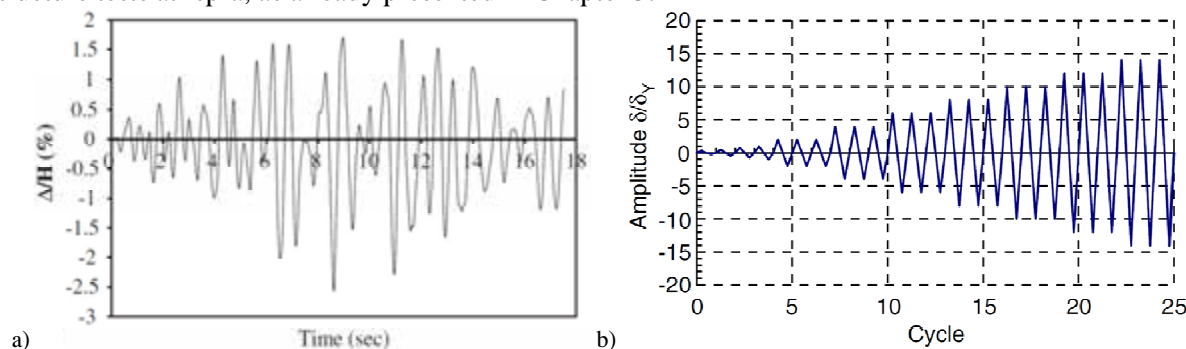


**Figure 5. 37:** a) time history used for PSD simulations, b) cyclic displacement history on CJ1 joint in Pisa.

As widely presented in Braconi et al. (2008), the behaviour of joints under PSD tests at Ispra laboratory was accurately investigated: in addition to demonstrating the good overall seismic behaviour of the full 3D frame, the PSD test program was carried out to also examine in detail the performance of the steel-concrete composite PS joints adopted in the design. As an example, strain gauges were suitably installed on the composite columns in order to estimate internal forces acting in the composite members. Bending moments in the composite columns could then be obtained from the curvatures determined from strain gauge measurements assuming linear material response and plane cross-section

behaviour. Shear forces in the individual columns could be computed using bending moment values so-determined at two different locations along the storey heights, assuming linear variation of the bending moments. The total storey shear forces obtained from these calculations were checked against the applied forces during the PSD programme. Excellent correlation was obtained, as illustrated in the figures 5.38. More details about the behaviour of internal joints under PSD tests can be found in Braconi et al. (2008).

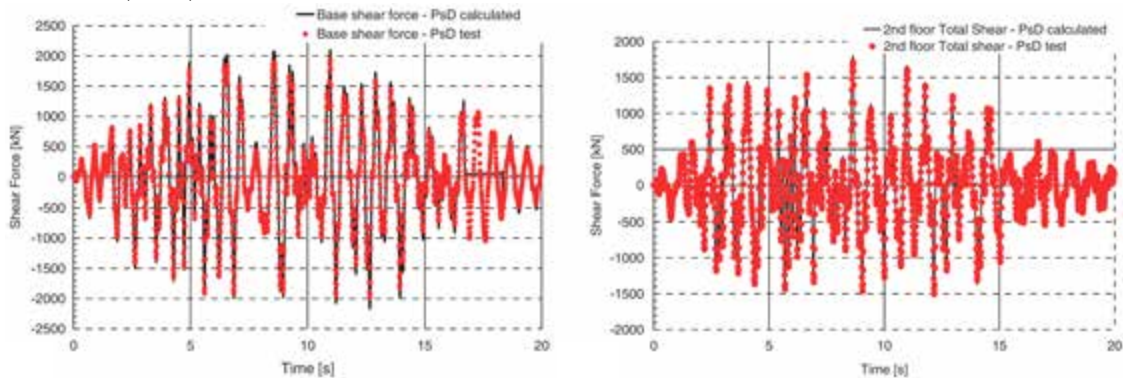


**Figure 5. 38:** Correlation between shear force calculated and obtained from PSD tests.

The maximum bending moment capacity of the exterior joint was reached in the third PsD test ( $PGA \approx 1.40g$ ), while the interior joints reached their total capacity, i.e. the sum of the left and right joint capacities, during the fourth PSD test ( $PGA \approx 1.80g$ ).

The maximum bending moment resistance values developed during the PSD test programme were in good agreement with the values obtained in the cyclic pilot tests conducted on the beam-to-column sub-structures at University of Pisa. As clearly represented in the figure 5.40, some of exterior joints presented a decrease in strength during the fourth PSD test. In these joints, yielding tended to concentrate in the beam connection (end plate) rather than in the column web shear panel as the demand increased, resulting in a more rapid cyclic degradation of the capacity of the connection, mainly due to damage to the concrete slab. However, the strength degradation observed in the exterior joints remained well below the 20% limit imposed by Eurodoce 8 for the classification of structural components as ductile dissipative elements. On the contrary, the interior joints reached their maximum resistance during the fourth PSD test, confirming the absence of strength degradation.

The joint behaviour during the PSD test program was compared with the joint response measured in the test program on beam-to-column sub-structures. The cyclic tests on the joint sub-assemblages were more demanding than the frame tests, as illustrated by the moment-rotation response from the two test programs. In all cases, the cyclic quasi-static test response on beam-to-column sub-structures represents an envelope of the cyclic behaviour of the beam to column joints during the PSD tests. Figures 5.39 show the good match between peak resistances developed by the joints in the two test programs.

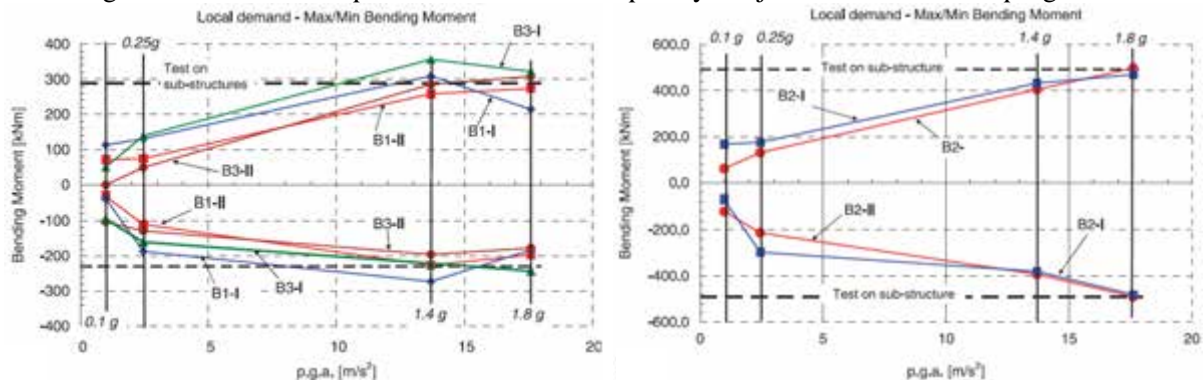


**Figure 5. 39:** Agreement with peak results obtained from teh two different test setup (PSD and cyclic tests).

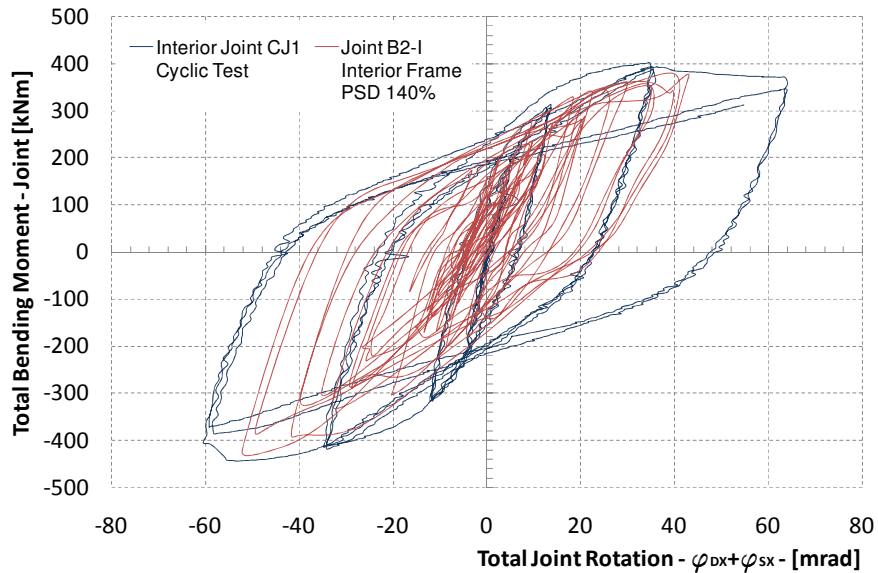


**Figure 5. 40:** Comparison between joint's behaviour obtained from PSD tests on full scale structure ( joint B2-I) and from cyclic tests on single sub-assembly (joint CJ1).

### 5.3.1 Calibration of the numerical model of the joint

On the base of what already presented, a numerical model of joint CJ1, representative of interior joint of Ispra frame (B2-I), was accurately calibrated (figure 5.41). Starting from what widely presented in Braconi et al. (2007) a component model was developed to reproduce the observed response of the entire sub-assembly beam-to-column test specimens, including beam and column flexural behaviour. In the model, the connections between the beam endplates and the column flanges were represented by equivalent T-stubs localized at top and bottom beam flanges. As shown in figure 5.52 for the interior joint CJ1, the model accounted for the response of: the unconfined concrete in compression (1), the confined concrete in compression (2), the lower T-stub in tension under positive moment (3), the upper T-stub in compression under positive moment (4), the wire mesh (6), the reinforcing bar (7) and the concrete in tension (11). Two rigid elements were introduced to simulate the connection between composite beam and PS joint. A fibre representation was adopted for the concrete slab in compression and in tension to adequately capture the non-uniform stress distribution over the slab thickness.

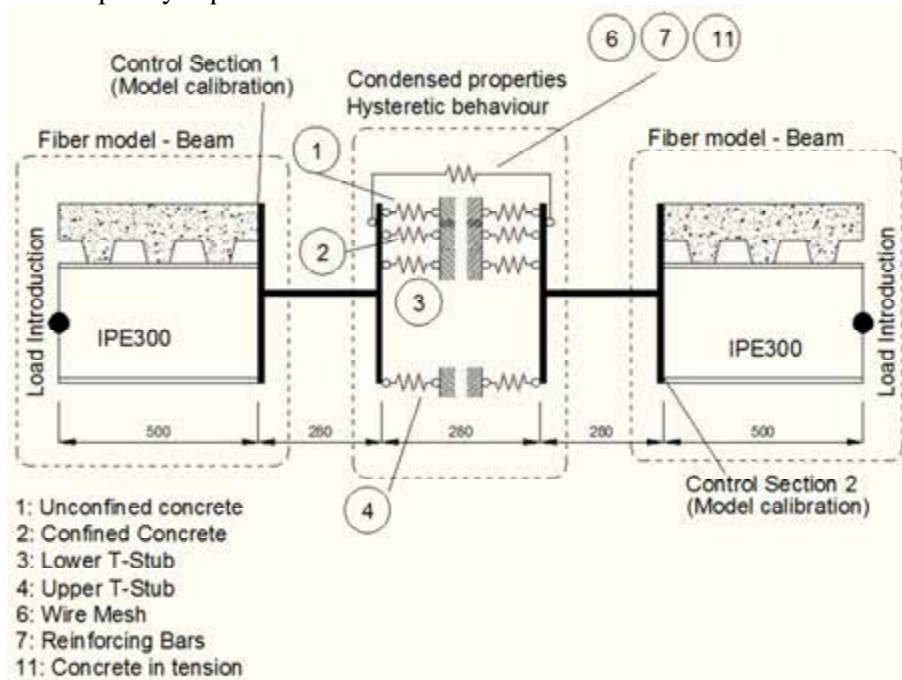


**Figure 5. 41:** Component model of joint CJ1.

The model was accurately calibrated on the base of the results obtained from cyclic tests on joint sub-assemblages executed in Pisa; as an example, in the figure 5.42 the comparison between data coming

from experimental tests, related to what registered by strain gauges positioned in correspondence of control section and what obtained from the numerical model is presented. As visible, results are in good agreement, even if some differences between model and experimental data are mainly due to progressive damaging in the concrete slab, that was not directly included in the model. Moreover, it's necessary to note that the highest level of demand was individuated in correspondence of steel reinforcing bars in correspondence of PS joint, as represented by the blue colour in figure 5.42 (component element n°7).

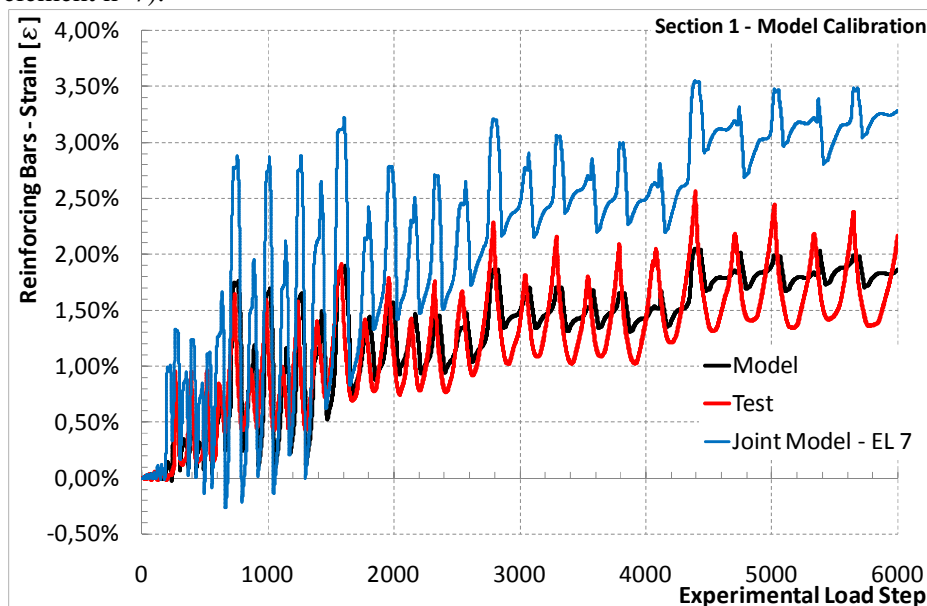
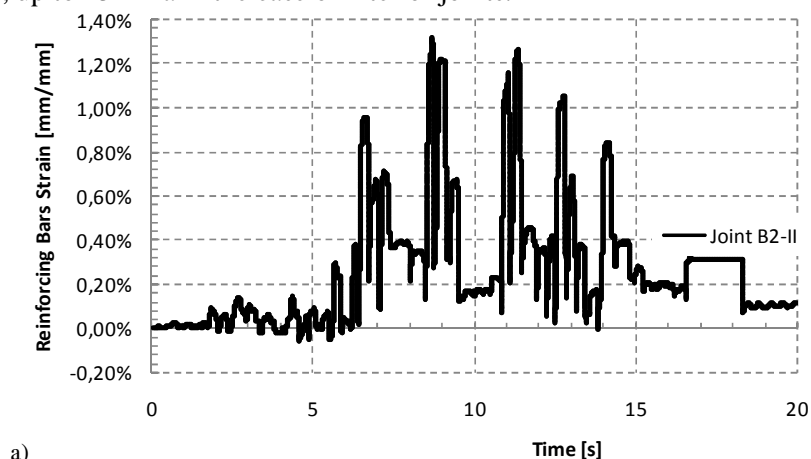


Figure 5. 42: Comparison between experimental and numerical results for joint CJ1.

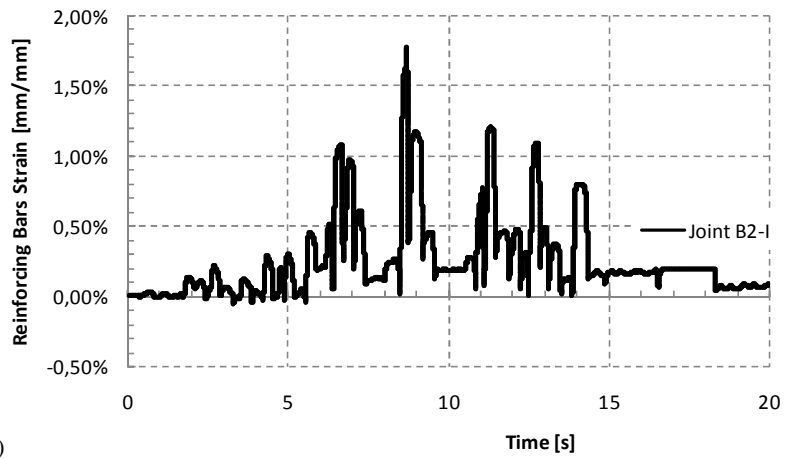
Stating the good agreement obtained from the calibration of the joint model, experimental data in terms of bending moments coming from PSD tests executed at Ispra laboratory were used for the individuation of the effective seismic ductility demand on the steel reinforcing bars present in correspondence of joints of steel/concrete composite structures. Results coming from PSD tests executed using an accelerogram scaled for a PGA equal to 1.40 g were adopted, since more representative of the effective conditions induced by real seismic action.

Bending moments obtained from PSD tests executed at Ispra laboratory were consequently redistributed among the different components constituting the model of the joint, obtaining in such a way the level of effective strain in correspondence of steel reinforcing bars, as presented in the following figures 5.43.

As visible, the maximum level of strain was reached in correspondence of bars inserted in interior joint (like the calibrated CJ1) was equal to 1.78%. Stress-strain histories were then obtained, as presented in the figure 5.44; in general, as already presented in the case of r.c. buildings, steel reinforcing bars were not able to completely reverse the sign of the deformation, resulting in lower values of the density of dissipated energy, up to 45 MPa in the case of interior joints.



a)



b)

Figure 5. 43: Strain history for steel reinforcing bars of interior joints.

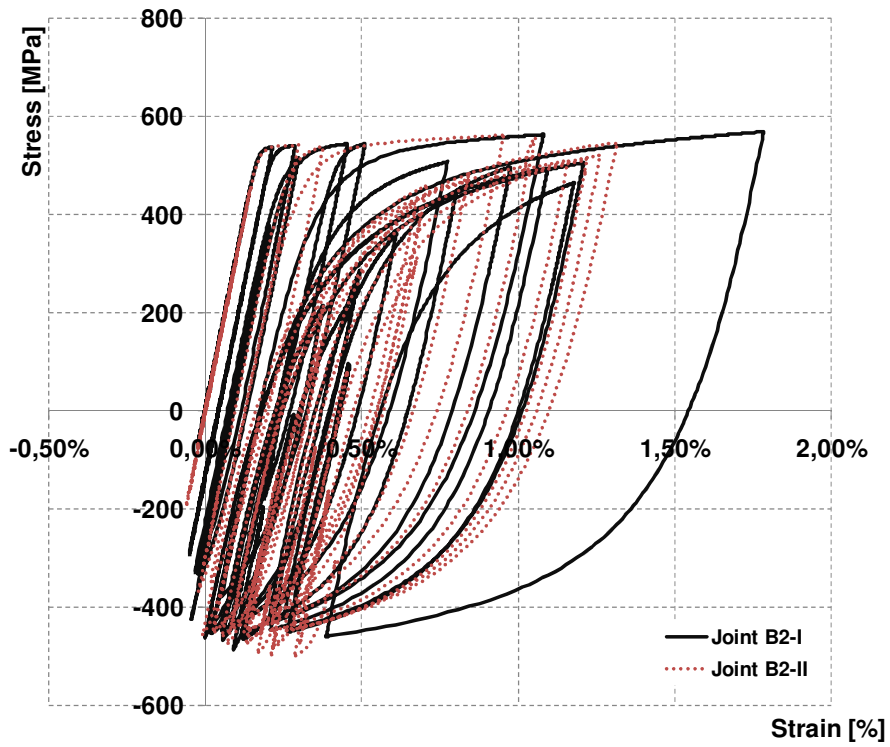


Figure 5. 44: Stress-strain histories for steel reinforcing bars of interior joints.

## 6. DURABILITY PROBLEMS IN R.C. STRUCTURES

---

As widely presented in the Introduction, durability problems were often individuated in existing reinforced concrete structures, affecting the mechanical properties of both concrete and steel reinforcing bars; in particular, the decrease of strength and ductility characteristics was evidenced for steel reinforcements (Apostolopoulos et al. 2006) both under monotonic and cyclic loading conditions, while concrete elements are often affected by carbonation phenomena.

In the present work, a detailed investigation of corrosion phenomena in existing r.c. buildings was executed, aiming to the individuation of the effective degradation of bars exposed to different environmental conditions: in particular, three different existing structures, realized in countries characterized by different seismicity (one in Italy, one in Portugal and one in Greece) were considered and deeply analyzed for what concerns the mechanical characteristics of concrete and steel bars, obtained through the execution of experimental tests on opportunely extracted specimens. The detailed description of existing case study buildings and of the consequences of corrosion exposition on the mechanical properties of materials were already described in the Mid Term Report and are reported in the corresponding deliverables. It's necessary to underline that in general, reinforcing steel bars present in existing reinforced concrete buildings are different from the ones actually adopted for new constructions, and consequently a detailed investigation shall be executed in order to individuate the effective ductility and strength capacity of actual steel reinforcing bars (TempCore, Micro-Alloyed and Stretched steels) when subjected to corrosion attack in different external conditions. In order to pursue this objective, a detailed analysis of actual techniques for laboratory tests able to reproduce aggressive condition was executed, an opportune procedure and a specific protocol were elaborated for the execution of experimental corrosion tests on the representative steel reinforcing bars previously selected.

### 6.1 Selection of accelerated corrosion testing procedures

According to what already discussed in the Introduction of the present work, many studies in the current literature evidenced the durability problems of r.c. structures affecting the ductile behaviour of steel reinforcing bars and usually leading to the decrease of their mechanical properties, both in terms of strength and, in particular, ductility.

In order to assess the ability of corroded steel reinforcing bars to still sustain the ductility demand imposed by earthquakes, experimental tensile and low-cycle fatigue tests were executed on a set of representative steel reinforcements, opportunely pre-corroded in order to represent the effective condition due to the presence of aggressive environmental conditions.

Different methodologies and techniques for the execution of accelerated corrosion tests on steel reinforcing bars are provided by standards and deeply presented in the scientific literature.

The testing conditions artificially reproduced in laboratory are strictly related to the effective environmental situation that wants to be obtained; consequently, a lot of attention shall be used not to over (or under) estimate the reality of external ambient and, in particular, to provide a reliable interpretation of the experimental results derived.

Most common accelerated corrosion techniques, in the following briefly presented, are electrochemical corrosion methods, immersion tests and salt spray chamber tests.

*Electrochemical corrosion methods* (figure 6.1) were widely used in the past for the study of uniform, galvanic and localized corrosion, for the analysis of environmental cracking, for the evaluation of protective coatings and films and for many different other aims. The large diffusion of electrochemical techniques was related to their simplicity of application: the corrosion process consisted in an electron flow between anodic and cathodic areas whose speed was directly related to the rates of the oxidation and reduction reactions occurring in correspondence of the surface of the specimen. The monitoring of the electron flow provided the assessment of the kinetics of corrosion process, the thermodynamic tendency to occur spontaneously and the accumulated metal loss registered after the test. Despite their large applicability both for laboratory and in situ applications, some limitations were individuated, mainly related to the representation of relevant environmental conditions, the preparation of alloy and surface and the presence of mechanical perturbations, affecting the possibility to correctly reproduce the desired situation and the execution of the test.

*Immersion test* (including complete, partial and intermittent immersion tests) were often used for reproducing specific external environmental conditions; despite the apparently simplicity, a lot of parameters need to be opportunely controlled in order to ensure adequate reproducibility of test results

(solution composition, temperature, aeration, volume, velocity, and waterline effects, specimen surface preparation, method of immersion of specimens, duration of test, and method of cleaning specimens at conclusion of the exposure).

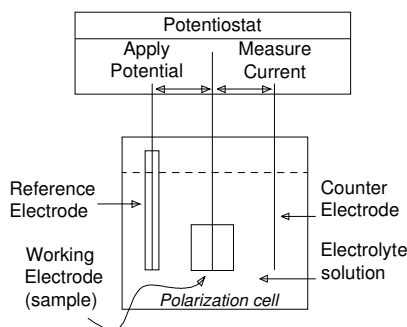


Figure 6. 1: Simplified scheme for electrochemical tests.

In the case of *Impressed Current Density tests*, reinforced concrete prisms (of dimensions generally equal to 150x250x300 mm, figure 6.2) with embedded steel reinforcing bars are used; a 5.0% of NaCl by weight of cement is generally added to the concrete mix in order to exceed the chloride threshold. The level of impressed current density generally varies between 100 and 500  $\mu\text{A}/\text{cm}^2$ . The corrosion rate is measured from strains at the faces of the prisms using Digital Image Correlation.

The Impressed Current Density test is a relatively simple and cheap method, able to provide useful information related to the spalling of the concrete cover, the mass loss and the mechanical properties of embedded rebars after extraction from the prisms. On the other hand, no specific codes for the execution of the test are provided, the interpretation of results is mainly optical, the depassivation rate of rebars cannot be evaluated and, moreover, the mass loss is the only parameter that can be directly related to the effective environmental conditions. Several studies, on the other hand, were presented in the current literature dealing with the investigation of the efficiency of impressed current density tests for the artificial reproduction of aggressive environmental conditions, taking into account parameters such as, for example, the variation of the intensity of impressed current (El Maaddawy T.A. et al. 2003).

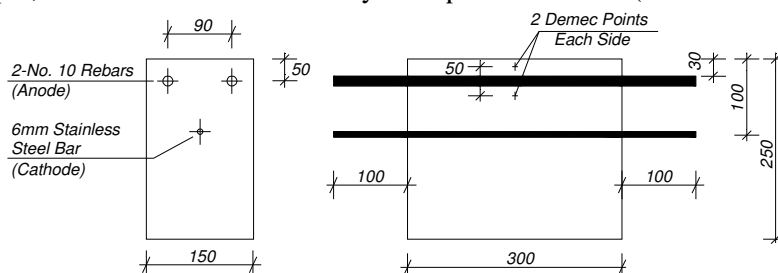
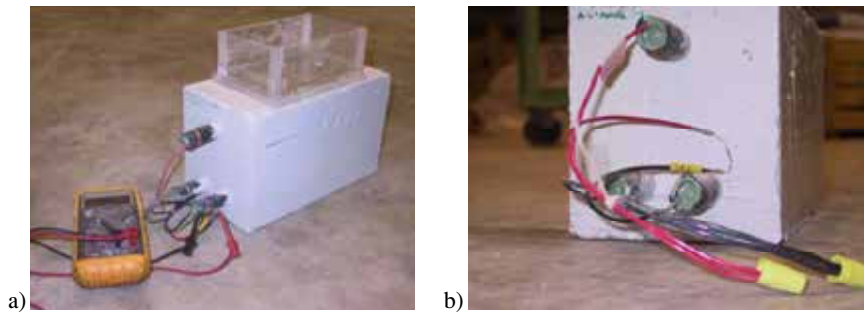


Figure 6. 2: Details of the specimens used for impressed current density tests (El Maaddawy T.A. et al. 2003).

American standard ASTM G109, on the other hand, provides a specific protocol for the execution of corrosion tests on steel reinforcements embedded in concrete. The test specimen consists of a small r.c. beam provided by two layers of steel reinforcements, a top layer with only one bar and a bottom layer with two rebars (figure 6.3). The layers are connected electrically with a 10-ohm resistor and the sides of the concrete are sealed with epoxy; a reservoir is secured to the beam to retain liquid on the upper surface. The solution in the reservoir ranges from 3.5-5% NaCl.

The half-cell corrosion potentials for the top and bottom layers are preliminarily measured as an indicator for the onset of corrosion. At the initiation of corrosion, concrete powder samples are obtained by impact-drilling at the level of the top reinforcement to estimate the chloride-ion concentration required for corrosion initiation. Additionally, corrosion current and the corresponding corrosion rates are determined by measuring the voltage drop across the resistor.



**Figure 6. 3:** Testing samples for accelerated corrosion tests following ASTM G109 (T. J. Wipf et al. 2006).

The main advantages in the application of this methodology for the execution of accelerated corrosion tests consist in the standardization of the testing procedure, the possibility of using steel reinforcements for further mechanical tests and to evaluate the chlorides' content; afterwards, generally long times of exposure are required and the rate of hydrogen diffusion remains unknown.

As an example, Al Hashemi (2007) executed artificial corrosion tests on steel reinforcing bars applying an electric current through the concrete between the reinforcing bars and two stainless steel grids (figure 6.4); the direction of the electric current inside the concrete blocks was applied in order to use the reinforcing bars as an anode and the two stainless steel grids as a cathode. The concrete blocks, characterized by dimensions equal to 200 mm long with a cross section of 200 x56 mm, were reinforced using four bars B450C (Tempcore) and two stainless steel grids, as presented in the figure 6.30. Tests were executed following the procedure provided by ASTM G109.

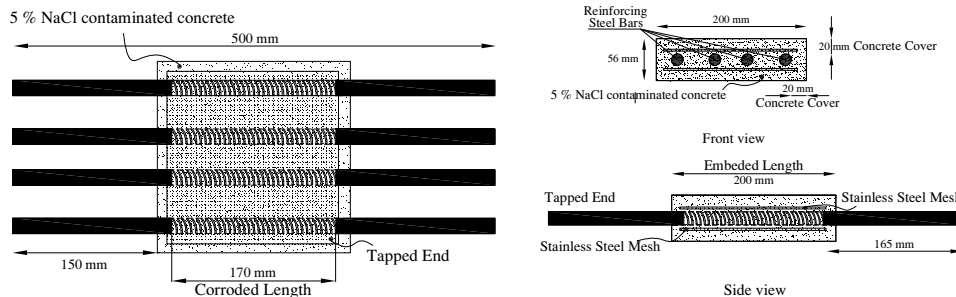


**Figure 6. 4:** Testing set up for accelerated corrosion tests following ASTM G109 (Al Hashemi 2007).

*Rapid Macrocell* procedure is another possible methodology for the execution of accelerated corrosion tests on both bare or embedded steel reinforcements. The contact surface between the mortar and the bar is used for simulating the effective interface steel bar/concrete in real structures. A single bar, either bare or mortar-clad, is placed in a 1-quart container with a simulated pore solution containing a 3.0% concentration of sodium chloride. Two bars are placed in a second 5-quart container and immersed in simulated pore solution with no chlorides added. The solution in both containers places 76 mm of reinforcement below the surface, as presented in the figure 6.5. The solutions in the two containers are connected by a salt bridge and the test specimen in the pore solution containing sodium chloride (anode) is electrically connected through a single 10-ohm resistor to the two specimens in the simulated pore solution (cathode). Air is bubbled into the pore solution surrounding the cathode to ensure an adequate supply of oxygen is present for the cathodic reaction. The air causes some evaporation, which is countered by adding distilled water to this container to maintain a constant volume of solution. The main advantages of this type of accelerated corrosion test consist in the possibilities of identifying the chloride content, adding CO<sub>2</sub> (carbonation), executing further mechanical tests on the specimens; moreover, lower times are required for the execution of test. Afterwards, the test is not codified by standards, and, once again, the hydrogen content cannot be evaluated. Many experimental Rapid Macrocell accelerated tests were executed in the current literature, in order to compare the results obtained using different techniques for reproducing the effects of aggressive environmental conditions on reinforcing steel bars (T.J.Wipf et al. 2006).

*Salt spray tests*, widely used during the last century as accelerated tests, allows the determination of the corrodibility of ferrous and nonferrous metals and the degree of protection due to both inorganic and organic coatings on a metallic base. Many revisions and improvements to the salt spray testing procedures were executed over the years through the efforts of the National Bureau of Standards, ASTM, equipment manufacturers, automotive industry and governmental agencies, eliminating many of the critic variables directly involved in this test procedure. The salt spray (fog) test is actually

considered the most useful accelerated laboratory corrosion test for reproducing the effects of marine atmospheres on different metals, with or without protective coatings.

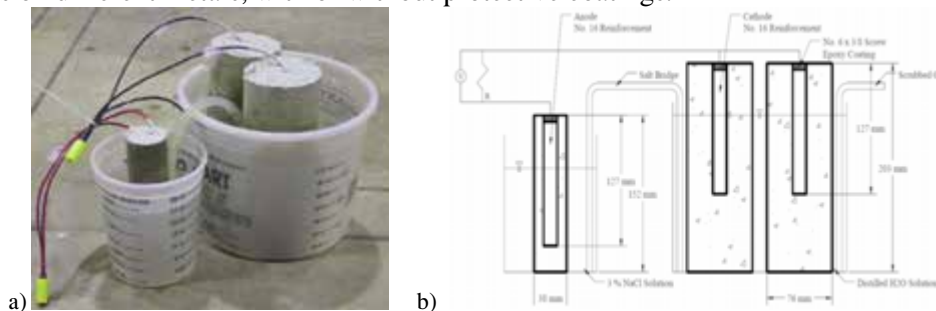


Figure 6. 5: Scheme of Rapid Macrocell accelerated corrosion test.

In a typical salt-spray chamber (figure 6.6) wet/dry cycles are introduced; in general, the number of cycles per day varies between 5 and 10. Different approaches can be adopted: in order to represent the “full concrete cover condition”, a solution of saturated  $\text{Ca}(\text{OH})_2 + 0.5\text{M NaCl}$  is generally used for reproduce a concrete pH in the range 12.5-13.6 and the humidity is generally maintained between 50-60% for the whole duration of the experiment. On the other hand, for recreating the “broken cover condition”, a percentage of NaCl between 3.5 and 5.0% is used simulating a pH of the solution around 5.8-7.2; also in this case, the humidity is kept constant (50-60%) for the whole duration of the experiment. The main advantage of this procedure consists in the reduced period of exposure, generally varying between 10 and 90 days, and in the fact that ASTM codified a specific protocol for the execution of the test. Moreover, the estimation of mass loss and the hydrogen charging are individuated. Afterwards, the negative aspects of this procedure are mainly related to the fact that the effects of corrosion on the specimens are strongly influenced by the number of wet-dry cycles adopted, the differences among different types of concrete cannot be taken into account and, finally, the chloride threshold is only artificially induced.

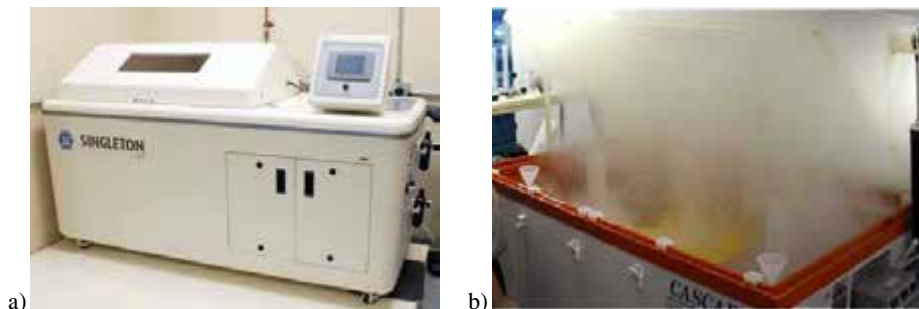


Figure 6. 6: Example of salt spray chamber.

Many studies in the current literature presented the results of mechanical tests (both monotonic and LCF) on reinforcing bars subjected to preliminarily exposure in salt spray chamber.

As an example, Apostolopoulos and Papadakis (2008) conducted salt spray (fog) tests according to the ASTM B117-94 specifications. The salt solution was prepared dissolving 5 parts by mass of sodium chloride (NaCl) into 95 parts of distilled water (pH range between 6.5 and 7.2). The temperature in the zone of the reinforcement material exposed inside the salt spray chamber was maintained at  $35\text{ }^\circ\text{C}$  ( $+1.1\text{--}1.7$ ) $^\circ\text{C}$ . When exposure was completed, the specimens were washed with clean running water to remove any salt deposits from their surfaces, and then were air dried. The accelerated salt spray corrosion was carried out for 10, 20, 30, 40 and 60 days and then, reinforcing bars (steel grade BSt 420) were subjected to experimental mechanical tests. The same procedure was also adopted by Apostolopoulos et al. (2006) for rebars BSt 500. In relation to the ability of correctly reproduce the aggressive environmental conditions and in particular, to the necessity of moderate required times for the execution of tests, accelerated corrosion procedure in salt spray chamber was adopted inside Rusteel project in order to pre-corrode steel reinforcing bars to be further subjected to experimental tensile and LCF tests, allowing the individuation of the ductility capacity of corroded specimen and their ability to withstand seismic action.

## 6.2 Accelerated corrosion tests in salt spray chamber

### 6.2.1 Elaboration of a protocol for the execution of accelerated corrosion test

In relation to what already presented, in the framework of *Rusteel* project a specific protocol for the execution of accelerated corrosion test in salt spray chamber, selected as the more useful and appropriate for the aims of the present work, was elaborated.

Two different exposure periods, respectively equal to 45 and 90 days, were considered for accelerated corrosion tests in salt spray chamber. The protocol was organized into 8 different steps and for the preparation of the specimens, standard ISO 9227 (2006) was adopted.

In particular, a lot of attention was paid to the preparation of samples, their positioning inside the salt spray chamber and, moreover, to their cleaning after the end of the exposure period for the execution of tensile and LCF tests, as well as for the evaluation of the effective mass loss.

Moreover, specific indications were provided for the maintenance of corroded specimens before the execution of mechanical tests in order to allow the exact evaluation of Hydrogen content.

Artificial corrosion tests in salt spray chamber were executed by three different Italian Laboratories, able to specifically reproduce the conditions required by the protocol, in the following individuated as Laboratory 1, 2 and 3.

#### - STEP 1: Preparation of the testing apparatus

The chamber, piping and solution tank shall be perfectly cleaned from previous experiments, using at least 120 liters of de-ionized water. The chamber can be considered ready for the execution of tests when the Ph ranges between 5.5 and 6.2. Moreover, the bottom corners of the chamber shall be cleaned by hand using a wet sponge, springer nozzles shall be removed and cleaned for 10 minutes into vinegar and then rinsed with tap water. In general, the prescriptions suggested by ISO 9227:2006 were adopted.

#### - STEP 2: Loading solution to the chamber

Before the placing of the specimens, at least 50 liters of solution shall be inserted in the chamber and circulate for about 6 hours under the pre-determined wet/dry cycle, in order to stabilize the pH of the chamber itself.

#### - STEP 3: Preparation of the testing articles

The length of the specimens shall be established following the prescriptions suggested by ASTM or DIN standards, with a minimum gauge length equal to 150 mm. In general, the length of the specimens varies between 500 and 600 mm, in order to allow execution of tensile tests on corroded rebars and the direct individuation of the stress-strain diagram.

In the middle section of the testing article, a high temperature aluminum (non adhesive) tape around the rebar shall be placed; the width of the tape usually varies between 20 mm or, at least, the distance between two following ribs: this length coincides with the unprotected part of the specimen, as presented in figure 6.7a. A tube of diameter at least 40 mm and length similar to that of the testing article shall be filled with natural wax, using the external end cups. The tube with the wax is then placed inside an oven for 20 minutes and a temperature of about 90°. The tube is then removed from the oven and one end cup is opened. Within 30 seconds the testing article shall be placed inside the tube. The article shall be finally removed and allowed for 10 minutes to cool; at the end the tape shall be removed (figure 6.7b).

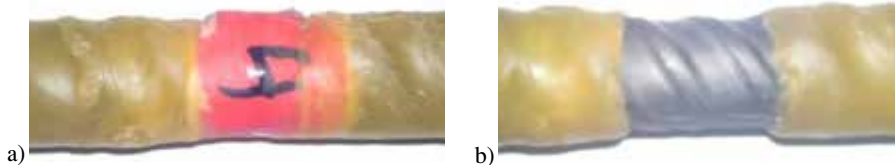


Figure 6. 7: a) The tape between two successive ribs, b) the article without tape.

#### - STEP 4: Placing the testing articles in the chamber

The testing article shall be placed at an angle of 45-60° to the supports (figure 6.8). During the full duration of the experiment the articles shall be rotated by 90° at least three times a day, in order to prevent the generation of salts, according to what prescribed by ISO 9227:2006.

- *STEP 5: Test Execution*

At least 8 wet/dry cycles shall be programmed per 24 hours, i.e. 90 minutes dry followed by 90 minutes wet. During the experiment a digital Ph meter is placed inside the chamber; the electrode shall be positioned at a bottom corner where solution is gathered.

- *STEP 6: Duration of the test and article handling*

Two different exposure periods, respectively equal to 45 and 90 days can be considered. At the end of the test, the specimens shall be rubbed with a fine steel brush and cleaned with tap water, without applying pressure of the article on the wheel to prevent heat generation. Moreover, specimens that cannot be immediately tested shall be maintained at a temperature of about  $-5^{\circ}$  to avoid the loss of the volatile part of hydrogen.

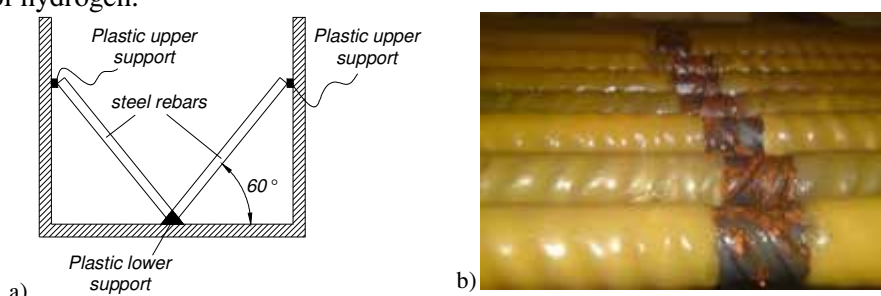


**Figure 6. 8:** a) Placing of the specimen inside the chamber, b) the articles on the salt spray chamber

- *STEP 7: Measuring of the damage before tensile tests*

Cross sectional analysis after the tensile test is prescribed as well as the use of SEM; the notch depth, crack depth and width shall be also measured. Moreover, mass loss and cross section reduction are the most significative parameters to take into account. The measurement of the hydrogen content is also recommended, according to what previously presented.

- *STEP 8: Execution of Mechanical tests on corroded rebars*

Upon removal from the freezer the article shall be allowed to reach ambient temperature before the execution of mechanical tests.

Experimental tensile tests shall be executed following the procedure provided by EN 15630:2010, according to what already presented for uncorroded specimens. In particular, to prepare the gripping ends, the wax shall be removed using a butane flame, keeping the temperature to low/moderate values and the wedged shall be cleaned from oil residues using an alcohol. The same preparation procedure is adopted also for rebars to test under LCF.

### 6.2.2 Individuation of a set of representative steel reinforcing bars

A set of representative steel reinforcements, reduced with respect to the one already presented and considered for mechanical tests in uncorroded condition, was individuated; once again, different steel grade (characteristic yielding strength  $R_e$  respectively equal to 400, 450 and 500 MPa), different ductility classes (A, B and C according to Eurocode 8, EN 1998-1:2005), different production processes (TempCore, Micro Alloyed, Stretched and Cold Worked bars) and finally different producer (producers 1 and 2) were considered. Table 6.1 summarizes reinforcing bars used in accelerated corrosion tests.

**Table 6. 1:** Reduced set of representative steel reinforcing bars subjected to accelerated corrosion tests.

| Steel grade | Ductility | Diameter | Process | Ribs   | Producer |
|-------------|-----------|----------|---------|--------|----------|
| B400        | C         | 16       | TEMP    | Ribbed | Prod.1   |
| B400        | C         | 16       | MA      | Ribbed | Prod.2   |
| B400        | C         | 25       | MA      | Ribbed | Prod.2   |
| B450        | C         | 12       | STR     | Ribbed | Prod.1   |
| B450        | C         | 16       | TEMP    | Ribbed | Prod.1   |
| B450        | C         | 25       | TEMP    | Ribbed | Prod.2   |
| B500        | A         | 12       | CW      | Ribbed | Prod.2   |
| B500        | B         | 12       | STR     | Ribbed | Prod.1   |
| B500        | B         | 16       | TEMP    | Ribbed | Prod.1   |
| B500        | B         | 25       | TEMP    | Ribbed | Prod.2   |

## 7. MECHANICAL TESTS ON CORRODED BARS

### 7.1 Tensile tests on corroded specimens

Accelerated corrosion tests were executed according to the protocol presented in the previous paragraph, using two different exposure durations (45 and 90 days). On the corroded specimens, mechanical tensile and low-cycle fatigue tests were executed: tensile tests were executed according to EN 15630-1:2010, while LCF tests followed the protocol presented in Chapter 2. The results are presented in terms of mechanical properties ( $R_e$ ,  $R_m$ ,  $A_{gt}$  and  $A$ ) and mass loss. In particular mass loss

was evaluated as  $\frac{M_i - M_f}{M_i^*}$ , in which  $M_i$  and  $M_f$  respectively the mass of the specimen before and after

corrosion tests in salt spray chamber and  $M_i^*$  represents the mass of a bar of length equal to the exposed length ( $L_{corr}$ ).  $L_{corr}$  can vary, due to practical operations during the preparation phase.

#### 7.1.1 Results of experimental tensile tests - UniPI

In the following paragraphs, the values obtained from experimental tensile tests on corroded steel rebars, after 45 and 90 days of exposure in salt spray chamber, are presented. Three different laboratories were selected for the execution of accelerated corrosion tests (ILVA s.p.a – Lab.1, Bavaro laboratory – Lab. 2 and Omeco laboratory – Lab.3).

**Table 7. 1:** Results of experimental tensile tests on corroded specimens B500A-Cold Worked, diameter 12 mm.

| Steel grade/diameter/<br>process/rib/producer | T <sub>corr</sub><br>[days] | L <sub>corr</sub><br>[mm] | ΔM<br>[g] | ΔM/M <sub>uncorr</sub><br>[%] | R <sub>e</sub><br>[MPa] | R <sub>m</sub><br>[MPa] | R <sub>m</sub> /R <sub>e</sub><br>[-] | A <sub>gt</sub><br>[%] | A <sub>5</sub><br>[%] | Lab    |
|---|-----------------------------|---------------------------|-----------|-------------------------------|-------------------------|-------------------------|---------------------------------------|------------------------|-----------------------|--------|
| B500A-12-CW-Prod.2-1                          | 45                          | 21,70                     | 3,26      | 17,17%                        | 489,5                   | 512,3                   | 1,05                                  | 1,30                   | 11,8                  | Lab. 1 |
| B500A-12-CW-Prod.2-2                          | 45                          | 23,30                     | 2,91      | 14,27%                        | 495,0                   | 518,6                   | 1,05                                  | 0,90                   | 10,7                  | Lab. 1 |
| B500A-12-CW-Prod.2-3                          | 45                          | 21,50                     | 4,23      | 22,47%                        | 498,6                   | 517,8                   | 1,04                                  | 0,80                   | 10,8                  | Lab. 1 |
| B500A-12-CW-Prod.2 5.6                        | 90                          | 24,90                     | 2,71      | 12,56%                        | 461,0                   | 480,0                   | 1,04                                  | 0,90                   | 13,3                  | Lab. 2 |
| B500A-12-CW-Prod.2 5.5                        | 90                          | 20,95                     | 0,82      | 4,50%                         | 508,0                   | 532,6                   | 1,05                                  | 2,40                   | 14,7                  | Lab. 2 |
| B500A-12-CW-Prod.2 5.2                        | 90                          | 182,50                    | 8,41      | 5,29%                         | 505,0                   | 535,0                   | 1,06                                  | 5,10                   | 14,2                  | Lab. 2 |

**Table 7. 2:** Results of experimental tensile tests on corroded specimens B400C TempCore, 16 mm (Prod. 1)

| Steel grade/diameter/<br>process/rib/producer | T <sub>corr</sub><br>[days] | L <sub>corr</sub><br>[mm] | ΔM<br>[g] | ΔM/M <sub>uncorr</sub><br>[%] | R <sub>e</sub><br>[MPa] | R <sub>m</sub><br>[MPa] | R <sub>m</sub> /R <sub>e</sub><br>[-] | A <sub>gt</sub><br>[%] | A <sub>5</sub><br>[%] | Lab    |
|---|-----------------------------|---------------------------|-----------|-------------------------------|-------------------------|-------------------------|---------------------------------------|------------------------|-----------------------|--------|
| B400C-16-TEMP-Prod.1-1                        | 90                          | 30,00                     | 6,26      | 13,54%                        | 398,4                   | 525,3                   | 1,32                                  | 7,1                    | 17,1                  | Lab. 1 |
| B400C-16-TEMP-Prod.1-2                        | 90                          | 28,40                     | 8,29      | 18,94%                        | 401,4                   | 520,6                   | 1,30                                  | 5,8                    | 14,8                  | Lab. 1 |
| B400C-16-TEMP-Prod.1-3                        | 90                          | 30,00                     | 5,63      | 12,18%                        | 404,9                   | 524,8                   | 1,30                                  | 6,4                    | 15,1                  | Lab. 1 |
| B400C-16-TEMP-Prod.1-4                        | 90                          | 24,90                     | 6,11      | 15,93%                        | 417,3                   | 518,5                   | 1,24                                  | 7,5                    | 19,4                  | Lab. 1 |
| B400C-16-TEMP-Prod.1-5                        | 90                          | 25,25                     | 6,24      | 16,03%                        | 410,8                   | -                       | -                                     | 7,6                    | 16,8                  | Lab. 1 |
| B400C-16-TEMP-Prod.1-6                        | 90                          | 25,05                     | 8,34      | 21,62%                        | 414,6                   | 522,6                   | 1,26                                  | 8,0                    | 15,4                  | Lab. 1 |
| B400C-16-TEMP-Prod.1-1                        | 45                          | 31,00                     | 4,79      | 10,03%                        | 444,5                   | 550,2                   | 1,24                                  | 8,4                    | 19,6                  | Lab. 1 |
| B400C-16-TEMP-Prod.1-2                        | 45                          | 30,50                     | 6,34      | 13,48%                        | 449,2                   | 548,2                   | 1,22                                  | 7,5                    | 17,5                  | Lab. 1 |
| B400C-16-TEMP-Prod.1-3                        | 45                          | 31,70                     | 7,47      | 15,30%                        | 436,5                   | 554,6                   | 1,27                                  | 9,0                    | 17,6                  | Lab. 1 |

**Table 7. 3:** Results of experimental tensile tests on corroded specimens B450C TempCore, 16 mm (Prod. 1)

| Steel grade/diameter/<br>process/rib/producer | T <sub>corr</sub><br>[days] | L <sub>corr</sub><br>[mm] | ΔM<br>[g] | ΔM/M <sub>uncorr</sub><br>[%] | R <sub>e</sub><br>[MPa] | R <sub>m</sub><br>[MPa] | R <sub>m</sub> /R <sub>e</sub><br>[-] | A <sub>gt</sub><br>[%] | A <sub>5</sub><br>[%] | Lab    |
|---|-----------------------------|---------------------------|-----------|-------------------------------|-------------------------|-------------------------|---------------------------------------|------------------------|-----------------------|--------|
| B450C-16-TEMP-Prod.1-1                        | 90                          | 20,90                     | 4,91      | 14,57                         | 481,4                   | 599,5                   | 1,25                                  | 4,3                    | 15,4                  | Lab. 1 |
| B450C-16-TEMP-Prod.1-2                        | 90                          | 26,40                     | 2,59      | 6,08                          | 484,4                   | 598,0                   | 1,23                                  | 4,4                    | 15,6                  | Lab. 1 |
| B450C-16-TEMP-Prod.1-3                        | 90                          | 27,20                     | 3,83      | 8,74                          | 499,8                   | 610,5                   | 1,22                                  | 5,1                    | 16,6                  | Lab. 1 |
| B450C-16-TEMP-Prod.1-4                        | 90                          | 28,85                     | 3,20      | 6,87                          | 497,4                   | 607,9                   | 1,22                                  | 5,7                    | 17,8                  | Lab. 1 |
| B450C-16-TEMP-Prod.1-5                        | 90                          | 24,20                     | 3,25      | 8,32                          | 480,9                   | 600,0                   | 1,25                                  | 4,1                    | 14,1                  | Lab. 1 |
| B450C-16-TEMP-Prod.1-6                        | 90                          | 24,50                     | 6,82      | 17,26                         | 502,8                   | 613,8                   | 1,22                                  | 5,5                    | 16,3                  | Lab. 1 |
| B450C-16-TEMP-Prod.1-1                        | 45                          | 30,50                     | 3,87      | 7,87                          | 509,2                   | 614,3                   | 1,21                                  | 6,9                    | 16,4                  | Lab. 1 |
| B450C-16-TEMP-Prod.1-2                        | 45                          | 29,50                     | 3,54      | 7,44                          | 511,2                   | 615,9                   | 1,20                                  | 6,2                    | 16,9                  | Lab. 1 |
| B450C-16-TEMP-Prod.1-3                        | 45                          | 28,80                     | 5,18      | 11,15                         | 504,3                   | 607,9                   | 1,21                                  | 5,7                    | 16,4                  | Lab. 1 |

**Table 7. 4:** Results of experimental tensile tests on corroded specimens B500B TempCore, 16 mm (Prod. 1)

| Steel grade/diameter/<br>process/rib/producer | T <sub>corr</sub><br>[days] | L <sub>corr</sub><br>[mm] | ΔM<br>[g] | ΔM/M <sub>uncorr</sub><br>[%] | R <sub>e</sub><br>[MPa] | R <sub>m</sub><br>[MPa] | R <sub>m</sub> /R <sub>e</sub><br>[-] | A <sub>gt</sub><br>[%] | A <sub>5</sub><br>[%] | Lab    |
|---|-----------------------------|---------------------------|-----------|-------------------------------|-------------------------|-------------------------|---------------------------------------|------------------------|-----------------------|--------|
| B500B-16-TEMP-Prod.1-1                        | 90                          | 28,60                     | 11,22     | 24,34%                        | 492,4                   | 607,9                   | 1,23                                  | 5,7                    | 14,8                  | Lab. 1 |
| B500B-16-TEMP-Prod.1-2                        | 90                          | 30,50                     | 8,34      | 16,97%                        | 476,5                   | 596,4                   | 1,25                                  | 4,6                    | 15,5                  | Lab. 1 |
| B500B-16-TEMP-Prod.1-3                        | 90                          | 20,00                     | 14,46     | 44,86%                        | 481,9                   | 610,5                   | 1,27                                  | 5,0                    | 14,9                  | Lab. 1 |
| B500B-16-TEMP-Prod.1-4                        | 90                          | 24,45                     | 6,66      | 16,91%                        | 485,4                   | 606,3                   | 1,25                                  | 5,1                    | 15,4                  | Lab. 1 |
| B500B-16-TEMP-Prod.1-5                        | 90                          | 26,40                     | 11,80     | 27,75%                        | 491,4                   | 603,2                   | 1,23                                  | 5,0                    | 15,6                  | Lab. 1 |
| B500B-16-TEMP-Prod.1-6                        | 90                          | 24,20                     | 6,82      | 17,48%                        | 490,3                   | 605,6                   | 1,24                                  | 5,5                    | 16,4                  | Lab. 1 |
| B500B-16-TEMP-Prod.1-1                        | 45                          | 31,50                     | 10,57     | 20,83%                        | 500,0                   | 610,3                   | 1,22                                  | 9,1                    | 19,4                  | Lab. 1 |
| B500B-16-TEMP-Prod.1-2                        | 45                          | 31,20                     | 9,62      | 19,13%                        | 490,9                   | 604,3                   | 1,23                                  | 6,3                    | 17,8                  | Lab. 1 |
| B500B-16-TEMP-Prod.1-3                        | 45                          | 23,20                     | 9,55      | 25,55%                        | 492,0                   | 604,2                   | 1,23                                  | 7,5                    | 16,5                  | Lab. 1 |

**Table 7. 5:** Results of experimental tensile tests on corroded specimens B400C Micro Alloyed, 16 mm (Prod. 2)

| Steel grade/diameter/<br>process/rib/producer | T <sub>corr</sub><br>[days] | L <sub>corr</sub><br>[mm] | ΔM<br>[g] | ΔM/M <sub>uncorr</sub><br>[%] | R <sub>e</sub><br>[MPa] | R <sub>m</sub><br>[MPa] | R <sub>m</sub> /R <sub>e</sub><br>[-] | A <sub>gt</sub><br>[%] | A <sub>5</sub><br>[%] | Lab    |
|---|-----------------------------|---------------------------|-----------|-------------------------------|-------------------------|-------------------------|---------------------------------------|------------------------|-----------------------|--------|
| B400C-16-MA-Prod.2-1                          | 45                          | 31,50                     | 5,98      | 11,75%                        | 427,2                   | 562,1                   | 1,32                                  | 10,6                   | 21,6                  | Lab. 1 |
| B400C-16-MA-Prod.2-2                          | 45                          | 29,50                     | 5,05      | 10,59%                        | 437,5                   | 562,0                   | 1,28                                  | 9,8                    | 21,0                  | Lab. 1 |
| B400C-16-MA-Prod.2-3                          | 45                          | 31,20                     | 11,19     | 22,19%                        | 424,0                   | 560,0                   | 1,32                                  | 10,3                   | 20,9                  | Lab. 1 |

**Table 7. 6:** Results of experimental tensile tests on corroded specimens B400C Micro Alloyed, 25 mm (Prod. 2)

| Steel grade/diameter/<br>process/rib/producer | T <sub>corr</sub><br>[days] | L <sub>corr</sub><br>[mm] | ΔM<br>[g] | ΔM/M <sub>uncorr</sub><br>[%] | R <sub>e</sub><br>[MPa] | R <sub>m</sub><br>[MPa] | R <sub>m</sub> /R <sub>e</sub><br>[-] | A <sub>gt</sub><br>[%] | A <sub>5</sub><br>[%] | Lab    |
|---|-----------------------------|---------------------------|-----------|-------------------------------|-------------------------|-------------------------|---------------------------------------|------------------------|-----------------------|--------|
| B400C-25-MA-Prod.2 8.10                       | 90                          | 22,80                     | 4,50      | 5,06%                         | 442,7                   | 569,5                   | 1,29                                  | 12,9                   | 23,6                  | Lab. 2 |
| B400C-25-MA-Prod.2 8.11                       | 90                          | 21,95                     | 8,50      | 9,95%                         | 437,7                   | 563,4                   | 1,29                                  | 15,0                   | 27,4                  | Lab. 2 |
| B400C-25-MA-Prod.2 8.9                        | 90                          | 17,05                     | 6,50      | 9,80%                         | 438,7                   | 573,5                   | 1,31                                  | 16,1                   | 26,5                  | Lab. 2 |
| B400C-25-MA-Prod.2-1                          | 45                          | 25,90                     | 0,66      | 0,65%                         | 427,5                   | 575,7                   | 1,35                                  | 11,6                   | 20,0                  | Lab. 1 |
| B400C-25-MA-Prod.2-2                          | 45                          | 22,15                     | 0,75      | 0,86%                         | 425,8                   | 576,2                   | 1,35                                  | 12,7                   | 14,0                  | Lab. 1 |
| B400C-25-MA-Prod.2-3                          | 45                          | 21,85                     | 0,62      | 0,73%                         | 424,0                   | 576,0                   | 1,36                                  | 13,3                   | 15,7                  | Lab. 1 |

**Table 7. 7:** Results of experimental tensile tests on corroded specimens B450C TempCore, 25 mm (Prod. 2)

| Steel grade/diameter/<br>process/rib/producer | T <sub>corr</sub><br>[days] | L <sub>corr</sub><br>[mm] | ΔM<br>[g] | ΔM/M <sub>uncorr</sub><br>[%] | R <sub>e</sub><br>[MPa] | R <sub>m</sub><br>[MPa] | R <sub>m</sub> /R <sub>e</sub><br>[-] | A <sub>gt</sub><br>[%] | A <sub>5</sub><br>[%] | Lab    |
|---|-----------------------------|---------------------------|-----------|-------------------------------|-------------------------|-------------------------|---------------------------------------|------------------------|-----------------------|--------|
| B450C-25-TEM-Prod2 10.3                       | 90                          | 21,55                     | 1,0       | 1,20%                         | 502,4                   | 623,7                   | 1,24                                  | 9,6                    | 18,9                  | Lab. 2 |
| B450C-25-TEM-Prod2 10.9                       | 90                          | 20,40                     | 1,5       | 1,89%                         | 515,5                   | 630,8                   | 1,22                                  | 10,0                   | 17,8                  | Lab. 2 |
| B450C-25-TEM-Prod2 10.10                      | 90                          | 21,55                     | 7,0       | 8,37%                         | 515,5                   | 628,8                   | 1,22                                  | 8,5                    | 19,3                  | Lab. 2 |
| B450C-25-TEM-Prod2-1                          | 45                          | 22,00                     | 0,3       | 0,37%                         | 500,3                   | 622,1                   | 1,24                                  | 9,1                    | 19,8                  | Lab. 1 |
| B450C-25-TEM-Prod2-2                          | 45                          | 25,50                     | 0,7       | 0,70%                         | 495,0                   | 618,1                   | 1,25                                  | 8,3                    | 19,2                  | Lab. 1 |
| B450C-25-TEM-Prod2-3                          | 45                          | 22,90                     | 0,7       | 0,78%                         | 497,4                   | 617,2                   | 1,24                                  | 8,5                    | 18,2                  | Lab. 1 |

**Table 7. 8:** Results of experimental tensile tests on corroded specimens B500B TempCore, 25 mm (Prod. 2)

| Steel grade/diameter/<br>process/rib/producer | T <sub>corr</sub><br>[days] | L <sub>corr</sub><br>[mm] | ΔM<br>[g] | ΔM/M <sub>uncorr</sub><br>[%] | R <sub>e</sub><br>[MPa] | R <sub>m</sub><br>[MPa] | R <sub>m</sub> /R <sub>e</sub><br>[-] | A <sub>gt</sub><br>[%] | A <sub>5</sub><br>[%] | Lab    |
|---|-----------------------------|---------------------------|-----------|-------------------------------|-------------------------|-------------------------|---------------------------------------|------------------------|-----------------------|--------|
| B500B-25-TEMP-Prod.2 6.9                      | 90                          | 21,70                     | 3,00      | 3,56%                         | 533,1                   | 640,1                   | 1,20                                  | 8,8                    | 18,6                  | Lab. 2 |
| B500B-25-TEMP-Prod.2 6.1                      | 90                          | 23,20                     | 18,5      | 20,57%                        | 537,1                   | 646,2                   | 1,20                                  | 8,1                    | 18,6                  | Lab. 2 |
| B500B-25-TEMP-Prod.2 6.8                      | 90                          | 22,80                     | 2,50      | 2,81%                         | 535,1                   | 640,1                   | 1,20                                  | 8,7                    | 19,9                  | Lab. 2 |
| B500B-25-TEMP-Prod.2-1                        | 45                          | 26,40                     | 1,72      | 1,67%                         | 518,4                   | 637,1                   | 1,23                                  | 8,5                    | 19,2                  | Lab. 1 |
| B500B-25-TEMP-Prod.2-2                        | 45                          | 23,00                     | 1,67      | 1,86%                         | 524,3                   | 643,2                   | 1,23                                  | 9,3                    | 18,2                  | Lab. 1 |
| B500B-25-TEMP-Prod.2-3                        | 45                          | 24,20                     | 11,99     | 2,13%                         | 513,7                   | 633,6                   | 1,23                                  | 8,2                    | 18,1                  | Lab. 1 |

### 7.1.2 Results of experimental tensile tests – ISQ

Results of the experimental tensile tests on corroded specimens executed by ISQ are presented in the tables 7.9-7.14 in terms of yielding and tensile strength, ultimate elongation and elongation corresponding to maximum load in relation to bars' diameter, considering the two exposure periods of 45 and 90 days in salt spray chamber,

**Table 7. 9:** Results of experimental tensile tests on corroded specimens of diameter 12.0 mm (45 days of corrosion).

| Steel grade/diameter/<br>process/rib/producer | ID  | D<br>(mm) | R <sub>e</sub><br>MPa | R <sub>m</sub><br>MPa | A <sub>5</sub><br>% | A <sub>gt</sub><br>% |
|---|-----|-----------|-----------------------|-----------------------|---------------------|----------------------|
| B500A-12-CW-I-Prod. 2                         | B3  | 12        | 608                   | 639                   | 8,2                 | 2,3                  |
|   | B4  |           | 534                   | 569                   | 6,2                 | 2,9                  |
|   | B6  |           | 573                   | 610                   | 6,4                 | 2,2                  |
|   | B7  |           | 558                   | 593                   | 4,6                 | 2,9                  |
|   | B41 |           | 500                   | 534                   | 6,6                 | 3,5                  |
|   | B43 |           | 498                   | 533                   | 6,4                 | 3,9                  |
|   | B45 |           | 498                   | 538                   | 7,2                 | 3,9                  |
| B450C-12-TEMP-R-Prod. 1                       | I7  | 12        | 464                   | 612                   | 10,2                | 7,9                  |
|   | I1  |           | 467                   | 615                   | 10,4                | 7,7                  |
|   | I9  |           | 460                   | 615                   | 10,6                | 7,9                  |
|   | I8  |           | 465                   | 615                   | 11,4                | 7,9                  |
|   | I5  |           | 470                   | 621                   | ----                | 7,8                  |

**Table 7. 10:** Results of experimental tensile tests on corroded specimens of diameter 16.0 mm (45 days of corrosion).

| Steel grade/diameter/<br>process/rib/producer | ID   | D<br>(mm) | R <sub>e</sub><br>MPa | R <sub>m</sub><br>MPa | A <sub>5</sub><br>% | A <sub>gt</sub><br>% |
|---|------|-----------|-----------------------|-----------------------|---------------------|----------------------|
| B400C-16-MA-R-Prod. 2                         | MA4  | 16        | 468                   | 609                   | 20,3                | 15,2                 |
|   | MA5  |           | 468                   | 609                   | 20,3                | 15,2                 |
|   | MA9  |           | 478                   | 623                   | 20,9                | 18,7                 |
|   | MA10 |           | 483                   | 624                   | 17,7                | 17,2                 |
|   | MA15 |           | 478                   | 623                   | 20,9                | 18,7                 |
|   | MA20 |           | 475                   | 616                   | 17,7                | 13,5                 |
|   | MA21 |           | 474                   | 619                   | ---(a)              | 14,4                 |
|   | MA26 |           | 476                   | 621                   | 19,5                | 15,1                 |
|   | MA22 |           | 474                   | 620                   | ---(a)              | 15,2                 |
| B400C-16-TEMP-R-Prod. 1                       | S9   | 16        | 412                   | 545                   | 18,7                | 13,0                 |
|   | S15  |           | 412                   | 545                   | 16,1                | 12,9                 |
|   | S6   |           | 417                   | 546                   | 17,2                | 11,8                 |
|   | S25  |           | 415                   | 544                   | 17,1                | 14,0                 |
|   | S8   |           | 418                   | 548                   | 17,5                | 13,4                 |
|   | S4   |           | 423                   | 552                   | 16,8                | 14,1                 |
|   | S19  |           | 404                   | 546                   | 16,0                | 15,3                 |
|   | SE8  |           | 427                   | 550                   | 17,3                | 13,8                 |
|   | SE24 |           | 428                   | 557                   | 17,1                | 13,2                 |
|   | SE23 |           | 420                   | 553                   | 16,7                | 14,0                 |
|   | SE17 |           | 408                   | 546                   | 15,9                | 10,2                 |
|   | SE20 |           | 421                   | 547                   | 16,2                | 13,2                 |
|   | SE7  |           | 425                   | 551                   | 16,5                | 14,0                 |
| SE22  | 422  | 550       | 15,5                  | 13,6                  |                     |                      |
| B450C-16-TEMP-R-Prod. 1                       | P3C  | 16        | 568                   | 666                   | 12,4                | 9,2                  |
|   | P5C  |           | 538                   | 656                   | 12,3                | 6,9                  |
|   | P8C  |           | 578                   | 674                   | 12,4                | 9,1                  |
|   | P11C |           | 567                   | 670                   | 13,0                | 9,9                  |
|   | P12C |           | 546                   | 654                   | 14,2                | 10,6                 |
|   | P13C |           | 576                   | 665                   | 11,6                | 8,2                  |
|   | P16C |           | 581                   | 679                   | 12,6                | 8,8                  |
| P17C  | 557  | 661       | 13,1                  | 10,4                  |                     |                      |

|                         |      |    |     |     |      |      |
|-------------------------|------|----|-----|-----|------|------|
|                         | R24  |    | 493 | 609 | 15,3 | 12,4 |
|                         | R22  |    | 508 | 626 | 16,1 | 13,2 |
|                         | R16  |    | 496 | 615 | 15,1 | 13,0 |
|                         | R20  |    | 495 | 616 | 13,8 | 12,4 |
|                         | R21  |    | 487 | 608 | 15,6 | 13,1 |
|                         | R15  |    | 480 | 598 | 16,2 | 12,6 |
|                         | R6   |    | 485 | 604 | 16,7 | 12,9 |
| B500B-16-TEMP-R-Prod. 1 | P8B  |    | 540 | 658 | 16,9 | 12,1 |
|                         | P13B | 16 | 531 | 647 | 15,3 | 11,6 |
|                         | P2B  |    | 524 | 645 | 14,7 | 10,1 |

**Table 7. 11:** Results of experimental tensile tests on corroded specimens of diameter 25.0 mm(45 days of corrosion).

| Steel grade/diameter/<br>process/rib/producer | ID  | D<br>(mm) | R <sub>e</sub><br>MPa | R <sub>m</sub><br>MPa | A <sub>5</sub><br>% | A <sub>gt</sub><br>% |
|---|-----|-----------|-----------------------|-----------------------|---------------------|----------------------|
| B400C-25-MA-R-Prod. 2                         | B22 | 25        | 455                   | 591                   | ---                 | 17,1                 |
|   | B23 |           | 455                   | 593                   | 22,0                | 16,2                 |
|   | B26 |           | 450                   | 592                   | 22,5                | 17,9                 |
|   | B27 |           | 451                   | 590                   | 26,9                | 16,9                 |
|   | B30 |           | 446                   | 588                   | 22,3                | 17,3                 |
|   | B54 |           | 456                   | 596                   | ----                | 8,2                  |
|   | B57 |           | 457                   | 596                   | 27,0                | 8,7                  |
|   | B56 |           | 455                   | 597                   | 26,2                | 8,3                  |
| B450C-25-TEMP-R-Prod. 2                       | B32 | 25        | 524                   | 635                   | 19,2                | 14,4                 |
|   | B35 |           | 522                   | 633                   | 20,5                | 13,9                 |
|   | B36 |           | 522                   | 634                   | 17,9                | 14,9                 |
|   | B38 |           | 524                   | 637                   | 22,4                | 13,7                 |
|   | B40 |           | 521                   | 630                   | 19,6                | 14,9                 |
|   | B64 |           | 533                   | 645                   | 16,2                | 6,3                  |
|   | B62 |           | 523                   | 638                   | 17,3                | 6,3                  |
|   | B60 |           | 528                   | 637                   | 17,0                | 6,6                  |
| B500B-25-TEMP-R-Prod. 2                       | B11 | 25        | 539                   | 653                   | 19,3                | 14,9                 |
|   | B12 |           | 545                   | 657                   | ---                 | 14,8                 |
|   | B13 |           | 543                   | 656                   | 20,0                | 13,9                 |
|   | B16 |           | 555                   | 657                   | 19,3                | 14,5                 |
|   | B18 |           | 541                   | 658                   | 16,7                | 13,5                 |
|   | B50 |           | 544                   | 652                   | 16,0                | 5,9                  |
|   | B49 |           | 549                   | 659                   | 16,7                | 6,2                  |

**Table 7. 12:** Results of experimental tensile tests on corroded specimens of diameter 12.0 mm(90 days of corrosion).

| Steel grade/diameter/<br>process/rib/producer | ID  | D<br>(mm) | R <sub>e</sub><br>MPa | R <sub>m</sub><br>MPa | A <sub>5</sub><br>% | A <sub>gt</sub><br>% |
|---|-----|-----------|-----------------------|-----------------------|---------------------|----------------------|
| B500A-12-CW-I-Prod. 2                         | B1  | 12        | 477                   | 504                   | 6,4                 | 2,3                  |
|   | B2  |           | 489                   | 516                   | 4,9                 | 2,2                  |
|   | B8  |           | 467                   | 487                   | 4,1                 | 1,7                  |
|   | B46 |           | 528                   | 553                   | 5,4                 | 2,4                  |
|   | B42 |           | 503                   | 529                   | 5,5                 | 2,4                  |
|   | B44 |           | 502                   | 503                   | 5,0                 | 2,4                  |
| B450C-12-TEMP-R-Prod. 1                       | I2  | 12        | 480                   | 624                   | 9,0                 | 7,7                  |
|   | I10 |           | 471                   | 613                   | 9,3                 | 6,9                  |
|   | I14 |           | 474                   | 611                   | 7,8                 | 6,1                  |
|   | I3  |           | 458                   | 603                   | 9,0                 | 6,9                  |
|   | I6  |           | 456                   | 612                   | 9,9                 | 7,1                  |

**Table 7. 13:** Results of experimental tensile tests on corroded specimens of diameter 16.0 mm(90 days of corrosion).

| Steel grade/diameter/<br>process/rib/producer | ID   | D<br>(mm) | R <sub>e</sub><br>MPa | R <sub>m</sub><br>MPa | A <sub>5</sub><br>% | A <sub>gt</sub><br>% |
|---|------|-----------|-----------------------|-----------------------|---------------------|----------------------|
| B400C-16-MA-R-Prod. 2                         | MA8  | 16        | 443                   | 573                   | 12,3                | 4,9                  |
|   | MA18 |           | 432                   | 582                   | 12,4                | 9,9                  |
|   | MA19 |           | 458                   | 568                   | 9,8                 | 5,0                  |
|   | MA25 |           | 454                   | 597                   | 13,7                | 16,7                 |
|   | MA23 |           | 453                   | 600                   | 16,0                | 15,6                 |
|   | MA24 |           | 466                   | 600                   | 16,9                | 15,0                 |
| B400C-16-TEMP-R-Prod. 1                       | S12  | 16        | 412                   | 544                   | 16,1                | 11,6                 |
|   | S17  |           | 434                   | 553                   | 14,5                | 9,6                  |
|   | S3   |           | 421                   | 543                   | 15,1                | 11,4                 |
|   | SE21 |           | 416                   | 541                   | 17,7                | 12,7                 |
|   | SE14 |           | 404                   | 544                   | 13,9                | 13,4                 |
|   | SE25 |           | 422                   | 544                   | 16,2                | 13,8                 |
|   | SE16 |           | 431                   | 548                   | 14,5                | 12,7                 |
|   | SE4  |           | 403                   | 537                   | 12,3                | 12,6                 |
|   | SE19 |           | 423                   | 543                   | 14,2                | 12,1                 |
|   | SE18 |           | 409                   | 543                   | 14,6                | 14,7                 |
|   | S16  |           | 417                   | 540                   | 13,0                | 13,4                 |
| S18   | 428  | 545       | 15,1                  | 12,9                  |                     |                      |
| S22   | 425  | 544       | 14,2                  | 12,8                  |                     |                      |
| S5  | 408  | 545       | 15,2                  | 13,9                  |                     |                      |
| B450C-16-TEMP-R-Prod. 1                       | P2C  | 16        | 472                   | 606                   | 11,2                | 6,9                  |
|   | P4C  |           | 482                   | 607                   | 14,3                | 7,4                  |
|   | P6C  |           | 476                   | 599                   | 9,7                 | 6,9                  |
|   | P7C  |           | 480                   | 604                   | 10,6                | 6,7                  |
|   | P9C  |           | 472                   | 605                   | 9,9                 | 7,6                  |
|   | P10C |           | 483                   | 596                   | 10,0                | 6,9                  |
|   | P14C |           | 477                   | 606                   | 9,1                 | 6,3                  |
| B450C-16-TEMP-R-Prod. 1                       | P15C | 16        | 480                   | 608                   | 10,4                | 6,8                  |
|   | R12  |           | 461                   | 583                   | 14,5                | 12,5                 |
| B500B-16-TEMP-R-Prod. 1                       | P6B  | 16        | 512                   | 629                   | 17,7                | 7,3                  |
|   | P4B  |           | 521                   | 640                   | 11,7                | 11,3                 |
|   | P14B |           | 521                   | 634                   | 12,3                | 11,8                 |

**Table 7. 14:** Results of experimental tensile tests on corroded specimens of diameter 25.0 mm(90 days of corrosion).

| Steel grade/diameter/<br>process/rib/producer | ID  | D<br>(mm) | R <sub>e</sub><br>MPa | R <sub>m</sub><br>MPa | A <sub>5</sub><br>% | A <sub>gt</sub><br>% |
|---|-----|-----------|-----------------------|-----------------------|---------------------|----------------------|
| B400C-25-MA-R-Prod. 2                         | B24 | 25        | 458                   | 589                   | 19,3                | 13,3                 |
|   | B25 |           | 458                   | 589                   | 19,8                | 14,5                 |
|   | B28 |           | ---                   | 592                   | 19,8                | 11,9                 |
|   | B29 |           | 453                   | 590                   | 19,7                | 15,2                 |
|   | B58 |           | 455                   | 594                   | 22,1                | 13,8                 |
|   | B55 |           | 456                   | 594                   | 16,8                | 14,7                 |
|   | B53 |           | 453                   | 591                   | 21,5                | 14,4                 |
| B450C-25-TEMP-R-Prod. 2                       | B33 | 25        | 529                   | 623                   | 12,8                | 9,8                  |
|   | B34 |           | 529                   | 622                   | 16,3                | 10,2                 |
|   | B37 |           | 531                   | 632                   | 16,7                | 11,1                 |
|   | B39 |           | ---                   | 627                   | 17,0                | 5,8                  |
|   | B59 |           | 523                   | 631                   | 16,3                | 11,9                 |

|                         |     |    |     |     |      |      |
|-------------------------|-----|----|-----|-----|------|------|
|                         | B63 |    | 519 | 626 | 14,8 | 11,2 |
|                         | B61 |    | 521 | 629 | 16,8 | 11,5 |
|                         | B14 |    | 551 | 643 | 13,1 | 9,7  |
|                         | B17 |    | 550 | 645 | 15,9 | 9,5  |
|                         | B19 |    | --- | 649 | 16,0 | 6,8  |
| B500B-25-TEMP-R-Prod. 2 | B20 | 25 | 540 | 634 | 17,5 | 10,3 |
|                         | B47 |    | 544 | 648 | 16,0 | 11,5 |
|                         | B51 |    | 544 | 643 | 16,4 | 11,2 |
|                         | B52 |    | 538 | 650 | 16,9 | 10,8 |

### 7.1.3 Results of experimental tensile tests – UPA

Results of the experimental tensile tests on corroded specimens executed by UPA are presented in the table below in terms of yielding and tensile strength, ultimate elongation and elongation corresponding to maximum load in relation to bars' diameter, considering the two exposure periods of 45 and 90 days in salt spray chamber.

**Table 7. 15:** Results of experimental tensile tests on corroded bars.

| Steel grade/diameter/<br>process/rib/producer | T <sub>corr</sub><br>[days] | ΔM<br>[g]   | L <sub>corr</sub><br>[mm] | ΔM/M <sub>unc</sub><br>[%] | R <sub>e</sub><br>[MPa] | R <sub>m</sub><br>[MPa] | R <sub>m</sub> /R <sub>e</sub><br>[-] | A <sub>5</sub><br>[%] | A <sub>gt</sub><br>[%] |
|---|-----------------------------|-------------|---------------------------|----------------------------|-------------------------|-------------------------|---------------------------------------|-----------------------|------------------------|
| B400C-16-TEMP-R-Prod.1 - 4                    | 45                          | 1,91        | 21                        | 5,9                        | 435                     | 518                     | 1,19                                  | 28,2                  | 6,3                    |
| B400C-16-TEMP-R-Prod.1 - 5                    | 45                          | 1,87        | 22                        | 5,5                        | 431                     | 520                     | 1,21                                  | 25,1                  | 5,7                    |
| B400C-16-TEMP-R-Prod.1 - 6                    | 45                          | 1,58        | 21,4                      | 4,8                        | 429                     | 520                     | 1,21                                  | 28,1                  | 6,3                    |
| <i>Average</i>                                |                             | <i>1,79</i> |                           | <i>5,4</i>                 | <i>432</i>              | <i>519</i>              | <i>1,20</i>                           | <i>27,1</i>           | <i>6,1</i>             |
| B400C-16-TEMP-R-Prod.1 - 7                    | 90                          | 2,97        | 22,7                      | 8,5                        | 400                     | 497                     | 1,24                                  | 22,2                  | 5,2                    |
| B400C-16-TEMP-R-Prod.1 - 8                    | 90                          | 3,12        | 21,0                      | 9,7                        | 414                     | 494                     | 1,19                                  | 17,7                  | 4,1                    |
| B400C-16-TEMP-R-Prod.1 - 9                    | 90                          | 3,2         | 21,6                      | 9,6                        | 408                     | 488                     | 1,19                                  | 20,1                  | 4,7                    |
| <i>Average</i>                                |                             | <i>3,10</i> |                           | <i>9,3</i>                 | <i>407</i>              | <i>493</i>              | <i>1,21</i>                           | <i>20,0</i>           | <i>4,7</i>             |
| B450C-16-TEMP-R-Prod.1 - 4                    | 45                          | 2,42        | 25                        | 6,0                        | 528                     | 614                     | 1,16                                  | 24,6                  | 4,6                    |
| B450C-16-TEMP-R-Prod.1 - 5                    | 45                          | 2,28        | 23                        | 6,2                        | 534                     | 613                     | 1,15                                  | 22,2                  | 4,1                    |
| B450C-16-TEMP-R-Prod.1 - 6                    | 45                          | 2,45        | 25,0                      | 6,1                        | 533                     | 617                     | 1,16                                  | 22,8                  | 4,3                    |
| <i>Average</i>                                |                             | <i>2,38</i> |                           | <i>6,1</i>                 | <i>532</i>              | <i>615</i>              | <i>1,16</i>                           | <i>23,2</i>           | <i>4,3</i>             |
| B450C-16-TEMP-R-Prod.1 - 7                    | 90                          | 4,63        | 25,7                      | 11,2                       | 512                     | 566                     | 1,11                                  | 11,7                  | 2,4                    |
| B450C-16-TEMP-R-Prod.1 - 8                    | 90                          | 4,61        | 25,3                      | 11,3                       | 509                     | 581                     | 1,14                                  | 13,2                  | 2,7                    |
| B450C-16-TEMP-R-Prod.1 - 9                    | 90                          | 4,13        | 25,3                      | 10,1                       | 496                     | 575                     | 1,16                                  | 14,9                  | 3,0                    |
| <i>Average</i>                                |                             | <i>4,46</i> |                           | <i>10,9</i>                | <i>506</i>              | <i>574</i>              | <i>1,14</i>                           | <i>13,3</i>           | <i>2,7</i>             |
| B500B-16-TEMP-R-Prod.1 - 4                    | 45                          | 1,74        | 23                        | 4,7                        | 529                     | 620                     | 1,17                                  | 29,0                  | 5,4                    |
| B500B-16-TEMP-R-Prod.1 - 5                    | 45                          | 2,17        | 25                        | 5,4                        | 515                     | 608                     | 1,18                                  | 23,9                  | 4,9                    |
| B500B-16-TEMP-R-Prod.1 - 6                    | 45                          | 2,58        | 26,0                      | 6,1                        | 514                     | 595                     | 1,16                                  | 21,8                  | 4,3                    |
| <i>Average</i>                                |                             | <i>2,16</i> |                           | <i>5,4</i>                 | <i>519</i>              | <i>608</i>              | <i>1,17</i>                           | <i>24,9</i>           | <i>4,9</i>             |
| B500B-16-TEMP-R-Prod.1 - 7                    | 90                          | 4,2         | 23,3                      | 11,3                       | 488                     | 562                     | 1,15                                  | 12,9                  | 2,7                    |
| B500B-16-TEMP-R-Prod.1 - 8                    | 90                          | 3,94        | 25,6                      | 9,9                        | 492                     | 572                     | 1,16                                  | 17,0                  | 3,4                    |
| B500B-16-TEMP-R-Prod.1 - 9                    | 90                          | 4,58        | 25,7                      | 11,2                       | 491                     | 570                     | 1,12                                  | 14,8                  | 3,0                    |
| <i>Average</i>                                |                             | <i>4,24</i> |                           | <i>10,8</i>                | <i>490</i>              | <i>568</i>              | <i>1,14</i>                           | <i>14,9</i>           | <i>3,0</i>             |
| B450C-16-TEMP-R-Prod.2 - 4                    | 45                          | 2,02        | 19,93                     | 6,4                        | 462                     | 587                     | 1,27                                  | 23,6                  | 4,7                    |
| B450C-16-TEMP-R-Prod.2 - 6                    | 45                          | 2,07        | 21                        | 6,2                        | 473                     | 589                     | 1,25                                  | 28,7                  | 5,6                    |
| B450C-16-TEMP-R-Prod.2 - 8                    | 45                          | 1,98        | 20,1                      | 6,2                        | 473                     | 589                     | 1,25                                  | 28,1                  | 5,5                    |
| <i>Average</i>                                |                             | <i>2,02</i> |                           | <i>6,3</i>                 | <i>469</i>              | <i>588</i>              | <i>1,25</i>                           | <i>26,8</i>           | <i>5,3</i>             |
| B450C-16-TEMP-R-Prod.2 - 5                    | 90                          | 4,63        | 25,7                      | 9,5                        | 479                     | 567                     | 1,18                                  | 17,8                  | 3,6                    |
| B450C-16-TEMP-R-Prod.2 - 11                   | 90                          | 4,61        | 25,3                      | 9,0                        | 487                     | 582                     | 1,20                                  | 22,4                  | 4,4                    |
| B450C-16-TEMP-R-Prod.2 - 12                   | 90                          | 4,13        | 25,3                      | 9,2                        | 458                     | 584                     | 1,28                                  | 24,0                  | 4,8                    |
| <i>Average</i>                                |                             | <i>4,46</i> |                           | <i>9,2</i>                 | <i>475</i>              | <i>578</i>              | <i>1,22</i>                           | <i>21,4</i>           | <i>4,3</i>             |
| B500B-12-ST R-Prod.1- 1                       | 90                          | 3,52        | 22,9                      | 9,8                        | 533                     | 570                     | 1,07                                  | 6,1                   | 1,3                    |
| B500B-12- STR-Prod.1- 2                       | 90                          | 3,38        | 19,6                      | 11,0                       | 523                     | 573                     | 1,10                                  | 12,0                  | 2,4                    |

|                         |    |             |      |             |              |              |             |            |             |
|-------------------------|----|-------------|------|-------------|--------------|--------------|-------------|------------|-------------|
| B500B-12- STR-Prod.1- 3 | 90 | 3,40        | 22,0 | 9,9         | 515          | 569          | 1,10        | 11,4       | 2,3         |
| <i>Average</i>          |    | <i>3,43</i> |      | <i>10,2</i> | <i>524</i>   | <i>571</i>   | <i>1,09</i> | <i>9,8</i> | <i>2,0</i>  |
| B400C-16- MA-Prod.2- 1  | 90 | -           | -    | 6,01        | 453          | 577          | 1,27        | -          | 7,88        |
| B400C-16- MA-Prod.2- 1  | 90 | -           | -    | 7,60        | 454          | 565          | 1,24        | -          | 7,41        |
| <i>Average</i>          |    | -           | -    | <i>6,81</i> | <i>453,3</i> | <i>570,7</i> | <i>1,26</i> | -          | <i>7,65</i> |

#### 7.1.4 Evaluation of necking of tested steel reinforcing bars

For all the specimens subjected to monotonic tensile tests, necking of the cross section area was evaluated, considering the two different exposure periods in salt spray chamber.

In the following tables  $d_i$  and  $d_f$  represent the diameter of the cross section area of the bar respectively before and after the rupture of the specimen; in particular,  $d_{fmin}$  and  $d_{fmax}$  refer to the maximum and minimum diameter, considering the presence of the rib.  $A_i$ ,  $A_{fmin}$  and  $A_{fmax}$  are the corresponding cross section areas and  $Z_{min}$  and  $Z_{max}$  are the necking of the minimum and maximum cross section evaluated as presented by equation 7.1:

$$Z_{min} = \frac{A_i - A_{fmin}}{A_i} \times 100, Z_{max} = \frac{A_i - A_{fmax}}{A_i} \times 100 \quad (7.1)$$

Looking at the rupture surfaces of rebars, some examples are presented in the figure 7.1-7.2, comparing also different production processes (TempCore and Micro Aligned).

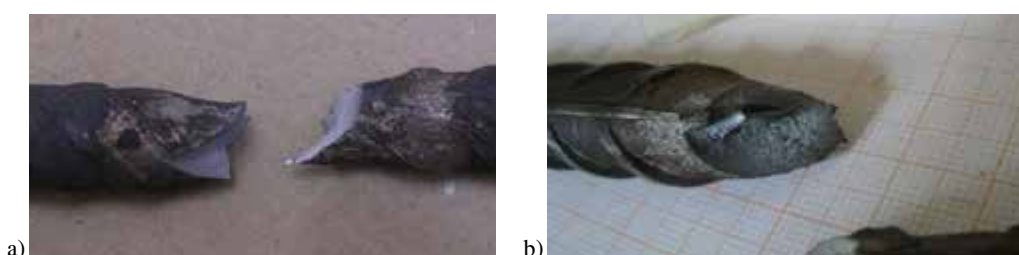


Figure 7. 1: Rupture surfaces of bars a) B400C, 16 Micro Aligned (prod. 2) and b) B400C, 16 TempCore (prod. 1).

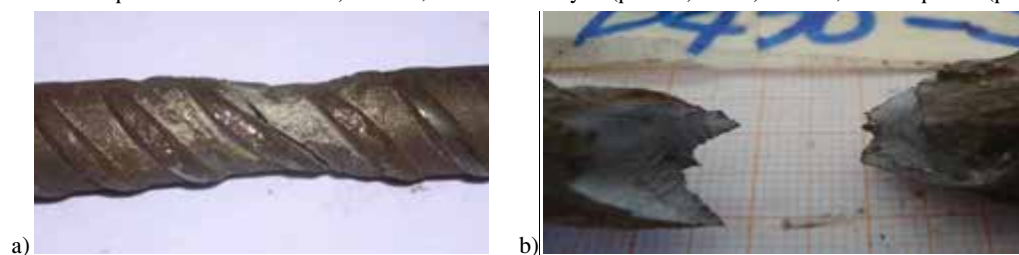


Figure 7. 2: Rupture surfaces of bars a) B500B, 16mm TempCore (prod. 1) and b) B460C, 16 mm TempCore (prod. 1).

Table 7. 16: Evaluation of the necking of corroded specimens after 45 days of exposure in salt spray chamber (UniPI).

| Steel grade/diameter/<br>process/producer | $d_i$<br>[mm] | $A_i$<br>[mm <sup>2</sup> ] | $d_{fmin}$<br>[mm] | $d_{fmax}$<br>[mm] | $A_{fmin}$<br>[mm <sup>2</sup> ] | $A_{fmax}$<br>[mm <sup>2</sup> ] | $Z_{min}$<br>[%] | $Z_{max}$<br>[%] |
|---|---------------|-----------------------------|--------------------|--------------------|----------------------------------|----------------------------------|------------------|------------------|
| B500A-12-CW- Prod.2-01                    | 11,87         | 110,65                      | 8,2                | 8,4                | 52,81                            | 55,42                            | 52,27            | 49,92            |
| B500A-12-CW- Prod.2-02                    | 11,87         | 110,75                      | 7,9                | 7,9                | 49,02                            | 49,02                            | 55,74            | 55,74            |
| B500A-12-CW- Prod.2-03                    | 11,86         | 110,40                      | 8,5                | 8,6                | 56,75                            | 58,09                            | 48,60            | 47,38            |
| B400C-16-MA- Prod.2-01                    | 16,13         | 204,30                      | 11,1               | 11,3               | 96,77                            | 100,29                           | 52,64            | 50,91            |
| B400C-16-MA- Prod.2-02                    | 16,14         | 204,54                      | 10,8               | 11,6               | 91,61                            | 105,68                           | 55,21            | 48,33            |
| B400C-16-MA- Prod.2-03                    | 16,08         | 202,97                      | 10,6               | 11,3               | 88,25                            | 100,29                           | 56,52            | 50,59            |
| B400C-16-TEMP- Prod.1-01                  | 15,76         | 195,02                      | 10,9               | 12,3               | 93,31                            | 118,82                           | 52,15            | 39,07            |
| B400C-16-TEMP- Prod.1-02                  | 15,74         | 194,62                      | 10,5               | 11,5               | 86,59                            | 103,87                           | 55,51            | 46,63            |
| B400C-16-TEMP- Prod.1-03                  | 15,73         | 194,34                      | 11,3               | 13,1               | 100,29                           | 134,78                           | 48,39            | 30,65            |
| B450C-16-TEMP- Prod.1-01                  | 16,13         | 204,41                      | 12,4               | 13,0               | 120,76                           | 132,73                           | 40,92            | 35,07            |
| B450C-16-TEMP- Prod.1-02                  | 16,14         | 204,50                      | 11,1               | 12,6               | 96,77                            | 124,69                           | 52,68            | 39,03            |
| B450C-16-TEMP- Prod.1-03                  | 16,12         | 204,06                      | 12,0               | 12,4               | 113,10                           | 120,76                           | 44,58            | 40,82            |
| B500B-16-TEMP- Prod.1-01                  | 16,06         | 202,47                      | 11,5               | 12,1               | 103,87                           | 114,99                           | 48,70            | 43,21            |
| B500B-16-TEMP- Prod.1-02                  | 16,07         | 202,81                      | 11,9               | 12,2               | 111,22                           | 116,90                           | 45,16            | 42,36            |
| B500B-16-TEMP- Prod.1-03                  | 16,07         | 202,75                      | 11,6               | 12,6               | 105,68                           | 124,69                           | 47,87            | 38,50            |
| B500B-25-TEMP- Prod.2-01                  | 25,15         | 496,78                      | 17,5               | 19,7               | 240,53                           | 304,81                           | 51,58            | 38,64            |
| B500B-25-TEMP- Prod.2-02                  | 25,15         | 496,79                      | 17,8               | 19,5               | 248,85                           | 298,65                           | 49,91            | 39,88            |

|                          |       |        |      |      |        |        |       |       |
|--------------------------|-------|--------|------|------|--------|--------|-------|-------|
| B500B-25-TEMP- Prod.2-03 | 25,08 | 494,14 | 17,5 | 19,0 | 240,53 | 283,53 | 51,32 | 42,62 |
| B450C-25-TEMP- Prod.2-01 | 25,12 | 495,50 | 18,5 | 20,1 | 268,80 | 317,31 | 45,75 | 35,96 |
| B450C-25-TEMP- Prod.2-02 | 25,11 | 495,40 | 17,5 | 19,9 | 240,53 | 311,03 | 51,45 | 37,22 |
| B450C-25-TEMP- Prod.2-03 | 25,11 | 495,40 | 17,5 | 19,7 | 240,53 | 304,81 | 51,45 | 38,47 |
| B400C-25-MA- Prod.2-01   | 25,20 | 498,68 | -    | -    | -      | -      | -     | -     |
| B400C-25-MA- Prod.2-02   | 25,20 | 498,66 | 17,3 | 18,0 | 235,06 | 254,47 | 52,86 | 48,97 |
| B400C-25-MA- Prod.2-03   | 25,20 | 498,69 | 16,5 | 18,2 | 213,82 | 260,16 | 57,12 | 47,83 |

**Table 7. 17:** Evaluation of the necking of corroded specimens after 90 days of exposure in salt spray chamber (UniPI).

| Steel grade/diameter/<br>process/producer | $d_i$<br>[mm] | $A_i$<br>[mm <sup>2</sup> ] | $d_{fmin}$<br>[mm] | $d_{fmax}$<br>[mm] | $A_{fmin}$<br>[mm <sup>2</sup> ] | $A_{fmax}$<br>[mm <sup>2</sup> ] | $Z_{min}$<br>[%] | $Z_{max}$<br>[%] |
|---|---------------|-----------------------------|--------------------|--------------------|----------------------------------|----------------------------------|------------------|------------------|
| B500A-12-CW- Prod.2 (5.6)                 | 11,81         | 109,61                      | 8,7                |                    | 59,4                             |                                  | 45,8             |                  |
| B500A-12-CW- Prod.2 (5.5)                 | 11,86         | 110,52                      | 8,2                |                    | 52,8                             |                                  | 52,2             |                  |
| B500A-12-CW- Prod.2 (5.2)                 | 11,79         | 109,18                      | 8,5                |                    | 56,7                             |                                  | 48,0             |                  |
| B400C-16-TEMP-Prod.1-01                   | 15,74         | 194,58                      | 12,7               | 13,5               | 126,68                           | 143,14                           | 34,90            | 26,44            |
| B400C-16-TEMP- Prod.1-02                  | 15,72         | 194,09                      | 11,6               | 13,0               | 105,68                           | 132,73                           | 45,55            | 31,61            |
| B400C-16-TEMP- Prod.1-03                  | 15,75         | 194,76                      | 11,0               | 12,9               | 95,03                            | 130,70                           | 51,21            | 32,89            |
| B400C-16-TEMP- Prod.1-04                  | 15,74         | 194,66                      | 11,0               | 13,0               | 95,03                            | 132,73                           | 51,18            | 31,81            |
| B400C-16-TEMP- Prod.1-05                  | 15,74         | 194,61                      | 12,8               | 13,5               | 128,68                           | 143,14                           | 33,88            | 26,45            |
| B400C-16-TEMP- Prod.1-06                  | 15,72         | 194,05                      | 11,5               | 12,0               | 103,87                           | 113,10                           | 46,47            | 41,72            |
| B450C-16-TEMP- Prod.1-01                  | 16,12         | 204,14                      | 10,8               | 12,5               | 91,61                            | 122,72                           | 55,12            | 39,88            |
| B450C-16-TEMP- Prod.1-02                  | 16,15         | 204,73                      | 11,2               | 12,3               | 98,52                            | 118,82                           | 51,88            | 41,96            |
| B450C-16-TEMP- Prod.1-03                  | 16,13         | 204,42                      | 11,2               | 12,9               | 98,52                            | 130,70                           | 51,80            | 36,06            |
| B450C-16-TEMP- Prod.1-04                  | 16,14         | 204,59                      | 9,9                | 11,5               | 76,98                            | 103,87                           | 62,38            | 49,23            |
| B450C-16-TEMP- Prod.1-05                  | 16,14         | 204,57                      | 11,2               | 12,4               | 98,52                            | 120,76                           | 51,84            | 40,97            |
| B450C-16-TEMP- Prod.1-06                  | 16,10         | 203,62                      | 11,2               | 12,6               | 98,52                            | 124,69                           | 51,62            | 38,76            |
| B500B-16-TEMP- Prod.1-01                  | 16,05         | 202,28                      | 11,2               | 11,7               | 98,52                            | 107,51                           | 51,30            | 46,85            |
| B500B-16-TEMP- Prod.1-02                  | 16,08         | 203,07                      | 11,0               | 12,2               | 95,03                            | 116,90                           | 53,20            | 42,43            |
| B500B-16-TEMP- Prod.1-03                  | 16,02         | 201,44                      | 11,2               | 12,5               | 98,52                            | 122,72                           | 51,09            | 39,08            |
| B500B-16-TEMP- Prod.1-04                  | 16,10         | 203,50                      | 10,7               | 12,5               | 89,92                            | 122,72                           | 55,81            | 39,70            |
| B500B-16-TEMP- Prod.1-05                  | 16,04         | 202,14                      | 11,4               | 11,7               | 102,07                           | 107,51                           | 49,51            | 46,81            |
| B500B-16-TEMP- Prod.1-06                  | 16,05         | 202,42                      | 11,9               | 12,1               | 111,22                           | 114,99                           | 45,05            | 43,19            |
| B500B-25-TEMP- Prod.2 (6.9)               | 25,09         | 494,58                      | 17,4               | 18,8               | 237,79                           | 277,59                           | 51,92            | 43,87            |
| B500B-25-TEMP- Prod.2 (6.1)               | 24,98         | 489,96                      | 15,9               | 18,8               | 198,56                           | 277,59                           | 59,47            | 43,34            |
| B500B-25-TEMP- Prod.2 (6.8)               | 25,13         | 495,87                      | 16,9               | 19,5               | 224,32                           | 298,65                           | 54,76            | 39,77            |
| B450C-25-TEMP- Prod.2 (10.3)              | 25,09         | 494,40                      | 17,9               | 19,9               | 251,65                           | 311,03                           | 49,10            | 37,09            |
| B450C-25-TEMP- Prod.2 (10.9)              | 25,10         | 494,62                      | 15,8               | 17,9               | 196,07                           | 251,65                           | 60,36            | 49,12            |
| B450C-25-TEMP- Prod.2 (10.10)             | 25,05         | 492,99                      | 17,4               | 20,0               | 237,79                           | 314,16                           | 51,77            | 36,28            |
| B400C-25-MA- Prod.2 (8.10)                | 25,13         | 495,99                      | 17,4               | 18,8               | 237,79                           | 277,59                           | 52,06            | 44,03            |
| B400C-25-MA- Prod.2 (8.11)                | 25,08         | 493,87                      | 15,9               | 18,8               | 198,56                           | 277,59                           | 59,80            | 43,79            |
| B400C-25-MA- Prod.2 (8.9)                 | 25,08         | 494,22                      | 16,9               | 19,5               | 224,32                           | 298,65                           | 54,61            | 39,57            |

As visible from tables 7.16 and 7.17, in general the necking of the cross section areas of the rebars after 45 and 90 days of exposure were similar, with some exceptions. In the case of steel bars B450C and B500B diameter 16 mm (TempCore process), the average reduction of the cross section was quite the same after 45 and 90 days, passing from 42.2% to 47.63% in the case of rebars B450C and from 44.30% to 47.0% in the case of B500B.

Similar values were individuated also in the case of steel reinforcements of diameter 25 mm (steel grade B450C and B500B), while big differences were found in the case of steel bars of small diameter: in the case B500A Cold Worked (diameter 12 mm) the cross section reduction passed from the 51.61% (45 days of exposure) to the 74.33% (90 days). In this last case, the salt spray chamber used was not the same (Laboratories 1 and 2) and the high reduction of the cross section was confirmed by very low values of the elongation to maximum load.

Some comparisons were made also with reference to the values of the cross section reduction obtained from uncorroded specimens. For example, table 7.18 provides the values obtained from steel rebars provided by producer 2; as visible, no big differences were individuated, with average percentage

values of the cross section reduction of about 45-50% with the exception of bars B500A (12 mm, Cold Worked) for which a reduction of about 60% was evidenced.

**Table 7. 18:** Evaluation of the necking of uncorroded specimens (Producer 2) (UniPI).

| Steel grade/diameter/<br>process/producer | $d_i$<br>[mm] | $A_i$<br>[mm <sup>2</sup> ] | $d_{fmin}$<br>[mm] | $d_{fmax}$<br>[mm] | $A_{fmin}$<br>[mm <sup>2</sup> ] | $A_{fmax}$<br>[mm <sup>2</sup> ] | $Z_{min}$<br>[%] | $Z_{max}$<br>[%] |
|---|---------------|-----------------------------|--------------------|--------------------|----------------------------------|----------------------------------|------------------|------------------|
| B500A-12-CW Prod. 2-01                    | 11,91         | 111,34                      | 6,95               | 37,94              | 7,40                             | 43,01                            | 65,92            | 61,37            |
| B500A-12-CW Prod. 2-02                    | 11,91         | 111,34                      | 7,05               | 39,04              | 7,35                             | 42,43                            | 64,94            | 61,89            |
| B500A-12-CW Prod. 2-03                    | 11,91         | 111,34                      | 7,13               | 39,93              | 7,46                             | 43,71                            | 64,14            | 60,74            |
| B400C-16-MA Prod. 2-01                    | 16,14         | 204,59                      | 10,31              | 83,48              | 11,71                            | 107,69                           | 59,20            | 47,36            |
| B400C-16-MA Prod. 2-02                    | 16,16         | 205,10                      | 10,26              | 82,67              | 11,50                            | 103,87                           | 59,69            | 49,36            |
| B400C-16-MA Prod. 2-03                    | 16,14         | 204,59                      | 10,84              | 92,29              | 11,60                            | 105,68                           | 54,89            | 48,35            |
| B450C-25-TEMP Prod. 2-01                  | 25,15         | 496,82                      | 17,15              | 230,99             | 20,10                            | 317,30                           | 53,51            | 36,13            |
| B450C-25-TEMP Prod. 2-02                  | 25,11         | 495,03                      | 17,33              | 235,87             | 18,95                            | 282,03                           | 52,35            | 43,03            |
| B450C-25-TEMP Prod. 2-03                  | 25,16         | 497,32                      | 16,20              | 206,11             | 18,66                            | 273,46                           | 58,56            | 45,01            |
| B500B-25-TEMP Prod. 2-01                  | 25,15         | 496,82                      | 17,10              | 229,65             | 18,96                            | 282,33                           | 53,78            | 43,17            |
| B500B-25-TEMP Prod. 2-02                  | 25,20         | 498,60                      | 16,67              | 218,25             | 18,71                            | 274,93                           | 56,23            | 44,86            |
| B500B-25-TEMP Prod. 2-03                  | 25,16         | 497,32                      | 16,60              | 216,42             | 18,80                            | 277,58                           | 56,48            | 44,18            |
| B400C-25-MA Prod. 2-01                    | 25,24         | 500,38                      | 15,24              | 182,41             | 17,22                            | 232,89                           | 63,55            | 53,46            |
| B400C-25-MA Prod. 2-02                    | 25,25         | 500,89                      | 15,69              | 193,34             | 18,26                            | 261,87                           | 61,40            | 47,72            |
| B400C-25-MA Prod. 2-03                    | 25,29         | 502,17                      | 16,37              | 210,46             | 18,47                            | 267,92                           | 58,09            | 46,65            |

Values obtained from specimens testes at University of Patras are presented in the table 7.19.

**Table 7. 19:** Evaluation of necking of corroded and uncorroded specimens.

| Steel grade/diameter/<br>process/rib/producer | $T_{corr}$<br>(days)      | $A_i$<br>(mm <sup>2</sup> ) | $A_f$<br>(mm <sup>2</sup> ) | $\Delta A_i$<br>(%) | Necking<br>(%) | $\Delta M$<br>(gr) | $\Delta M/M_{unc}$<br>(%) |       |       |
|---|---------------------------|-----------------------------|-----------------------------|---------------------|----------------|--------------------|---------------------------|-------|-------|
| B450C-16-TEMP-R<br>Prod.2                     | 1                         | 205,48                      | 141,59                      | 31,09               | 32,7           | -                  | -                         |       |       |
|   | 2                         |                             | 129,73                      | 36,86               |                | -                  | -                         |       |       |
|   | 3                         |                             | 143,54                      | 30,14               |                | -                  | -                         |       |       |
|   | 4                         |                             | 45                          | 118,16              | 42,5           | 48,29              | 2,02                      | 6,4   |       |
|   | 6                         |                             | 45                          | 107,19              | 47,83          |                    | 2,07                      | 6,23  |       |
|   | 8                         |                             | 45                          | 93,44               | 54,53          |                    | 1,98                      | 6,23  |       |
|   | 5                         |                             | 90                          | 84,49               | 58,88          |                    | 3,5                       | 9,46  |       |
|   | 11                        |                             | 90                          | 107,5               | 47,68          |                    | 52,28                     | 2,93  | 8,95  |
|   | 12                        |                             | 90                          | 102,18              | 50,27          | 3,38               | 9,2                       |       |       |
|   | B500B-16-Prod.1           |                             | 13                          | 204,09              | 131,2          | 35,72              | 36,58                     | -     | -     |
|   |                           |                             | 4                           |                     | 127,68         | 37,44              |                           | -     | -     |
|   |                           |                             | 11                          |                     | 129,43         | 36,58              |                           | -     | -     |
| 1   |                           | 90                          | 114,13                      |                     | 44,08          | 51,05              | 3,52                      | 9,8   |       |
| 2   |                           | 90                          | 92,15                       |                     | 54,85          |                    | 3,38                      | 10,96 |       |
| 3   |                           | 90                          | 93,42                       |                     | 54,23          |                    | 3,40                      | 9,88  |       |
| B400C-16-TEMP-R-<br>Prod.1                    | 1                         | 196,22                      | 123,77                      | 36,92               | 38,2           | -                  | -                         |       |       |
|   | 2                         |                             | 118,34                      | 39,69               |                | -                  | -                         |       |       |
|   | 3                         |                             | 121,71                      | 37,97               |                | -                  | -                         |       |       |
|   | 5                         |                             | 45                          | 88,73               | 54,78          | 47,25              | 1,91                      | 5,54  |       |
|   | 6                         |                             | 45                          | 118,29              | 39,72          |                    | 1,58                      | 4,81  |       |
|   | 7                         |                             | 90                          | 105,01              | 46,48          |                    | 2,97                      | 8,55  |       |
|   | 8                         |                             | 90                          | 91,46               | 53,39          |                    | 49,94                     | 3,12  | 9,70  |
|   | B450C-16-TEMP-R<br>Prod.1 |                             | 1                           | 207,01              | 143,87         |                    | 30,5                      | 29,71 | -     |
| 2   |                           | 147,15                      | 28,91                       |                     | -              | -                  |                           |       |       |
| 5   |                           | 45                          | 144,22                      |                     | 30,33          | 34,59              | 2,28                      |       | 6,16  |
| 6   |                           | 45                          | 126,57                      |                     | 38,86          |                    | 2,45                      | 6,08  |       |
| 8   |                           | 90                          | 110,1                       |                     | 46,82          |                    | 45,14                     | 4,61  | 11,32 |
| 9   |                           | 90                          | 117,04                      |                     | 43,46          | 4,13               | 10,13                     |       |       |

|                 |   |    |        |        |       |       |      |       |
|-----------------|---|----|--------|--------|-------|-------|------|-------|
| B500B-16-Prod.1 | 1 | 0  |        | 124,28 | 38,8  |       | -    | -     |
|                 | 2 | 0  |        | 120,44 | 40,69 | 39,75 | -    | -     |
|                 | 5 | 45 | 203,08 | 109,35 | 46,15 |       | 2,17 | 5,41  |
|                 | 6 | 45 |        | 109,65 | 46,01 | 46,08 | 2,58 | 6,15  |
|                 | 7 | 90 |        | 96,8   | 52,34 |       | 4,2  | 11,31 |
|                 | 8 | 90 |        | 89,98  | 55,7  | 54,02 | 3,94 | 9,85  |

### 7.1.5 Preliminary observations on experimental tensile tests' results on corroded bars

Tensile tests on corroded steel specimens evidenced a progressive decrease of the mechanical properties of steel reinforcing bars, especially for what concerns the ductility of the bar, expressed in terms of elongation to maximum load ( $A_{gt}$ ).

In the case of steel grade B500A (Cold Worked process), bars of diameter 12 mm evidenced a strong decrease of the elongation to maximum load, dropping from an initial average value of 6.82% (mean value coming from experimental tests on three different specimens) to values equal to 1.30%, 0.90% and 0.80% and 0.90%, 2.40% and 5.10% respectively after 45 and 90 days in salt spray chamber (results coming from UniPi). Similar results were found also considering the values provided by ISQ, in which  $A_{gt}$  after 90 days reached values around 2.0%

Considering the results coming from UniPi, the mass loss measured in relation to the exposed length of the sample was varied between 17 and 22% in the case of corrosion period equal to 45 days; on the other hand, for 90 days of exposure period, lower values (varying between 4.29% and 12.57%) were individuated.

Looking at the effective damages on the rebars, in the case of specimen B500A-12 (Cold Worked) n°5.2 the corrosion deterioration was diffused on a higher length (equal to 182 mm, probably due to some detachment of the covering wax during the exposition period in salt spray chamber), resulting in a relatively low value of the mass loss; on the other hand, for the specimen 5.6 corrosion phenomena were concentrated on a small portion of the rebars ( $L_{corr}=24.90$  mm), resulting in higher values of mass loss and higher decrease of elongation to maximum load (figure 7.3). Similar considerations can be made also for the values obtained for elongation at failure (figure 7.3), even if the percentage decrease was lower.

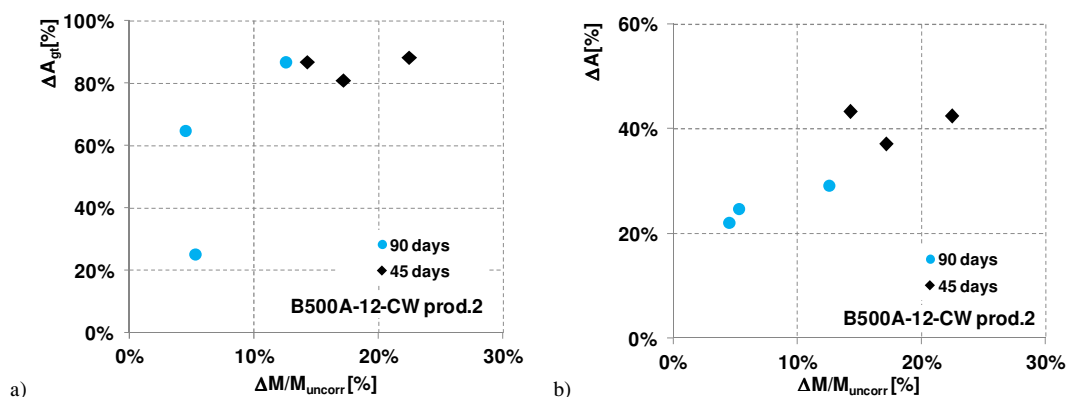


**Figure 7. 3:** Decrease of a) elongation to maximum load and of b) total elongation at failure in relation to the mass loss for steel bars B500A-12-CW (Producer 2), after 45 and 90 days.

As regards the modification of mechanical properties in terms of strength, the reduction of yielding and tensile resistance after 45 days of exposure in salt spray chamber was around 12-14%, while higher reductions (up to about 18.5%) were individuated in the case of 90 days of corrosion in salt spray chamber. As an example, in the case specimen n°5.6 the tensile strength dropped from an average value of 564 MPa to 461 MPa, with correspondent tensile strength equal to 480 MPa respect to the average one of uncorroded specimen equal to 586.5 MPa; the percentage decrease of yielding and tensile strength were around 18 % (figure 7.4).

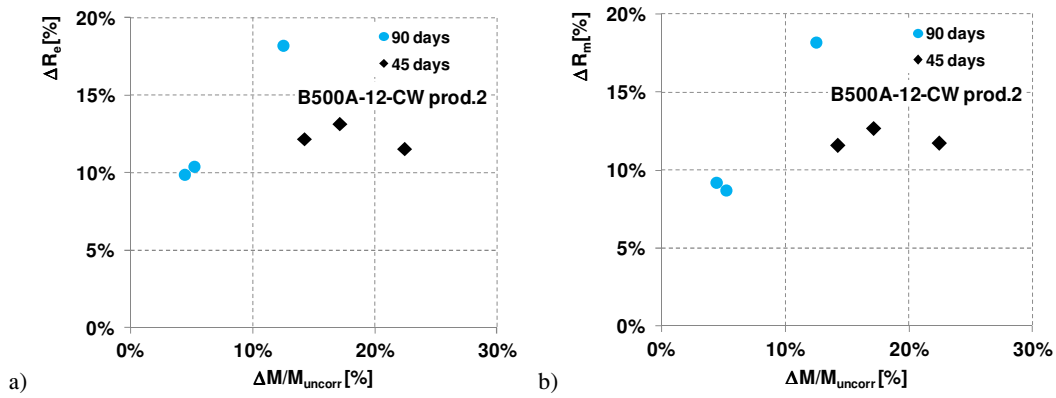


**Figure 7. 4:** Decrease of a) yielding strength and of b) tensile strength in relation to the mass loss for steel bars B500A-12-CW (Producer 2), after 45 and 90 days.

In the case of steel reinforcing bars of diameter 16 mm (tested at UniPI), different steel grades and production process were considered. In general, the ratio  $\Delta M / M_{uncorr}$  was quite higher in the case of exposure period equal to 90 days respect to the one corresponding to 45 days, with the exception of steel bars B450C (TempCore, producer 1) for which the mass losses in relation to the exposed lengths were substantially the same for the two different corrosion periods considered.

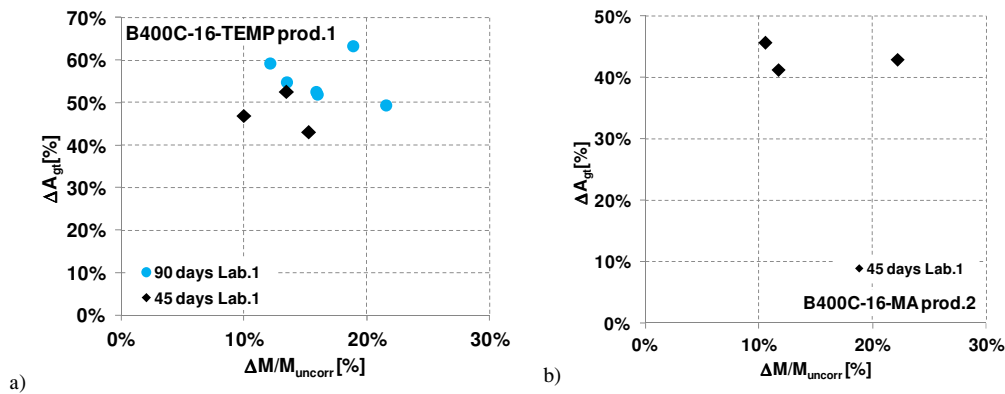


**Figure 7. 5:** Decrease of elongation to maximum load for steel bars a) B400C-16 TempCore (producer 1) and b) B400C-16 Micro Alloyed (producer 2).

As visible, the percentage average decrease of  $A_{gt}$  in the case of steel reinforcing bar B400C diameter 16 mm (Tempcore process) was around 55% after 90 days and 47% after 45 days of exposure period; in the case of specimen n°2, as an example, the  $A_{gt}$  value dropped from an average value equal to 15.52% (obtained from experimental tests on the uncorroded specimens) to 5.8%; moreover, the maximum value obtained from corroded samples (90 days) was equal to 8.0% (specimen n°6).

Lower reductions of ductility were, on the other hand, individuated in the case of Micro Alloyed steel rebars; in particular, the average percentage decrease of  $A_{gt}$  was about equal to 43%, with a minimum value up to 9.80%, respect to the 18.0% reference value obtained from experimental tests on uncorroded specimens. The average mass loss was equal to 15%.

In the case of reinforcing steel bars B450C (TempCore process), the  $A_{gt}$  passed from levels around 13.6% (average value obtained from uncorroded specimens) to 4.19% (minimum result) or 5.7% (maximum result). In this case, the mass loss varied between 6.08% and 17.3% in the case of 90 days of exposure and between 7.4% and 11.2% after 45 days in salt spray chamber; anyway, but not a strict relationship was individuated between mass loss and ductility decrease (figure 7.6a), and the decrease of elongation to maximum load was in general between 60% and 70%. Similar values were obtained also from steel rebars B500B diameter 16mm (TempCore, figure 7.6b); in particular, in the case of 90 days of exposure reduction of  $A_{gt}$  between 53% and 62% were found in correspondence of a mass loss varying between 17% and 28% (with a sparse value), while after 45 days of corrosion, lower reductions of  $A_{gt}$  were found.

For what concerns steel reinforcing bars of diameter 25mm, accelerated corrosion tests were executed in two different laboratories (Laboratory 1 for exposure period equal to 45 days and Laboratory 2 for 90 days). With respect to other corroded specimens, the reduction of ductility showed by rebars of higher diameter were lower, with a maximum value up to 42.6% (steel bars B450C, TempCore), evaluated

considering the average values provided by experimental tests on uncorroded samples. Moreover, no significant reductions of yielding and tensile strength were individuated.

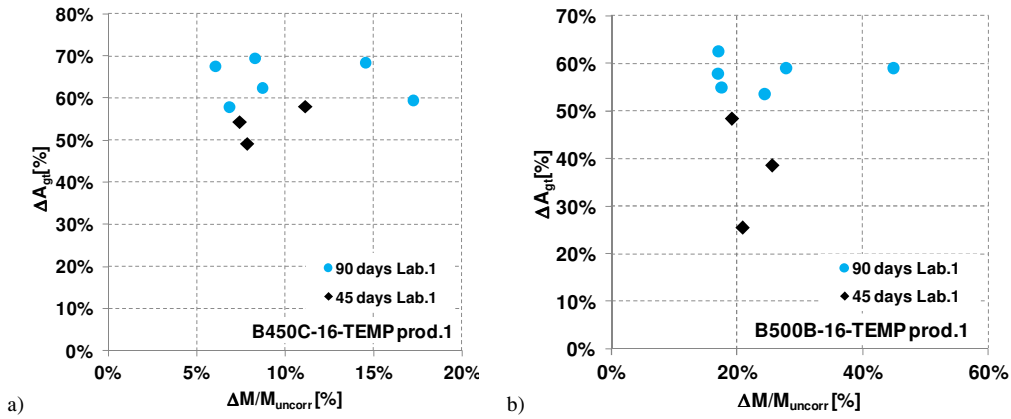


Figure 7. 6: Decrease of  $A_{gt}$  for steel Tempcore bars a) B450C-16 (prod. 1) and b) B500B-16 (prod.1).

Figures 7.7-7.9 present the diagrams of the reduction of elongation to maximum load and elongation at failure ( $A_{gt}$  and  $A$ ) in relation to the percentage mass loss for all the specimens of diameter 25 mm tested (including both TempCore and Micro Alloyed process).

As well as already presented for steel reinforcement of diameter equal to 16 mm, in the case of Micro Alloyed process the reduction of  $A_{gt}$  was generally lower respect to the other cases: the minimum value obtained was equal to 12.9% (respect to the initial average one of 18.4%), while in the other cases (respectively B450C and B500B TempCore) the minimum values were equal to 8.30% and 8.10% (respect to initial average values equal to 14.80% and 12.70%).

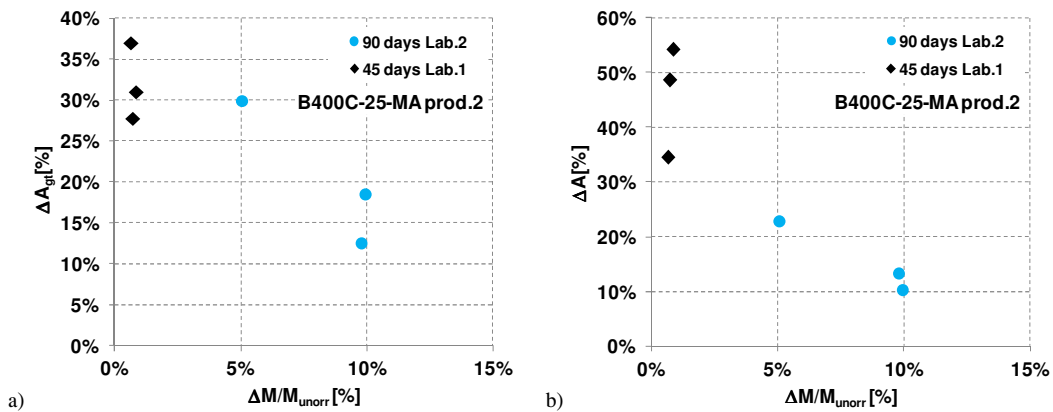


Figure 7. 7: Decrease of a)  $A_{gt}$  and b)  $A$  for steel bars B400C-25, Micro Alloyed process (Producer 2).

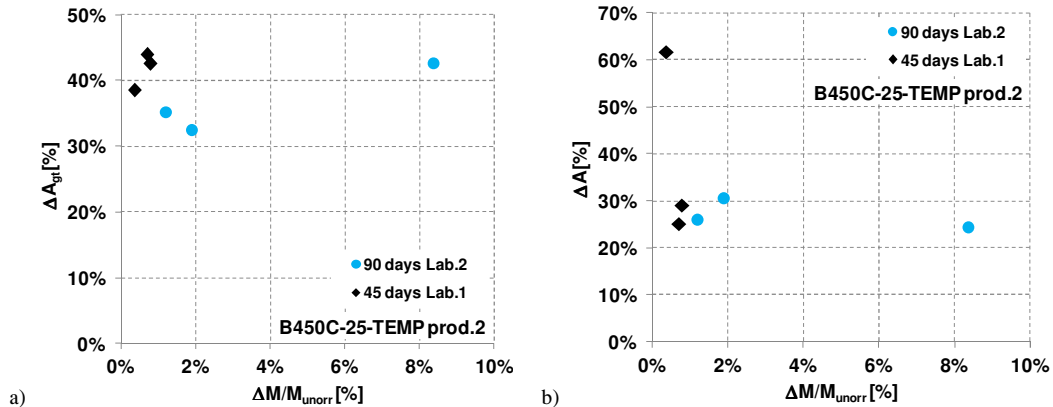
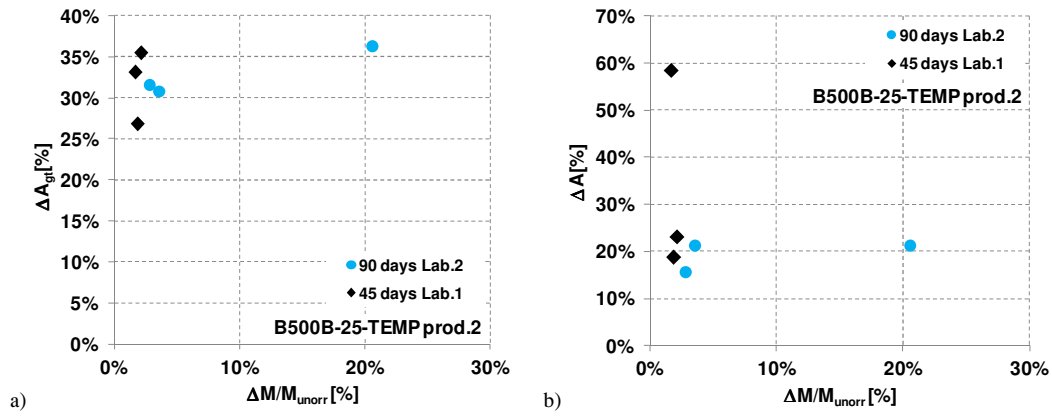
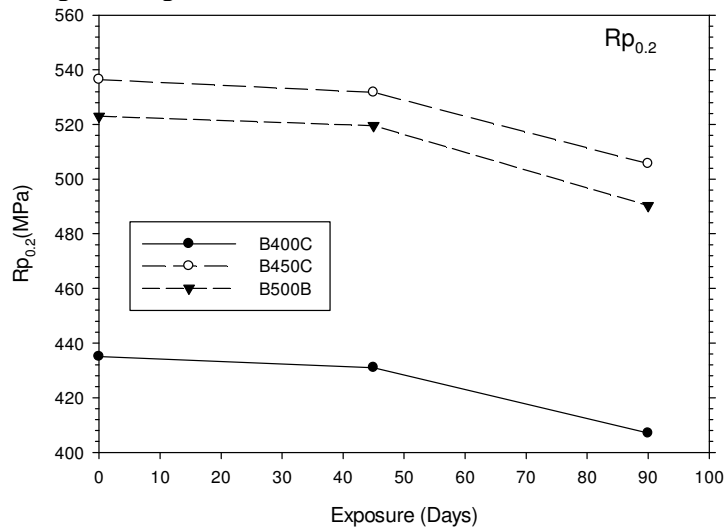


Figure 7. 8: Decrease of a)  $A_{gt}$  and b)  $A$  for steel bars B450C-25, TempCore process (Producer 2).



**Figure 7. 9:** Decrease of a)  $A_{gt}$  and b)  $A$  for steel bars B500B-25, TempCore process (Producer 2).

Considering the results obtained from UPA, the effect of corrosion exposure on yielding stress (figure 7.10) appears to follow two distinct rates. From 0 to 45 days of exposure, all steel grades exhibit small reduction slopes indicating that elastic stress concentrations effects, i.e. pits are not pronounced. Herein it is rational to assume that the reduction is attributed to generalized mass loss. In the exposure range 45-90 days, there is a distinct increase in the slope indicating that elastic stress concentrations, in the form of pits, might be the governing feature.



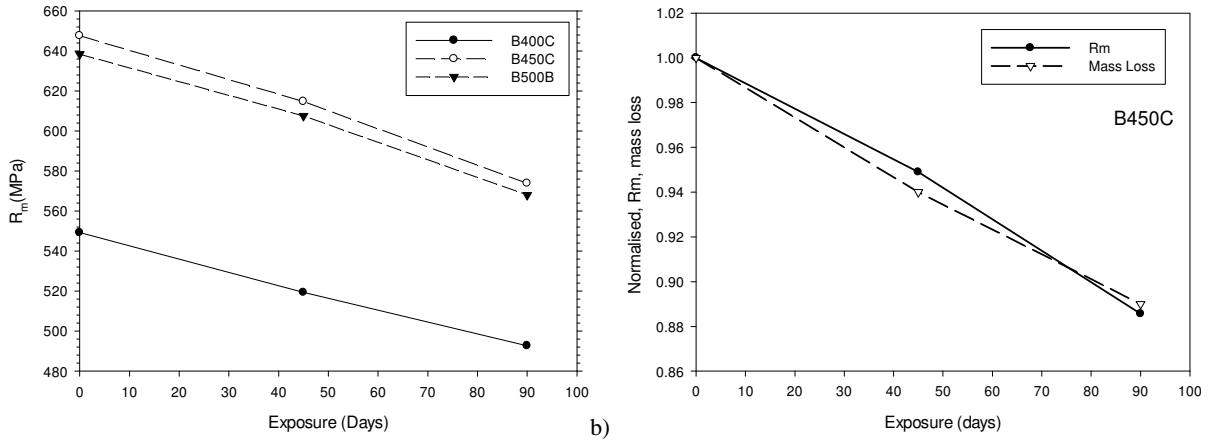
**Figure 7. 10:** Effect of corrosion exposure on yield stress.

The effect of corrosion exposure on the ultimate tensile strength ( $R_m$ ) (figure 7.11a), appears to maintain an almost constant slope with corrosion exposure. Considering that fact that there is a linear relationship between ultimate tensile strength and martensite thickness and that ultimate tensile strength is insensitive to geometrical features. The above are confirmed in figure 7.11b, where normalised mass loss and  $R_m$  are plotted as a function of exposure time. Herein the slopes appear to almost identical, fact that substantiates that mass loss is related to reduction of the martensite layer.

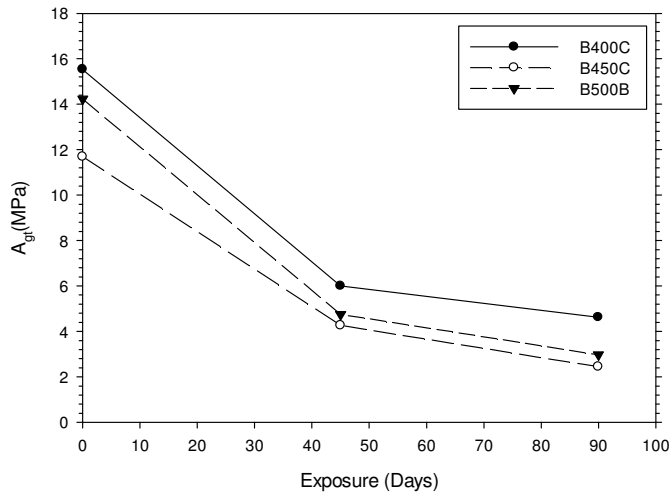
Elongation to failure ( $A_{gt}$ ) delivers the strongest degradation effect from corrosion exposure. The exposure range 0-45 has the sharpest slope gradient followed by the 45-90 day range, Figure 7.12..

Summarizing the behavior of steel rebars the effect of corrosion in the mechanical properties is presented (Figure 7.13 a,b) indicatively for B400C-16-TEMP and B450C-16-TEMP respectively.

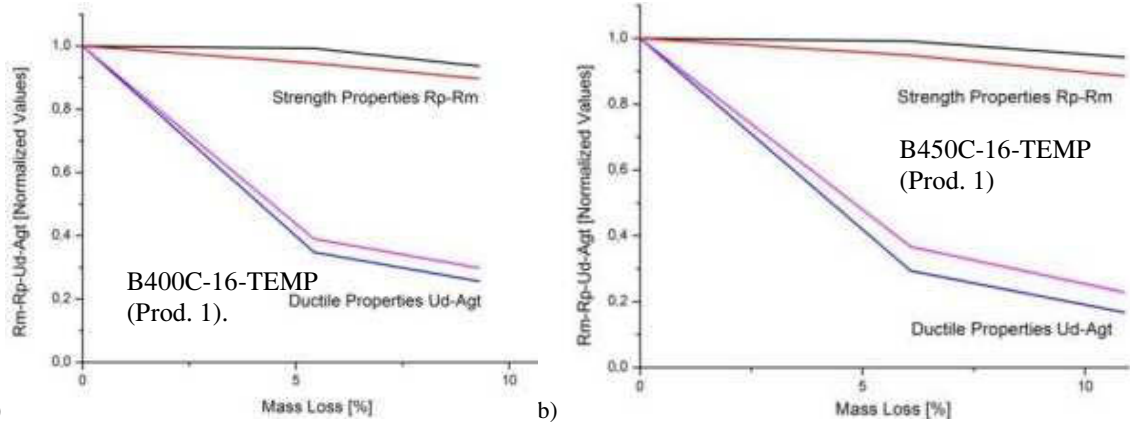
The slopes indicate that the degradation mechanism should not be sought in terms of a single dominant mechanism, i.e. hydrogen embrittlement, but rather as multi-parametric outcome. Such initial assumption is also supported by the failure surface appearance. In all cases it is apparent that the martensite zone failed in a semi-brittle manner even after the initiation of necking. At this point it is necessary to point out that necking in the as-received articles was not profound. This type of failure is not necessarily associated with hydrogen embrittlement but can also be the result of fast fracture. Confirmation can be found in Figure 7.14.



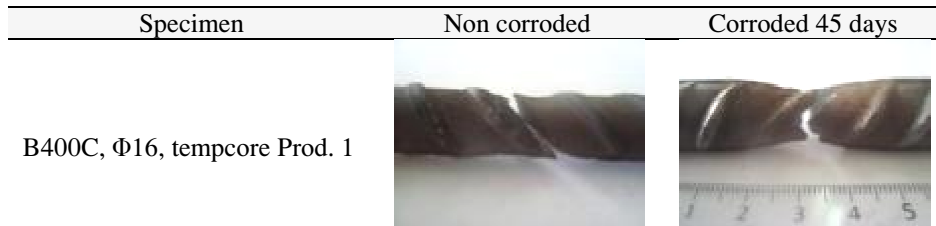
**Figure 7.11:** a) Effect of corrosion exposure on Ultimate Tensile Strength. b) Normalized mass loss and ultimate tensile strength as a function of exposure.



**Figure 7.12:** Effect of corrosion exposure on elongation to failure.



**Figure 7.13:** a) Effect of corrosion exposure on Mechanical properties of B400C-16-TEMP (Prod.1), b) Effect of corrosion exposure on Mechanical properties of B450C-16-TEMP (Prod.1).



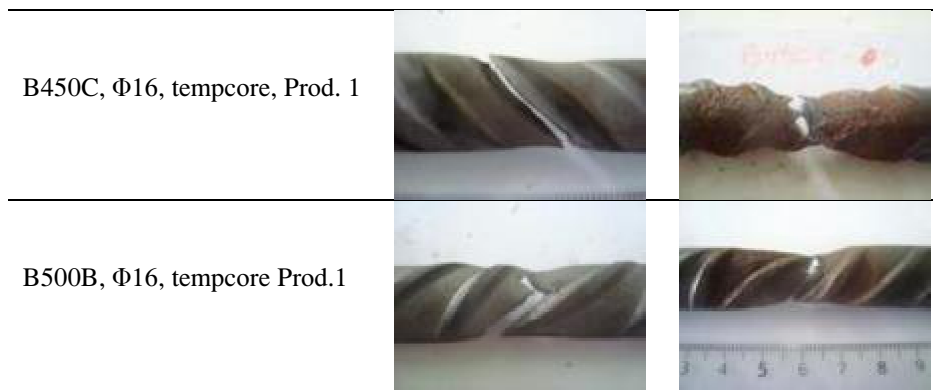


**Figure 7. 14:** Necking of testing articles taken from the as-received and 45 days exposure.

In the case of the low ductility class B (B500B), the fracture surface of the as-received article appears to follow multiple shear failure sites (zig-zag effect), while both high ductility classes (B400C and B450C) exhibit failure by single shear. However all articles exhibit multiple shear failure sites after 45 days exposure.

Moreover, SEM and EDX analyses were executed on several samples corroded at UPA laboratory; in particular, steel bars B450C, diameter 16mm (TempCore) after 45 and 90 days of exposure in salt spray chamber were considered.

Specimens were examined after 45 days of exposure and without be subjected to any stress. Figure 7.15 shows evidence where the segregation sites turned into a) crevice corrosion or, and b) pitting. The two corrosion mechanisms should be seen as being governed by the segregation road (the presence of impurities as a function of depth from the surface). Of particular importance is the presence of active corrosion sites at some depth from near-surface (Figure 7.15c). These sites were found to contain  $Cl^-$  and can lead to segment decohesion (Figure 7.16). Chloride ions however appear to be trapped within the region where MnS inclusions have been dissolved. Yet outside these region were MnS inclusions are present,  $Cl^-$  is not registered (figure 7.17).

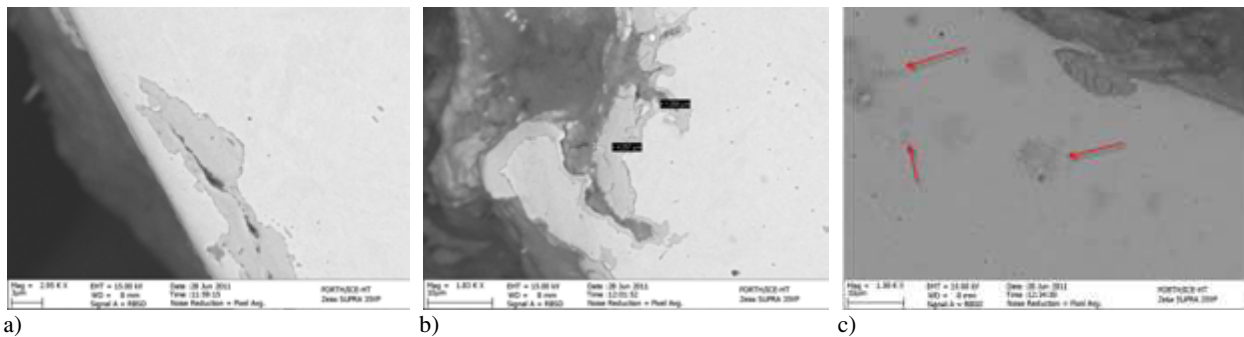


**Figure 7. 15:** Depending on the depth of the segregation corrosion can lead to either a) crevice type corrosion, b) pitting and c) a mixture along with subsurface active corrosion sites.

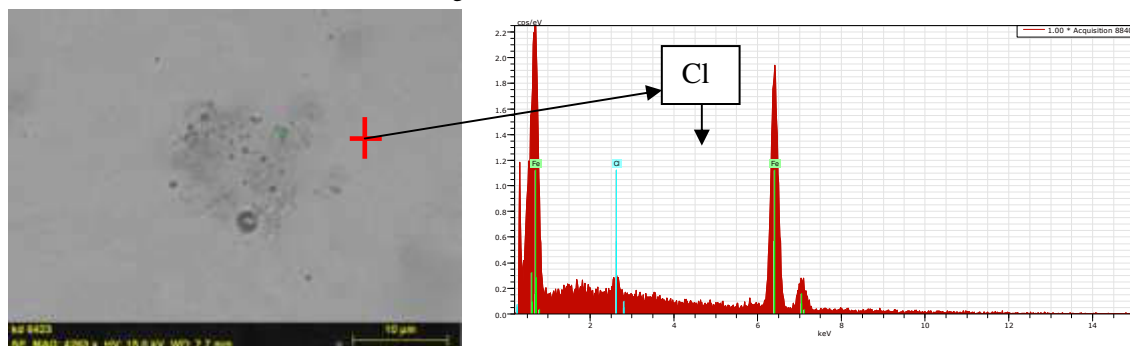


**Figure 7. 16:**  $Cl^-$  diffusion at sub-surface region of segregated inclusions after MnS dissolution.

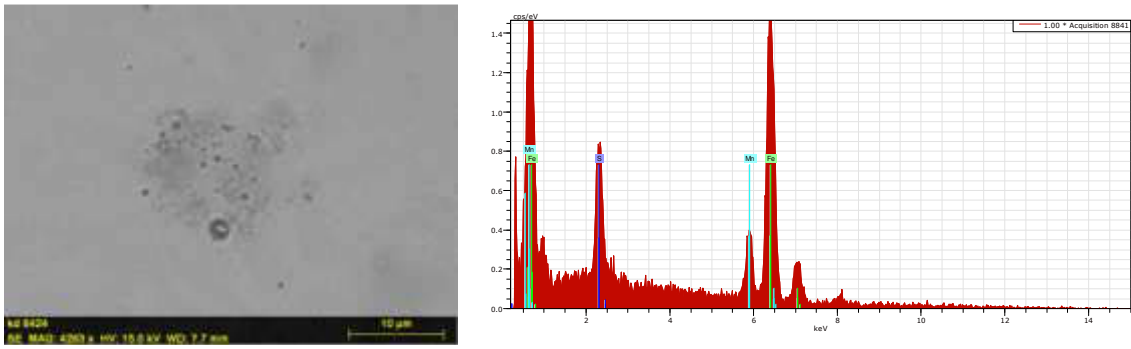


**Figure 7.17:** The presence of non-dissolved MnS inclusions negates the presence of Cl<sup>-</sup>.

Longer exposure (90 days) enhances the phenomenon of either close to surface or sub surface MnS dissolution creating a variety of side effects. Figure 7.18a, shows a well established pit being the result of close to surface dissolution. At this point it is necessary to take into consideration that the original diameter and hence the surface has been significantly consumed. Figure 7.18b, shows expansive dissolution leading to subsurface cracking. Of the most critical side effects in terms of mechanical properties is the sub-surface material dissolution creating severe internal stress concentrations (Fig. 7.18c).

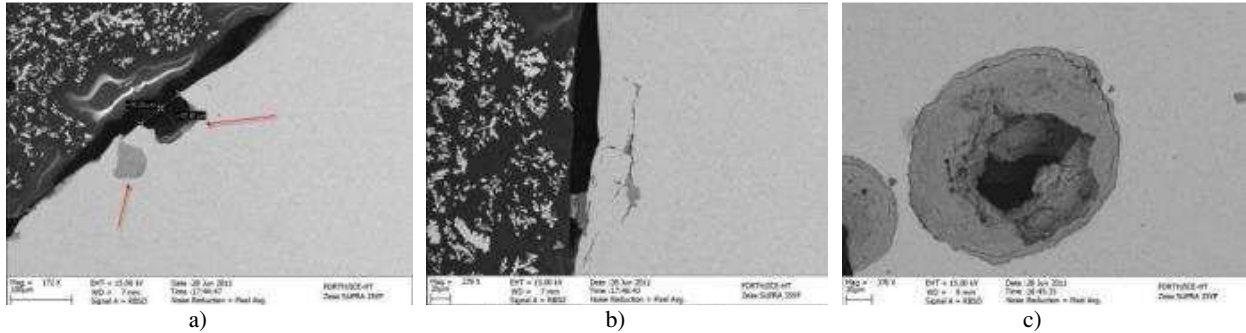


**Figure 7.18:** Side effects of MnS segregation sites subjected to extensive corrosion.

Looking at the effects of segregation of impurities after 90 days exposure on fracture behavior B450C-16-TEMP (Prod.1), dissolution of MnS segregation sites by Cl<sup>-</sup> appears to generate local stress concentrations with the possible generation of hydrogen. Due to the position of the MnS sites at depths below up to 500µm from the surface, the fracture surface exhibits sites of partial debonding of sections approximately equal the above critical depth (Figure 7.19).

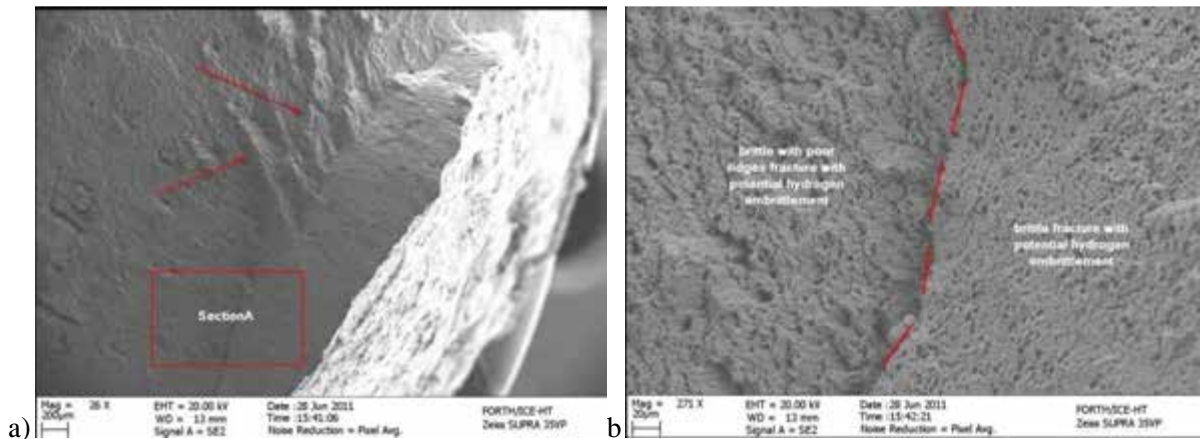


**Figure 7.19:** Partial debonding of martensite zone due to MnS segregation. Both the shape of the zone as well as the ridges found at the top site indicate variation in ductility; b) high magnification of section A shows infinitesimal ductility variation with due to poor defined ridges left on the left side.

## 7.2 Low-Cycle Fatigue (LCF) tests on corroded specimens

Low-Cycle Fatigue (LCF) tests were executed on several steel reinforcing bars previously corroded in salt spray chamber; the protocol already presented in Chapter 2 was generally followed. All the specimens were cleaned and the corresponding mass loss was evaluated. Results obtained by tests executed by UniPI, ISQ and UPA are presented in the following tables.

### 7.2.1 Tests executed by UniPi

In relation to the effective capability of the machine used for the LCF tests, corroded steel reinforcing bars of diameter 20 and 25 mm were not finally tested (table 7.20). Results are presented in terms of mass loss, maximum and minimum effective deformation and stress, total dissipated energy and number of cycles up to failure.

**Table 7. 20:** Corroded specimens subjected to Low Cycle Fatigue tests.

| ID | Steel grade | Ductility | Diameter | Process | Ribs          | Producer |
|----|-------------|-----------|----------|---------|---------------|----------|
| 1  | B500        | B         | 16 mm    | R       | Ribbed        | Prod. 1  |
| 2  | B450        | C         | 16 mm    | R       | Ribbed        | Prod. 1  |
| 3  | B400        | C         | 16 mm    | R       | Ribbed        | Prod. 1  |
| 4  | B400        | C         | 16 mm    | R       | Micro Alloyed | Prod. 2  |
| 5  | B500        | A         | 12 mm    | CW      | Ribbed        | Prod.2   |
| 9  | B450        | C         | 12 mm    | STR     |               | Prod. 1  |

**Table 7. 21:** Mass loss and values adopted for the execution of LCF tests for bars B400C-16 MA, producer 2.

| B400C-16 - MA Prod. 2 90 days (Laboratory 2) |                         |        |                      |                        |        |                            |                     |        |         |
|--|-------------------------|--------|----------------------|------------------------|--------|----------------------------|---------------------|--------|---------|
| ID   | M <sub>uncorr</sub> [g] | L [mm] | M <sub>cor</sub> [g] | L <sub>corr</sub> [mm] | ΔM [g] | ΔM/M <sub>uncorr</sub> [%] | L <sub>0</sub> [mm] | Δε [%] | ΔL [mm] |
| 4.1  | 940,64                  | 594    | 938,55               | 24,05                  | 2,093  | 5,49%                      | 128                 | ±4,0%  | 5,12    |
| 4.2  | 956,57                  | 599    | 954,48               | 20,15                  | 2,094  | 6,51%                      | 96                  | ±4,0%  | 3,84    |
| 4.3  | 973,28                  | 602    | 970,32               | 25,90                  | 2,957  | 7,06%                      | 128                 | ±2,5%  | 3,2     |
| 4.4  | 952,14                  | 595    | 949,37               | 21,70                  | 2,773  | 7,98%                      | 128                 | ±2,5%  | 3,2     |
| 4.6  | 964,27                  | 602    | 962,06               | 21,70                  | 2,211  | 6,36%                      | 128                 | ±4,0%  | 5,12    |
| 4.7  | 947,69                  | 594    | 944,77               | 24,30                  | 2,921  | 7,53%                      | 128                 | ±2,5%  | 3,2     |
| 4.8  | 961,91                  | 601    | 958,90               | 23,60                  | 3,011  | 7,97%                      | 96                  | ±2,5%  | 2,4     |
| 4.9  | 960,31                  | 601    | 957,94               | 22,10                  | 2,375  | 6,73%                      | 96                  | ±2,5%  | 2,4     |
| 4.10   | 958,35                  | 600    | 954,98               | 20,90                  | 3,374  | 10,11%                     | 128                 | ±4,0%  | 5,12    |
| 4.11   | 963,86                  | 602    | 960,11               | 23,80                  | 3,752  | 9,85%                      | 96                  | ±2,5%  | 2,4     |
| 4.12   | 959,78                  | 597    | 956,32               | 18,75                  | 3,464  | 11,49%                     | 96                  | ±4,0%  | 3,84    |
| 4.15   | 955,22                  | 597    | 952,29               | 21,50                  | 2,930  | 8,52%                      | 96                  | ±4,0%  | 3,84    |

**Table 7. 22:** Experimental results of LCF tests on corroded specimen B400C-16-MA-R (producer 2).

| Spec. | L <sub>0</sub> [mm] | F [Hz] | Max σ [MPa] | Min σ [MPa] | Max ε [%] | Min ε [%] | Energy [MPa] | N <sub>cycles</sub> |
|-------|---------------------|--------|-------------|-------------|-----------|-----------|--------------|---------------------|
| 4.1   | 128                 | 0,5    | 528         | -511        | 4,05%     | -3,84%    | 216          | 6                   |
| 4.2   | 96                  | 0,5    | 537         | -525        | 4,02%     | -3,66%    | 324          | 8                   |
| 4.3   | 128                 | 0,5    | 500         | -515        | 2,52%     | -2,36%    | 230          | 11                  |
| 4.4   | 128                 | 0,5    | 496         | -506        | 2,51%     | -2,35%    | 247          | 12                  |
| 4.6   | 128                 | 0,5    | 527         | -496        | 4,04%     | -3,88%    | 247          | 8                   |
| 4.7   | 128                 | 0,5    | 492         | -491        | 2,51%     | -2,38%    | 178          | 9                   |
| 4.8   | 96                  | 0,5    | 523         | -519        | 2,51%     | -2,18%    | 449          | 17                  |
| 4.9   | 96                  | 0,5    | 519         | -507        | 2,50%     | -2,17%    | 350          | 14                  |
| 4.10  | 128                 | 0,5    | 523         | -507        | 4,07%     | -3,83%    | 197          | 6                   |
| 4.11  | 96                  | 0,5    | 498         | -485        | 2,57%     | -2,19%    | 305          | 13                  |
| 4.12  | 96                  | 0,5    | 533         | -514        | 4,12%     | -3,65%    | 314          | 8                   |
| 4.15  | 96                  | 0,5    | 537         | -523        | 4,02%     | -3,71%    | 289          | 7                   |

**Table 7. 23:** Mass loss and values adopted for the execution of LCF tests for bars B450C-16 TempCore, producer 1.

| B450C-16 -TEMP Prod. 1 90 days (Laboratory 2) |                        |        |                      |                        |        |                            |                     |        |         |
|---|------------------------|--------|----------------------|------------------------|--------|----------------------------|---------------------|--------|---------|
| ID  | M <sub>uncor</sub> [g] | L [mm] | M <sub>cor</sub> [g] | L <sub>corr</sub> [mm] | ΔM [g] | ΔM/M <sub>Uncorr</sub> [%] | L <sub>0</sub> [mm] | Δε [%] | ΔL [mm] |
| 2.1   | 809,35                 | 500,00 | 806,75               | 20,75                  | 2,60   | 7,74%                      | 96                  | ±4.0%  | 3,84    |
| 2.2   | 810,34                 | 501,00 | 806,89               | 22,40                  | 3,45   | 9,53%                      | 96                  | ±4.0%  | 3,84    |
| 2.3   | 806,88                 | 500,00 | 804,18               | 21,15                  | 2,70   | 7,91%                      | 96                  | ±4.0%  | 3,84    |
| 2.4   | 808,42                 | 501,00 | 805,96               | 19,90                  | 2,46   | 7,66%                      | 96                  | ±2.5%  | 2,40    |
| 2.5   | 810,50                 | 500,00 | 807,69               | 21,20                  | 2,81   | 8,18%                      | 128                 | ±2.5%  | 3,20    |
| 2.6   | 805,92                 | 500,00 | 802,48               | 22,65                  | 3,44   | 9,43%                      | 96                  | ±2.5%  | 2,40    |
| 2.7   | 810,25                 | 501,00 | 808,04               | 18,60                  | 2,21   | 7,33%                      | 96                  | ±2.5%  | 2,40    |
| 2.8   | 806,38                 | 500,00 | 803,71               | 23,90                  | 2,67   | 6,92%                      | 128                 | ±4.0%  | 5,12    |
| 2.9   | 809,54                 | 501,00 | 807,39               | 20,55                  | 2,15   | 6,49%                      | 128                 | ±4.0%  | 5,12    |
| 2.10  | 808,78                 | 501,00 | 804,68               | 27,10                  | 4,10   | 9,36%                      | 128                 | ±2.5%  | 3,20    |
| 2.11  | 808,11                 | 501,00 | 804,58               | 23,83                  | 3,53   | 9,18%                      | 128                 | ±2.5%  | 3,20    |
| 2.12  | 810,58                 | 502,00 | 808,27               | 20,75                  | 2,31   | 6,89%                      | 128                 | ±2.5%  | 3,20    |

**Table 7. 24:** Experimental results of LCF tests on corroded specimen B450C-16-TEMP-R (producer 1).

| Spec. | L <sub>0</sub> [mm] | F [Hz] | Max σ [MPa] | Min σ [MPa] | Max ε [%] | Min ε [%] | Energy [MPa] | N <sub>cycles</sub> |
|-------|---------------------|--------|-------------|-------------|-----------|-----------|--------------|---------------------|
| 2.1   | 96                  | 0.5    | 533,67      | -518,70     | 4,024%    | -3,709%   | 307          | 7                   |
| 2.2   | 96                  | 0.5    | 516,81      | -509,08     | 4,082%    | -3,728%   | 291          | 7                   |
| 2.3   | 96                  | 0.5    | 531,15      | -521,06     | 4,077%    | -3,728%   | 307          | 7                   |
| 2.4   | 96                  | 0.5    | 512,48      | -524,74     | 2,495%    | -2,204%   | 371          | 14                  |
| 2.5   | 128                 | 0.5    | 498,12      | -511,11     | 2,502%    | -2,367%   | 214          | 10                  |
| 2.6   | 96                  | 0.5    | 512,42      | -528,17     | 2,531%    | -2,215%   | 371          | 15                  |
| 2.7   | 96                  | 0.5    | 509,72      | -518,78     | 2,501%    | -2,201%   | 377          | 15                  |
| 2.8   | 128                 | 0.5    | 511,48      | -479,41     | 4,057%    | -3,845%   | 207          | 6                   |
| 2.9   | 128                 | 0.5    | 503,90      | -495,95     | 4,025%    | -3,889%   | 173          | 5                   |
| 2.10  | 128                 | 0.5    | 507,99      | -484,72     | 2,511%    | -2,385%   | 215          | 11                  |
| 2.11  | 128                 | 0.5    | 513,42      | -528,16     | 2,494%    | -2,374%   | 273          | 13                  |
| 2.12  | 128                 | 0.5    | 496,39      | -507,23     | 2,538%    | -2,331%   | 290          | 16                  |

**Table 7. 25:** Mass loss and values adopted for the execution of LCF tests for B500B-16 TempCore, prod. 1 (90 days).

| B500B-16 - TEMP Prod. 1 90 days (Laboratory 2) |                        |        |                      |                        |        |                            |                     |        |         |
|--|------------------------|--------|----------------------|------------------------|--------|----------------------------|---------------------|--------|---------|
| ID   | M <sub>uncor</sub> [g] | L [mm] | M <sub>cor</sub> [g] | L <sub>corr</sub> [mm] | ΔM [g] | ΔM/M <sub>Uncorr</sub> [%] | L <sub>0</sub> [mm] | Δε [%] | ΔL [mm] |
| 1.1  | 823,04                 | 512    | 820,68               | 20,6                   | 2,36   | 7,13%                      | 128                 | ±2.5%  | 3,2     |
| 1.2  | 809,34                 | 508    | 807,24               | 19,85                  | 2,1    | 6,64%                      | 96                  | ±2.5%  | 2,4     |
| 1.4  | 812,11                 | 506    | 809,6                | 19,75                  | 2,51   | 7,91%                      | 96                  | ±2.5%  | 2,4     |
| 1.6  | 809,82                 | 508    | 807,76               | 17,8                   | 2,06   | 7,25%                      | 128                 | ±4.0%  | 5,12    |
| 1.8  | 819,21                 | 511    | 816,95               | 19,55                  | 2,26   | 7,20%                      | 96                  | ±2.5%  | 2,4     |
| 1.9  | 819,57                 | 511    | 817,37               | 23,2                   | 2,21   | 5,93%                      | 128                 | ±2.5%  | 3,2     |
| 1.10   | 823,1                  | 514    | 820,38               | 22,5                   | 2,72   | 7,56%                      | 96                  | ±4.0%  | 3,84    |
| 1.11   | 799,48                 | 502    | 797,25               | 19,5                   | 2,23   | 7,18%                      | 128                 | ±4.0%  | 5,12    |
| 1.12   | 807,23                 | 505    | 805,19               | 24,15                  | 2,04   | 5,28%                      | 96                  | ±4.0%  | 3,84    |
| 1.13   | 816,52                 | 511    | 814,68               | 18,9                   | 1,84   | 6,08%                      | 128                 | ±2.5%  | 3,2     |

**Table 7. 26:** Experimental results of LCF tests on corroded specimen B500B-16-TEMP-R (producer 1).

| Spec. | L <sub>0</sub> [mm] | F [Hz] | Max σ [MPa] | Min σ [MPa] | Max ε [%] | Min ε [%] | Energy [MPa] | N <sub>cycles</sub> |
|-------|---------------------|--------|-------------|-------------|-----------|-----------|--------------|---------------------|
| 1.1   | 128                 | 1      | 540         | -570        | 2,49%     | -2,35%    | 271          | 13                  |
| 1.2   | 96                  | 1      | 539         | -565        | 2,54%     | -2,16%    | 537          | 21                  |
| 1.4   | 96                  | 1      | 536         | -545        | 2,49%     | -2,41%    | -553         | 19                  |
| 1.6   | 128                 | 1      | 533         | -553        | 2,47%     | -2,29%    | 223          | 8                   |
| 1.8   | 96                  | 1      | 536         | -564        | 2,58%     | -2,23%    | 486          | 19                  |
| 1.9   | 128                 | 1      | 519         | -518        | 2,53%     | -2,36%    | 289          | 14                  |

|      |     |   |     |      |       |        |     |    |
|------|-----|---|-----|------|-------|--------|-----|----|
| 1.10 | 96  | 1 | 555 | -578 | 4,04% | -3,74% | 295 | 7  |
| 1.11 | 128 | 1 | 505 | -529 | 4,02% | -3,89% | 203 | 7  |
| 1.12 | 96  | 1 | 558 | -551 | 3,98% | -3,83% | 440 | 12 |
| 1.13 | 128 | 1 | 536 | -545 | 2,49% | -2,41% | 319 | 17 |

**Table 7. 27:** Mass loss and values adopted for the execution of LCF tests for B400C-16 TempCore, prod. 1 (90 days).

| B400C- 16- TEMP-Producer 1 - 90 days (Laboratory 3) |                        |        |                      |                        |        |                            |                     |        |         |
|---|------------------------|--------|----------------------|------------------------|--------|----------------------------|---------------------|--------|---------|
| ID  | M <sub>uncor</sub> [g] | L [mm] | M <sub>cor</sub> [g] | L <sub>corr</sub> [mm] | ΔM [g] | ΔM/M <sub>Uncorr</sub> [%] | L <sub>0</sub> [mm] | Δε [%] | ΔL [mm] |
| 3.2   | 777,92                 | 498    | 777,33               | 15,20                  | 0,589  | 2,48%                      | 96                  | ±2.5%  | 2,4     |
| 3.3   | 779,38                 | 500    | 777,94               | 15,00                  | 1,442  | 6,17%                      | 128                 | ±4.0%  | 5,12    |
| 3.4   | 778,25                 | 499    | 777,10               | 17,00                  | 1,151  | 4,34%                      | 96                  | ±2.5%  | 2,4     |
| 3.5   | 764,69                 | 492    | 763,88               | 19,85                  | 0,815  | 2,64%                      | 128                 | ±4.0%  | 5,12    |
| 3.6   | 778,90                 | 500    | 778,30               | 12,20                  | 0,605  | 3,18%                      | 96                  | ±4.0%  | 3,84    |
| 3.7   | 777,37                 | 499    | 776,89               | 13,70                  | 0,485  | 2,27%                      | 96                  | ±4.0%  | 3,84    |
| 3.8   | 778,59                 | 500    | 778,14               | 13,60                  | 0,453  | 2,14%                      | 128                 | ±5.0%  | 6,4     |
| 3.9   | 776,83                 | 499    | 776,16               | 17,30                  | 0,673  | 2,50%                      | 128                 | ±5.0%  | 6,4     |
| 3.10  | 777,55                 | 499    | 776,53               | 14,00                  | 1,021  | 4,68%                      | 128                 | ±4.0%  | 5,12    |
| 3.12  | 776,25                 | 499    | 776,19               | 11,00                  | 0,061  | 0,36%                      | 128                 | ±2.5%  | 3,2     |

**Table 7. 28:** Experimental results of LCF tests on corroded specimen B400C-16-TEMP-R (producer 1).

| Spec. | L <sub>0</sub> [mm] | F [Hz] | Max σ [MPa] | Min σ [MPa] | Max ε [%] | Min ε [%] | Energy [MPa] | N <sub>cycles</sub> |
|-------|---------------------|--------|-------------|-------------|-----------|-----------|--------------|---------------------|
| 3.2   | 96                  | 0.5    | 482         | -485        | 2,49%     | -2,22%    | 468          | 19                  |
| 3.4   | 96                  | 0.5    | 481         | -475        | 2,52%     | -2,23%    | 424          | 17                  |
| 3.6   | 96                  | 0.5    | 506         | -482        | 4,13%     | -3,79%    | 335          | 8                   |
| 3.7   | 96                  | 0.5    | 509         | -484        | 4,03%     | -3,74%    | 322          | 8                   |
| 3.8   | 96                  | 0.5    | 514         | -495        | 5,00%     | -4,69%    | 305          | 6                   |
| 3.9   | 96                  | 0.5    | 511         | -465        | 5,10%     | -4,83%    | 295          | 6                   |
| 3.11  | 128                 | 0.5    | 470         | -482        | 2,18%     | -2,13%    | 263          | 13                  |
| 3.12  | 128                 | 0.5    | 452         | -467        | 2,21%     | -2,16%    | 277          | 15                  |
| 3.3   | 128                 | 0.5    | 456         | -476        | 4,03%     | -3,85%    | 171          | 6                   |
| 3.5   | 128                 | 0.5    | 455         | -486        | 4,00%     | -3,89%    | 219          | 8                   |
| 3.10  | 128                 | 0.5    | 480         | -489        | 4,03%     | -3,88%    | 217          | 7                   |

**Table 7. 29:** Mass loss and values adopted for the execution of LCF tests for bars B450C-12 Stretched, producer 1.

| B450C-12-STR Prod.1 - 90 days – Laboratory 3 |                        |        |                      |                        |         |                            |                     |        |         |
|--|------------------------|--------|----------------------|------------------------|---------|----------------------------|---------------------|--------|---------|
| ID   | M <sub>uncor</sub> [g] | L [mm] | M <sub>cor</sub> [g] | L <sub>corr</sub> [mm] | ΔM [g]  | ΔM/M <sub>Uncorr</sub> [%] | L <sub>0</sub> [mm] | Δε [%] | ΔL [mm] |
| 9.1  | 451,24                 | 501    | 450,24               | 18,95                  | 0,998   | 5,84%                      | 6φ                  | ±2.5%  | 1,80    |
| 9.7  | 449,94                 | 500    | 440,05               | 38,00                  | 9,895   | 28,94%                     | 6φ                  | ±2.5%  | 1,80    |
| 9.14   | 449,27                 | 500    | 448,19               | 25,80                  | 1,081   | 4,66%                      | 6φ                  | ±4.0%  | 2,88    |
| 9.18   | 449,87                 | 500    | 449,28               | 20,15                  | 0,595   | 3,28%                      | 6φ                  | ±4.0%  | 2,88    |
| 9.19   | 451,38                 | 501    | 451,07               | 10,50                  | 0,311   | 3,29%                      | 6φ                  | ±3.0%  | 2,16    |
| 9.6  | 450,97                 | 501    | 450,28               | 21,25                  | 0,691   | 3,61%                      | 6φ                  | ±3.0%  | 2,16    |
| 9.12   | 449,48                 | 500    | 448,71               | 26,35                  | 0,771   | 3,26%                      | 8φ                  | ±2.5%  | 2,40    |
| 9.13   | 450,82                 | 500    | 449,86               | 14,65                  | 0,959   | 7,26%                      | 8φ                  | ±2.5%  | 2,40    |
| 9.11   | 450,12                 | 501    | 448,47               | 38,00                  | 1,652   | 4,84%                      | 8φ                  | ±3.0%  | 2,88    |
| 9.2  | 449,45                 | 501    | 448,02               | 23,45                  | 1,434   | 6,82%                      | 8φ                  | ±3.0%  | 2,88    |
| 9.8  | 450,27                 | 501    | 449,69               | 15,80                  | 0,584   | 4,11%                      | 8φ                  | ±4.0%  | 3,84    |
| 9.9  | 450,18                 | 501    | 449,20               | 19,60                  | 0,985   | 5,59%                      | 8φ                  | ±4.0%  | 3,84    |
| 9,3  | 452,06                 | 502    | 450,95               | 13,75                  | 1,1075  | 8,94%                      | 6φ                  | ±4.0%  | 2,88    |
| 9,4  | 450,21                 | 500    | 449,05               | 15,00                  | 1,165   | 8,63%                      | 8φ                  | ±4.0%  | 3,84    |
| 9,5  | 449,15                 | 500    | 448,03               | 15,30                  | 1,1225  | 8,17%                      | 6φ                  | ±2.5%  | 1,80    |
| 9,17   | 451,14                 | 501    | 450,33               | 16,10                  | 0,81125 | 5,60%                      | 8φ                  | ±2.5%  | 2,40    |

**Table 7. 30:** Experimental results of LCF tests on corroded specimen B450C-12-STR-R (producer 1).

| Spec. | L <sub>0</sub> [mm] | F [Hz] | Max $\sigma$ [MPa] | Min $\sigma$ [MPa] | Max $\epsilon$ [%] | Min $\epsilon$ [%] | Energy [MPa] | N <sub>cycles</sub> |
|-------|---------------------|--------|--------------------|--------------------|--------------------|--------------------|--------------|---------------------|
| 9.1   | 72                  | 0,5    | 551                | -536               | 2,07%              | -1,99%             | 591          | 20                  |
| 9.7   | 72                  | 0,5    | 561                | -529               | 2,08%              | -1,99%             | 362          | 16                  |
| 9.6   | 72                  | 0,5    | 573                | -550               | 2,60%              | -2,56%             | 485          | 16                  |
| 9.19  | 72                  | 0,5    | 566                | -541               | 2,61%              | -2,61%             | 502          | 16                  |
| 9.14  | 72                  | 0,5    | 573                | -522               | 3,50%              | -3,59%             | 346          | 8                   |
| 9.18  | 72                  | 0,5    | 587                | -539               | 3,70%              | -3,72%             | 315          | 7                   |
| 9.12  | 96                  | 0,5    | 560                | -488               | 2,52%              | -2,50%             | 265          | 12                  |
| 9.13  | 96                  | 0,5    | 556                | -477               | 2,21%              | -2,29%             | 275          | 13                  |
| 9.11  | 96                  | 0,5    | 558                | -467               | 2,73%              | -2,79%             | 198          | 8                   |
| 9.2   | 96                  | 0,5    | 564                | -472               | 2,69%              | -2,81%             | 221          | 9                   |
| 9.8   | 96                  | 0,5    | 574                | -470               | 3,70%              | -3,81%             | 258          | 8                   |
| 9.9   | 96                  | 0,5    | 585                | -471               | 3,76%              | -3,84%             | 207          | 7                   |
| 9,3   | 72                  | 0,5    | 589                | -531               | 4,08%              | -3,70%             | 288          | 7                   |
| 9,4   | 96                  | 0,5    | 591                | -487               | 4,02%              | -3,91%             | 235          | 7                   |
| 9,5   | 72                  | 0,5    | 555                | -525               | 2,54%              | -2,25%             | 471          | 18                  |
| 9,17  | 96                  | 0,5    | 562                | -483               | 2,50%              | -2,39%             | 514          | 12                  |

### 7.2.2 Tests executed by UPA

Low-cycle fatigue tests were executed on specimens of diameter 12 and 16mm, considering 45 and 90 days of exposure; results are presented in terms of maximum and minimum stress, stress corresponding to the minimum deformation, mass loss of the corroded specimens, number of cycles up to failure and total dissipated energy.

**Table 7. 31:** Experimental results of LCF tests on corroded specimen diameter 12 mm.

| B450C-12-STR – Prod. 1 (45 days of corrosion) |                |                  |                      |                              |                      |                     |              |          |
|---|----------------|------------------|----------------------|------------------------------|----------------------|---------------------|--------------|----------|
| ID  | L <sub>0</sub> | $\Delta\epsilon$ | $\sigma_{max}$ [MPa] | $\sigma_{MIN\epsilon}$ [MPa] | $\sigma_{min}$ [MPa] | N <sub>cycles</sub> | Energy [MPa] | M.L. [%] |
| B450C-21                                      |                |                  | 523,25               | -530,4                       | -531,2               | 30                  | 669          | 3,34     |
| B450C-22                                      | 6 $\Phi$       |                  | 535,9                | -554,2                       | -555,6               | 32                  | 718          | 2,91     |
| B450C-23                                      |                |                  | 537,3                | -546,2                       | -548,8               | 36                  | 801,4        | 3,32     |
| B450C-1                                       |                | $\pm 2,5\%$      | 530,5                | -446                         | -493,1               | 16                  | 303          | 2,93     |
| B450C-2                                       | 8 $\Phi$       |                  | 538,26               | -466,2                       | -503,4               | 20                  | 380          | 4,16     |
| B450C-3                                       |                |                  | 536,6                | -460,47                      | -497                 | 16                  | 341,5        | 3,18     |
| B450C-4                                       |                |                  | 566,9                | -491,4                       | -497                 | 7                   | 213          | 2,97     |
| B450C-5                                       | 8 $\Phi$       |                  | 567,7                | -484                         | -484,26              | 7                   | 234,19       | 4,12     |
| B450C-6                                       |                |                  | 559,3                | -485,7                       | -484,26              | 7                   | 250,7        | 3,51     |
| B450C-10                                      |                | $\pm 4\%$        | 575,2                | -549,5                       | -549,6               | 11                  | 428,2        | 2,61     |
| B450C-30                                      | 6 $\Phi$       |                  | 573,3                | -560                         | -560,4               | 11                  | 428,74       | 3,41     |
| B450C-40                                      |                |                  | 570,5                | -539,7                       | -540,1               | 10                  | 374,31       | 2,87     |
| B450C-12-STR – Prod. 1 (90 days of corrosion) |                |                  |                      |                              |                      |                     |              |          |
| B450C-36                                      |                |                  | 528,98               | 525,4                        | -532,8               | 30                  | 643,01       | 7,55     |
| B450C-37                                      |                |                  | 531,42               | -524                         | -531,8               | 21                  | 461,01       | 8,46     |
| B450C-38                                      | 6 $\Phi$       |                  | 530,73               | -526,3                       | -532                 | 36                  | 778,32       | 6,81     |
| B450C-39                                      |                |                  | 530,27               | -529                         | -535,9               | 26                  | 568,55       | 6,52     |
| B450C-20                                      |                | $\pm 2,5\%$      | 514,47               | -499                         | -482,7               | 31                  | 637,52       | 7,12     |
| B450C-11                                      |                |                  | 539,8                | -429                         | -483,1               | 12                  | 227,27       | 8,75     |
| B450C-12                                      | 8 $\Phi$       |                  | 547,7                | -456                         | -501,5               | 18                  | 333,9        | 10,55    |
| B450C-13                                      |                |                  | 547,65               | -457,1                       | -500,7               | 15                  | 293,57       | 7,28     |
| B450C-14                                      |                |                  | 548,4                | -438,7                       | -483,6               | 19                  | 346,23       | 5,45     |

| B450C-15                                     |                |       | 560,67           | -340                    | -465,8                 | 7                   | 218,63       | 6,57     |
|--|----------------|-------|------------------|-------------------------|------------------------|---------------------|--------------|----------|
| B450C-16                                     |                |       | 553,89           | -341                    | -457,5                 | 7                   | 224,22       | 6,75     |
| B450C-17                                     | 8Φ             |       | 556,64           | -324                    | -446,1                 | 8                   | 242,19       | 6,98     |
| B450C-18                                     |                |       | 555,57           | -331                    | -450,5                 | 8                   | 243,78       | 8,93     |
| B450C-19                                     |                |       | 556,9            | -362                    | -469                   | 8                   | 241,6        | 8,47     |
| B450C-32                                     |                | ±4%   | 576,14           | -504                    | -531,6                 | 9                   | 365,8        | 5,3      |
| B450C-33                                     |                |       | 577,51           | -490,7                  | -528,9                 | 6                   | 250,71       | 7,86     |
| B450C-34                                     | 6Φ             |       | 574,7            | -503                    | -537,1                 | 8                   | 342,55       | 10,08    |
| B450C-35                                     |                |       | 575,9            | -505                    | -534,5                 | 10                  | 393,39       | 7,67     |
| B450C-31                                     |                |       | 557              | -512,7                  | -529                   | 11                  | 414,2        | 6,89     |
| B500A-12-CW – Prod. 2 (45 days of corrosion) |                |       |                  |                         |                        |                     |              |          |
| ID   | L <sub>0</sub> | Δε    | σ <sub>max</sub> | σ <sub>MINε</sub> [MPa] | σ <sub>min</sub> [MPa] | N <sub>cycles</sub> | Energy [MPa] | M.L. [%] |
| B500A-21                                     |                |       | 540,2            | -511,3                  | -525,4                 | 27                  | 565,4        | 3,43     |
| B500A-22                                     | 6Φ             |       | 538,8            | -505,7                  | -530,4                 | 25                  | 519          | 3,91     |
| B500A-23                                     |                |       | 537,8            | -508                    | -526                   | 24                  | 513,5        | 3,77     |
| B500A-1                                      |                | ±2,5% | 542,8            | -406,5                  | -518,2                 | 12                  | 214          | 3,37     |
| B500A-2                                      | 8Φ             |       | 540,2            | -419,3                  | -509,9                 | 14                  | 250          | 3,82     |
| B500A-3                                      |                |       | 531,8            | -405                    | -491,95                | 13                  | 241,7        | 3,6      |
| B500A-4                                      |                |       | 541,7            | -320,41                 | -493,7                 | 7                   | 184,7        | 3,86     |
| B500A-5                                      | 8Φ             |       | 544,8            | -326,6                  | -491,7                 | 7                   | 195,4        | 3,43     |
| B500A-6                                      |                |       | 547,5            | -307                    | -485,4                 | 7                   | 182,6        | 3,63     |
| B500A-10                                     |                | ±4%   | 532,6            | -424,89                 | -502                   | 9                   | 288,6        | 4,95     |
| B500A-30                                     | 6Φ             |       | 546,1            | -516,8                  | -516,6                 | 6                   | 237,1        | 5,42     |
| B500A-40                                     |                |       | 562,7            | -518,9                  | -518,9                 | 9                   | 311,8        | 1,62     |
| B500A-12-CW – Prod. 2 (90 days of corrosion) |                |       |                  |                         |                        |                     |              |          |
| B500A-36                                     |                |       | 513,8            | -456,4                  | -498,2                 | 17                  | 315,17       | 10,5     |
| B500A-37                                     |                |       | 513,5            | -473,1                  | -503,3                 | 15                  | 284,22       | 10,5     |
| B500A-38                                     | 6Φ             |       | 524,8            | -497,3                  | -526,6                 | 15                  | 291,73       | 4,8      |
| B500A-39                                     |                |       | 525,4            | -484                    | -510                   | 14                  | 286,73       | 8,4      |
| B500A-20                                     |                | ±2,5% | 525,2            | -492,6                  | -508,3                 | 17                  | 344,1        | 6,56     |
| B500A-11                                     |                |       | 540,56           | -359                    | -447,5                 | 12                  | 192          | 6,76     |
| B500A-12                                     |                |       | 544,2            | -365                    | -514,8                 | 12                  | 190,26       | 8,08     |
| B500A-13                                     | 8Φ             |       | 537,74           | -350                    | -484                   | 12                  | 195,34       | 7,73     |
| B500A-14                                     |                |       | 533,85           | -356                    | -494,7                 | 12                  | 194,1        | 8,83     |
| B500A-15                                     |                |       | 534,46           | -256                    | -445,5                 | 6                   | 157,2        | 8,66     |
| B500A-16                                     |                |       | 536              | -244,1                  | -447                   | 6                   | 150,8        | 7,37     |
| B500A-17                                     | 8Φ             |       | 558,4            | -281,3                  | -473,4                 | 6                   | 177,59       | 8,34     |
| B500A-18                                     |                |       | 540              | -264,3                  | -463,5                 | 6                   | 169,16       | 7,16     |
| B500A-19                                     |                |       | 536,26           | -315,23                 | -483                   | 5                   | 147,04       | 6,71     |
| B500A-32                                     |                | ±4%   | 545              | -405                    | -496                   | 6                   | 227          | 8,1      |
| B500A-33                                     |                |       | 520              | -370                    | -489                   | 6                   | 194          | 11,7     |
| B500A-34                                     | 6Φ             |       | 533              | -414                    | -511                   | 6                   | 209,1        | 10,7     |
| B500A-35                                     |                |       | 528              | -378,2                  | -485                   | 6                   | 211,7        | 10,3     |
| B500A-31                                     |                |       | 524,8            | -426,5                  | -500                   | 6                   | 218,9        | 10,5     |

**Table 7. 32:** Experimental results of LCF tests on corroded specimens diameter 16 mm.

| Steel grade/diameter/process | L <sub>0</sub>           | Δε [%] | T <sub>corr</sub> [days] | N <sub>cycles</sub> | Energy [MPa] | Mass Loss [%] |      |
|------------------------------|--------------------------|--------|--------------------------|---------------------|--------------|---------------|------|
| B450C-16-TEMP-R- Prod. 1     | 6φ                       | 2,50   | 45                       | 20                  | 454,00       | 6,65          |      |
|                              | 6φ                       | 2,50   | 45                       | 20                  | 450,10       | 6,52          |      |
|                              | 6φ                       | 2,50   | 45                       | 23                  | 503,62       | 5,37          |      |
|                              | 8φ                       | 2,50   | 45                       | 16                  | 308,83       | 7,00          |      |
|                              | 8φ                       | 2,50   | 45                       | 17                  | 324,64       | 5,31          |      |
|                              | 8φ                       | 2,50   | 45                       | 16                  | 312,79       | 6,35          |      |
|                              | 8φ                       | 4,00   | 45                       | 7                   | 204,27       | 4,39          |      |
|                              | 8φ                       | 4,00   | 45                       | 8                   | 237,69       | 6,65          |      |
|                              | 8φ                       | 4,00   | 45                       | 9                   | 253,67       | 6,06          |      |
|                              | 6φ                       | 4,00   | 45                       | 10                  | 380,55       | 5,56          |      |
|                              | 6φ                       | 4,00   | 45                       | 10                  | 382,88       | 7,01          |      |
|                              | 6φ                       | 4,00   | 45                       | 11                  | 418,26       | 4,94          |      |
|                              | B450C-16-TEMP R- Prod. 1 | 6φ     | 2,50                     | 90                  | 16           | 416,06        | 8,81 |
|                              |                          | 6φ     | 2,50                     | 90                  | 18           | 470,93        | 9,40 |
| 6φ                           |                          | 2,50   | 90                       | 13                  | 343,23       | 9,38          |      |
| 8φ                           |                          | 2,50   | 90                       | 18                  | 329,11       | 10,22         |      |
| 8φ                           |                          | 2,50   | 90                       | 16                  | 304,55       | -             |      |
| 8φ                           |                          | 2,50   | 90                       | 13                  | 295,17       | 8,29          |      |
| 8φ                           |                          | 2,50   | 90                       | 11                  | 262,70       | 7,45          |      |
| 8φ                           |                          | 4,00   | 90                       | 6                   | 240,12       | 7,44          |      |
| 8φ                           |                          | 4,00   | 90                       | 6                   | 197,51       | 8,51          |      |
| 8φ                           |                          | 4,00   | 90                       | 6                   | 231,91       | 9,20          |      |
| 8φ                           |                          | 4,00   | 90                       | 6                   | 236,70       | 7,91          |      |
| 6φ                           |                          | 4,00   | 90                       | 8                   | 374,10       | 9,34          |      |
| 6φ                           |                          | 4,00   | 90                       | 8                   | 365,80       | 8,17          |      |
| 6φ                           |                          | 4,00   | 90                       | 12                  | 296,20       | 10,10         |      |
| B400C-16-TEMP R- Prod. 1     | 6φ                       | 4,00   | 90                       | 7                   | 296,20       | 8,15          |      |
|                              | 6φ                       | 2,50   | 45                       | 19                  | 440,97       | 6,25          |      |
|                              | 6φ                       | 2,50   | 45                       | 22                  | 484,09       | 5,94          |      |
|                              | 6φ                       | 2,50   | 45                       | 15                  | 345,42       | 6,50          |      |
|                              | 8φ                       | 2,50   | 45                       | 14                  | 243,87       | 6,40          |      |
|                              | 8φ                       | 2,50   | 45                       | 13                  | 235,85       | 5,24          |      |
|                              | 8φ                       | 2,50   | 45                       | 8                   | 177,89       | 6,50          |      |
|                              | 8φ                       | 4,00   | 45                       | 6                   | 161,51       | 5,72          |      |
|                              | 8φ                       | 4,00   | 45                       | 6                   | 187,14       | 6,20          |      |
|                              | 8φ                       | 4,00   | 45                       | 6                   | 186,33       | 6,63          |      |
|                              | 6φ                       | 4,00   | 45                       | 8                   | 292,66       | 6,40          |      |
|                              | 6φ                       | 4,00   | 45                       | 7                   | 244,63       | 6,60          |      |
|                              | 6φ                       | 4,00   | 45                       | 7                   | 288,69       | 6,30          |      |
|                              | B400C-16-TEMP R- Prod. 1 | 6φ     | 2,50                     | 90                  | 13           | 337,21        | 9,57 |
| 6φ                           |                          | 2,50   | 90                       | 15                  | 360,62       | 9,60          |      |
| 6φ                           |                          | 2,50   | 90                       | 25                  | 560,50       | 8,40          |      |
| 8φ                           |                          | 2,50   | 90                       | 12                  | 223,22       | 8,77          |      |
| 8φ                           |                          | 2,50   | 90                       | 12                  | 204,01       | 8,71          |      |
| 8φ                           |                          | 2,50   | 90                       | 12                  | 231,53       | 9,42          |      |
| 8φ                           |                          | 4,00   | 90                       | 6                   | 152,80       | 10,21         |      |
| 8φ                           |                          | 4,00   | 90                       | 6                   | 161,53       | 8,81          |      |
| 8φ                           |                          | 4,00   | 90                       | 4                   | 145,45       | 9,49          |      |
| 8φ                           |                          | 4,00   | 90                       | 5                   | 174,02       | 8,50          |      |
| 6φ                           |                          | 4,00   | 90                       | 7                   | 311,30       | 8,79          |      |
| 6φ                           |                          | 4,00   | 90                       | 7                   | 318,40       | 9,65          |      |
| 6φ                           |                          | 4,00   | 90                       | 7                   | 327,40       | 9,20          |      |

|                         |    |      |    |    |        |       |
|-------------------------|----|------|----|----|--------|-------|
| B400C-16-MA- R- Prod. 2 | 6φ | 2,50 | 45 | 17 | 401,00 | 6,66  |
|                         | 6φ | 2,50 | 45 | 24 | 564,50 | 5,34  |
|                         | 6φ | 2,50 | 45 | 21 | 480,10 | 6,59  |
|                         | 8φ | 2,50 | 45 | 11 | 220,30 | 6,15  |
|                         | 8φ | 2,50 | 45 | 11 | 209,50 | 5,98  |
|                         | 8φ | 4,00 | 45 | 7  | 210,00 | 6,03  |
|                         | 8φ | 4,00 | 45 | 6  | 185,50 | 5,87  |
|                         | 6φ | 4,00 | 45 | 8  | 311,70 | 6,38  |
|                         | 6φ | 4,00 | 45 | 9  | 349,10 | 5,79  |
|                         | 6φ | 4,00 | 45 | 8  | 312,40 | 5,68  |
|                         | 6φ | 2,50 | 90 | 19 | 475,80 | 8,90  |
| B400C-16-MA- R- Prod. 2 | 6φ | 2,50 | 90 | 18 | 480,90 | 9,65  |
|                         | 6φ | 2,50 | 90 | 17 | 438,70 | 9,95  |
|                         | 8φ | 2,50 | 90 | 15 | 290,00 | 10,73 |
|                         | 8φ | 2,50 | 90 | 13 | 280,01 | 9,55  |
|                         | 8φ | 2,50 | 90 | 12 | 273,83 | 18,90 |
|                         | 8φ | 2,50 | 90 | 13 | 288,60 | 8,45  |
|                         | 8φ | 4,00 | 90 | 6  | 212,95 | 9,09  |
|                         | 8φ | 4,00 | 90 | 5  | 181,47 | 9,43  |
|                         | 8φ | 4,00 | 90 | 6  | 221,36 | 8,90  |
|                         | 8φ | 4,00 | 90 | 6  | 208,41 | 8,75  |
|                         | 8φ | 4,00 | 90 | 5  | 181,46 | 9,20  |
|                         | 6φ | 4,00 | 90 | 7  | 347,40 | 8,48  |
|                         | 6φ | 4,00 | 90 | 6  | 296,10 | 9,71  |
|                         | 6φ | 4,00 | 90 | 7  | 347,10 | 8,72  |
|                         | 6φ | 4,00 | 90 | 7  | 317,50 | 8,65  |

### 7.2.3 Tests executed by ISQ

Low-cycle fatigue tests were executed on specimens of diameter 12, 16 and 25 mm adopting different testing frequencies; results are presented in terms of number of cycles up to failure and total dissipated energy.

**Table 7. 33:** Experimental results of LCF tests on corroded specimen tested by ISQ.

| Steel grade/diameter/<br>process/ rib/ producer | Uncorroded<br>ref.  | ID        | f<br>[Hz] | L <sub>0</sub><br>[mm] | Δε<br>[%] | N <sub>cycles/<br/>break</sub> | Tot. Energy<br>[MPa] |         |        |        |
|---|---------------------|-----------|-----------|------------------------|-----------|--------------------------------|----------------------|---------|--------|--------|
| B400C-16-MA-R-Prod.2                            | Ref. <sup>a</sup> C | C5/C6     | 2,00      | 6φ                     | ±2.5      | 18B/20                         | 452,52               | 510,76  |        |        |
|   |                     | C7/C8     |           |                        |           | 9B/7B                          | 364,71               | 316,51  |        |        |
|   |                     | C13/C14   |           |                        |           | 8φ                             | ±2.5                 | 15B/14B | 286,76 | 271,83 |
|   |                     | C15/C16   |           |                        |           |                                | ±4.0                 | 6B/6B   | 200,41 | 191,00 |
| B400C-25-MA-R-Prod.2                            | Ref. <sup>a</sup> B | B69/B70   | 0,05      | 6φ                     | ±2.5      | 20/20B                         | 535,19               | 491,72  |        |        |
|   |                     | B71/B72   |           |                        |           | ±4.0                           | ----                 | ----    | ----   |        |
|   |                     | B75/B76   |           |                        |           | 8φ                             | ±2.5                 | 12B/15B | 262,97 | 286,77 |
|   |                     | B77/B78   |           |                        |           |                                | ±4.0                 | 6B/5B   | 200,12 | 181,20 |
| B450C-25-TEMP-R-<br>Prod.2                      | Ref. B              | B85/B86   | 0,05      | 6φ                     | ±2.5      | 20/20B                         | 556,18               | 556,65  |        |        |
|   |                     | B87/B88   |           |                        |           | ±4.0                           | ----                 | ----    | ----   |        |
|   |                     | B92/B93   |           |                        |           | 8φ                             | ±2.5                 | 15B/13B | 301,98 | 269,50 |
|   |                     | B94/B96   |           |                        |           |                                | ±4.0                 | 6B/8B   | 205,61 | 234,13 |
| B500A-12-CW-R-Prod.2                            | Ref. <sup>a</sup> D | D1/D2     | 2,00      | 6φ                     | ±2.5      | 20b/18B                        | 447,36               | 387,04  |        |        |
|   |                     | D7/D8     |           |                        |           | ±4.0                           | 7B/8B                | 276,68  | 258,38 |        |
|   |                     | D11/D13   |           |                        |           | 8φ                             | ±2.5                 | 14B/13B | 231,07 | 242,45 |
|   |                     | D15/D16   |           |                        |           |                                | ±4.0                 | 6B/6B   | 191,70 | 200,18 |
| B500B-25-TEMP-R-<br>Prod.2                      | Ref. <sup>a</sup> B | B99/B100  | 0,05      | 6φ                     | ±2.5      | 21/21                          | 571,23               | 493,21  |        |        |
|   |                     | B102/B104 |           |                        |           | ±4.0                           | ----                 | ----    | ----   |        |
|   |                     | B105/B106 |           |                        |           | 8φ                             | ±2.5                 | 15B/12B | 297,59 | 253,60 |
|   |                     | B107/B108 |           |                        |           |                                | ±4.0                 | 7B/7B   | 233,83 | 242,08 |

|                        |                          |          |      |    |      |         |        |        |
|------------------------|--------------------------|----------|------|----|------|---------|--------|--------|
| B450C-16-TEMP-R-Prod.1 | Ref. <sup>a</sup> R      | R10/R11  | 2,00 | 6φ | ±2.5 | 20B/20  | 483,76 | 485,91 |
|                        |                          | R29/R30  |      |    | ±4.0 | 7B/7B   | 312,37 | 330,01 |
|                        |                          | R3/R8    |      | 8φ | ±2.5 | 13B/15B | 254,88 | 287,15 |
|                        |                          | R13/R18  |      |    | ±4.0 | 6B/6B   | 208,56 | 210,12 |
| B450C-12-STR-R-Prod.1  | Ref. <sup>a</sup> I      | I17/I18  | 2,00 | 6φ | ±2.5 | 20/20   | 489,44 | 490,04 |
|                        |                          | I20/I21  |      |    | ±4.0 | 9B/9B   | 399,62 | 385,88 |
|                        |                          | I25/I27  |      | 8φ | ±2.5 | 15B/13B | 290,71 | 268,83 |
|                        |                          | I31/I32  |      |    | ±4.0 | 6B/6B   | 213,25 | 238,03 |
| B500B-16-TEMP-R-Prod.1 | Ref. <sup>a</sup> PB     | P7B      | 2,00 | 6φ | ±2.5 | 20B     | 499,40 |        |
|                        |                          | P1B      |      |    | ±4.0 | 7B      | 326,73 |        |
|                        |                          | P3B      |      | 8φ | ±2.5 | 13B/15B | 273,10 |        |
|                        |                          | P16B     |      |    | ±4.0 | 5B      | 196,56 |        |
| SAM                    | Ref. <sup>a</sup> T      | T1/T3    | 2,00 | 6φ | ±2.5 | 20B/20  | 486,40 | 518,08 |
|                        |                          | T7/T8    |      |    | ±4.0 | 9B/15B  | 345,79 | 381,24 |
|                        |                          | T10/T11  |      | 8φ | ±2.5 | 15B/20  | 299,54 | 344,30 |
|                        |                          | T12/T14  |      |    | ±4.0 | 7B/6B   | 236,53 | 216,04 |
| B400C-16-TEMP-R-Prod.1 | Ref. <sup>a</sup> S e SE | SE2/SE3  | 2,00 | 6φ | ±2.5 | 20/15B  | 498,63 | 342,40 |
|                        |                          | SE6/SE10 |      |    | ±4.0 | 6B/6B   | 273,43 | 265,35 |
|                        |                          | S2/S7    |      | 8φ | ±2.5 | 13B/11B | 223,57 | 216,19 |
|                        |                          | S11/S22  |      |    | ±4.0 | 5B/6B   | 176,18 | 164,78 |

#### 7.2.4 Hydrogen concentration measurements of corroded rebars after low-fatigue test

After the low-fatigue tests (UniPI), several samples were stored at low temperature in order to limit the hydrogen out-gassing. Then a piece of rebar in the corroded region close to the fracture surface has been collected by using a cooled saw. Finally, the hydrogen content has been measured by hot extraction method. Hydrogen concentration measured on several as-received rebars of different classes and grades have all shown values in the range  $0.1 \div 0.2$  ppm, that can be considered as the background value. Results are summarized in the following table.

**Table 7. 34:** Hydrogen concentration values of samples of different corroded rebars after low-cycle fatigue tests.

| Steel grade/diameter/process/producer    | ID   | $\Delta M/M$ (%) | $C_H$ |
|--|------|------------------|-------|
| B 500B-16-TEMP Prod. 1 90 days (Lab. 2)  | 1.4  | 7.91             | 0.2   |
|  | 1.6  | 7.25             | 0.3   |
|  | 1.8  | 7.20             | 0.2   |
|  | 1.9  | 5.93             | 0.3   |
|  | 1.10 | 7.56             | 0.4   |
|  | 1.11 | 7.18             | 0.3   |
|  | 1.12 | 5.28             | 0.3   |
|  | 1.13 | 6.08             | 0.2   |
| B 450C-16-TEMP Prod. 1 90 days (Lab. 2)  | 2.1  | 7.74             | 0.5   |
|  | 2.2  | 9.53             | 0.6   |
|  | 2.6  | 9.43             | 0.3   |
|  | 2.7  | 6.92             | 0.5   |
| B400C-16-TEMP-Prod. 1 - 90 days (Lab. 3) | 2.10 | 9.36             | 0.4   |
|  | 3.3  | 6.17             | 0.3   |
|  | 3.5  | 2.64             | 0.2   |
| B 400C-16- MA Prod. 2 90 days (Lab. 2)   | 3.10 | 4.68             | 0.2   |
|  | 4.6  | 6.36             | 0.2   |
|  | 4.10 | 10.11            | 0.3   |
|  | 4.13 | 5.81             | 0.6   |
|  | 4.15 | 8.52             | 0.4   |
| B 500B- 12- STR Prod. 1 90 days (Lab. 2) | 7.3  | 2.62             | 0.3   |
|  | 7.7  | 5.53             | 0.4   |
|  | 7.8  | 2.81             | 0.8   |
|  | 7.14 | 6.24             | 0.2   |
|  | 7.15 | 5.11             | 0.2   |

|                                     |      |      |     |
|-------------------------------------|------|------|-----|
|                                     | 7.17 | 4.97 | 0.4 |
|                                     | 7.18 | 3.41 | 0.3 |
| B 450C-12-STR RIVA 90 days (Lab. 3) | 9.3  | 8.94 | 0.6 |
|                                     | 9.4  | 8.63 | 0.5 |
|                                     | 9.5  | 8.17 | 0.6 |
|                                     | 9.17 | 5.60 | 0.4 |

Although data belonging to the same class are affected to high scattering, it is possible to note that, in case of TempCore rebars of same diameter and ductility class (B400C-16-TEMP, B450C-16-TEMP), the hydrogen content absorbed during corrosion increases with the increase of the yielding stress. This, in turn, is driven by the martensite skin thickness. Thus, as expected, a higher martensite volume fraction gives higher hydrogen concentration, thanks to the higher hydrogen solubility of this phase. Notwithstanding, the hydrogen concentration values measured after low-cycle fatigue tests, seems too low to induce a sensitive decrease of mechanical properties of steels with yield strength between 400 and 500 MPa, or also 800 MPa (considering the mechanical properties of the skin layer of TempCore rebars). This behaviour is confirmed by the fractographic analysis performed after the low fatigue test. In fact, the most part of investigated samples have revealed only ductile fracture mode in their fracture surface (see, for example, Fig.7.20). In some cases, brittle areas and secondary cracks have been highlighted, but no correlation have been found with their grades, ductility class and hydrogen content (Fig.7.21). Moreover, it is worth noting that low-cycle fatigue tests impose high deformation on samples and, after the fracture onset, it can induce a heavy compression load between the two just opened halves of fracture that, locally, can induce the rubbing of the as-formed fracture surfaces (see Fig.7.22 and Fig.7.23). This can limit the surface area effective for the fractographic investigations.

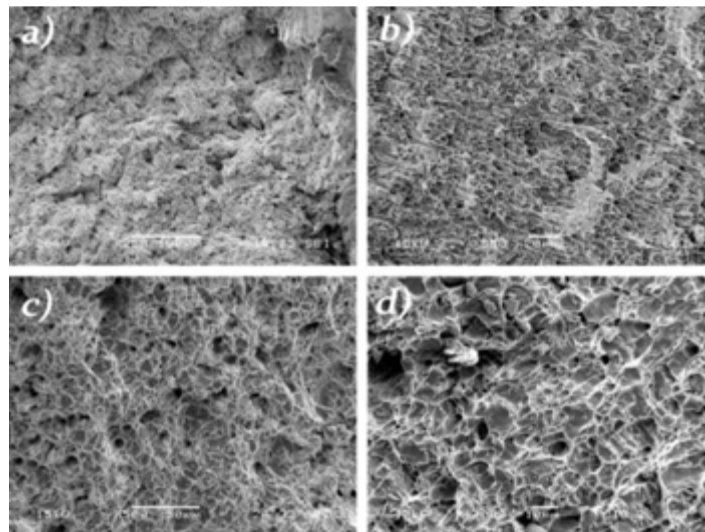


**Figure 7. 20:** Fractographs of bars after LCF test: a) B450C-16-TEMP, b) B500B-16-TEMP, c) B450C-12-STR, d) B500A-12-CW.

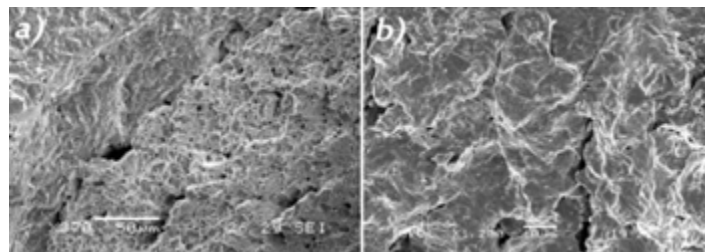


**Figure 7. 21:** Fractographs of rebars after LCF test showing secondary cracks: a) B450C-12-STR, b) B 500A-12-CW.

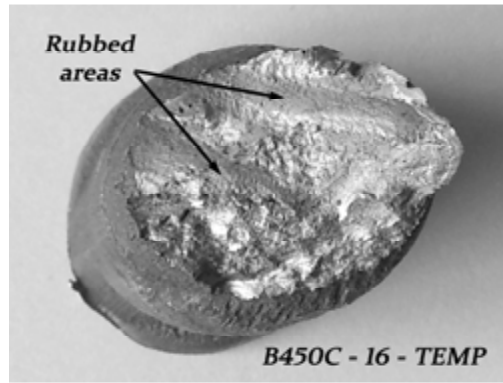


Figure 7.22: Picture of the fracture surface of a B450C – 16 – TEMP sample after LCF test showing rubbed areas.

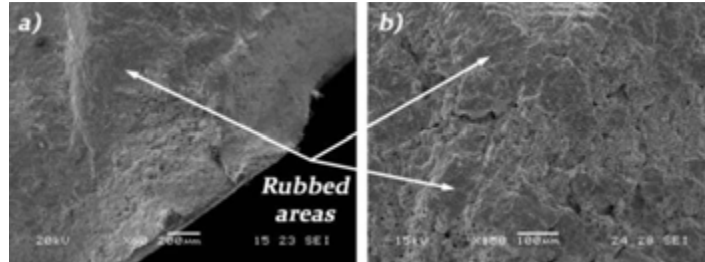


Figure 7.23: Fractographs of rebars samples after low-cycle fatigue test showing presence of rubbed areas. a) B 450 C – 16 TEMP, b) B 500 B – 12 STR.

### 7.2.5 Considerations on the results of LCF tests on corroded bars

In the figure 7.24, the dissipated energy per cycle is presented for steel reinforcing bars B400C (tested by UniPI), diameter 16mm (TempCore process), for the two free lengths considered and for imposed deformation equal to  $\pm 2.5\%$  and  $\pm 4.0\%$ . The values of mass loss were around 2.40%, with the two exceptions of specimens 3.4 (4.34%) and 3.12 (0.36%); the above mentioned differences in the corrosion attack were not directly related to a different LCF behaviour: as an example, in the case of  $L_0=6\phi$  (HDC), specimens n° 3.6 and 3.7 (imposed deformation equal to  $\pm 4.0\%$ ) showed a percentage difference in the mass loss of 30% (the values of the ratio  $\Delta M / M_{uncor}$  were respectively equal to 3.2% and 2.3%), but the number of complete cycles before failure was, in both cases, equal to 8 and the following dissipated energy 334 and 322 MPa, respectively; analogous considerations were executed for higher levels of imposed deformation and free length equal to 8 diameters (figure 7.24b). No specific correlation were individuated between the values of mass loss and the corresponding density of dissipated energy, and specimens characterized by high differences between mass loss (up to 30%) presented a similar LCF behaviour.

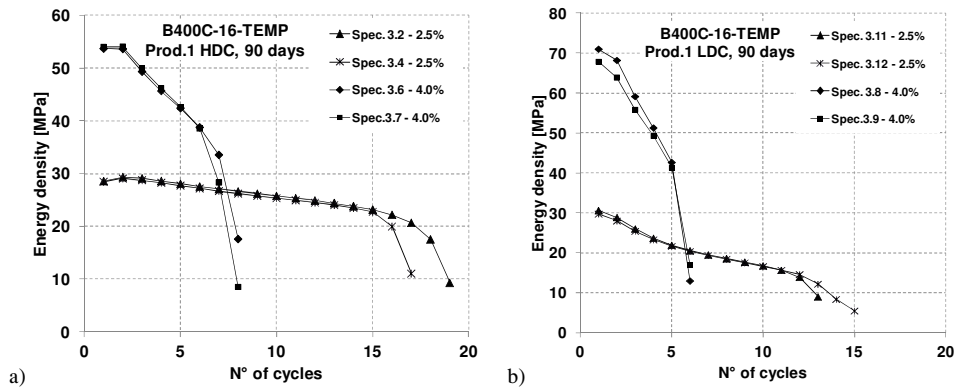


Figure 7.24: Dissipated energy for cycles, corroded steel bars B400C-16-TempCore: a) HDC, b) LDC (UniPI).

In the case of steel grade B400C-16-MA (Prod. 2, tested by UniPI), despite some differences in the dissipated energy per cycle, a more stable behaviour of the uncorroded specimens was evidenced, considering both the two different free lengths and the imposed deformation (Figure 7.25). Values of mass loss generally varied between 5.0% and 11.0% and in general, the lower total dissipated energy was associated to the higher levels of mass loss (Figure 7.26), even if no big differences were evidenced.

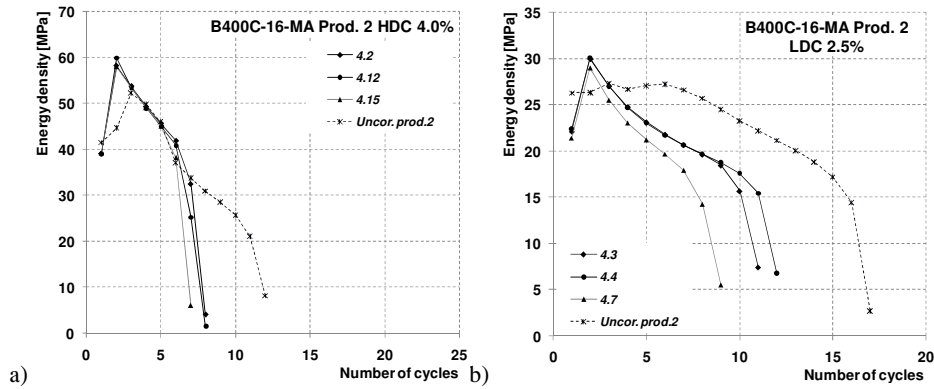


Figure 7.25: Dissipated energy for cycles, corroded steel bars B400C-16-MA: a) HDC 4.0%, b) LDC 2.5% (UniPI).

Similar considerations can be executed also for steel grades B450C and B500B (diameter 16 mm, TempCore process, Figure 7.27), with a more stable behaviour (in terms of dissipated energy per cycle and number of cycles up to failure). Values of mass loss due to exposition in salt spray chamber generally varied between 6 and 10% for B450C and between 5 and 8% for B500B; the comparison in terms of total dissipated energy vs mass loss are presented in the figures 7.28.

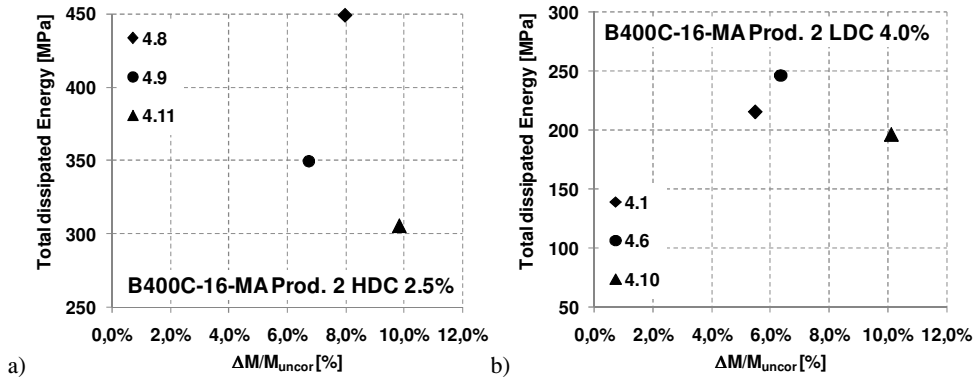


Figure 7.26: Total dissipated energy vs mass loss, corroded steel bars B400C-16-MA: a) HDC 4.0%, b) LDC 4.0%.

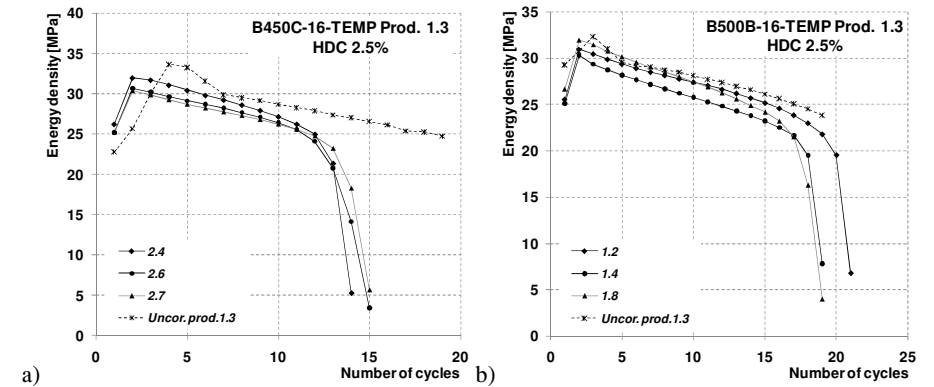


Figure 7.27: Dissipated energy for cycles, corroded steel bars a) B450C-16-TEMP HDC 2.5%, b) B500B-16-TEMP HDC 2.5%.

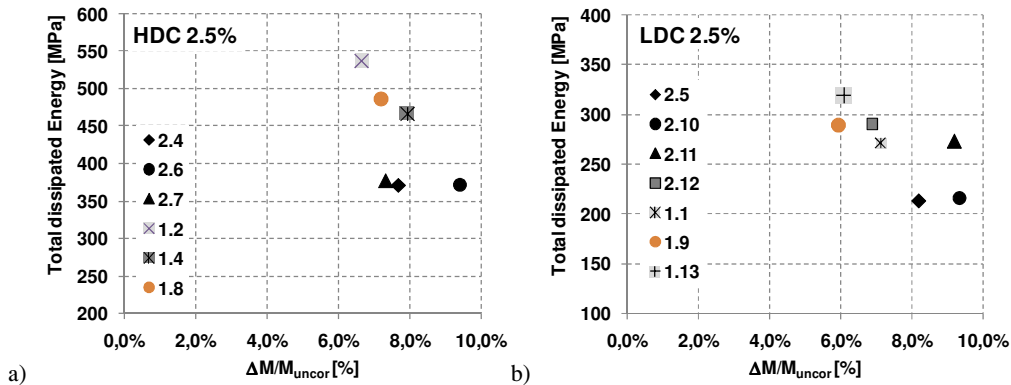


Figure 7.28: Total energy vs mass loss, corroded bars B450C-16-TEMP and B500B-16-TEMP: a) HDC 2.5%, b) LDC 2.5%.

Considering steel reinforcing bars B450C-12-STR, a more evident correlation between mass loss and the ductile behaviour of steel bars was individuated: corroded samples characterized by higher values of the mass loss ratio were associated, in general, to a more brittle behaviour, lower values of the dissipated energy and lower complete cycles executed. The behaviour of specimens 9.6 and 9.19 under imposed deformation equal to  $\pm 3.0\%$  was similar, in terms of number of cycles before failure and total density of dissipated energy, corresponding also to comparable values of mass loss, respectively equal to 42 and 30 mg/mm. The same considerations can be executed also for the specimens tested under imposed deformation equal to  $\pm 4.0\%$  (n° 9.14 and 9.18). Some differences were revealed between specimens 9.1 and 9.7, subjected to an imposed deformation equal to  $\pm 2.5\%$ : as visible from figure 7.29a, specimen 9.7, characterized by higher mass losses (28.94% against 5.84% of specimen 9.1) showed a more brittle behaviour, resulting in a total dissipated energy of 362.3 MPa versus the 529.3 MPa of sample 9.1 (the corresponding number of cycles before failure was respectively equal to 16 and 20, even if failure was not reached after 20 cycles by specimen 9.1).

Some considerations can be also executed about specimens B500A, diameter 12mm (Cold Worked process). In this case, only one test for each level of imposed deformation was executed, and consequently no specific remarks can be made about the relationship between dissipated energy and mass loss. On the other hand, as visible from the figures 7.29, the behaviour of rebars under increasing levels of deformation, considering both the adopted free lengths, evidenced a progressive degradation, translated in a progressive lower number of complete cycles before failure. As an example the behaviour was very stable for deformation levels of about 1.0-1.5%, resulting in total density of dissipated energy respectively equal to 135 and 277 MPa for  $L_0=6\phi$  and 150 and 226 MPa for  $L_0=8\phi$ , with 20 cycles always completed. On the other hand, for high levels of imposed deformation, only few cycles were completed: for example, in the case of HDC the total number of cycles was respectively equal to 4 and for  $\pm 4.0\%$  and  $\pm 5.0\%$ , with corresponding dissipated energy equal to 169 and 102 MPa. Similar considerations can be executed also in the case of LDC (figure 7.29b).

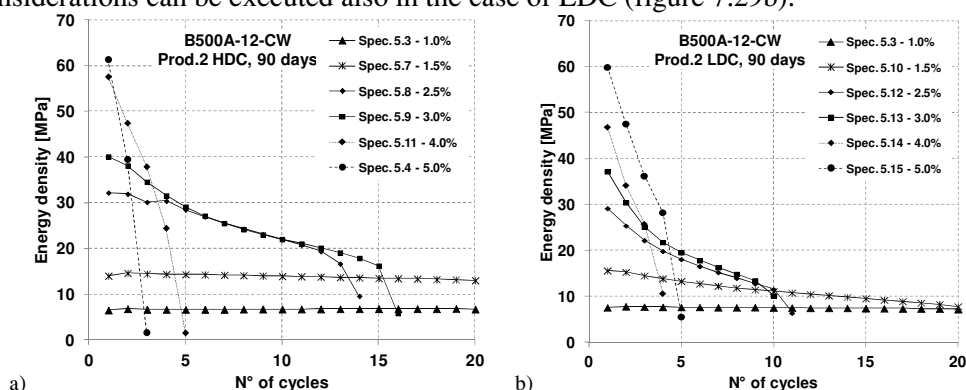


Figure 7. 29: Dissipated energy /cycle, corroded steel bars B500A-12-Cold Worked: a) HDC, b) LDC.

Similar results were obtained also from tests executed at UPA laboratory. In the figures below the diagrams obtained from steel bars of diameter 12 mm for the three grades are presented; the effects of strain, free length and corrosion time can be clearly individuated.

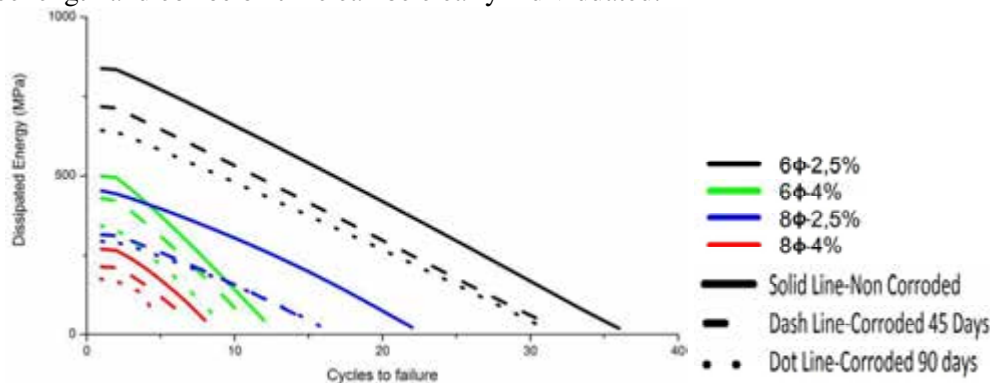
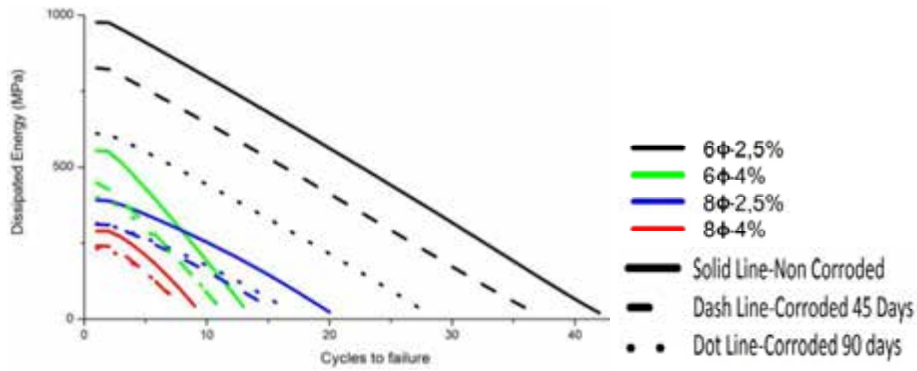
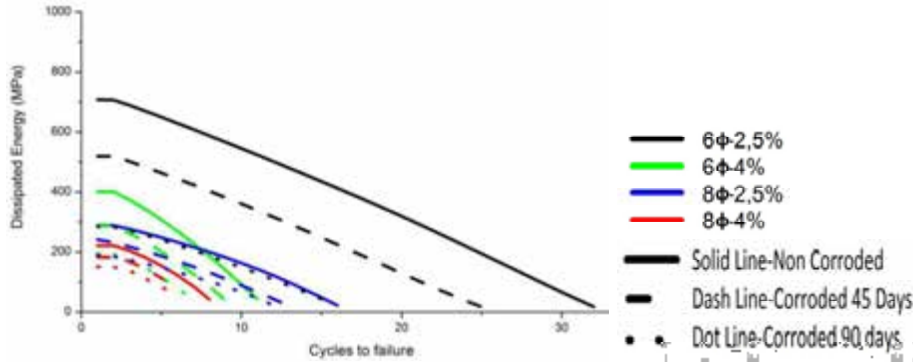


Figure 7. 30: Dissipated energy /cycle vs n° of cycles for B450C-12-STR (Prod. 1), tested by UPA.



**Figure 7.31:** Dissipated energy /cycle vs n° of cycles for B500B-12-STR (Prod. 1), tested by UPA.



**Figure 7.32:** Dissipated energy /cycle vs n° of cycles for B500A-12-CW (Prod. 2), tested by UPA.

Moreover, SEM and EDX analyses were executed on corroded specimens. It was evidenced that the exposure in salt spray chamber for 45/90 days caused important degradation in the structural properties of all materials resulting in brittle fracture. In all fracture surfaces holes and impurities were observed (for example figures 7.33, 7.34). In the SEM images, crack initiations along the samples located in the martensitic zone were visible. Also inside the crack Mn and regions of MnS were identified, and detailed studies were executed, since apparently crack initiation site varies from surface to subsurface depending on original position of the MnS inclusions (Figure 7.35). A more detailed description of the SEM results is reported in the deliverable D.4.3.

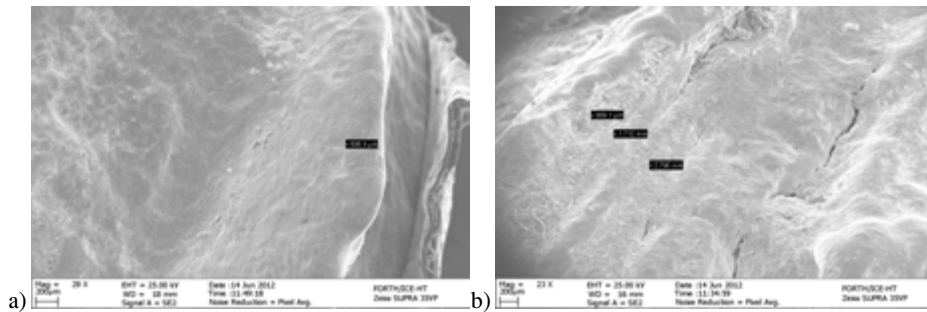


**Figure 7.33:** B450C-16-TEMP (Prod.1) with 34.66% martensite under LCF  $\pm 2.50\%$ , a) Failure initiation at the edges (45 days) b) Creases and cracks «ripples» from the top of the cross-section towards the bottom of the fracture surface (45 days).

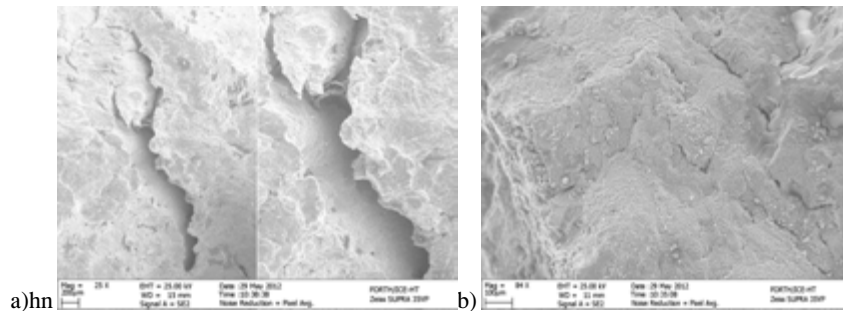


**Figure 7.34:** B500B-12-STR 90 days corroded, without martensite under LCF  $\pm 2.50\%$ , strain controlled with 6Φ gauge length. The study of the fracture surfaces of 90 days pre-corroded samples shows the appearance of cracks (not grown in the outer surface) oblique on the near perimeter (a), and other cracks starting from outside surface (the perimeter) and penetrate (b).

As a consequence of what obtained from experimental tests and metallurgical investigations, the following failure mechanism due to cyclic loadings can be individuated:

- Corrosion causes internal pitting of MnS particles. They follow their original particle congregation prior to pitting. The pitting has significant surface dimension while it is expected that the damage extends in depth.
- Upon loading these locations act as internal stress concentration leading eventually to the formation of cracks. However due to their proximity they force a multiple cracking phenomenon. As such crack coalescence will become critical with the number of loading cycles leading to fast crack growth. The direction of the crack appears to tend to expand towards the surface taking advantage of the free surface effect.
- This rapid expansion of the crack produces brittle ridge-like fracture surface negating any remaining ductility left in the material. Yet pits which are not congregate in a similar way (single MnS particles) will produce some sort of quasi brittle LCF surface.
- Buckling appeared from the first loading cycles, creating increasing tension on a single side of the rebar. The process was so strong as to produce rapid ductility exhaustion (hardening plateau) and therefore pits within this region propagated into cracks without any significant ductility signs in their crack path.
- The fracture surface of the rebar can be considered a mixture of more than 2 failure mechanisms which due to their nature produced in nature a mainly brittle type failure with limited signs of traditional LCF. Due to buckling and buckling reversal, the material's ductility especially at 4% is particularly limited and can be exhausted prior to the formation of the cracks..
- From a Fracture Mechanics perspective the case postulates void growth analysis according to Dugdale's theory.
- When cyclically stresses, MnS sites will host crack nucleation leading to sub-surface crack propagation. The case becomes very complex in terms of analysis, especially under fully reverse loading and high plastic strain levels leading to buckling. In this case, all slip planes (dislocation accommodation planes) will be engaged leading to premature ductility exhaustion. As such the martensitic zone will fracture following a semi-ductile appearance. Debonding of the martensitic zone is possible under the case when the agglomeration of the MnS inclusions/micro-cracks are positioned close to the interfacial zone. In such case, crack coalescence, being the result of crack growth, could lead to crack of the interfacial circumference (appearing as debonding).

### **7.3 Definition of Corrosion Damage Indicators (CDI) for each type of corrosion induced damage previously classified**

The corrosion phenomena on reinforcing steel in concrete have been classified in relation to the exposure classes given in EN 1992-1-1. It can be derived that mass loss (corrosion rates and erosion rates respectively) is a valid CDI for both types of corrosion:

- Uniform corrosion due to carbonation
- Local (pit) corrosion due to chloride ingress

Furthermore the pit depth related to local corrosion and the hydrogen absorption subsequent to the above described two corrosion types are possible candidates for CDI, in the following deeply analyzed. In Gräfen (1980) the influence of absorbed hydrogen on mechanical performance was studied for sensitive quenched and tempered prestressing steels. These results can be used so far, because some reinforcing steels are made by TempCore production technology which leads to a quenched and tempered martensitic microstructure in the outer layer of the steel. Figure 7.35a shows for different nominal tensile strength levels the drop of ductility (elongation at rupture) depending on hydrogen contents.

The relevance of hydrogen content for the performance of reinforcing steels under low cycle fatigue loads can be estimated with results presented by Riecke (1978) . In the figure 7.35b the results of a study to the influence of the strain rate after hydrogen absorption (high hydrogen activities) on the elongation are presented for a quenched and tempered prestressing steel. With increasing strain rate the elongation values in solution (hydrogen absorption conditions) converges to the values of the elongation

of the CERT-Test in air. The strain rates used for low cycle fatigue tests ranges from  $10^{-3}$  to  $10^{-2}$  [1/s]. According to figure 7.35b a loss of elongation of about 20% was observed for such strain rates.

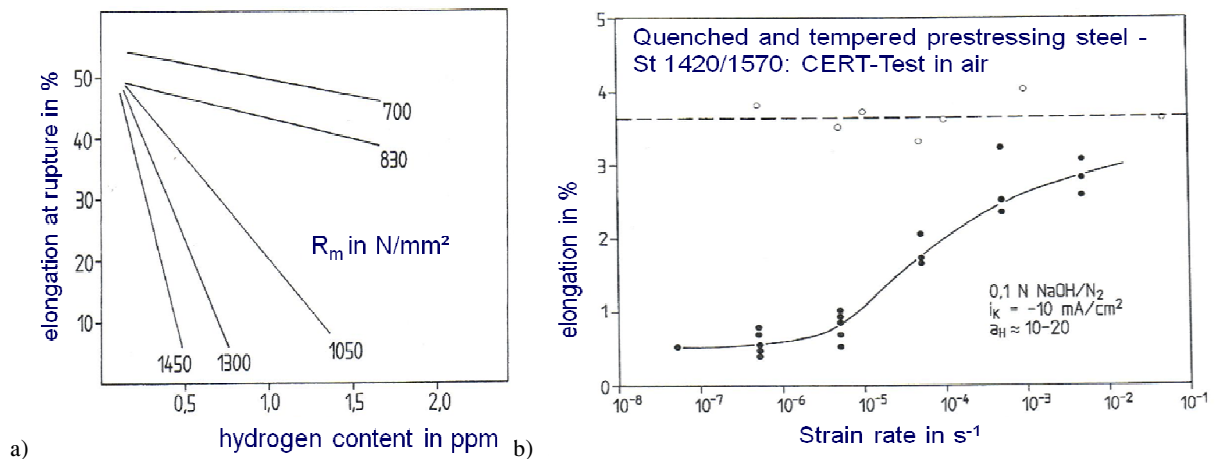


**Figure 7.35:** a) Influence of hydrogen content on different steel types and b) Influence of strain rate after hydrogen absorption on elongation.

The other possible damage indicator is the pit depth of the reinforcing steel. Chloride induced corrosion causes damages to the surfaces (pitting holes) which can be compared from their mechanical effect to notches. A notch depth of about 0.5 mm causes a loss of elongation at fracture of about 30 % (curve 2) for a very sensitive high strength quenched and tempered prestressing steel.

The relation between exposure class XS3, corrosion erosion depth due to chloride induced corrosion and notch depth was studied in Rehm (1988). The results are presented in figure 7.36 and table 7.35.

**Table 7.35:** Degree of corrosion depending on exposure condition XS3 and an exposure duration of 30 years.

| Corrosion erosion depth - Uniform [mm] | Notch depth [mm] |
|--|------------------|
| $\ll 0,1$                              | $\ll 1$          |
| $\leq 0,2$                             | $< 1,5$          |
| $\leq 0,5$                             | $< 2$            |
| $\leq 3$                               | $< 3$            |

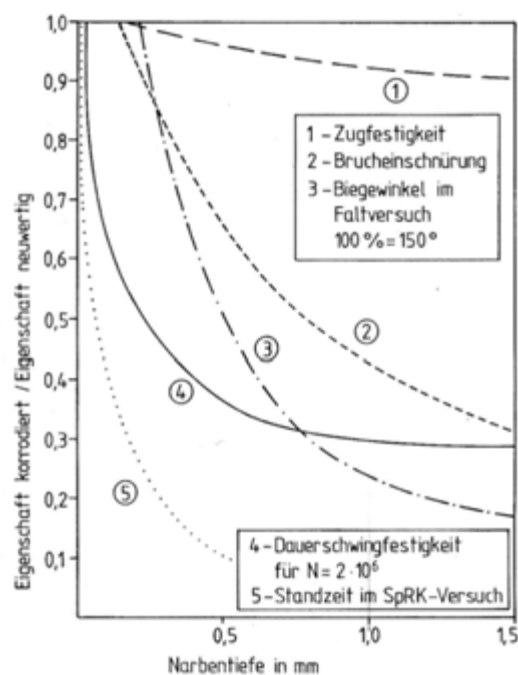


**Figure 7.36:** Influence of local corrosion on mechanical performance of high strength quenched and tempered prestressing steel.

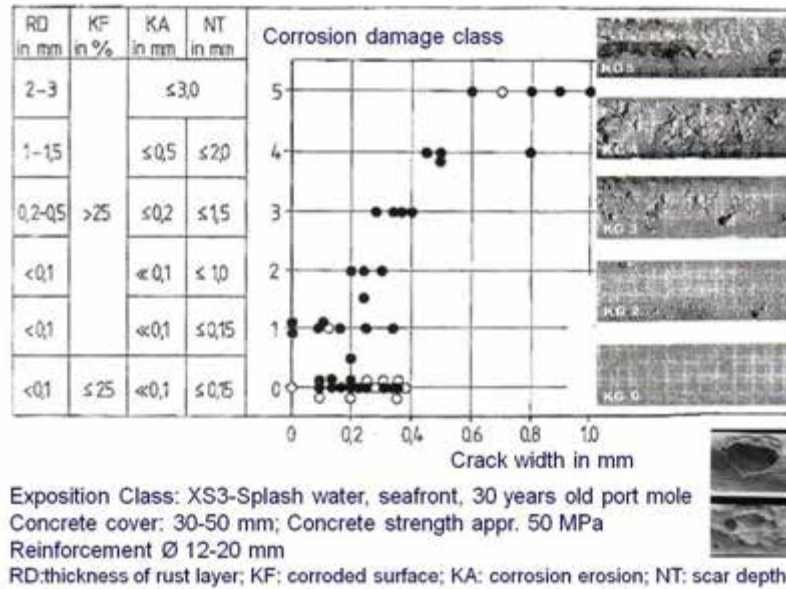


**Figure 7. 37:** Degree of corrosion depending on crack width for exposure condition XS3 and an exposure duration of 30 years. The evaluation of relevant corrosion damage indicators leads to the following result:

- For the analysis of the relation between CDI and Performance Indexes mass loss is the most appropriate damage indicator. Mass loss can be easily measured accurately and can be related through calculation to exposure classes and exposure durations.
- Using mass loss as damage indicator, it is necessary to distinguish between mass loss in circumstances where local corrosion (pitting corrosion) or uniform corrosion is probable.
- Hydrogen content seems to play no important role in static conditions but may be relevant to low cycle fatigue performance.

#### 7.4 Correlation between corrosion attacks intensity on existing buildings and increasing corrosion damaging levels obtained by accelerated corrosion tests – Corrosion Damage Indicators (CDI)

##### 7.4.1 Correlation of mass loss

The corrosion process of reinforcing steel in concrete is divided into two periods (figure 7.38). The initiation period is the time before the onset of corrosion. Within this period the carbonation front is moving towards the steel surface or the chloride concentration is rising to its critical value. The duration of this period is influenced strongly by concrete performance and exposure conditions. After critical corrosion conditions at the surface of the reinforcing steel are fulfilled, propagation period starts with the initiation of corrosion.

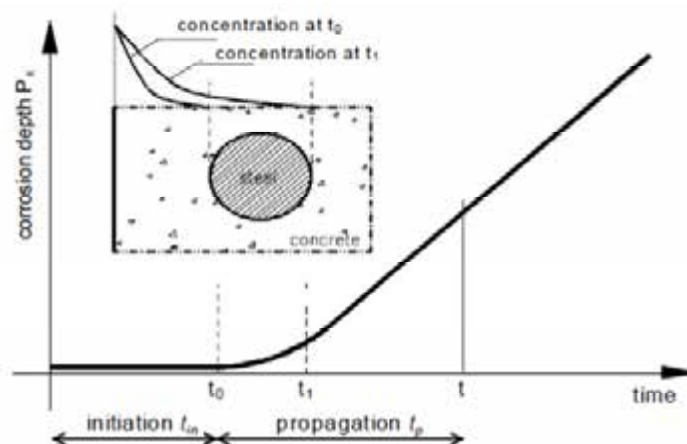


**Figure 7. 38:** Corrosion process over time

In the following only the propagation period is treated. To predict the initiation period, a lot of detailed information about the building, the concrete, the cover and the exposure conditions are required and

normally unique for every building. The classification of the corrosion phenomena in the propagation period according to paragraph 6 relates practical exposure classes to corrosion rates in  $\mu\text{m}/\text{year}$  and hydrogen activities. Corrosion rates can also be expressed in current densities according to equation 7.2:

$$c = \frac{V \cdot I \cdot t}{z \cdot F} \quad (7.2)$$

*c*: corrosion rates in  $\mu\text{m}/\text{year}$

*V*: molar Volume of Iron [ $7,10 \text{ cm}^3/\text{mol}$ ]

*I*: current [A]

*t*: time [s]

*z*: number of elektrons [2]

*F*: Faradays constant [ $1F = 96487 \text{ As/mol}$ ]

This leads to table 7.36. The relation between current densities and erosion rates are given. The current densities are suggested by Rodriguez et al. (2006). The calculated erosion rates are in good agreement with the results previously presented.

**Table 7. 36:** Suggested ranges for  $i_{\text{corr}}$  for exposure classes (shortly after corrosion initiation).

| Exposure class | Corrosion current density $i_{\text{corr}}$ in | Erosion rate in $\mu\text{m}/\text{year}$ |
|----------------|--|---|
| X0             | $\approx 0,01$                                 | 0,12                                      |
| XC1            | $\approx 0,01$                                 | 0,12                                      |
| XC2            | 0,1 – 0,5                                      | 1,16 – 5,8                                |
| XC3            | 0,05-0,2                                       | 0,58 – 2,32                               |
| XC4            | 0,01-0,5                                       | 0,12 – 5,8                                |
| XD1            | 0,1-0,2  | 1,16 – 2,32                               |
| XD2            | 0,1-0,5  | 1,16 – 5,8                                |
| XD3            | 0,5-5  | 5,8 – 58,1                                |
| XS1            | 0,5-5  | 5,8 – 58,1                                |
| XS2            | 0,1-1  | 1,16 – 11,6                               |
| XS3            | 1-10   | 11,6 - 116                                |

After the corrosion initiation has happened, the development of the corrosion rates over time is required for the mass loss calculation. The extreme case is that corrosion rates are constant over time. This approach could be used in cases where concrete strength is very low and only a very small concrete cover and/or significant cracks are present and the environmental conditions are supporting corrosion. In the case of a good concrete and a sufficient cover and only very small cracks (less than 0,1 mm) it is more likely that corrosion rates are decreasing due to e. g. diffusion resistance for ions away from the steel surface via the oxidation layer. According to Rodriguez et al. (1996) the corrosion current densities decrease significantly over time (see equation 7.3).

$$i_{\text{corr}(t)} = i_{\text{corr}(1)} \cdot 0,85 \cdot t^{-0,29} \quad (7.3)$$

$i_{\text{corr}(t)}$ : current density during the propagation period [ $\mu\text{A}/\text{cm}^2$ ]

$i_{\text{corr}(1)}$ : current density at the initiation time [ $\mu\text{A}/\text{cm}^2$ ]

*t*: time

Figure 7.39 exhibits the development of the specified corrosion rate  $c(t)/c(t_0)$  over the propagation period. After a corrosion period of about 10 years the curve converges towards a residual corrosion rate of about 20% of the initial corrosion rate immediately after corrosion initiation.

The results of the CDI mass loss of the accelerated corrosion tests can be correlated to practical corrosion conditions classified in the exposure conditions according to what already presented. The CDI mass loss is relevant to uniform and local corrosion phenomena.

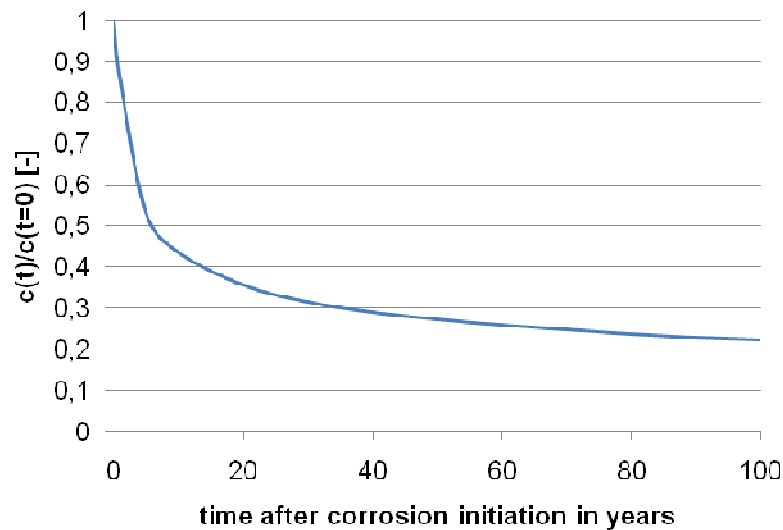


Figure 7.39: Development of corrosion rate over time (Rodriguez et al. 1996).

#### 7.4.2 Correlation of pit depth

It's necessary to distinguish between the local and uniform corrosion phenomena. In order to understand the relation between pit depth in accelerated salt spray test and pit depth in salt containing mortar (embedded samples – practical conditions), measurements of pit depth were carried out on the corroded samples. The results can be summarized as follows:

- The distribution of pit depth on an embedded bar can be approximated with a gamma function. For the salt spray tests not enough results were available to analyze the distribution function.
- The regression to calculate the 10% quantile value, estimated value (mean value) and 90% quantile value was estimated using a potency approximation (see figure 7.40).
- For the same mass loss only 20% of the mean pit depth of embedded samples was observed for the mean pit depth for salt spray samples in the range up to 5% mass loss (see figure 7.41).

It can be concluded that salt spray testing results in a more uniform corrosion attack than chloride induced corrosion under practical conditions. Thus, results of salt spray tests represent more carbonation induced corrosion and corrosion in cracked concrete (wider cracks). In the case of corrosion in uncracked concrete due to chloride attack one has to take into consideration that pit depth might be higher than in salt spray testing.

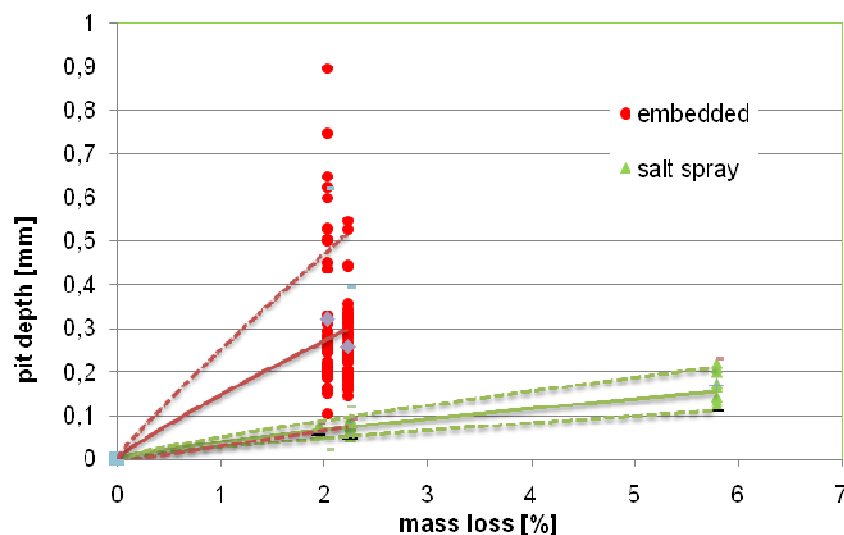


Figure 7.40: Pit depth depending on mass loss for embedded samples and salt spray samples



#### 7.4.4 Example for the correlation of CDI from accelerated corrosion tests to practical corrosion conditions

The mass loss results in the salt spray tests can now be translated into corrosion time under practical conditions using the equations 7.2 and 7.3. As an example the following case study is carried out:

- Nominal rebar diameter: 16 mm
- Mass loss in salt spray test: 5%
- Column in exposure condition XS2

| Class designation                               | Description of the environment | Informative examples where exposure classes may occur |
|---|--------------------------------|---|
| 4. Corrosion induced by chlorides from seawater |                                |   |
| XS2   | Permanently submerged          | Parts of marine structures                            |

- Practical corrosion rates and hydrogen activities for XS2

| Class designation                                | Degree of corrosion                                   | Hydrogen activity   |
|--|---|---|
| 4. Corrosion induced by chlorides from sea water |   |   |
| XS2  | Average erosion rates<br>10 $\mu\text{m}/\text{year}$ | 1-15 for: <ul style="list-style-type: none"> <li>• pH-value <math>\geq 12.6</math></li> <li>• critical chloride content for corrosion exceeded:</li> <li>• oxygen poverty: 10-100 mol Cl<sup>-</sup>/mol OH<sup>-</sup>,</li> <li>• oxygen saturation: 0.1-1 mol Cl<sup>-</sup>/mol OH<sup>-</sup></li> </ul> 5-45 for: <ul style="list-style-type: none"> <li>• pH-value <math>&lt; 12.6</math></li> <li>• critical chloride content for corrosion exceeded:</li> <li>• oxygen poverty: 10-100 mol Cl<sup>-</sup>/mol OH<sup>-</sup>,</li> <li>• oxygen saturation: 0.1-1 mol Cl<sup>-</sup>/mol OH<sup>-</sup></li> </ul> |

| Exposure class | Corrosion current density $i_{\text{corr}}$ in $\mu\text{A}/\text{cm}^2$ | Erosion rate in $\mu\text{m}/\text{year}$ |
|----------------|--|---|
| XS2            | 0,1-1  | 1,16 – 11,6                               |

- To calculate the duration until for exposure condition XS2 a mass loss of 5% is achieved the following assumptions are valid: For poor concrete, low concrete cover and/or cracked concrete the linear approach is used. For uncracked concrete the degressive approach according to equation 7.3 is used.

The results are:

- For the correlation of mass loss and corrosion time:

| Erosion rate in $\mu\text{m}/\text{year}$ | Time in years to reach a mass loss of 5% for the following conditions: |   |
|---|--|---|
|   | Poor concrete, low concrete cover and/or cracked concrete              | Uncracked concrete or only small cracks together with a good concrete and a sufficient concrete cover |
| Low: 1,16                                 | > 150  | > 150   |
| High: 11,6                                | < 20   | < 45  |

- The pitting depth can be expected according to 4.2 at 0,1 mm for poor concrete and 0,5 mm for uncracked concrete.
- The hydrogen concentration due to corrosion would be expected according to 4.3 at about 0,3 ppm. This value seems to be too high. A calculation of H-activity derived from literature data is given in the following table 7.37. The hydrogen activities measured for practical conditions (Vu and Stewart 2005) were in maximum for exposure class XS2  $a_{\text{H}}=45$ . The results of the hydrogen content measurements within this project are at least three times higher. This could be expected because of the testing protocol for salt spray chamber conditions which are aggressive. Therefore it is concluded that hydrogen concentration in practice are much lower and according to literature survey not relevant for the mechanical performance of reinforcing steel.

**Table 7. 37:** Hydrogen activities in salt spray tests

| Material                                 | Measured range of H-concentration in salt spray tests [ppm] | Derived H-activity [-]<br>$C_0=10^{-8}$ [mol H/cm <sup>3</sup> Fe] /2/ |
|--|---|--|
| Tempcore – Martensitic microstructure    | 0,5 – 1,1   | 156 to 859   |
| Micro-alloyed – Pearlitic microstructure | 0,2   | 156  |

## 7.5 Correlation of CDI and Classes of Exposure for buildings with the static and LCF PI's

### 7.5.1 Performance indicators for static performance - correlation of relevant PI's to CDI

All measured mechanical performance characteristics for static loading after corrosion ( $R_{e,corr}$ ,  $R_{m,corr}$ ,  $(R_m/R_e)_{corr}$ ,  $A_{gt,corr}$  and  $Z_{corr}$ ) have been related to the performance characteristics at delivery conditions (Ex.: res.  $A_{gt} = 100A_{gt,corr}/A_{gt,0}$  [%]). The most important PI for static loads is strain at maximum load  $A_{gt}$ . All other performance characteristics does not exhibit a significant decrease with increasing mass loss.

A strong reduction of  $A_{gt}$  was observed already for small mass losses. Another significant factor on the result is the nominal diameter. With increasing diameter the PI residual  $A_{gt}$  decreases less important with mass loss. Whereas for diameter 16 mm the mean value for residual  $A_{gt}$  is at a mass loss of 5% at about 50%, it is for diameter 25 mm at about 85% (see figures 7.43 and 7.44). The parameters ductility class and production type are playing also a role. There is the tendency that with increasing ductility the reduction of residual  $A_{gt}$  decreases less important with mass loss. The decrease of residual  $A_{gt}$  decreases less important with mass loss in the order MA (micro alloyed), T (Tempcore) and STR (stretched material). It needs to be taken into account that nominal diameter, ductility class and production type are partly linked parameters and not as independent as required for an ANOVA.

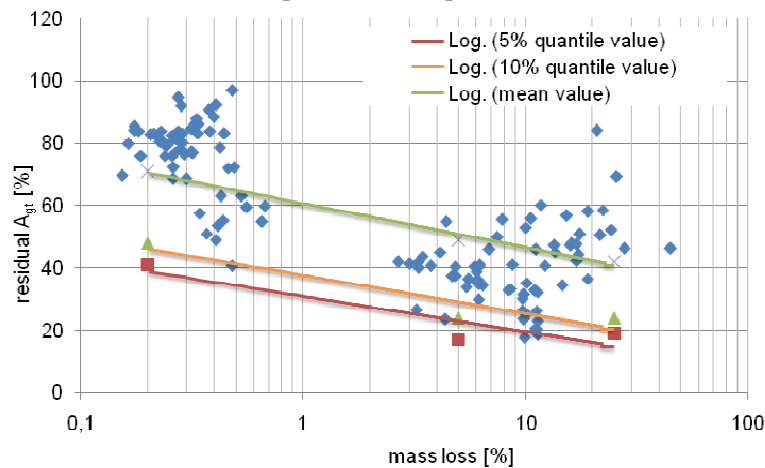


**Figure 7. 43:** Influence of mass loss on residual  $A_{gt}$  for nominal diameter 16 mm.

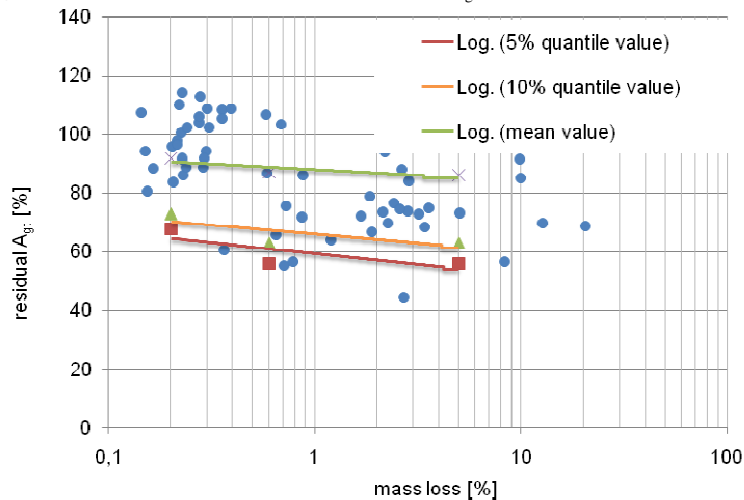


**Figure 7. 44:** Influence of mass loss on residual  $A_{gt}$  for nominal diameter 25 mm.

### 7.5.2 Performance indicators for LCF performance - correlation of relevant PI's to CDI

The nominated PI's for low cycle fatigue tests with corrosion are dissipated Energy (dE) for the cumulated number of load cycles till fracture of the sample or stop of test and the Number of cycles (N) till fracture or stop of the test. The results of the test programme can be summarized as follows:

- The most significant influence on number of cycles and dissipated energy is the strain followed by the free test length. The influence of corrosion is visible but not very significant on N and dE due to the large scatter of the mass loss results out of the salt spray tests.
- No influence was detectable for the other independent parameters Institute, nominal yield, nominal diameter, ductility class and production type.

For the next step of analysis the influence of strain and free test length is excluded. This is done via specified values for dE and N. The residual dissipated energy ( $100 \cdot dE(\text{corr})/dE(0)$  [%]) and the specified number of load cycles ( $N(\text{corr})/N(0)$  [-]) are now independent of strain and free test length and it can be derived that both PI's res. N and res. dE are strongly influenced by corrosion.

In order to estimate the PI's res. N and res. dE as a function of mass loss the following approximations are made:

- The mass loss is normal distributed in a mass loss range from 0 to 5% and from 5 to 10%.
- In these mass loss ranges res. N and res. dE are normal distributed

With these approximations the 5% and 10% quantile values for res. N and res. dE can be calculated and implemented in the diagram at the mean value for mass loss in the pre-defined mass loss range (Example: mass loss range from 5% to 10%: mean value for mass loss = 7,41 %; 5% quantile value for res. dE = 48,79%). The full set of data is given in the following table 7.38 and implemented in the figures 7.45 and 7.46. The PI's res. N and res. dE decrease more or less in the same slope with mass loss. A strong decrease at low mass loss values lower than 5% is followed by a flat slop for mass loss values higher than 5%. The residual performance at 8% mass loss is approximately at about 50%.

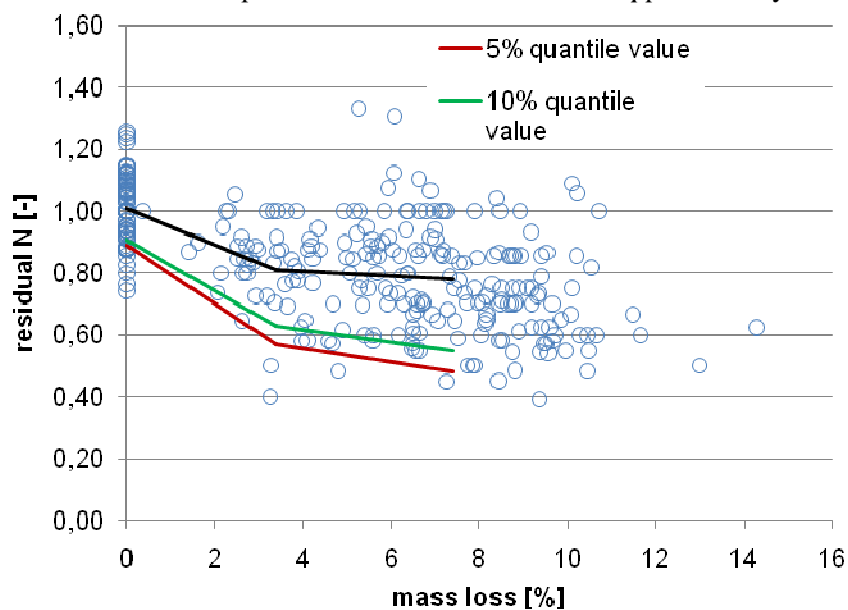


Figure 7. 45: Scatterplot for res. N versus mass loss and quantile slopes for res. N

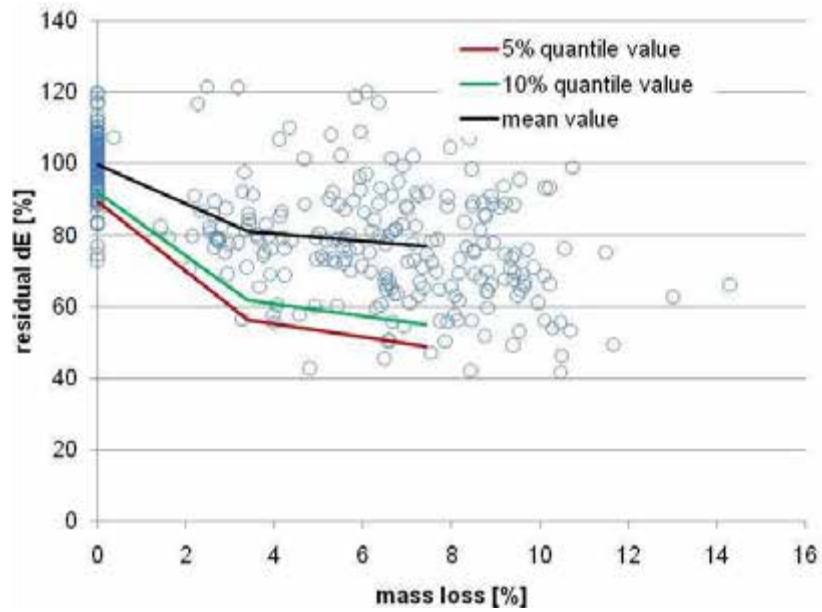


Figure 7. 46: Scatterplot for res. dE versus mass loss and quantile slopes for res. dE.

Table 7. 38: Evaluation of quantile values

| mass loss range [%] | Statistical value     | mass loss | res. N [-] | res. dE [%] |
|---------------------|-----------------------|-----------|------------|-------------|
| 0                   | Mean                  | 0         | 1,01       | 99,80       |
|                     | Standard deviation    | 0         | 0,07       | 6,24        |
|                     | Variation coefficient | 0         | 7,29       | 6,25        |
|                     | 5% quantile           | 0         | 0,89       | 89,53       |
|                     | 10% quantile          | 0         | 0,91       | 91,80       |
| 0 < m ≤ 5           | Mean                  | 3,39      | 0,81       | 81,04       |
|                     | Standard deviation    | 0,95      | 0,15       | 15,08       |
|                     | Variation coefficient | 28,04     | 17,93      | 18,61       |
|                     | 5% quantile           | 1,83      | 0,57       | 56,23       |
|                     | 10% quantile          | 2,17      | 0,63       | 61,71       |
| 5 < m ≤ 10          | Mean                  | 7,41      | 0,78       | 77,08       |
|                     | Standard deviation    | 1,36      | 0,18       | 17,20       |
|                     | Variation coefficient | 18,39     | 22,93      | 22,31       |
|                     | 5% quantile           | 5,17      | 0,48       | 48,79       |
|                     | 10% quantile          | 5,66      | 0,55       | 55,03       |

### 7.5.3 Correlation of PI's and CDI's with practical corrosion conditions

According to the results presented, the relevant PI's are:

- For static loads it is the strain at maximum load  $A_{gt}$  [%]
- For low cycle fatigue it is the dissipated Energy [MPa] and/or the number of load cycles [-] till fracture or stop of the test.

The relevant CDI is the mass loss [%]. The pit depth and the hydrogen concentration can be roughly estimated. In order to get more reliable results for the last both CDI's more results are required. The relation of CDI in laboratory tests to practical corrosion conditions is described in paragraph 7.4.4. Extending the example will lead to the following table 7.39. For a reinforced concrete building in exposure condition XS2 a mass loss of 5% is reached after approximately 45 years. The related 5% quantile values for res. N/res. dE is approximately 55% and for res.  $A_{gt}$  is approximately 25%. In other words: 95% of the reinforcing steel in this building in the defined condition will have a residual N/dE of 55% and a residual  $A_{gt}$  of 25% of the performance characteristics in the as produced condition. For a reinforcing steel with an initial  $A_{gt}$  of 10% the residual performance res.  $A_{gt}$  after a mass loss of 5% is about 2,5% and it will sustain at least 10 load cycles at a strain of 2,5%.

**Table 7. 39:** Relation of CDI and PI's to practical corrosion conditions.

| CDI - Nominal diameter: 16 mm  |   |   |                        |                                 |
|--|---|---|------------------------|---------------------------------|
| Time in years to reach a mass loss of 5% for the following conditions: |   |   |                        |                                 |
| Erosion rate in $\mu\text{m}/\text{year}$                              | Poor concrete, low concrete cover and/or cracked concrete | Uncracked concrete or only small cracks together with a good concrete and a sufficient concrete cover |                        |                                 |
| Low: 1,16  | > 150   | > 150   |                        |                                 |
| High: 11,6   | < 20  | < 45  |                        |                                 |
| PI's - Nominal diameter: 16 mm   |   |   |                        |                                 |
| mass loss [%]  | Mean value res. N [-]                                     | 5% quantile value res. N [-]  | Mean value res. dE [%] | 5% quantile value res. dE [MPa] |
| 5  | 0,8   | 0,55  | 80%                    | 55%                             |
| mass loss [%]  | Mean value res. $A_{gt}$ [%]                              | 5% quantile value res. $A_{gt}$ [%]   |                        |                                 |
| 5  | 50  | 25  |                        |                                 |

For each exposure condition according to EN 1992-1-1 and concrete strength, concrete cover and crack width the corrosion rate can be estimated according to table 7.38 Using the equations 7.2 and 7.3 it is possible to calculate for each pre-defined mass loss in salt spray test the duration in practice when the mass loss is reached under practical conditions. The mass loss in salt spray testing is related to the residual mechanical performance for static - and low cycle fatigue loads. Thus it is possible to predict mechanical performance depending on the degree of corrosion.

## 8. CONCLUSIONS

---

### 8.1 Exploitation and impact of the research results

According to what already presented in the introduction of the report, the main aim of *Rusteel* research project consists in the analysis of the combined effects of seismic action (low-cycle fatigue loading condition) and corrosion phenomena on the mechanical behaviour of reinforcing steel bars in r.c. and steel/concrete composite buildings.

This requires the individuation and the fully knowledge of the effective mechanical *capacity* of steel reinforcing bars under low-cycle fatigue in both uncorroded (reference) and corroded conditions and the following comparison with the ductility *demand* required by earthquakes to bars, opportunely investigated through the elaboration of numerical and experimental analyses (respectively for the case of r.c. and steel/concrete composite structures). The comparison between demand and capacity allows the elaboration of a procedure for the execution of LCF tests taking into account what really necessary for modern buildings in terms of ductility (i.e. strain and energy dissipation).

The main aim of the research project consequently correctly reflects what required by Mandate M115 (inside the revision of the European standard EN 10080), according to which a codified procedure for the execution of experimental LCF tests, able to reproduce the effective loading condition due to earthquake events, shall be elaborated. Nowadays in fact, only few European standards for reinforcing steels (i.e. Spanish, Portuguese and Polish codes) introduce a protocol for the execution of LCF tests on bars, but the testing frequency, the free length adopted for the specimens and the required energy dissipation (in terms of number of cycles and imposed deformation) are different from one another and not based on an accurate scientific approach investigating the effective behaviour of r.c. and composite buildings under seismic action. Moreover, the real seismic behaviour of steel reinforcing bars (i.e. demand) is not widely described in the current literature, in which a lot of information are provided for the characterization of the cyclic behaviour of structural components and sub-assemblages but with very few details for what happens on bars.

Finally, despite several information regarding the mechanical monotonic behaviour of corroded TempCore steel reinforcing bars, only few experimental tests are presented in the current literature concerning the cyclic behaviour of corroded rebars, needing consequently further investigations to establish if corroded bars are still able to sustain what required by earthquakes.

Stating the actual scenario of European standards for reinforcing steels what provided by the current scientific literature for both demand and capacity of steel bars, the fundamental contributions given by the present research can be summarized in the following points:

1. for what concerns the *ductility capacity* of bars:
  - Individuation of a codified procedure for the mechanical characterization of the LCF behaviour of steel reinforcing bars, in agreement with the prescriptions imposed by Mandate M115.
  - Characterization of the LCF behaviour of the most common steel grades (MA, STR, TEMP and CW steels) and diameters (ranging from 8 to 25 mm) of reinforcing bars.
  - Elaboration of a protocol for the execution of accelerated corrosion tests in salt spray chamber aiming to reproduce the real effects of aggressive environmental conditions in modern buildings.
  - Individuation of the mechanical capacity of corroded steel reinforcing bars under both monotonic (tensile tests) and cyclic (LCF tests) condition.
  - Selection of the most significant damage index parameters (CDI - mass loss, necking, ecc.) and analysis of their correlation with the performance indicators (PI - mechanical properties like  $A_{gt}$ ,  $R_e$ ,  $R_m$ , dissipated energy and number of cycles up to failure).
  - Provision of simple prescriptions to prevent and limit corrosion of steel reinforcements in r.c. and composite structures, in addition to what already provided by Eurocodes.
2. for what concerns the *ductility demand* on bars:
  - Elaboration of a simplified model for the representation of the behaviour of steel reinforcing bars embedded in concrete, able to take into account the effects of relative slips between steel reinforcing bars and concrete, necessary when structures are subjected to cyclic loadings (i.e. seismic action) and easy to be implemented in common software.

- Individuation of the effective ductility demand on steel reinforcing bars (i.e. maximum deformation and total dissipated energy) due to earthquake events, evaluated through the execution of numerical analyses on r.c. structures (IDAs with opportunely selected accelerograms) and experimental tests on substructures for steel/concrete composite buildings.

In the following pages, a more detailed description of the protocol elaborated as codified procedure for the low-cycle fatigue mechanical characterization of steel reinforcing bars is provided. It's necessary to underline that the elaboration of a codified procedure for the execution of LCF tests on bars will have consequently an important role in the revision process of actual European standards: moreover, two of the partners involved in Rusteel project (UniPI with Prof. Salvatore and ISB with Dr. Moersch) are members of the commission *ECISS/TC104 "reinforcing and prestressing steel products"*, leading to the possibility of an immediate dissemination of the results obtained by the research project inside the European normative scenario.

Moreover, a critical analysis of the behaviour of corroded steel reinforcing bars under monotonic and cyclic condition is provided, in relation to the structural behaviour of r.c. and composite buildings, providing indication for the prevention of corrosion attack of reinforcements.

Finally, for the scientific dissemination of results, a lot of works regarding the individuation of the ductility demand on bars and on their mechanical capacity in uncorroded and corroded condition are under preparation or already presented for scientific journals and conferences. A list of papers based on Rusteel results is provided at the end of the present report.

## 8.2 Background document for the execution of LCF tests

The results of the investigations about *ductility demand* evidenced that steel reinforcing bars in modern buildings are subjected to two different stress-strain conditions, leading to the necessity of satisfying two main requirements in terms of ductility, respectively related to the monotonic and the cyclic LCF behaviour. In particular:

1. The first condition is characterized by high levels of deformation essentially in tension or in compression, with higher absolute values of the strain but low total dissipated energy, since no complete reversed tension/compression cycles are executed. An example of this situation is represented in the figure 8.1 (beams and columns of r.c. structures), consequently requiring enough ductility in terms of monotonic behaviour ( $PI - A_{gt}$ ).
2. The second condition is characterized by lower levels of absolute deformation but higher values of the total dissipated energy, due to the complete reversal of the tension/compression cycle. An example of this situation is presented in the figure 8.2, evidencing the requiring of enough ductility in terms of LCF behaviour ( $PI - dE$  or  $N_{cycles}$ ). In general, only few complete tension/compression cycles are executed

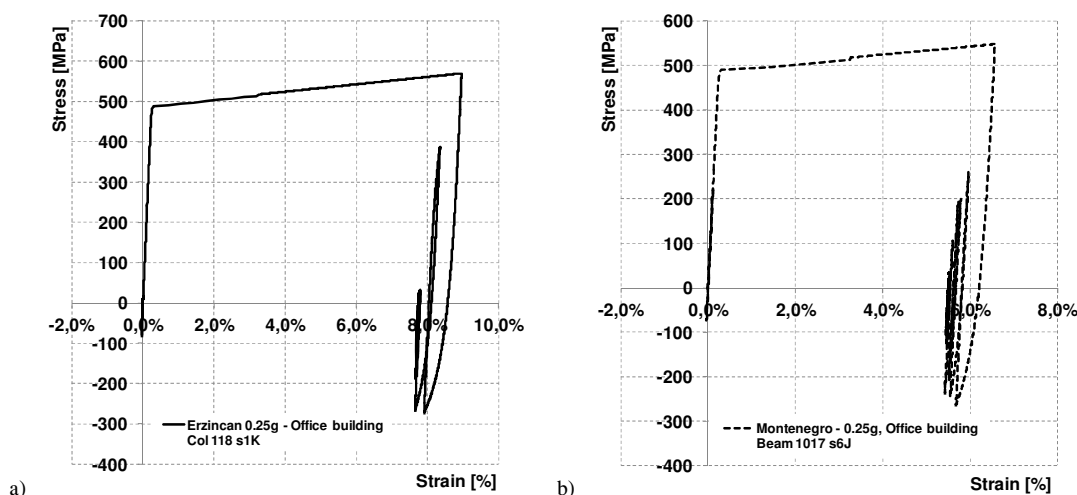
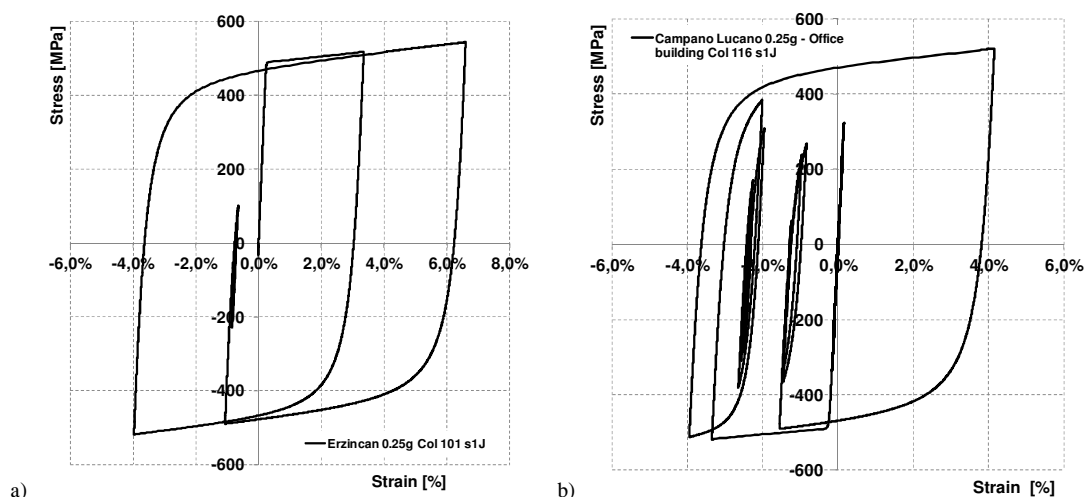


Figure 8. 1: Stress-strain histories on bars characterized by mainly tension or compression.



**Figure 8. 2:** Stress-strain histories on bars subjected to complete reversed tension/compression cycles.

As a consequence, to guarantee a ductile behaviour towards seismic actions steel reinforcing bars shall be able to satisfy:

- the ductile requirements in terms of  $A_{gt}$  prescribed by actual standards for different ductility classes, according to Eurocodes 2 and 8;
- the ductile requirements in terms of energy dissipation and number of cycles to failure, for which a specific protocol shall be elaborated on the base of results obtained, since not a unique experimental procedure is nowadays provided by standards.

The results coming from LCF tests on specimens evidence a dissipation of energy per cycle equal to 25-30 MPa for imposed deformation  $\pm 2.5\%$  and  $L_0=6\phi$  (HDC), value usually reached in the first cycles and followed by a progressive reduction due to degradation of the rebar and buckling phenomena. After the execution of 6 cycles the total dissipated energy is around 175 MPa for  $\phi 16$  mm, 154 MPa for  $\phi 20$  mm, 149 MPa and 158 MPa respectively for  $\phi 12$  mm and  $\phi 8$  mm (tables 1-4). In the case of experimental tests executed for  $L_0=8\phi$  (LDC) and imposed deformation  $\pm 2.5\%$ , the dissipated energy per cycle varies between 26 and 32 MPa; after 6 complete cycles, the average values of the total dissipated energy are 162 MPa ( $\phi 16$  mm), 146 MPa ( $\phi 20$  mm) and 130 MPa ( $\phi 12$  mm and  $\phi 8$  mm).

The results of IDAs on buildings in HDC evidence a maximum total dissipated energy equal to 124 MPa (columns) and 120 MPa (beams), while for residential building in MDC the maximum dissipated energy is equal to 72 MPa (columns) and 50 MPa (beams).

**Table 8. 1:** Dissipated energy after 6 cycles with  $\pm 2.5\%$  of imposed strain (16 mm) for HDC and MDC.

| Steel reinforcing bars diameter 16 mm: dissipated energy [MPa] | $L_0=6\phi$   | $L_0=8\phi$   |
|--|---------------|---------------|
|  | 6 cycles      | 6 cycles      |
| B400C-16-MA-R (Producer 2)                                     | 150,26        | 160,85        |
| B400C-16-TEMP-R (Producer 1)                                   | 161,26        | 140,59        |
| B450C-16-TEMP-R (Producer 1.1)                                 | 184,69        | 160,89        |
| B450C-16-TEMP-R (Producer 1.2)                                 | 164,83        | 170,68        |
| B450C-16-TEMP-R (Producer 1.3)                                 | 176,75        | 167,10        |
| B450C-16-TEMP-R (Producer 2)                                   | 190,52        | 161,65        |
| B500B-16-TEMP-R (Producer 1.1)                                 | 179,90        | 161,10        |
| B500B-16-TEMP-R (Producer 1.2)                                 | 191,96        | 180,14        |
| B500B-16-TEMP-R (Producer 1.3)                                 | 181,99        | 162,65        |
| B500B-16-TEMP-R (Producer 2)                                   | 171,35        | 159,43        |
| <i>Mean value [MPa]</i>  | <i>175,35</i> | <i>162,51</i> |

**Table 8. 2:** Dissipated energy after 6 cycles with  $\pm 2.5\%$  of imposed strain (20 mm) for HDC and LDC.

| Steel reinforcing bars diameter 20 mm: dissipated energy [MPa] | $L_0=6\phi$   | $L_0=8\phi$   |
|--|---------------|---------------|
|  | 6 cycles      | 6 cycles      |
| B400C-20-MA-R (Producer 2)                                     | 153,61        | 145,78        |
| B400C-20-TEMP-R (Producer 2)                                   | 146,07        | -             |
| B450C-20-TEMP-R (Producer 2)                                   | 167,64        | 189,64        |
| B500B-20-TEMP-R (Producer 2)                                   | 158,82        | 172,24        |
| <i>Mean value [MPa]</i>  | <i>153,61</i> | <i>145,78</i> |

**Table 8. 3:** Dissipated energy after 6 cycles with  $\pm 2.5\%$  of imposed strain (12 mm) for HDC and LDC.

| Steel reinforcing bars diameter 12 mm: dissipated energy [MPa] | $L_0=6\phi$   | $L_0=8\phi$   |
|--|---------------|---------------|
|  | 6 cycles      | 6 cycles      |
| B450C-12-STR-R (Producer 2)                                    | 153,61        | 138,39        |
| B500A-12-CW-R (Producer 2)                                     | 143,49        | 122,21        |
| <i>Mean value [MPa]</i>  | <i>148,55</i> | <i>130,30</i> |

**Table 8. 4:** Dissipated energy after 6 cycles with  $\pm 2.5\%$  of imposed strain (8 mm) for, HDC and LDC.

| Steel reinforcing bars diameter 12 mm: dissipated energy [MPa] | $L_0=6\phi$   | $L_0=8\phi$   |
|--|---------------|---------------|
|  | 6 cycles      | 6 cycles      |
| B450C-8-STR-R (Producer 1)                                     | 159,63        | 125,56        |
| B400C-8-TEMP-R (Producer 1)                                    | 159,59        | 120,46        |
| B500A-8-CW-R (Producer 1)                                      | 161,42        | 127,16        |
| B500A-8-CW-R (Producer 2)                                      | 132,92        | 113,01        |
| B500B-8-STR-R (Producer 1)                                     | 158,22        | 131,48        |
| B500B-8-TEMP-R (Producer 2)                                    | 173,14        | 159,77        |
| <i>Mean value [MPa]</i>  | <i>157,49</i> | <i>129,57</i> |

By comparing the mechanical *capacity* and the ductility *demand* on steel reinforcing bars in terms of dissipated energy equivalence, a protocol for the execution of low-cycle fatigue (LCF) tests has been elaborated: the procedure consists in the execution of 6 complete hysteretic cycles with imposed deformation equal to  $\pm 2.5\%$ , a free length of the tested specimens equal to 8 diameters (the most critical testing situation in terms of dissipated energy) and a testing frequency equal to 2.0 Hz or 0.5 Hz for large diameters. (table 8.5). According to what presented in Chapter 2 in fact, the values of the adopted testing frequency does not influence in a significative way the experimental results.

Finally, it's suggested to execute at least three tests for each steel grade/diameter/process.

**Table 8. 5:** Protocol for the execution of LCF tests on specimens.

|                     |  |                                 |
|---------------------|--|---------------------------------|
| Testing frequency   | 0,5÷2,0 Hz (in relation to the diameter) |                                 |
| Imposed deformation | $\pm 2.5\%$                              |                                 |
| Free Length         | 8 $\phi$                                 | <i>i.e. Low Ductility Class</i> |
| N° of cycles        | 6  |                                 |

### 8.3 Behaviour of corroded steel reinforcing bars: considerations and practical guidelines

The results of experimental tests on corroded specimens evidenced the high decrease of the mechanical properties of steel reinforcing bars, in all the cases of TempCore, Micro-Alloyed, Stretched and Cold Worked production processes, leading to the determination of the effective ductility capacity of corroded steel bars. Tests were executed considering both the monotonic and the low-cycle fatigue/seismic condition, according respectively to EN 15630-1:2010 and to the LCF protocol and already presented in Chapter 2. The results of the experimental tests on corroded rebars were deeply analyzed, as described in Chapter 7, individuating for both the monotonic and the cyclic behaviour of bars specific performance indexes (PI) to be related with the most significant corrosion damage indicators (CDI).

More in details, the following aspects were evidenced concerning the behaviour of corroded bars:

1) for the monotonic/tensile behaviour:

- The degradation of the mechanical properties in terms of ductility ( $A_{gt}$ ) is more significant than the decrease of the yielding and tensile strength ( $R_e$ ,  $R_m$ ).
- The decrease of the mechanical properties is directly related to the exposure time to aggressive environmental conditions, and consequently is directly connected to the corresponding mass loss, evaluated with reference to the exposed corrosion length.
- The ductile behaviour of corroded Micro-Alloyed steel reinforcing bars is higher than the one of TempCore rebars: the reduction of the  $A_{gt}$ , in relation to the mass loss, is lower in the case of MA steels than in the case of TEMP ones, leading to higher residual values of  $A_{gt}$ , also due to the fact that the initial "reference" behaviour is characterized by higher values of elongation to maximum load.
- The values of  $A_{gt}$  after 90 days of corrosion exposure evaluated for steel reinforcing bars of diameter 16 mm (medium diameter) are lower than the maximum levels of deformation according to the IDAs executed; obviously, bars have further capacities after the reaching of  $A_{gt}$ , as visible from the stress-strain diagrams obtained.
- The effects of the corrosion in terms of reduction of ductility ( $A_{gt}$ ) increase with the decrease of the diameter.
- The effects of the corrosion in terms of reduction of ductility ( $A_{gt}$ ) increase with the decrease of the exposure length: as visible in the case of bars B500A-CW diameter 12 mm, bars subjected to a more uniform corrosion (due to the dislocation of the cover wax during the salt spray chamber tests) are characterized by a more ductile behaviour, with higher residual values of the elongation to maximum load.
- The most critical condition is evidenced in the case of Cold Worked steel reinforcing bars (diameter 12 mm) in which higher levels of the mass loss are related to a strong reduction of the  $A_{gt}$ , with residual values in some cases lower than 1.0%.

2) for the low-cycle fatigue behaviour:

- The cyclic behaviour of uncorroded steel reinforcing bars is obviously more stable than the one of corroded specimens, with a more gradual decrease of the dissipated energy per cycle and an higher number of complete cycles executed before failure. This situation has been revealed for all the steel grades, processes (MA, TEMP, STR and CW) and diameters.
- The LCF behaviour of MA steel reinforcing bars appears more stable than the one of TEMP rebars, considering bars characterized by an equal yielding strength of 400 MPa.
- The degradation of the ductile cyclic behaviour of steel reinforcing bars ( $dE$ ,  $N_{cycles}$ ) is higher for higher levels of the mass loss.
- The degradation of the ductile cyclic behaviour of steel reinforcing bars is directly related to the increase of the imposed deformation: the higher is the strain, the lower is the ductile capacity of corroded bars in terms of dissipated energy and number of cycles up to failure.
- The effects of the corrosion in terms of reduction of ductility ( $dE$ ,  $N_{cycles}$ ) increase with the decrease of the diameter.

As a consequence of what already presented, the selected PI are:

- $A_{gt}$  [%] for static/monotonic loads
- dissipated Energy density [MPa] and/or the number of load cycles until fracture for LCF loads.

The relevant CDI is the mass loss [%], since pit depth and the hydrogen concentration cannot be easily estimated. The relation of CDI in laboratory tests to practical corrosion conditions, widely described in paragraph 7.4.4, allows the correlation between erosion rates and exposure conditions and the following estimation of the possible decrease of the mechanical properties of rebars (i.e. a sort of prediction of the mechanical performance of corroded bars), expressed through the selected PI.

Trying to summarize results of the experimental tests showed in Chapter 7, the worst condition is evidenced in the case of tensile tests (monotonic behaviour): the ductility demand related to the LCF behaviour (i.e. PI: dissipated energy,  $N_{cycles}$ ) does not represent the most critical situation, while the ductility monotonic demand (i.e. PI:  $A_{gt}$ ) is the most conditioning parameter for the mechanical characterization of the behaviour of corroded specimens.

For example, in the case of bars 16 mm, after an artificial exposition in salt spray chamber for 90 days, an average decrease of the PI  $A_{gt}$  equal to 55% was obtained (53% for B400C, 60% for B450C and 50% for B500B) for an average mass loss up to 15% for B400C, 10% for B450C and 24% for B500B.

The values obtained for  $A_{gt}$  are often lower than 5% for both ductility classes “C” and “B”; the same situation is individuated also in the case of specimens B500A (CW process, diameter 12 mm), for which the  $A_{gt}$  drops from initial values of about 6-7% to values between 0.80% and 5.10%, in relation to the mass loss and to a more localized or uniform corrosion.

The reduction of the  $A_{gt}$  is lower in the case of MA steel: in the case of specimens of diameter 16 mm the percentage decrease of  $A_{gt}$  is equal to 40%, while for bars of diameter 25 mm the reduction is around the 25%. The influence of corrosion phenomena on the monotonic behaviour of steel reinforcing bars has been widely explained in Chapter 7, and can be summarized in the Figure 8.3, in which is evident the progressive decrease of the residual ductility in terms of  $A_{gt}$  (PI) for increasing levels of mass loss (CDI).

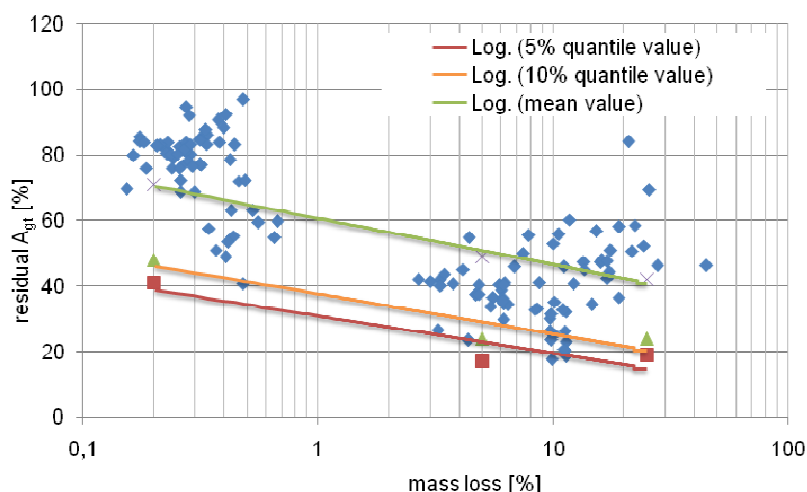


**Figure 8. 3:** Correlation between PI  $A_{gt}$  (for monotonic condition) and CDI mass loss for steel bars diameter 16 mm.

On the other hand, considering the LCF behaviour of corroded steel reinforcements, in the case of tests executed for low values of the imposed deformation ( $\pm 2.5\%$ ) no significant reduction of the total dissipated energy is revealed for bars of large diameter, while some modifications can be individuated in the case of smaller rebars, characterized by a lower number of complete cycles up to failure. The situation, on the other hand, is more critical in the case of higher levels of the imposed deformation, for which the number of cycles executed rapidly drops with a strong decrease of the total dissipated energy. The wide description of results obtained is presented in Chapter 7, while Figure 8.4 briefly summarizes what already presented for the total dissipated energy.

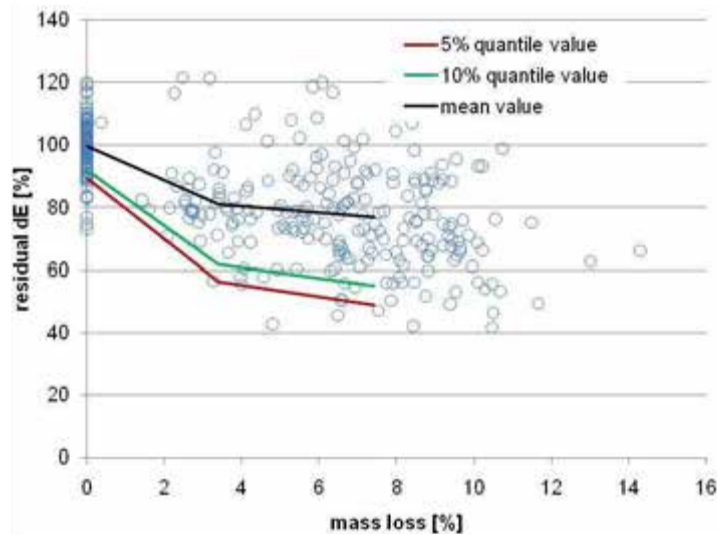


**Figure 8. 4:** Residual dissipation of energy (PI for cyclic condition) in relation to CDI mass loss.

What already presented about the results of mechanical tests on corroded steel rebars evidences the possible critical condition of steel reinforcing bars in buildings affected by different corrosion phenomena: rebars might be subjected to levels of imposed deformation higher than the ones they are able to sustain, requiring consequently further devices or design specifications in order to avoid the above described situation.

Considering for example the results of the Incremental Dynamic Analyses presented in Chapter 6 for r.c. structures, the level of strain due to real seismic inputs in some cases reaches values around 10% with average values equal to 6-7%.

In many cases, rebars are subjected to a complete reversed tension/compression cycle with imposed strain equal, for example, to +6.30% - 4.25%. Looking at the figures 8.5, the behaviour of corroded rebars (in this case steel grade B450C, diameter 16 mm) is compared with the results of analysis for steel reinforcements in one column or in one beam of the first floor; the maximum strains imposed by seismic event were respectively equal to about 11% and 9%, while the average  $A_{gt}$  of corroded rebars varied between 4.3% and 5.7% (manually measured values). Obviously, corroded rebars also presented a residual deformation capacity, as presented in the figures 8. 5, leading to values of the total elongation varying between 14% and 16%.

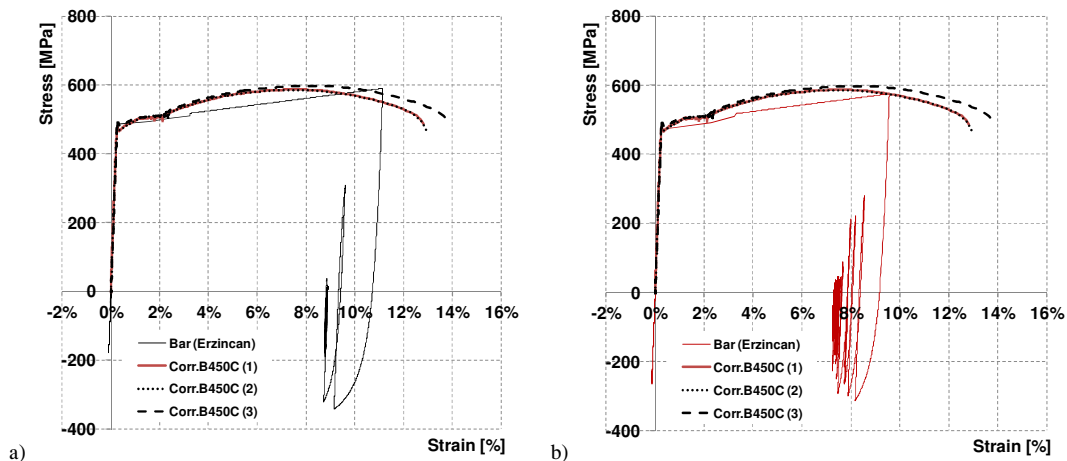


**Figure 8. 5:** Comparison between the ductility demand imposed by Erzincan time history on a) 1<sup>st</sup> floor column's bar and b) beam's 1<sup>st</sup> floor bar and monotonic behaviour of corroded steel reinforcements (bar B450C, diameter 16 mm).

As a consequence of what already discussed and in relation also to what presented about the relationship between Corrosion Damage Indicators (CDI) and Performance Indexes (PI's), some practical guidelines and recommendations can be provided for common applications and for designers, aiming to prevent corrosion attacks on steel reinforcing bars in new buildings in different exposure conditions.

In order to fully satisfy the seismic ductile requirements in exposure conditions with significant corrosion rates (i.e. XC2 to XC4, XD2 and XD3, XS1 to XS3) and to prevent damage due to aggressive

environmental conditions with the following degradation of the mechanical properties, the following indications, completing and improving what already presented in Eurocodes, are provided.

1. The strength of concrete used can be increase by (at least) one strength class or, similarly, the concrete cover can be increased by 5.0 mm maintaining the initial concrete strength class.
2. The crack width can be limited to 0.15 mm;

Moreover, the analysis executed using ANOVA evidenced that the influence of corrosion, in terms of mass loss, on the decrease of the elongation to maximum load generally decreases with the increase of the diameter (i.e. for higher diameters the effects of corrosion on the  $A_{gt}$  are lower). As a consequence, despite an accurate analysis of the effects of large diameter for what concerns the bond condition between steel and concrete, probably the adoption of higher diameters can be suggested (for example for a required reinforcement of 24cm<sup>2</sup> use 8 diameter 20mm instead of 12 diameter 16 mm).

Obviously, the higher are the initial values of ductility ( $A_{gt}$ ), the higher are the residual values after corrosion attack: for example this is what happens in the case of MA steels (both diameters 16 mm and 25 mm).

Finally, in the case of very aggressive environment perhaps additional measures are useful (i.e. coating of the surface of the concrete, cathodic protection, inspection systems with repair options).

#### 8.4 Dissemination

In the framework of the results obtained in Rusteel research project, the following papers were presented in International conferences, published on scientific journal and are, in some cases under preparation.

- A. Braconi, F. Braga, S. Caprili, R. Gigliotti, W. Salvatore “*Influence of low-cycle fatigue and corrosion phenomena on the ductile behaviour of steel reinforcing bars*”, COMPDYN 2013 4th ECCOMAS Thematic Conference on Computational Methods in Structural Dynamics and Earthquake Engineering, Kos Island, Greece, 12–14 June 2013.
- A. Braconi, F. Braga, S. Caprili, R. Gigliotti, W. Salvatore “*Ductility Demand on Steel Reinforcing Bars in Concrete Buildings*” 11<sup>th</sup> International Conference on Computational Structures Technology, Dubrovnik, 4-7 September 2012.
- A. Braconi, F. Braga, S. Caprili, R. Gigliotti, W. Salvatore “*Influence of low-cycle fatigue and corrosion phenomena on the structural behaviour of steel reinforcing bars*”, 15<sup>th</sup> World Conference on Earthquake Engineering, Lisbona, 24-28 Settembre 2012.
- A. Braconi, F. Braga, S. Caprili, R. Gigliotti, W. Salvatore “*Seismic demand on steel reinforcing bars in reinforced concrete frame structures*”, Bulletin of Earthquake Engineering (under review).
- A. Braconi, F. Braga, S. Caprili, R. Gigliotti, W. Salvatore “*Hardening slip model for reinforcing steel bars*”, Journal of Earthquake Engineering (under review)
- S. Caprili, W. Salvatore “*Corrosion effects on mechanical properties of steel reinforcing bars*”, under preparation.
- S. Caprili, W. Salvatore “*Low cycle fatigue behaviour of steel reinforcing bars in uncorroded and corroded conditions*”, under preparation.
- S. Caprili, W. Salvatore, J. Moersch, G.F. Pimenta, C. Apostolopoulos, M. Finetto, L. Bianco, C. Ascanio “*Corrosion effects on mechanical performance of steel reinforcing bars*”, under preparation.

## LIST OF FIGURES

- Figure I: a) Stress-strain curves for B500St rebars (Apostolopoulos 2006), b) relationship between exposure period and dissipated energy (Apostolopoulos and Michalopoulos 2006).
- Figure II: Simplified scheme of the adopted methodology.
- Figure III: Execution of experimental tensile (a) and low-cycle fatigue (b) tests on corroded specimens.
- Figure 1. 1: Different ductility levels (structure, element, material).
- Figure 1. 2: TempCore production process and cross-section of TempCore rebar.
- Figure 1. 3: a) Starting and b) advanced corrosion in bars due to carbonation of concrete (Schießl P., 1976).
- Figure 1. 4: Pitting corrosion due to a) low and b) high concentration of chlorides (Nürnberger U., 2005).
- Figure 1. 5: Effects of corrosion on bars: a) yielding, b) elongation (Apostolopoulos and Papadakis 2008).
- Figure 1. 6: Effects of corrosion on the LCF behaviour of bars (Apostolopoulos and Papadopoulos 2007).
- Figure 1. 7: Simplified scheme of the methodology adopted for the assessment of the seismic performance of steel bars.
- Figure 1. 8: Scheme of the methodology adopted for the assessment of the seismic capacity of corroded steel bars.
- Figure 2. 1: Typical microstructures present in a cross-section of B450C-16-TEMP-2.1Tempcore reinforcing bar, a) skin: tempered martensite, b) intermediate zone: bainite/ferrite mixture, and c) core: ferrite-pearlite.
- Figure 2. 2: a) Typical micro structural in a cross-section of B400C-16 (Prod. 2) Micro alloyed rebar: ferrite-pearlite.
- Figure 2. 3: Typical micro structural in a cross-section of B500B-8-STR (Producer 1) rebar: ferrite-pearlite.
- Figure 2. 4: a) Stress-strain curve from LCF tests on specimens B450C-Tempcore (producer 2) 16 mm, for imposed deformation equal to  $\pm 2.5\%$ , free length equal to 6 diameters and frequency equal to 0.05 and 2.0 Hz and b) Stress-strain curve from LCF tests on specimens B450C-Tempcore (producer 2) 16 mm, for imposed deformation equal to  $\pm 2.5\%$ , free length equal to 8 diameters and frequency equal to 0.05 and 2.0 Hz.
- Figure 3. 1: Geometrical schemes adopted for residential buildings.
- Figure 3. 2: Geometrical schemes adopted for office building.
- Figure 3. 3: Geometrical schemes adopted for commercial building.
- Figure 3. 4: Response spectra used for the desing of case studies in HDC and MDC to 0.25g (D.M.14/01/2008).
- Figure 3. 5: Tridimensional linear model for residential, commercial and office buildings case studies.
- Figure 3. 6: Scheme of elements' sections disposition for residential building in HCD (main frame).
- Figure 3. 7: Typical sections of beam and column elements in residential building in HDC.
- Figure 3. 8: Scheme of elements' sections disposition for residential building in MCD (main frame).
- Figure 3. 9: Typical sections of beam and column elements in residential building in MDC.
- Figure 3. 10: Schemes of elements' sections for commercial building (main frame yz, secondary frame xz).
- Figure 3. 11: Typical sections of beam and column elements in commercial building in HDC.
- Figure 3. 12: Scheme of elements' sections disposition for office building in HCD (main frame).
- Figure 3. 13: Typical sections of beam and column elements in office building in HDC.
- Figure 3. 14: a) Simplified scheme of non linear model with beam with hinges elements, b) BWH element.
- Figure 3. 15: Shift from axial stress-slip model to axial stress-fictitious strain model for steel reinforcements.
- Figure 3. 16: Simplified stress-strain relationship assumed for steel constitutive law.
- Figure 3. 17: Bond stress-slip relationship assumed for the modified slip model.
- Figure 3. 18: Bond stress-slip relationship and trilinear equivalent model.
- Figure 3. 19: Designed prototype structure: a) moment-resisting frame and designed structure; b) concrete slab plan view of the realized prototype at JRC and concentrically braced frame, c) main geometrical features of composite beams and columns.
- Figure 3. 20: Sub-assembly beam-column experimental set-up.
- Figure 3. 21: Instrumented frame of the full-scale structure at Ispra (considered interior joint B2-I of the internal frame).
- Figure 3. 22: Detail of tested internal joint of full scale structure at Ispra laboratory (B2-I).
- Figure 3. 23: Substructure of an interior joint (CJ1) tested at the University of Pisa.
- Figure 4. 1: Subdivision of time-histories in homogeneous classes: same magnitude range and geological local conditions.
- Figure 4. 2: a) Peak counting technique, b) Level crossing counting technique.
- Figure 4. 3: Range counting technique using rain-flow method.
- Figure 4. 4: Example of application of the rain flow counting technique.
- Figure 4. 5: a)  $N_{cycles}$  – PGA of input, b)  $N_{cycles}$  – max amplitude of acceleration cycles, c)  $N_{cycles}$  – epicentre distance, d)  $N_{cycles}$  – strong motion duration.
- Figure 4. 6: a) PGA – epicentre distance, b) Max amplitude of cycles – epicentre distance.
- Figure 4. 7: a) Correlation between PGA and maximum cycles amplitude, b) Correlation between maximum amplitude cycles and earthquake magnitude
- Figure 4. 8: Pushover analysis on residential building in HDC and trilinear equivalent SDOF system.
- Figure 4. 9: a) Base shear vs lateral top displacement under cyclic and monotonic pushover analyses; b) Comparison between the cyclic response of the SDOF model and the trilinear equivalent hysteretic model.
- Figure 4. 10: Park & Ang damage index vs PGA for significative acclerograms for residential building in HDC.
- Figure 4. 11: a) Horizontal components of the selected time histories (ESMD); b) Response spectra for the selected time histories (ESMD).
- Figure 5. 1: a) Capacity curves obtained for the different time histories (kN-mm), b) Interstorey drift profiles for the different time histories and for PGA equal to 0.30g.

Figure 5. 2: Numbering of beam and column elements for residential building in HDC.

Figure 5. 3: Progressive evolution of the structural behaviour of residential building in HDC for Campano earthquake.

Figure 5. 4: Progressive evolution of the structural behaviour of residential building in HDC for Montenegro earthquake.

Figure 5. 5: Progressive evolution of the structural behaviour of residential building in HDC for Erzincan earthquake.

Figure 5. 6: a) Capacity curves for the different time histories (kN-mm), b) Interstorey drift profiles for different levels of PGA

Figure 5. 7: Numbering of beam and column elements for commercial building in HDC.

Figure 5. 8: Progressive evolution of the structural behaviour of commercial building in HDC for Campano earthquake.

Figure 5. 9: Progressive evolution of the structural behaviour of commercial building in HDC for Montenegro earthquake.

Figure 5. 10: Progressive evolution of the structural behaviour of commercial building in HDC for Erzincan earthquake.

Figure 5. 11: a) Capacity curves obtained for the different time histories and from pushover (kN-mm), b) drift profiles.

Figure 5. 12: Progressive evolution of the structural behaviour of office building in HDC for Campano earthquake.

Figure 5. 13: Progressive evolution of the structural behaviour of office building in HDC for Erzincan earthquake.

Figure 5. 14: Progressive evolution of the structural behaviour of office building in HDC for Montenegro earthquake.

Figure 5. 15: a) Capacity curves for the different time histories and from pushover analysis, b) Interstorey drift profiles.

Figure 5. 16: Development of shear mechanisms in beams and columns for increasing levels of PGA (Campano Lucano).

Figure 5. 17: Development of brittle shear mechanisms in beams and columns for increasing levels of PGA (Montenegro).

Figure 5. 18: Development of brittle shear mechanisms in beams and columns for increasing levels of PGA (Erzincan).

Figure 5. 19: Progressive evolution of the structural behaviour of residential building in MDC for Campano earthquake.

Figure 5. 20: Progressive evolution of the structural behaviour of residential building in MDC for Montenegro earthquake.

Figure 5. 21: Progressive evolution of the structural behaviour of residential building in MDC for Erzincan earthquake.

Figure 5. 22: Modified slip model: shift from axial stress-slip law to trilinear hysteretic stress-fictitious strain relationship.

Figure 5. 23: Formulation of the Steel02 material in OpenSees (Mazzoni et al. 2007) for deformations around 2.2%.

Figure 5. 24: Schematization of output section and steel fiber.

Figure 5. 25: Stress-strain histories on bars for Campano earthquake: a) columns 1<sup>st</sup> floor, b) beam 1<sup>st</sup> level.

Figure 5. 26: Stress-strain histories on bars for Montenegro time history: a) columns 1<sup>st</sup> floor, b) beams 1<sup>st</sup> level.

Figure 5. 27: Stress-strain histories on steel bars for Erzincan time history: a) columns 1<sup>st</sup> floor, b) beams 1<sup>st</sup> level.

Figure 5. 28: Stress-strain histories on bars for Campano Lucano: a) column 1<sup>st</sup> floor, b) beams 1<sup>st</sup> level.

Figure 5. 29: Stress-strain histories on steel bars for Montenegro time history: a) columns 1<sup>st</sup> floor, b) beams 1<sup>st</sup> level.

Figure 5. 30: Stress-strain histories on bars for Erzincan: a) columns 1<sup>st</sup> floor, b) beams 1<sup>st</sup> level.

Figure 5. 31: Stress-strain histories on bars for Campano Lucano time history: a) columns 1<sup>st</sup> floor, b) beams 1<sup>st</sup> level.

Figure 5. 32: Stress-strain histories on bars for Montenegro time history: a) columns 1<sup>st</sup> floor, b) beams 1<sup>st</sup> level.

Figure 5. 33: Stress-strain histories on bars for Erzincan: a) columns 1<sup>st</sup> floor, b) beams 1<sup>st</sup> level.

Figure 5. 34: Stress-strain histories on bars for Campano Lucano time history: a) columns 1<sup>st</sup> floor, b) beams 1<sup>st</sup> level.

Figure 5. 35: Stress-strain histories on bars for Montenegro time history: a) columns 1<sup>st</sup> floor, b) beams 1<sup>st</sup> level.

Figure 5. 36: Stress-strain histories on bars for Erzincan time history: a) columns 1<sup>st</sup> floor, b) beams 1<sup>st</sup> level.

Figure 5. 37: a) time history used for PSD simulations, b) cyclic displacement history on CJ1 joint in Pisa.

Figure 5. 38: Correlation between shear force calculated and obtained from PSD tests.

Figure 5. 39: Agreement with peak results obtained from the two different test setup (PSD and cyclic tests).

Figure 5. 40: Comparison between joint's behaviour obtained from PSD tests on full scale structure ( joint B2-I) and from cyclic tests on single sub-assembly (joint CJ1).

Figure 5. 41: Component model of joint CJ1.

Figure 5. 42: Comparison between experimental and numerical results for joint CJ1.

Figure 5. 43: Strain history for steel reinforcing bars of interior joints.

Figure 5. 44: Stress-strain histories for steel reinforcing bars of interior joints.

Figure 6. 1: Simplified scheme for electrochemical tests.

Figure 6. 2: Details of the specimens used for impressed current density tests (El Maaddawy T.A. et al. 2003).

Figure 6. 3: Testing samples for accelerated corrosion tests following ASTM G109 (T. J. Wipf et al. 2006).

Figure 6. 4: Testing set up for accelerated corrosion tests following ASTM G109 (Al Hashemi 2007).

Figure 6. 5: Scheme of Rapid Macrocell accelerated corrosion test.

Figure 6. 6: Example of salt spray chamber.

Figure 6. 7: a) The tape between two successive ribs, b) the article without tape.

Figure 6. 8: a) Placing of the specimen inside the chamber, b) the articles on the salt spray chamber

Figure 7. 1: Rupture surfaces of bars a) B400C, 16 Micro Alloyed (prod. 2) and b) B400C, 16 TempCore (prod. 1).

Figure 7. 2: Rupture surfaces of bars a) B500B, 16 mm TempCore (prod. 1) and b) B460C, 16 mm TempCore (prod. 1).

Figure 7. 3: Decrease of a) elongation to maximum load and of b) total elongation at failure in relation to the mass loss for steel bars B500A-12-CW (Producer 2), after 45 and 90 days.

Figure 7. 4: Decrease of a) yielding strength and of b) tensile strength in relation to the mass loss for steel bars B500A-12-CW (Producer 2), after 45 and 90 days.

Figure 7. 5: Decrease of elongation to maximum load for steel bars a) B400C-16 TempCore (producer 1) and b) B400C-16 Micro Alloyed (producer 2).

Figure 7. 6: Decrease of Agt for steel Tempcore bars a) B450C-16 (prod. 1) and b) B500B-16 (prod.1).

Figure 7. 7: Decrease of a) Agt and b) A for steel bars B400C-25, Micro Alloyed process (Producer 2).

Figure 7. 8: Decrease of a) Agt and b) A for steel bars B450C-25, TempCore process (Producer 2).

Figure 7. 9: Decrease of a)  $A_{gt}$  and b)  $A$  for steel bars B500B-25, TempCore process (Producer 2).

Figure 7. 10: Effect of corrosion exposure on yield stress.

Figure 7. 11: a) Effect of corrosion exposure on Ultimate Tensile Strength. b) Normalized mass loss and ultimate tensile strength as a function of exposure.

Figure 7. 12: Effect of corrosion exposure on elongation to failure.

Figure 7. 13: a) Effect of corrosion exposure on Mechanical properties of B400C-16-TEMP (Prod.1), b) Effect of corrosion exposure on Mechanical properties of B450C-16-TEMP (Prod.1).

Figure 7. 14: Necking of testing articles taken from the as-received and 45 days exposure. mixture along with subsurface active corrosion sites.

Figure 7. 15: Depending on the depth of the segregation corrosion can lead to either a) crevice type corrosion, b) pitting and c) a mixture along with subsurface active corrosion sites.

Figure 7. 16: Cl- diffusion at sub-surface region of segregated inclusions after MnS dissolution.

Figure 7. 17: The presence of non-dissolved MnS inclusions negates the presence of Cl-.

Figure 7. 18: Side effects of MnS segregation sites subjected to extensive corrosion.

Figure 7. 19: Partial debonding of martensite zone due to MnS segregation. Both the shape of the zone as well as the ridges found at the top site indicate variation in ductility; b) high magnification of section A shows infinitesimal ductility variation with due to poor defined ridges left on the left side.

Figure 7. 20: Fractographs of rebars after LCF test: a) B450C-16-TEMP, b) B500B-16-TEMP, c) B450C-12-STR, d) B500A-12-CW.

Figure 7. 21: Fractographs of rebars after LCF test showing secondary cracks: a) B450C-12-STR, b) B500A-12-CW.

Figure 7. 22: Picture of the fracture surface of a B450C-16-TEMP sample after LCF test showing rubbed areas.

Figure 7. 23: Fractographs of rebars samples after low-cycle fatigue test showing presence of rubbed areas. a) B450C-16-TEMP, b) B500B-12-STR.

Figure 7. 24: Dissipated energy for cycles, corroded steel bars B400C-16-TempCore: a) HDC, b) LDC (UniPI).

Figure 7. 25: Dissipated energy for cycles, corroded steel bars B400C-16-MA: a) HDC 4.0%, b) LDC 2.5% (UniPI).

Figure 7. 26: Total dissipated energy vs mass loss, corroded steel bars B400C-16-MA: a) HDC 4.0%, b) LDC 4.0%.

Figure 7. 27: Dissipated energy for cycles, corroded steel bars a) B450C-16-TEMP HDC 2.5%, b) B500B-16-TEMP HDC 2.5%.

Figure 7. 28: Total energy vs mass loss, corroded bars B450C-16-TEMP and B500B-16-TEMP: a) HDC 2.5%, b) LDC 2.5%.

Figure 7. 29: Dissipated energy /cycle, corroded steel bars B500A-12-Cold Worked: a) HDC, b) LDC.

Figure 7. 30: Dissipated energy /cycle vs  $n^\circ$  of cycles for B450C-12-STR (Prod. 1), tested by UPA.

Figure 7. 31: Dissipated energy /cycle vs  $n^\circ$  of cycles for B500B-12-STR (Prod. 1), tested by UPA.

Figure 7. 32: Dissipated energy /cycle vs  $n^\circ$  of cycles for B500A-12-CW (Prod. 2), tested by UPA.

Figure 7. 33: B450C-16-TEMP (Prod.1) with 34.66% martensite under LCF  $\pm 2.50\%$ , a) Failure initiation at the edges (45 days) b) Creases and cracks «ripples» from the top of the cross-section towards the bottom of the fracture surface (45 days).

Figure 7. 34: B500B-12-STR 90 days corroded, without martensite under LCF  $\pm 2.50\%$ , strain controlled with  $6\Phi$  gauge length. The study of the fracture surfaces of 90 days pre-corroded samples shows the appearance of cracks (not grown in the outer surface) oblique on the near perimeter (a), and other cracks starting from outside surface (the perimeter) and penetrate (b).

Figure 7. 35: a) Influence of hydrogen content on different steel types and b) Influence of strain rate after hydrogen absorption on elongation.

Figure 7. 36: Influence of local corrosion on mechanical performance of high strength quenched and tempered prestressing steel.

Figure 7. 37: Degree of corrosion depending on crack width for exposure condition XS3 and an exposure duration of 30 years.

Figure 7. 38: Corrosion process over time

Figure 7. 39: Development of corrosion rate over time (Rodriguez et al. 1996).

Figure 7. 40: Pit depth depending on mass loss for embedded samples and salt spray samples

Figure 7. 41: Pit depth relation between embedded samples and salt spray samples

Figure 7. 42: Hydrogen concentration due to corrosion for salt spray samples (90 days)

Figure 7. 43: Influence of mass loss on residual  $A_{gt}$  for nominal diameter 16 mm.

Figure 7. 44: Influence of mass loss on residual  $A_{gt}$  for nominal diameter 25 mm.

Figure 7. 45: Scatterplot for res. N versus mass loss and quantile slopes for res. N

Figure 7. 46: Scatterplot for res. N versus mass loss and quantile slopes for res. dE

Figure 8. 1: Stress-strain histories on bars characterized by mainly tension or compression.

Figure 8. 2: Stress-strain histories on bars subjected to complete reversed tension/compression cycles.

Figure 8. 3: Correlation between PI  $A_{gt}$  (for monotonic condition) and CDI mass loss for steel bars diameter 16 mm.

Figure 8. 4: Residual dissipation of energy (PI for cyclic condition) in relation to CDI mass loss.

Figure 8. 5: Comparison between the ductility demand imposed by Erzincan time history on a) 1<sup>st</sup> floor column's bar and b) beam's 1<sup>st</sup> floor bar and monotonic behaviour of corroded steel reinforcements (bar B450C, diameter 16 mm).



## LIST OF TABLES

---

- Table 1. 1: Mechanical properties of rebars according to UNI EN 1992-1-1:2005 prescriptions.
- Table 1. 2: Steel grades and mechanical properties of steel reinforcements in European Countries.
- Table 1. 3: Production control tests prescribed by the different standards presented in Table 1.2.
- Table 1. 4: Indicative design working life (EN 1990:2006, table 2.1).
- Table 1. 5: Nominal Life ( $V_N$ ) for different kind of structures (D.M. 14/01/2008, table 2.4.I).
- Table 1. 6: Values for use coefficient  $C_U$  (D.M. 14/01/2008, table 2.4.II).
- Table 1. 7: Extracted from table 4.1 of EN 206-1-1:2005 for corrosion classes.
- Table 1. 8: Minimum concrete cover for bond requirements (EN 1992-1-1:2005, table 4.2).
- Table 1. 9: Indicative strength classes (Appendix E of EN 1992-1-1:2005, table E 1N).
- Table 1. 10: Recommended structural classification (EN 1992-1-1:2005, table 4.3N).
- Table 1. 11: Minimum values of  $c_{min,dur}$  for different exposure conditions (EN 1992-1-1:2005) for ordinary bars.
- Table 2. 1: Mechanical properties of steel reinforcing bars (table C.1 Annex C of EN 1992-1-1:2005).
- Table 2. 2: Mechanical properties of steel reinforcements according to Greek standard for reinforcements (ELOT 1421-3:2007), being  $R_e$  the yielding strength,  $R_m$  the tensile strength and  $A_{gt}$  the elongation corresponding to maximum load.
- Table 2. 3: Mechanical properties of steel reinforcements according to Italian standard for constructions (D.M.14/01/2008), in which  $f_{yk}$  and  $f_{tk}$  are the characteristic yield and tensile strength for a 5% fractile.
- Table 2. 4: Mechanical properties of steel reinforcements according to Spanish standard for steel reinforcements (UNE 36065 EX:2000), being  $R_e$  the yielding strength,  $R_m$  the tensile strength and  $A_{gt}$  the elongation corresponding to maximum load and  $A_5$  the ultimate elongation. In the following table: (1) characteristic value, (2) means that for the evaluation of stresses it is necessary to use the nominal section of bar, (3) real value obtained from tests.
- Table 2. 5: Mechanical properties of steel reinforcements according to Portuguese standard for steel reinforcements (LNEC E460:2008 and LNEC E455:2008), being  $R_e$  the yielding strength,  $R_m$  the tensile strength and  $A_{gt}$  the elongation corresponding to maximum load. In the following table: (1) minimum characteristic value referred to a 5% fractile, (1) minimum characteristic value referred to a 10% fractile and (3) maximum characteristic value referred to a 90% fractile.
- Table 2. 6: Mechanical properties of steel reinforcements according to British standard for reinforcement of concrete (BS 4449:2005), being  $R_e$  the yielding strength,  $R_m$  the tensile strength and  $A_{gt}$  the elongation corresponding to maximum load. In the following table: (a) means that the ratio  $R_m/R_e$  is equal to 1.02 for diameters below 8.0 mm and (b) characteristic  $A_{gt}$  is 2.0 for diameters below 8.0 mm.
- Table 2. 7: Mechanical properties of steel reinforcements according to French standard for steel rebars (NF A35-016-1:2007), being  $R_e$  the yielding strength,  $R_m$  the tensile strength and  $A_{gt}$  the elongation corresponding to maximum load. In the following table: (a) means  $R_m/R_e$  equal to 1.03 for diameter 5.0 mm, (b) means  $A_{gt}$  equal to 2.0 for diameter 5.0 mm, (c) means  $R_m/R_e$  equal to 1.05 for diameter 5.0 mm, (d) means  $A_{gt}$  equal to 4.0 for diameter 5.0 mm.
- Table 2. 8: Mechanical properties of steel reinforcements according to German standard (DIN 488-1:1984-09), being  $R_e$  the yielding strength,  $R_m$  the tensile strength and  $A_{gt}$  the elongation corresponding to maximum load. In the following table (c) means that  $R_m/R_e$  is equal to 1.03 and minimum  $A_{gt}$  is equal to 2.0 % for diameters between 4.0 and 5.5 mm
- Table 2. 9: Mechanical properties of steel reinforcements according to Bulgarian standard for rebars (BG 9252:2007), being  $R_e$  the yielding strength,  $R_m$  the tensile strength and  $A_{gt}$  the elongation corresponding to maximum load.
- Table 2. 10: Mechanical properties of steel reinforcements according to Romanian standard (STAS 438/1:1989), in which  $R_e$  is the yielding strength,  $R_m$  is the tensile strength and  $A_{tot}$  is the ultimate total elongation. Steel grade "OB 37" is a kind of carbon.
- Table 2. 11: Mechanical properties of steel reinforcements according to Serbian standard for reinforcing steel (JUS C.K6.020:1987).  $R_{eH}$  is the nominal values for yielding strength.
- Table 2. 12: Mechanical properties of steel reinforcements according to Algerian standard for reinforcing steel (1997), being  $R_{e,min}$  the minimum yielding strength,  $R_{m,min}$  the minimum tensile strength,  $A_{min}$  the elongation to maximum load.
- Table 2. 13: Mechanical properties of reinforcements according to Egyptian standard for reinforcing steel (262/1988), being  $R_{e,min}$  the minimum yielding strength,  $R_{m,min}$  the minimum tensile strength,  $A_{min}$  the elongation to maximum load.
- Table 2. 14: Summarizing table for mechanical properties of steel reinforcements in European and other countries.
- Table 2. 15: Experimental tests prescribed by actual standards for steel reinforcements' production control.
- Table 2. 16: Representative set of steel reinforcements selected for mechanical characterization.
- Table 2. 17: Measured bars properties.
- Table 2. 18: Measured bars properties (Micro Alloyed specimens), b) Typical micro structural in a cross-section of B500A-8-CW (Producer 2) rebar: ferrite-pearlite.
- Table 2. 19: Measured bars properties (Cold Worked specimens).
- Table 2. 20: Measured bars properties (Stretched specimens).
- Table 2. 21: Mechanical properties of tested rebars.
- Table 2. 22: Mean values of the mechanical properties of specimens of different diameters.
- Table 2. 23: Mechanical properties of specimens of different diameters tested by UPA's laboratory.
- Table 2. 24: Low-cycle Fatigue testing procedures according to UNE 36065 EX:2000 and LNEC E455:2008.
- Table 2. 25: Preliminary protocol for the investigation of strain rate influence on low-cycle fatigue behaviour.
- Table 2. 26: Experimental results of LCF tests for different values of testing frequency.
- Table 2. 27: Testing procedure for different diameters.

Table 2. 28: Experimental results of LCF tests on bars.

Table 2. 29: Experimental results of LCF on specimens tested by ISQ.

Table 2. 30: Experimental results of LCF on specimens tested by UPA.

Table 3. 1: Designed reinforced concrete case studies.

Table 3. 2: Loads acting on r.c. case studies.

Table 3. 3: Values of the q factors adopted for designed buildings.

Table 3. 4: Dimensions and height of structural elements for residential building in HDC.

Table 3. 5: Dimensions and height of structural elements for residential building in MDC.

Table 3. 6: Dimensions and height of structural elements for commercial building in HDC.

Table 3. 7: Dimensions and height of structural elements for office building in HDC.

Table 3. 8: Mean values of experimental test on B450C-TempCore rebars and assumed values for simplified model.

Table 3. 9: Assumed values for the bond stress-slip relationship in modified slip model.

Table 3. 10: Assumed values for the axial stress-slip model.

Table 3. 11: Nominal and actual steel and concrete material properties.

Table 4. 1: Earthquakes belonging to group 5 and analyzed with rain flow technique.

Table 4. 2: First set of analyzed time-histories.

Table 4. 3: Second set of analyzed time-histories.

Table 4. 4: Park and Ang Damage Index Performance (Oyarzo Vera 2006).

Table 4. 5: Trilinear equivalent system for residential building in HDC: values of forces and displacements.

Table 4. 6: ID number assigned to the considered accelerograms ( $PGA \geq 0.15$  g, soil type B and magnitude  $\geq 5.5$ ).

Table 4. 7: Park & Ang damage index vs PGA for selected time histories (residential building in HDC).

Table 4. 8: Park & Ang damage index vs PGA for selected time histories (residential building in MDC).

Table 4. 9: Park & Ang damage index vs PGA for selected time histories (commercial building in HDC).

Table 4. 10: Park & Ang damage index vs PGA for selected time histories (office building in HDC).

Table 5. 1: Selected time histories for non linear dynamic analyses.

Table 5. 2: Values of the interstorey drift for PGA equal to 0.30g.

Table 5. 3: Values of the interstorey drift for the considered time histories and different PGA levels.

Table 5. 4: Values of the interstorey drift for the considered time histories and different PGA levels.

Table 5. 5: Values of the interstorey drift for the considered time histories and different PGA levels.

Table 5. 6: Maximum and minimum strength and deformation and density of dissipated energy for steel bars of representative columns of residential building in HDC for Campano Lucano earthquake.

Table 5. 7: Maximum and minimum strength and strain and density of dissipated energy for steel bars of significative beams of residential building in HDC (Campano Lucano).

Table 5. 8: Maximum and minimum strength and deformation and density of dissipated energy for steel bars (Montenegro).

Table 5. 9: Maximum and minimum strength and deformation and density of dissipated energy for steel bars of beams of residential building in HDC for Montenegro earthquake.

Table 5. 10: Maximum and minimum strength and deformation and dissipated energy for steel bars for Erzincan earthquake.

Table 5. 11: Maximum and minimum strength and deformation and dissipated energy for steel bars of beams (Erzincan).

Table 5. 12: Max and min strength and deformation and dissipated energy for steel bars of beams (Campano Lucano).

Table 5. 13: Max and min strength and deformation and dissipated energy for steel bars of columns (Campano Lucano).

Table 5. 14: Max and min strength and deformation and dissipated energy for steel bars of columns (Montenegro).

Table 5. 15: Max and min strength and deformation and dissipated energy for steel bars of (Montenegro).

Table 5. 16: Max and min strength and deformation and dissipated energy for steel bars of columns (Erzincan).

Table 5. 17: Max and min strength and deformation and dissipated energy for steel bars of beams (Erzincan).

Table 5. 18: Max and min strength and deformation and dissipated energy for steel bars of columns (Campano Lucano).

Table 5. 19: Max and min strength and deformation and dissipated energy for steel bars of beams (Campano Lucano).

Table 5. 20: Max and min strength and deformation and dissipated energy for steel bars of columns (Montenegro).

Table 5. 21: Max and min strength and deformation and dissipated energy for steel bars of beams (Montenegro).

Table 5. 22: Max and min strength and deformation and dissipated energy for steel bars of columns (Erzincan).

Table 5. 23: Max and min strength and deformation and dissipated energy for steel bars of beams (Erzincan).

Table 5. 24: Max and min strength and deformation and dissipated energy for steel bars of columns (Campano Lucano).

Table 5. 25: Max and min strength and deformation and dissipated energy for steel bars of beams (Campano Lucano).

Table 5. 26: Max and min strength and deformation and dissipated energy for steel bars of columns (Montenegro).

Table 5. 27: Max and min strength and deformation and dissipated energy for steel bars of beams (Montenegro).

Table 5. 28: Max and min strength and deformation and dissipated energy for steel bars of columns (Erzincan).

Table 5. 29: Max and min strength and deformation and dissipated energy for steel bars of beams (Erzincan).

Table 6. 1: Reduced set of representative steel reinforcing bars subjected to accelerated corrosion tests.

Table 7. 1: Results of experimental tensile tests on corroded specimens B500A-Cold Worked, diameter 12 mm.

Table 7. 2: Results of experimental tensile tests on corroded specimens B400C TempCore, 16 mm (Prod. 1)

Table 7. 3: Results of experimental tensile tests on corroded specimens B450C TempCore, 16 mm (Prod. 1)

Table 7. 4: Results of experimental tensile tests on corroded specimens B500B TempCore, 16 mm (Prod. 1)

Table 7. 5: Results of experimental tensile tests on corroded specimens B400C Micro Alloyed, 16 mm (Prod. 2)

Table 7. 6: Results of experimental tensile tests on corroded specimens B400C Micro Alloyed, 25 mm (Prod. 2)

Table 7. 7: Results of experimental tensile tests on corroded specimens B450C TempCore, 25 mm (Prod. 2)

Table 7. 8: Results of experimental tensile tests on corroded specimens B500B TempCore, 25 mm (Prod. 2)

Table 7. 9: Results of experimental tensile tests on corroded specimens of diameter 12.0 mm (45 days of corrosion).

Table 7. 10: Results of experimental tensile tests on corroded specimens of diameter 16.0 mm (45 days of corrosion).

Table 7. 11: Results of experimental tensile tests on corroded specimens of diameter 25.0 mm(45 days of corrosion).

Table 7. 12: Results of experimental tensile tests on corroded specimens of diameter 12.0 mm(90 days of corrosion).

Table 7. 13: Results of experimental tensile tests on corroded specimens of diameter 16.0 mm(90 days of corrosion).

Table 7. 14: Results of experimental tensile tests on corroded specimens of diameter 25.0 mm(90 days of corrosion).

Table 7. 15: Results of experimental tensile tests on corroded bars.

Table 7. 16: Evaluation of the necking of corroded specimens after 45 days of exposure in salt spray chamber (UniPI).

Table 7. 17: Evaluation of the necking of corroded specimens after 90 days of exposure in salt spray chamber (UniPI).

Table 7. 18: Evaluation of the necking of uncorroded specimens (Producer 2) (UniPI).

Table 7. 19: Evaluation of necking of corroded and uncorroded specimens.

Table 7. 20: Corroded specimens subjected to Low Cycle Fatigue tests.

Table 7. 21: Mass loss and values adopted for the execution of LCF tests for bars B400C-16 MA, producer 2.

Table 7. 22: Experimental results of LCF tests on corroded specimen B400C-16-MA-R (producer 2).

Table 7. 23: Mass loss and values adopted for the execution of LCF tests for bars B450C-16 TempCore, producer 1.

Table 7. 24: Experimental results of LCF tests on corroded specimen B450C-16-TEMP-R (producer 1).

Table 7. 25: Mass loss and values adopted for the execution of LCF tests for B500B-16 TempCore, prod. 1 (90 days).

Table 7. 26: Experimental results of LCF tests on corroded specimen B500B-16-TEMP-R (producer 1).

Table 7. 27: Mass loss and values adopted for the execution of LCF tests for B400C-16 TempCore, prod. 1 (90 days).

Table 7. 28: Experimental results of LCF tests on corroded specimen B400C-16-TEMP-R (producer 1).

Table 7. 29: Mass loss and values adopted for the execution of LCF tests for bars B450C-12 Stretched, producer 1.

Table 7. 30: Experimental results of LCF tests on corroded specimen B450C-12-STR-R (producer 1).

Table 7. 31: Experimental results of LCF tests on corroded specimen diameter 12 mm.

Table 7. 32: Experimental results of LCF tests on corroded specimens diameter 16 mm.

Table 7. 33: Experimental results of LCF tests on corroded specimen tested by ISQ.

Table 7. 34: Hydrogen concentration values of samples of different corroded rebars after low-cycle fatigue tests.

Table 7. 35: Degree of corrosion depending on exposure condition XS3 and an exposure duration of 30 years.

Table 7. 36: Suggested ranges for icorr for exposure classes (shortly after corrosion initiation).

Table 7. 38: Evaluation of quantile values

Table 7. 39: Relation of CDI and PI's to practical corrosion conditions.

Table 8. 1: Dissipated energy after 6 cycles with  $\pm 2.5\%$  of imposed strain (16 mm) for HDC and MDC.

Table 8. 2: Dissipated energy after 6 cycles with  $\pm 2.5\%$  of imposed strain (20 mm) for HDC and MDC.

Table 8. 3: Dissipated energy after 6 cycles with  $\pm 2.5\%$  of imposed strain (12 mm) for HDC and MDC.

Table 8. 4: Dissipated energy after 6 cycles with  $\pm 2.5\%$  of imposed strain (8 mm) for, HDC and MDC.

Table 8. 5: Protocol for the execution of LCF tests on specimens.



## LIST OF MAIN ABBREVIATIONS

---

|                  |                                     |
|------------------|-------------------------------------|
| BGL              | Braga-gigliotti Laterza model       |
| BWH              | Beam with hinges                    |
| CDI              | Corrosion Damage Indicators         |
| CW               | Cold-Worked                         |
| DCH              | high dissipation                    |
| DCL              | low dissipation                     |
| DCM              | medium dissipation                  |
| DI <sub>PA</sub> | Park and Ang index                  |
| DL               | Damage Limitation limit state       |
| ESMD             | European Strong Motion Database     |
| HDC              | High Ductility Class                |
| IDA              | Incremental Dynamic Analysis        |
| LCF              | Low-Cycle Fatigue                   |
| LDC              | Low Ductility Class                 |
| LS               | Life Safety limit state             |
| MA               | Micro-Alloyed                       |
| MDC              | Medium Ductility Class              |
| MDOF             | Multi degree of freedom             |
| MRF              | Moment Resisting Frames             |
| PGA              | Peak Ground Acceleration            |
| PI               | Low-Cycle Fatigue Performance Index |
| PS               | partial strength                    |
| PSD              | Pseudo-Dynamic                      |
| Rebar            | Reinforcing Steel bar               |
| SDOF             | Single degree of freedom            |
| STR              | Stretched                           |
| TEMP             | TempCore                            |



## LIST OF REFERENCES

---

- Al Hashemi M., De Sanctis M., Salvatore W., Valentini R. (2007). Effects of corrosion induced damages on the tensile and fatigue properties of concrete reinforcing bars, *XII Convegno ANIDIS L'Ingegneria Sismica in Italia*, Pisa, 10-14 Giugno 2007.
- Apostolopoulos C.A. (2007). Mechanical behavior of corroded reinforcing steel bars S500s tempcore under low cycle fatigue, *Construction and Building Materials*, Vol. 21, pp.1447–1456.
- Apostolopoulos C.A., Michalopoulos D. (2006). Effect of Corrosion on Mass Loss, and High and Low cycle fatigue on reinforcements, *Journal of Materials Engineering and Performance*, Vol. 15, No. 6., pp. 742-749.
- Apostolopoulos C.A., Papadakis V.G. (2008). Consequences of steel corrosion on the ductility properties of reinforcement bar, *Construction and Building Materials*, Vol. 22, pp. 2316–2324.
- Apostolopoulos C.A., Papadopoulos M.P. (2007). Tensile and low cycle fatigue behavior of corroded reinforcing steel bars S400, *Construction and Building Materials*, Vol. 21, pp. 855–864.
- Apostolopoulos C.A., Papadopoulos M.P., Pantelakis Sp. G. (2006). Tensile behavior of corroded reinforcing steel bars BSt 500s, *Construction and Building Materials*, Vol. 20, pp. 782-789.
- ASTM B 117-94 (1995). Standard practice for operating salt (fog) testing apparatus. In: Annual book of ASTM standards, section 3, Metal test methods and analytical procedures, West Conshohocken, ASTM, Philadelphia, USA.
- ASTM G109 – 07 (2007). Standard Test Method for Determining Effects of Chemical Admixtures on Corrosion of Embedded Steel Reinforcement in Concrete Exposed to Chloride Environments
- Attolico A., Biondi S., Nuti C., Petrangeli M. (2000). Influence of buckling of longitudinal rebars in finite element modelling of reinforced concrete structures subjected to cyclic loading, Proceedings of the 12<sup>th</sup> World Conference on Earthquake Engineering, Auckland, New Zealand.
- B.S.4449/2009 + A2:2009 “Steel for reinforcement of concrete – Weldable reinforcing steel – Bar, coil and decoiled product – Specification”, 2009.
- Bandstra J. et al., "Modeling void coalescence during ductile fracture of a steel", *Materials Science & Engineering*, A336, pp. 269-281, 2004.
- BG 9252 :2007 “Steel for the reinforcement of concrete – Weldable reinforcing steel B500”, 2007.
- Bozorgnia Y., Bertero V.V. (2001). Improved damage parameters for post-earthquake applications, *Proceedings of SMIP02 Seminar on Utilization of Strong-Motion Data*, Los Angeles, CA, May 2, pp. 61-82.
- Braconi A., Salvatore W., Tremblay R., Bursi O. S. (2007). Behaviour and modelling of partial-strength beam-to-column composite joints for seismic applications. *Earthquake Engng Struct. Dyn.* 2007, Vol. 36, pp. 142:161.
- Braconi A., Salvatore W., Tremblay R., Bursi O. S. (2008). Seismic performance of a 3D full-scale high-ductile steel–concrete composite moment-resisting frame Part I:Design and testing procedure. *Earthquake Engng Struct. Dyn.* 2008, Vol. 37.
- Braconi A., Salvatore W., Tremblay R., Bursi O. S. (2008). Seismic performance of a 3D full-scale high-ductile steel–concrete composite moment-resisting frame—Part II: Test results and analytical validation. *Earthquake Engng Struct. Dyn.* 2008, Vol. 37, pp. 1635:1655.
- Braga et al. (2006). Analytical Stress–Strain Relationship for Concrete Confined by Steel Stirrups and/or FRP Jackets, *Journal of Structural Engineering*, ASCE, Vol. 132, pp. 1402-1416.
- Braga F. et al. (2004). Analisi della risposta in c.a. esistente, da sottoporre a prove sismiche di laboratorio, utilizzando differenti tecniche di adeguamento sismico, *XI Congresso Nazionale “L'ingegneria Sismica in Italia”*. 25-29 Gennaio, Genova, Italy.
- Brown J., Kunnath S.K. (2004). Low-Cycle Fatigue Failure of Reinforcing Steel Bars, *ACI Materials Journal*, Vol.101, No. 6, pp. 457:466.
- Bursi OS, Caramelli S, Fabbrocino G, Molina J, Salvatore W, Taucer F. 3-D full-scale seismic testing of a steel– concrete composite building at ELSA. Contract No. HPR-CT-1999-00059, Eur Report, European Community, Brussels, Belgium, 2004
- CEB-FIP Model Code 1990 Design Code (1993), Comité Euro-International du Béton.
- Coffin L.F. (1954). A study of the effect of cyclic thermal stresses in ductile metals, *Transactions of the ASME*, Vol. 76, pp. 931–950.
- Corrosion Mechanisms in Theory and Practice, Third Edition, CRC press, Philippe Marcus, 2012
- Cosenza E., Manfredi G. (2000). Damage indices and damage measures, *Progress in Structural Engineering and Materials*, Vol. 2, No. 1, pp. 50-59.
- Cosenza E., Manfredi G., Ramasco R. (1993). The use of damage functionals in earthquake engineering: a comparison between different methods, *Earthquake Engineering and Structural Dynamics*, Vol. 22, pp. 855-868.

- Cosenza E., Prota A., De Cicco F. (2008). Comportamento ciclico sperimentale di barre d'acciaio lisce, Convegno Reluis "Valutazione e riduzione della vulnerabilità sismica di edifici esistenti in c.a.", Roma, 29-30 May 2008.
- Crespi P. (2002). Monotonic and cyclic behaviour of rebars in the plastic hinge of r.c. beams, PhD Thesis.
- D. M. Infrastrutture Trasporti 14 gennaio 2008, Norme Tecniche per le Costruzioni NTC 2008.
- D'Amato M. (2008). Analytical models for non linear analysis of RC structures: confined concrete and bond-slips of longitudinal bars, PhD Thesis, University of Basilicata, 2008.
- Delgado R., Costa A., Arede A., Vila Pouca N., Guedes J., Romão X., Delgado P., Rocha P. (2008). Ongoing research on seismic safety assessment, *Bulletin of Earthquake Engineering*, Vol. 8, pp. 181–199.
- DIN 488-1:2008 "Betonstahl — Stahlsorten, Eigenschaften, Kennzeichnung", 2008.
- Dodd L.L., Restrepo-Posada J.I. (1995). Model for predicting cyclic behavior of reinforcing steel, *Journal of Structural Engineering*, Vol. 121, pp. 433-445.
- ECSC. Steel RTD programme—applicability of composite structures to sway frames. ECSC Contract No. 7210- PR-250, edited by Stangenberg H, European Commission, Brussels, Belgium, 2002.
- El Maaddawy T.A., Soudki K. A. (2003). Effectiveness of Impressed Current Technique to Simulate Corrosion of Steel Reinforcement in Concrete, *Journal of Materials in Civil Engineering*, Vol. 15, pp. 41-47.
- El Maaddawy T.A., Soudki K. A. (2003). Effectiveness of Impressed Current Technique to Simulate Corrosion of Steel Reinforcement in Concrete, *Journal of Materials in Civil Engineering*, Vol. 15, pp. 41-47.
- ELOT 1421-3:2008. Acciai di armatura calcestruzzo – Acciai saldabili – Parte 3° : Classe tecnica B500C. Organismo greco standardizzazione s.a. (in italian).
- EN 10080:2005, Steel for the reinforcement of concrete - Weldable reinforcing steel – General, European Committee for Standardization – CEN, 2005.
- EN ISO 15630-1:2010, Steel for the reinforcement and prestressing of concrete -- Test methods - Part 1: Reinforcing bars, wire rod and wire, 2010.
- European Commission (EC), M/115 rev.1 EN, Revised mandate M115 to CEN/CENELEC concerning the execution of standardisation work for harmonized standards on Reinforcing and prestressing (for concrete), Brussels May 26<sup>th</sup> 2009.
- Fajfar P. (2000). A non linear analysis method for performance based seismic design, *Earthquake Spectra*, Vol. 16, No. 3, pp. 573-592.
- Fajfar P., Fischinger M. (1988). N2 – A method for non linear seismic analysis of regular buildings, *Proceeding of Ninth World Conference on Earthquake Engineering*, August 2-9, Tokyo-Kyoto, Japan.
- Fardis M. (1995). Damage measures and failure criteria for reinforced concrete members, *Proceedings of the 10<sup>th</sup> European Conference on Earthquake Engineering*, Vienna, Rotterdam: Balkema, pp. 1377–1382.
- FEMA 356 (2000). Pre-standard and Commentary for the Seismic Rehabilitation of Buildings, Federal Emergency Management Agency, Washington DC.
- Gomes A., Appleton J. (1997). Nonlinear cyclic stress-strain relationship of reinforcing bars including buckling, *Engineering Structures*, Vol. 19, No. 10, pp. 822-826.
- Gräfen H. Wasserstoffinduzierte Rissbildung, S. 153-178; In: Grundlagenkursus Korrosion, DECHEMA, Frankfurt 1980
- Hawileh R. A., Abdalla J.A., Oudah F., Abdelrahman K. (2010). Low-cycle fatigue life behaviour of BS 460B and BS B500B steel reinforcing bars, *Fatigue & Fracture of Engineering Materials & Structures*, Vol. 33, n. 7, pp. 397-407.
- ISO 9227 (2006). Corrosion tests in artificial atmospheres - Salt spray tests.
- JUS C.K6.020:1987 "Hot-rolled steel. Reinforcing steel. Technical requirement", 1987.
- Kappos A.J. (1997). Seismic damage indices for RC buildings: evaluation of concepts and procedures, *Progress in Structural Engineering and Materials*, Vol. 1, No. 1, pp. 78-87.
- Krawiec H, Vignal V, Oltra R, "Use of the electrochemical microcell technique and the SVET for monitoring pitting corrosion at MnS inclusions", *Electrochemistry Communications*, Volume 6, Issue 7, July 2004, Pages 655–660.
- LNEC E455-2008 – Vares de aço A400 NR de ductilidade especial para armaduras de betão armado: características, ensaios e marcação, 2008.
- LNEC E460-2008 – Vares de aço A500 NR de ductilidade especial para armaduras de betão armado: características, ensaios e marcação, 2008.
- MacDougall, B. and Cohen, M. (1978) in Frankenthal, R. and Kruger, J. (Eds), "Passivity of Metals ", The Electrochemical Society, Princeton, NJ, p. 827.
- Mander J.B., Panthaki F.D., Kasalanati A. (1994). Low-cycle fatigue behaviour of reinforcing steel, *Journal of Materials in Civil Engineering*, ASCE, Vol. 6, No. 4, pp. 453-468.
- Manson S.S. (1954). Behaviour of materials under conditions of thermal stress. NASA TN 2933. Hanover.
- Massone L.M., Moroder D. (2009). Buckling model of reinforcing bars with imperfections, *Engineering Structures*, Vol. 31, pp. 758-767.
- Mazzoni S., McKenna F., Scott M.H., Fenves G.L. et al. (2007). OpenSees Command Language Manual, University of California, Berkley, USA.

- McClintock, F A., "A criterion for ductile fracture by the growth of holes", *Journal of applied mechanics* June 1968, pp. 363-369 *Transactions of the ASME*, 1968.
- Menegotto M., Pinto P. (1973). Method of analysis for cyclically loaded RC plane frames including changes in geometry and non-elastic behavior of elements under combined normal force and bending, *Proc., Symp. Resistance and Ultimate Deformability of Structures Acted on by Well-Defined Repeated Loads, IABSE Reports*, Vol. 13, pp. 15-22.
- Moersch J. Zur wasserstoffinduzierten Spannungsrisskorrosion von hochfesten Spannstählen – Untersuchungen zur Dauerhaftigkeit von Spannbetontragwerken. Schriftenreihe Deutscher Ausschuss für Stahlbeton, Heft 563 (2005)
- Moersch J. (2005). Zur wasserstoffinduzierten Spannungsrisskorrosion von hochfesten Spannstählen – Untersuchungen zur Dauerhaftigkeit von Spannbetontragwerken. Schriftenreihe Deutscher Ausschuss für Stahlbeton (in English).
- Monti G., Nuti C. (1992). Nonlinear cyclic behaviour of reinforcing bars including buckling, *Journal of Structural Engineering*, Vol. 118, No. 12, pp. 3268:3284.
- Mpampatsikos V., Nascimbene R., Petrini L. (2008). A Critical Review of the R.C. Frame Existing Building Assessment Procedure According to Eurocode 8 an Italian Seismic Code, *Journal of Earthquake Engineering*, Vol. 12(S1), pp. 52–82.
- Neubert B., Nürnberger U. Untersuchungen der statischen Kenngrößen und des dynamischen Tragverhaltens von Spannstählen in Abhängigkeit vom Rostgrad, S. 149-150; Schriftenreihe des Deutschen Ausschuss für Stahlbeton, Heft 405 (1990)
- NF A35-016-1:2007 “Aciers pour béton armé - Aciers soudables à verrous - Partie 1 : Barres et couronnes”, 2007.
- Nürnberger U. (2005). Korrosion und Korrosionsschutz im Bauwesen, Bände 1 und 2 erschienen im Bauverlag.
- NZS 1170.5:2004, Structural Design Actions, Part 5, Earthquake actions, New Zealand, Standards New Zealand, 2004.
- NZS 3101:2006, Parts 1 & 2: Concrete Structures Standard, Standards New Zealand, 2006.
- Panagiotakos T.B., Fardis M.N. (2001). Deformations of Reinforced Concrete Members at Yielding and Ultimate, *ACI Structural Journal*, Vol. 98, No. 2, pp. 135-148.
- Paulay T., Priestley M.J.N. (1992). Seismic design of reinforced concrete and masonry structures, John Wiley and Sons, Inc.
- Perrone V. (2004). Il calcolo agli stati limite: progetto e verifica delle sezioni in c.a. Hevelius Edizioni srl, Benevento, Italy (in italian).
- Petrini L., Pinho R., Calvi G.M. (2004). Criteri di Progettazione Antisismica degli Edifici, IUSS Press, Pavia, Italy (in italian).
- Powell G.H., Allahabadi R. (1988). Seismic damage prediction by deterministic methods: concepts and procedures, *Earthquake Engineering and Structural Dynamics*, Vol. 16, pp. 719–734.
- prEN 10080:2012, rev. 19/01/2012 - Steel for the reinforcement of concrete - Weldable reinforcing steel – General, ECISS/TC-104/WG1, 2012.
- Rehm G., Nürnberger U., Neubert B. Chloridkorrosion von Stahl in gerissenem Beton. Schriftenreihe Deutscher Ausschuss für Stahlbeton 390 (1988) 43-144
- Rice, J R and Tracey, D M: "On the Ductile Enlargement of voids in triaxial stress Field", *J. Mech. Phys. Solids* 17, pp. 201-217, 1969.
- Riecke E. Die Wasserstoffaufnahme von Eisen beider Korrosion in neutralen bis schwach sauren Elektrolyten. *Werkstoffe und Korrosion* 29 (1978), S. 106 – 112
- Rodriguez J., Ortega L.M., Casal J., Diez J.M. Corrosion of reinforcement and service life of concrete structures. 7th Int. Conference on durability of building materials and components; Stockholm, 1996
- Rodriguez M.E., Boter J.C., Villa J. (1999) . Cyclic stress-strain behaviour of reinforcing steel including effect of buckling, *Journal of Structural Engineering*, Vol. 125, n. 6, pp. 605-612.
- Schießl p. (1976). Zur Frage der zulässigen Rißbreite und der erforderlichen Betondeckung im Stahlbetonbau unter besonderer Berücksichtigung der Karbonatisierung des Beton, Schriftenreihe Deutscher Ausschuss für Stahlbeton 255.
- Simioni P. (2009). Seismic response of reinforced concrete structures affected by reinforcement corrosion, PhD Thesis, University of Braunschweig and University of Firenze.
- STAS 438/1-89 “Hot rolled reinforcement steel”, 1989.
- Szklarska-Smialowska, Z. (1986), *Pitting Corrosion of Metals*, NACE, Houston, MA.
- UNE 36065 EX:2000, Norma Española Experimental 2000 – Barras corrugadas de acero soldable con características especiales de ductilidad para armaduras de horigòn armado, 2000.
- UNI EN 1990:2006, Eurocode – Basis of structural design, 2006.
- UNI EN 1992-1-1:2005, Eurocode 2 (Annex C) - Design of concrete structures - Part 1-1: General rules and rules for buildings, 2005.

- UNI EN 1998-1:2005, Eurocode 8 - Design of structures for earthquake resistance - Part 1: General rules, seismic actions and rules for buildings, 2005.
- UNI EN 206-1:2006, Concrete - Part 1: Specification, performance, production and conformity, 2006.
- Vu K.A.T., Stewart M.G., 2005. Predicting the likelihood and extent of reinforced concrete corrosion-induced cracking, *J. of Structural Engineering*, 131(11), 1681–1689.
- Wen Y.K., Ang A. H-S., Park Y.J. (1988). Seismic damage analysis and design of reinforced concrete buildings for tolerable damage, *Proceeding of Ninth World Conference on Earthquake Engineering*, August 2-9, Tokyo-Kyoto, Japan.
- Wipf T.J., Phares B.M., Fanous F.S., Lee Y.S., Jolley M.J. (2006). Evaluation of corrosion resistance of different steel reinforcement types, Final report, Center for Transportation Research and Education Iowa State University

## HOW TO OBTAIN EU PUBLICATIONS

### Free publications:

- one copy:  
via EU Bookshop (<http://bookshop.europa.eu>);
- more than one copy or posters/maps:  
from the European Union's representations ([http://ec.europa.eu/represent\\_en.htm](http://ec.europa.eu/represent_en.htm));  
from the delegations in non-EU countries ([http://eeas.europa.eu/delegations/index\\_en.htm](http://eeas.europa.eu/delegations/index_en.htm));  
by contacting the Europe Direct service ([http://europa.eu/eurodirect/index\\_en.htm](http://europa.eu/eurodirect/index_en.htm)) or  
calling 00 800 6 7 8 9 10 11 (freephone number from anywhere in the EU) (\*).

(\* ) The information given is free, as are most calls (though some operators, phone boxes or hotels may charge you).

### Priced publications:

- via EU Bookshop (<http://bookshop.europa.eu>).

### Priced subscriptions:

- via one of the sales agents of the Publications Office of the European Union  
([http://publications.europa.eu/others/agents/index\\_en.htm](http://publications.europa.eu/others/agents/index_en.htm)).

The dissipative capacity of modern r.c. and composite steel/concrete structures is directly related to the rotational capacity of the elements in which plastic hinges are located: it strictly depends on the geometrical and mechanical characteristics of the sections and, moreover, on the ductile capacity of the steel reinforcing bars (deformation and dissipated energy). Nowadays the low-cycle fatigue/seismic behaviour of steel reinforcing bars is not well known and, at European level, no production control tests are prescribed for the mechanical characterisation of the seismic performance of reinforcing steels. This situation is well reflected in the framework of the revision of European standard EN10080 and in Mandate M115 which tends to harmonise production control for reinforcing steels also introducing low-cycle fatigue tests. Full knowledge about the effective ductility requirements imposed on bars by real seismic events is necessary: a detailed analysis of the ductility demand on reinforcements, considering both r.c. and composite steel/concrete structures, is consequently necessary and deeply analysed in the project. At the same time, the ductility capacity of steel reinforcing bars has been investigated considering also the detrimental effects due to aggressive environmental conditions, generally resulting in a progressive decrease of the mechanical characteristics of deformation, strength and dissipative capacity. The evaluation of the ability of corroded steel bars to still sustain the ductile requirements due to seismic action has been analysed, finally providing practical indications for the protection of bars from corrosion, in addition to what was already suggested by Eurocode 2.

*Studies and reports*